AD-A111 901 APPLIED RESEARCH ASSOCIATES INC ALBUQUERQUE NM F/G 8/13
FUNDAMENTAL PROPERTIES OF SOILS FOR COMPLEX DYNAMIC LOADINGS.(U)
SEP 81 W C DASS, J L BRATTON, C J HIGGINS F49620-80-C-0088
UNCLASSIFIED AFOSR-TR-82-0101 NL

1 OF 2
AD A
111901

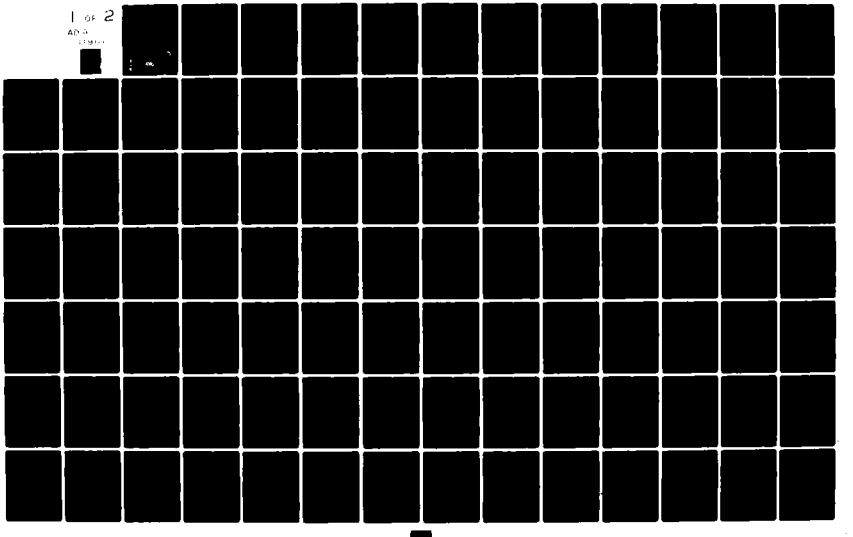

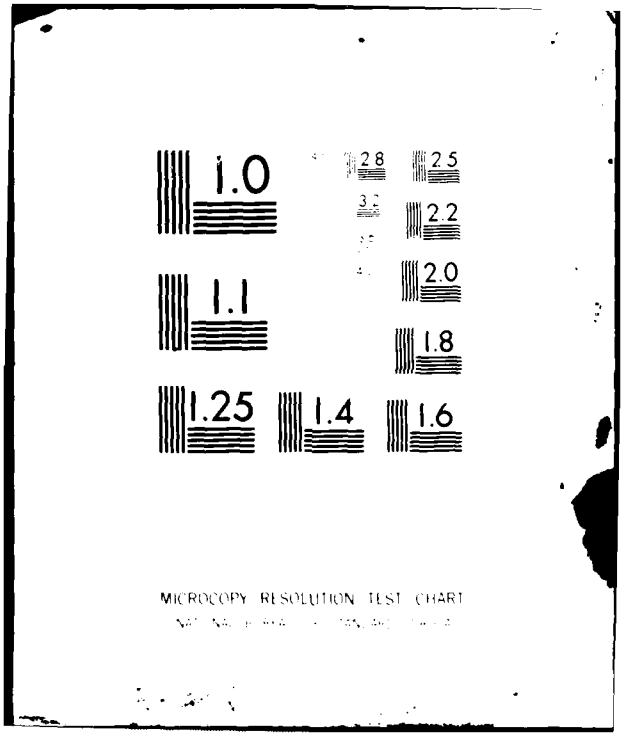
1.0
2.8
2.5
2.2
2.0
1.1
1.8
1.25
1.4
1.6
MICROCOPY RESOLUTION TEST CHART

AFOSR-TR- 82 -0101

F49620-80-C-0088

(11)

AD A111901

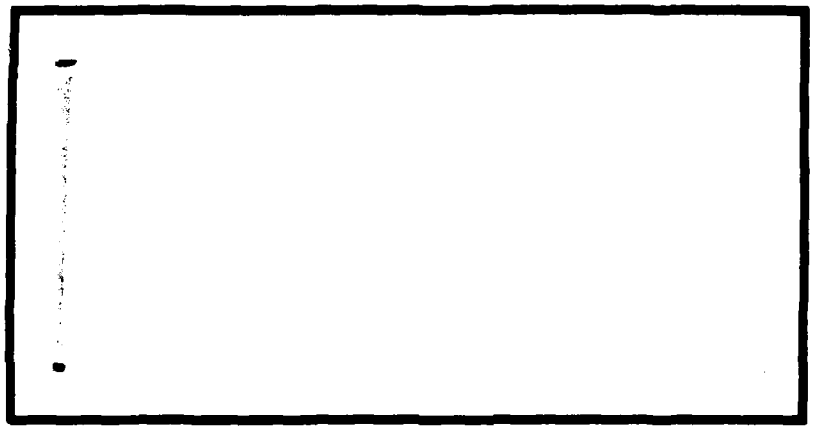

DTIC
ELECTE
MAR 11 1982
H

FILE COPY

APPLIED RESEARCH ASSOCIATES, INC.
Engineering and Applied Science

82 03 11 115

Approved for public release;
distribution unlimited.

FUNDAMENTAL PROPERTIES OF SOILS FOR COMPLEX DYNAMIC LOADINGS

ANNUAL TECHNICAL REPORT

on

Contract No. F49620-80-C-0088

by

William C. Dass
Jimmie L. Bratton
Cornelius J. Higgins

Applied Research Associates, Inc.
2101 San Pedro, N.E., Suite A
Albuquerque, NM 87110

Prepared for

Air Force Office of Scientific Research
Bolling Air Force Base
Washington, D.C. 20332

APPLIED RESEARCH ASSOCIATES, INC.

Conditions of Reproduction

APPLIED RESEARCH ASSOCIATES, INC.

SECURITY CLASSIFICATION OF THIS PAGE (When Data Entered)

REPORT DOCUMENTATION PAGE		READ INSTRUCTIONS BEFORE COMPLETING FORM
1. REPORT NUMBER AFOSR-TR- 82-0101	2. GOVT ACCESSION NO.	3. RECIPIENT'S CATALOG NUMBER
4. TITLE (and Subtitle) FUNDAMENTAL PROPERTIES OF SOILS FOR COMPLEX DYNAMIC LOADINGS		5. TYPE OF REPORT & PERIOD COVERED ANNUAL 1 Aug 80 - 31 Jul 81
		6. PERFORMING ORG. REPORT NUMBER
7. AUTHOR(s) WILLIAM C DASS JIMMIE L BRATTON CORNELIUS J HIGGINS		8. CONTRACT OR GRANT NUMBER(s) F49620-80-C-0088
9. PERFORMING ORGANIZATION NAME AND ADDRESS APPLIED RESEARCH ASSOCIATES, INC 2101 SAN PEDRO, NE, SUITE A ALBUQUERQUE, NM 87110		10. PROGRAM ELEMENT, PROJECT, TASK AREA & WORK UNIT NUMBERS 61102F 2307/C1
11. CONTROLLING OFFICE NAME AND ADDRESS AIR FORCE OFFICE OF SCIENTIFIC RESEARCH/NA BOLLING AFB, DC 20332		12. REPORT DATE 30 SEP 81
		13. NUMBER OF PAGES 173
14. MONITORING AGENCY NAME & ADDRESS(if different from Controlling Office)		15. SECURITY CLASS. (of this report) UNCLASSIFIED
		15a. DECLASSIFICATION/DOWNGRADING SCHEDULE

16. DISTRIBUTION STATEMENT (of this Report)

Approved for public release; distribution unlimited.

17. DISTRIBUTION STATEMENT (of the abstract entered in Block 20, if different from Report)

18. SUPPLEMENTARY NOTES

19. KEY WORDS (Continue on reverse side if necessary and identify by block number)

MATERIAL MODELING
INSITU BEHAVIOR
CIST
DYNAMIC PROPERTIES

20. ABSTRACT (Continue on reverse side if necessary and identify by block number)

An improved understanding of the fundamental behavior of soils under dynamic loads can lead to better modeling of many important soil and soil-structure phenomena. This report presents the initial results of a research program directed toward this goal. Constitutive modeling requirements are briefly reviewed, and results of a literature survey are summarized. A computer program for studying material models is described, and some preliminary examples are given. A study of insitu material behavior is presented in which several

DD FORM 1 JAN 73 1473 EDITION OF 1 NOV 65 IS OBSOLETE

UNCLASSIFIED
SECURITY CLASSIFICATION OF THIS PAGE (When Data Entered)

Two-dimensional simulations of cylindrical Insitu Test (CIST) events were performed. Basic CIST phenomena are investigated, as well as the response of specific soils. Insitu shear behavior and effective stress modeling of soils is discussed.

TABLE OF CONTENTS

LIST OF FIGURES

LIST OF FIGURES (Continued)

LIST OF FIGURES (Concluded)

LIST OF TABLES

1.0 INTRODUCTION

1.1 Philosophy

This year's research effort concentrated on evaluating the state-of-the-art in material modeling for dynamic loading conditions and developing some basic tools for further research.

Because complex dynamic loading of soils occurs under many different situations, it has been necessary to gather information from various disciplines within soil mechanics. The areas of earthquake and ground-shock seem to dominate, but other areas such as wave and wind effects, vehicle loading, machine vibrations and impact loading also are very much concerned with dynamic soil properties. The magnitude and nature of forces imposed on the soil varies quite widely among these types of loading. As a result, the people working in a specific area tend to concentrate on the soil behaviors which seem to be most important for their problem. The basic philosophy behind this research, however, is that a soil mass really has only a single fundamental behavior. The properties of a soil mass cannot be different just because the load is a vibrating machine or a 100 kt nuclear blast. Rather, certain properties will dominate soil behavior under certain load conditions. A truly accurate and complete constitutive model would be based on the most fundamental properties and cover all behaviors. Unfortunately, in developing a comprehensive soil model, one is limited by testing capabilities, both in the lab and field, by the ability to mathematically express and use complex models, and, to a varying degree, one is limited by imagination in recognizing fundamental soil properties.

In light of this, our effort is directed toward gaining a better understanding of both soil constitutive models and insitu soil behavior. In engineering, one must obtain the right mixture of accuracy and simplicity. If a soil model which is fundamentally correct can be suitably compartmentalized, and if one knows what properties are most pertinent to the problem at hand, then the necessary elements of the model can be chosen and the soil behavior may be suitably modeled.

1.2 Scope

This report deals primarily with material modeling in its current state as it applies to soils. A general discussion of soil models and their use is included. A description of a computer code which is presently being developed under this effort and which will be used to study material models is presented. In addition, there is a section on insitu material properties summarizing a series of two-dimensional finite difference calculations which has been done. And finally, some special topics which are important to material modeling, shear behavior and effective stress modeling, are discussed.

1.3 Methodology

In order to proceed with minimum duplication of effort, a review of the existing literature was undertaken. The general topics covered were:

i) Material Modeling
   a) Review Papers
   b) Specific Soil Models
   c) Calculational Studies/Modeling

ii) Insitu Testing
   a) Explosive Loading
   b) Insitu Shear Properties

iii) Laboratory Testing

Appendix A is a summary list (by topic) of the more important references. Please note that this list is continuously being updated and is certainly not exhaustive.

Evaluation of various material models has begun, using a computer code which is capable of simulating several different stress and strain loading paths. The computer program allows model study without having to perform

expensive boundary value calculations. It is by no means, however, a replacement for finite difference/element studies because it cannot reproduce overall geometry and material interaction effects. In view of this, several finite difference calculations of Cylindrical In-Situ Test (CIST) sites were also performed. This allowed the study of material behavior under insitu, large strain conditions. Because of the sizable CIST data base, the calculations also served as a basis for evaluating a modeling effort with actual field data.

This report summarizes the past years efforts as outlined in the statement of work contained in the following section. Soil modeling is reviewed in Section 2, the Soil Element Model is described in Section 3 and in-situ material behavior is presented in Section 4. Section 5 contains the results of two special study areas and the effort is summarized in Section 6.

1.4 Statement of work

The following are the tasks as outlined in Contract No. F49620-80-C-0088 "Fundamental Properties of Soils for Complex Dynamic Loadings".

TASK 1. Development of Plotting Routines for Data Display

ARA will prepare plot routines for 2-D finite difference codes to allow plots of the states of stress and strain, particle velocities and displacements. Included will be the variation of these parameters at various times as well as plots of the CIST data.

TASK 2. Perform Two-Dimensional Finite Difference Calculations of the Middle Gust Wet Site CIST (CIST-9) and Dry Lake Valley CIST (CIST-23)

Using the best available cavity pressure description for CIST-9 and CIST-23, ARA will perform the 2-D calculations using the following material models:

- Elastic Based on Seismic Wave Speeds

- Engineering Model (AFWL) Fit to Laboratory Recommended Properties
- Engineering Model Developed from 1-D Analysis of CIST-9 by AFWL
- Hydrostatic
- Elastic, Perfectly Plastic Using Seismic Wave Speeds and Laboratory Failure Surface
- Engineering Model with Revised Properties to Better Fit Experimental Velocity-Time Histories
- Engineering Model Updated (on basis of preceding calculation) to Better Fit Data

TASK 3. Perform Two-Dimensional Finite Difference Calculations of CIST Events in Saturated Sand

A series of calculations as described for CIST-9 will also be performed for saturated sands. CIST-10 and CIST-15, 16 will receive the primary focus. Perform additional calculations as necessary to better resolve the basic response of the dry clay, saturated clay, clay shale, dry sand, and saturated sand which will be studied in Tasks 2 and 3. It is estimated that 8-10 additional calculations will be required.

TASK 4. Interpretation of Calculational Studies to Describe the Fundamental Response of the Two Geologic Materials

The calculations performed in Tasks 2 and 3 will be used to develop an understanding of the effect of the assumption concerning the form of the material model on the behavior of the materials. The difference exhibited in the stress and strain paths by the various models will be compared to the implied behavior of the real materials. Comparisons of these stress paths to those utilized in laboratory tests and expected to occur in field conditions will be used to evaluate the potential of the models studied and to suggest improved laboratory testing procedures. In particular, the characteristics of constitutive models that would be required to

reproduce the measured response of these two materials will be described and compared to other available models that were not evaluated in this study.

Recommendations concerning constitutive model development necessary to better model these materials will be developed.

TASK 5. Development of a Soil Element Code

A computer code will be developed to allow study of the characteristics of the various material models to prescribed stress or strain paths. The code will be general enough to reproduce the stress paths representative of current laboratory tests as well as paths of interest which cannot be reproduced in current test apparatus.

This code will then be exercised for representative material models to develop a better understanding of the limitations and advantages of current models and laboratory testing devices. At least one model from each of the following groups will be evaluated:

- Elastic
- Viscoelastic
- One-Dimensional Curve Fit
- Ideal Elastic-Plastic
- Elastic Non-Ideally Plastic

As a minimum each model evaluated will be subjected to the following loading conditions:

- Repetitive Pure Shear
- Hydrostatic Compression
- Uniaxial Strain
- Biaxial Compression (Std. Triaxial Test)
- Plane Strain with Rotation of Principal Strain Direction

- True Triaxial Loading
- Biaxial Extension
- Complex Loading Histories

In all cases the response will be evaluated for various levels of loading and repetitions of load. The complex loading histories will be developed from study of CIST, earthquake, and explosive surface burst calculations.

TASK 6. Evaluation of Shear Response in In-Situ Material Property Tests

ARA will:

Perform theoretical and calculational studies of the shear stresses generated in the plane (DISK HEST), cylindrical (CIST) and spherical dynamic, high stress, *in-situ* tests. These studies will focus on the nature (location and magnitude) of the shear stresses and strains developed, their spacial and temporal variation, and how they might be measured and interpreted.

Analyze experimental data from representative tests of each type to corroborate the theoretical studies and establish experimental measurement limitations on the recovery of shear response data.

Develop alternatives to current in-situ test configurations and measurements to improve recovery of shear data.

TASK 7. Theoretical Analysis of Special Problems in Modeling Soil Behavior

Study the consequences, in terms of computer storage requirements, of using true multi-phase models in finite difference codes especially with respect to the AFWL CRAY computer.

Evaluate alternate approximate methods of treating effective stress in finite difference calculations.

Study the physical basis for soils increase in strength at very high (several kilobars) pressures.

Other issues identified in previous tasks.

The general result of this task will be input to future theoretical work on model development.

2.0 SOIL MODELING

2.1 Theoretical Requirements

Constitutive relations used to model physical phenomena must obey the laws of thermodynamics and other principles of continuum mechanics. (A model may consider the soil material to be particulate, but homogeneity is usually still assumed). The model should produce behavior which is smooth and continuous, as this seems to be the case for soil, and infinitesmal changes in load should produce infinitesimal changes in state.

Several material models in use today do not satisfy all the above criteria. This is primarily a result of the "ad hoc" nature of soil modeling to date. There is a tendency to develop a model which produces the required behavior under the given conditions with little concern for generality, completeness, or theoretical correctness. These models are then usually applied to different conditions by an unsuspecting modeler who soon discovers some unusual behavior.

2.2 Behavioral Requirements

Certain behavioral characteristics of soils have been observed in lab tests, insitu tests, and (in practice) under actual field loading conditions. Although it is impossible to completely summarize soil behavior in this report, a complete soil model would need to address each of the following:

a) Soils exhibit non-linear response, even at strains as low as 10^{-5}.

b) Permanent (irrecoverable) deformations occur under both pressure and deviatoric loading.

c) Initial unloading (shear and volumetric) is very often elastic in nature.

d) There usually is a convex (or "stiffening") shape to the volumetric pressure-strain response while there is a concave (or "softening") shape of the shear stress-strain behavior.

e) Soils display a shear strength, τ_{max}, beyond which shear "failure" takes place - usually defined as the development of large deformation under small increases in applied stress.

f) Normal stress (confining pressure) has a significant effect on properties.

g) There is a coupling of volume behavior and shear behavior often referred to as shear-dilatancy coupling.

h) The response of a soil up to a particular stress state depends on the stress path taken to obtain that state (stress path dependency).

i) Soils may exhibit anisotropy due to their history, i.e. deposition, overconsolidation, compaction, etc.

j) Stress induced anisotropy can occur as a result of current loading conditions.

k) At low stress levels, strain will occur in the direction of a stress increment, while at high stress levels, strain occurs in the direction of the overall stress state.

l) Soils may display a "peak" strength with subsequent strain softening to a "residual" strength.

m) Cyclic loads produce special effects such as "ratcheting" of hysteresis loops. If the cycled stress level is low enough an eventual equilibrium state will be reached. Energy dissipation (hysteresis) occurs even at low strain levels.

n) Multi-directional cycling produces different effects than unidirectional cycling.

o) The properties of soils vary with strain magnitude.

p) Soils may exhibit loss of structure (sensitivity).

q) Deformation in some soils may become highly localized, e.g. formation of "shear bands" in clay soils under triaxial test conditions.

r) Rate of deformation affects some soil properties.

If one considers that soil is actually a three-phase material (air-water-soil solids) there are many additional behaviors which must be accounted for. Some of the more important:

s) Liquefaction due to excessive pore pressure and subsequent loss of shear strength.

t) Pore fluids migrate depending on a number of gradient fields.

u) Pore fluids create additional rate effects.

As of yet, no soil model has taken all of these behaviors into account, and this may, in fact, not be possible.

2.3 Practical Requirements

To successfully apply a particular constitutive model to a practical engineering situation, it must meet certain requirements. First, it must be understandable. A model which is so complex to the point of being overly cumbersome is not very useful to an engineer. Second, the model must be physically meaningful. If each element of the model can be associated with one or more of the above soil behaviors, the model is much easier to work with and alter as necessary. Finally, a model must be suitable for use on existing computer hardware. This is a somewhat limiting factor, but capabilities are improving with each new generation of computer, and this greatly broadens the alternatives for choosing a suitable model.

2.4 Available Soil Models

The following is a list of the major models which are available for soil. (Each of these may have a number of subsets.) The models which have been installed in the soil element are summarized in Section 3.3. Information on the others may be found by consulting the appropriate references as outlined in Appendix A.

Simple Models

a) Elastic (Linear or Non-Linear)
b) Visco-Elastic
c) Elastic-Perfectly Plastic
d) Curve-Fit Models

More Complex Models

e) AFWL Engineering Model
f) Cam-Clay Model
g) Cap Model
h) Rate Type Fluid Models
i) Lade's Model
j) Prevost's Model
k) Endochronic Models
l) Multi-phase Models

3.0 SOIL ELEMENT MODEL

3.1 Purpose

There are many constitutive models for soils which have been developed and tested to varying degrees. Some models have their basis in elastic theory or the theory of plasticity. Others are developed specifically to produce one or more of the behaviors discussed earlier (Section 2.2, Behavioral Requirements). In order to bring several models into direct comparison, a computer code has been written which can drive these models at the user's discretion. This "Soil Element Model", is a tool for performing material modeling studies. It has been developed with generality in mind so that it may be useful in several ways. Parameter studies of a particular model may be performed, which provide a valuable understanding of how a model's behavior depends on the assigned coefficients. One may subject two or more models to identical boundary conditions and compare the results. Model behavior can also be compared with test data, either in an effort to fit a model to a set of data or to predict soil response for a particular test. And most important, the Soil Element Model (SEM) is useful for model development and syntnesis; new relationships may be tested or model elements may be combined to produce the best model behavior.

3.2 Description

The SEM is a small computer program which has been developed at ARA and presently is operational on the CRAY-1S computer at the Air Force Weapons Laboratory. It is basically an adaptation and generalization of a code called "SANDR" which was written by G. Baladi at WES for Sandia Laboratories (Ref. 1). SANDR is capable of simulating the behavior of the effective-stress cap model under standard triaxial test boundary conditions. SEM incorporates several material model options and can simulate, at present, true-triaxial, pure shear, and arbitrary boundary conditions as well as standard triaxial.

The program consists of a driver, a choice of constitutive model algorithms, and plotting routines. The basic idea is illustrated in Figure 3.1. The Driver's role is to handle input and output operations and provide

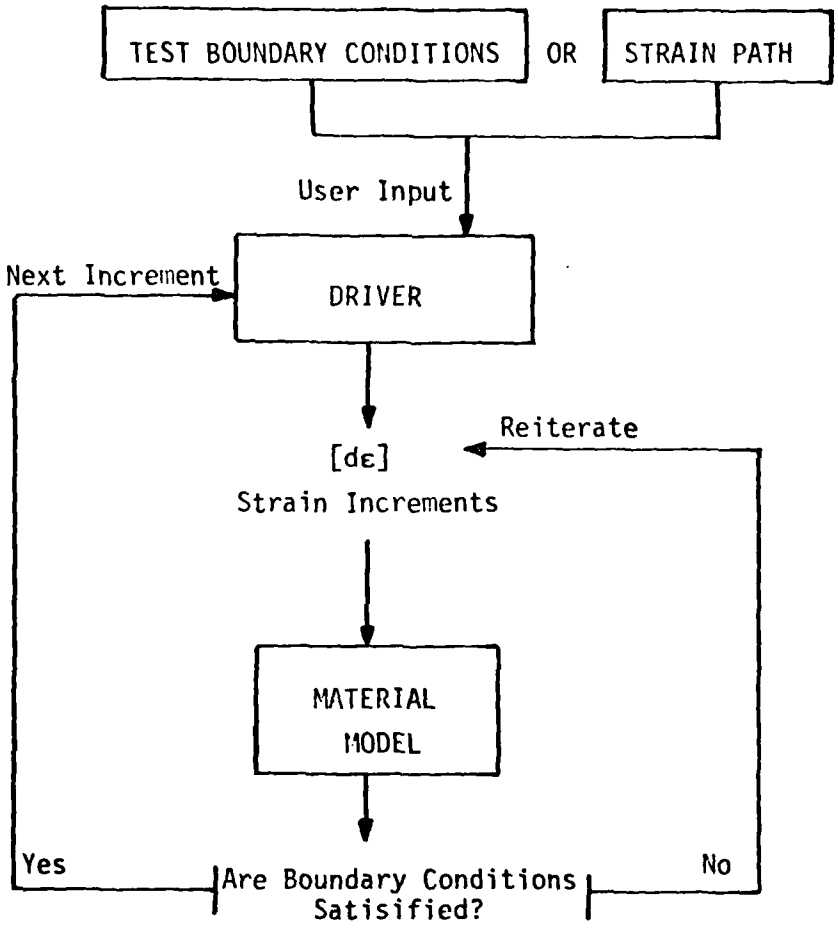

Figure 3.1. Basic soil element model logic.

the material model with a strain increment, while enforcing any specific boundary conditions which may be appropriate. For example, in the standard triaxial test, the strain increment tensor must be controlled so as to produce a stress state with $\sigma_R = \sigma_T$. The material models provide a constitutive relationship ([H]) which generates a new stress tensor:

$$[d\sigma] = [H]\,[d\epsilon] \tag{3.1}$$

It is important to keep the material model distinct from the driving mechanism to allow easy alteration and/or substitution.

All of the models are "strain controlled", as in equation 3.1 above. This is consistent with most finite element and finite difference code formulations. As a result, making a model follow a particular strain path is relatively easy. Most laboratory tests, however, are run under stress controlled conditions. In studying a particular model it would be convenient to subject it to a specific load path, i.e. that of a particular laboratory test. This is done in SEM via iteration. That is, if the stress state which is calculated with a particular material model does not meet the boundary stress conditions, the strain increment tensor is adjusted and the stress is recalculated. This involves finding an efficient method for adjusting the strain increment tensor. The more general test boundary conditions, such as true triaxial, are somewhat more difficiult to iteratively duplicate.

SEM uses any set of consistent units. Output appears in the same units as are input. A number of plot options may be chosen to graphically display the results.

3.3 Constitutive Relations

The soil element model has great potential for aiding in model study and is constantly developing. The following paragraphs will describe the present status of the SEM.

The following five constitutive models are presently incorporated into the the program:

1) Elastic
2) Elastic - Perfectly Plastic
3) One-Dimensional Curve Fit
4) AFWL Engineering Model
5) Effective Stress Cap Model

Appendix B describes the notation used in the model subroutines and gives some general definitions. An attempt was made to be consistent in going from one model to the next, although this is not always possible. Note that all models assume the material to be homogeneous and isotropic.

3.3.1. Elastic Model

The constitutive relationship here is simply Hooke's Law. Only two constants are required to completely define a linearly elastic, isotropic material, we use K and G, where

$$K = \frac{\sigma_{kk}}{3\,\epsilon_{kk}}$$

$$G = \frac{S_{ij}}{2e_{ij}} \qquad (3.2)$$

and S_{ij} and e_{ij} are deviatoric stress and strain, respectively. An expression for stress in terms of strain may then be derived:

$$S_{ij} = \sigma_{ij} - \frac{\sigma_{kk}}{3}(\delta_{ij})$$

$$e_{ij} = \epsilon_{ij} - \frac{\epsilon_{kk}}{3}(\delta_{ij})$$

combining,

$$\sigma_{ij} = S_{ij} + \frac{\sigma_{kk}}{3} (\delta_{ij})$$

and substituting,

$$\sigma_{ij} = 2\,G\,e_{ij} + K\,\varepsilon_{kk}\,(\delta_{ij})$$

$$\sigma_{ij} = 2\,G\,[\varepsilon_{ij} - 3\,\frac{\varepsilon_{kk}}{3}\,(\delta_{ij})] + K\,\varepsilon_{kk}\,(\delta_{ij})$$

$$\sigma_{ij} = 2\,G\,\varepsilon_{ij} + \left[\frac{3\,K - 2\,G}{3}\right]\,\varepsilon_{kk}\,(\delta_{ij}) \qquad (3.3)$$

Equation (3.3) describes both the volumetric and deviatortic response of an elastic material.

3.3.2. Elastic - Perfectly Plastic

In the elastic-plastic case, a failure surface is defined (in $\sqrt{J_2'}$, J_1 space) up to which a material behaves linearly elastically. When the stress path intersects the failure envelope, plastic strain occurs according to an associated flow rule and the devatoric stress may not exceed the failure surface.

The failure surface is defined as an exponential (see also figure 3.2a),

$$f\,(J_1) = A - C_e^{BJ_1} \qquad (3.4)$$

Because it is defined in terms of $\sqrt{J_2'}$, the intersection of the failure surface with the deviatoric plane is a circle (figure 3.2b).

When a stress increment based on eleastic behavior violates the failure surface (see figure 3.2c) some plastic strain occurs and a correction must be made to bring the stress state back to the failure surface. An

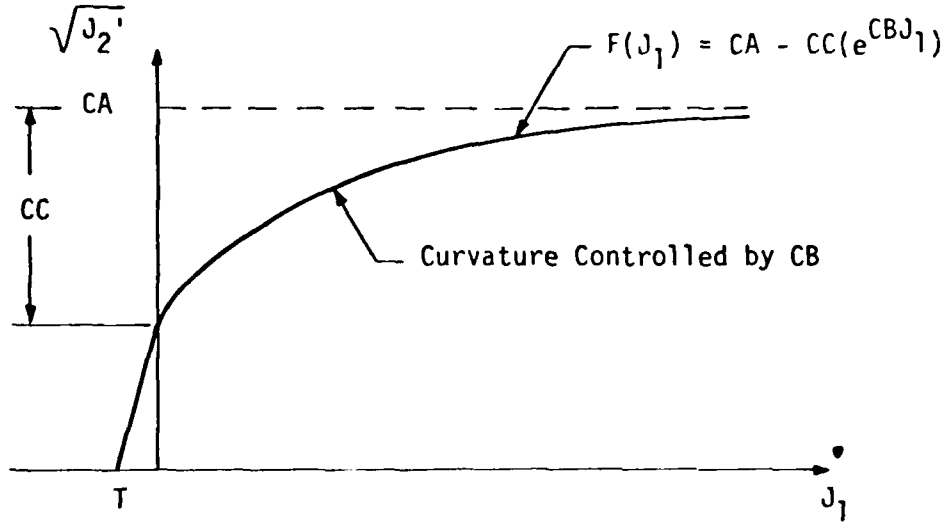

a) Failure Surface

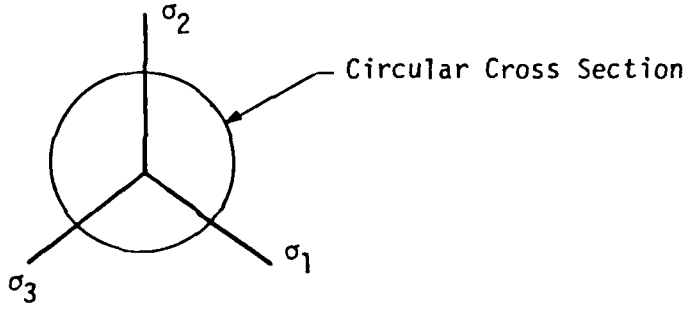

b) Deviator Plane

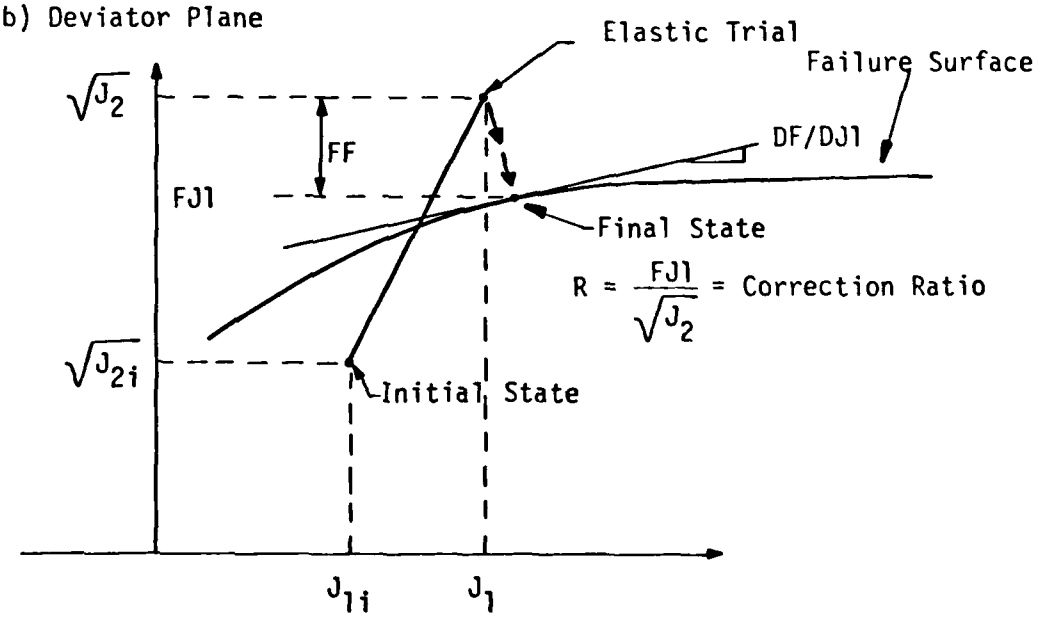

c) Correction Procedure for Violation of Failure Surface

Figure 3.2. Elastic-plastic model.

associative flow rule is enforced and corrections are made normal to the failure surface. First a volumetric plastic strain is calculated as follows:

$$d\,\varepsilon_{kk}^{p} = -\,3\left[\frac{\sqrt{J_2}^{E} - f(J_1^{E})}{9\,K\left(\frac{\delta f}{\delta f_1}\right)^2 + G}\right]\frac{\delta f}{\delta f_1} \tag{3.5}$$

then,

$$J_1 = J_1^{E} - 3\,K\,d\,\varepsilon_{kk}^{p} \tag{3.6}$$

A ratio is calculated based on the amount of necessary correction, and the stress deviators are multiplied by this adjustment:

$$S_{ij} = \frac{f(J_1)}{f(J_1^{E})}\,S_{ij}^{E} \tag{3.7}$$

3.3.3. One-Dimensional Curve Fit

Curve-fitting is an empirical method for modeling the behavior of a material. A trend is observed in some laboratory test data and a mathematical curve is fit to it which reproduces that data. The curve may be exponential, hyperbolic, polynomial, or any other convenient functional form.

The curve-fit routine in the SEM is aimed at reproducing the cyclic shearing behavior observed in soils. It is taken from a paper entitled "Nonlinear Soil Models for Irregular Cyclic Loadings" by Robert Pyke (Ref. 2). The soil model fits a hyperbolic expression to the intitial loading shear stress-strain curve, then uses extended "Masing" rules to model the hystresis loops. These rules postulate that the shear modulus on each loading reversal assumes a value equal to the initial tangent modulus for

the initial loading curve and that the shape of the unloading or reloading curves is the same as the initial curve, except that the scale is enlarged by some factor.

The model is basically a Davidenkov - class model, giving the shear stress in terms of shear strain:

$$\tau = \tau_c + G_{max} (\gamma - \gamma_c) \left[\frac{1}{1 + \frac{|\gamma - \gamma_c|}{n\gamma_y}} \right] \tag{3.8}$$

where $n = 1$ for initial loading,

and $n = \left| \pm 1 - \frac{\tau_c}{\tau_y} \right|$ $\quad$ + = reloading
$\quad$ - = unloading

The terms of the above equation are defined in figure 3.3.

The volumetric behavior is treated as linearly elastic with

$$\sigma_{kk} = 3 K \gamma_{kk}$$

although this can be modified so that K is any functional form, e.g.

$$K = K (\sigma_{kk}).$$

3.3.4. AFWL Engineering Model

A non-energy-dependent version of the AFWL engineering model has been installed into the SEM. The model is elastic-ideally plastic with volume hysteresis. The model is described in terms of a failure surface (in $\sqrt{J_2'}$ vs P space) and a hydrostat (in P vs μ space).

Pressure - volume behavior is controlled by the hydrostat, which is a series of linear segments (see figure 3.4b). Upon unloading the model

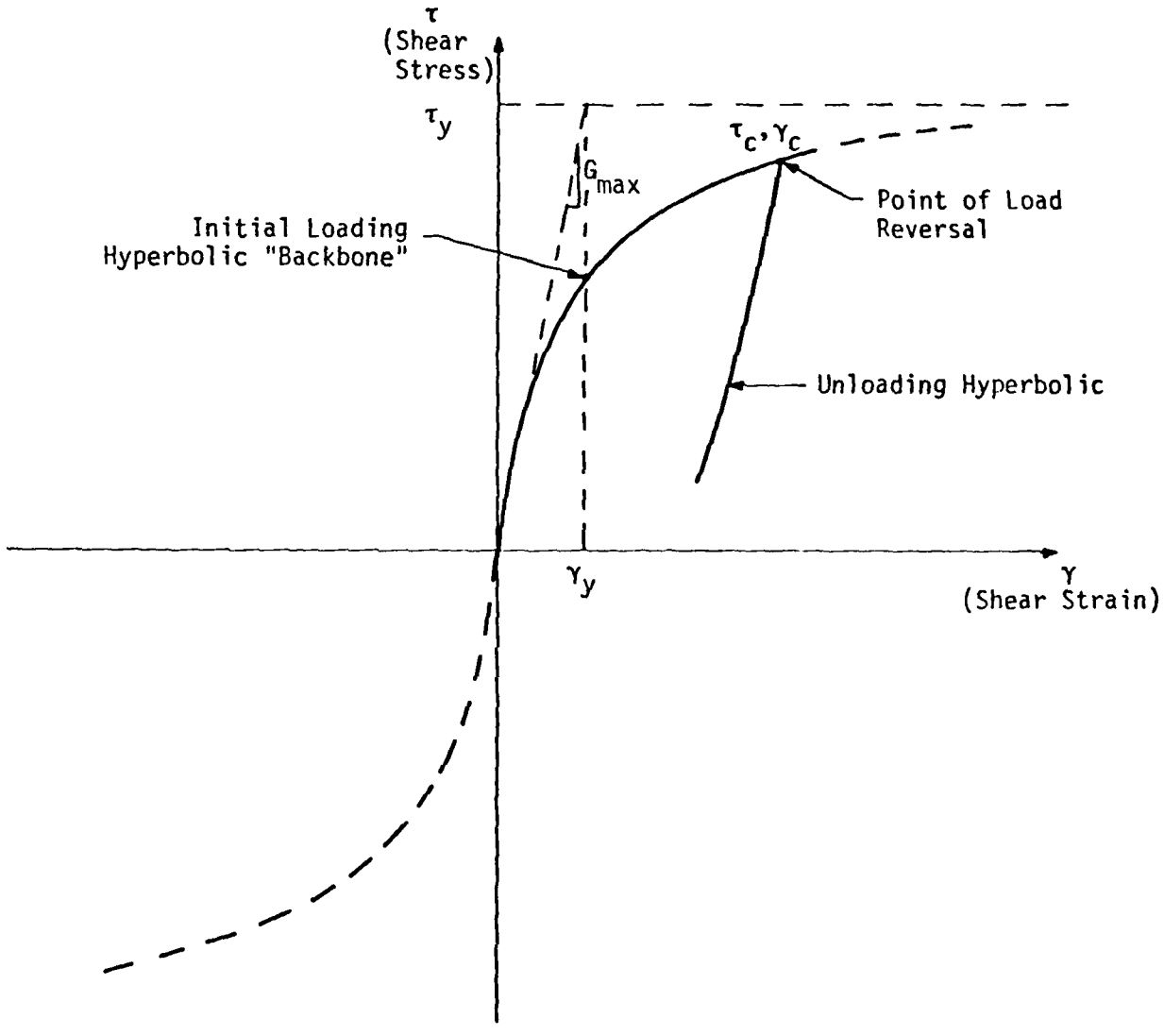

Figure 3.3. Hyperbolic shear model.

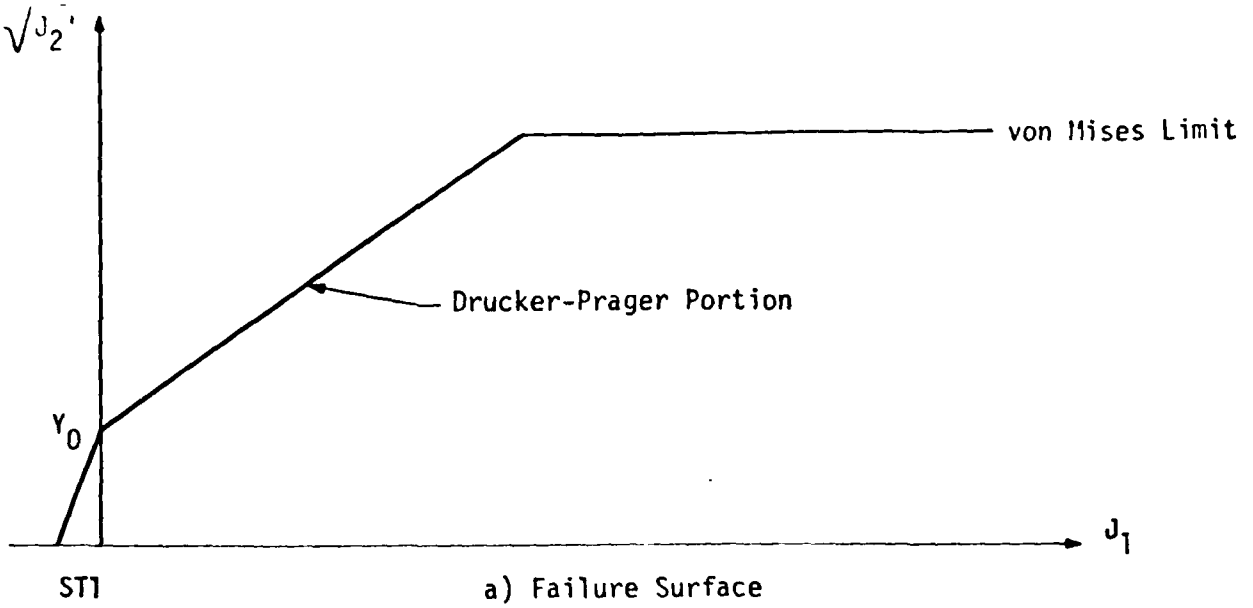

a) Failure Surface

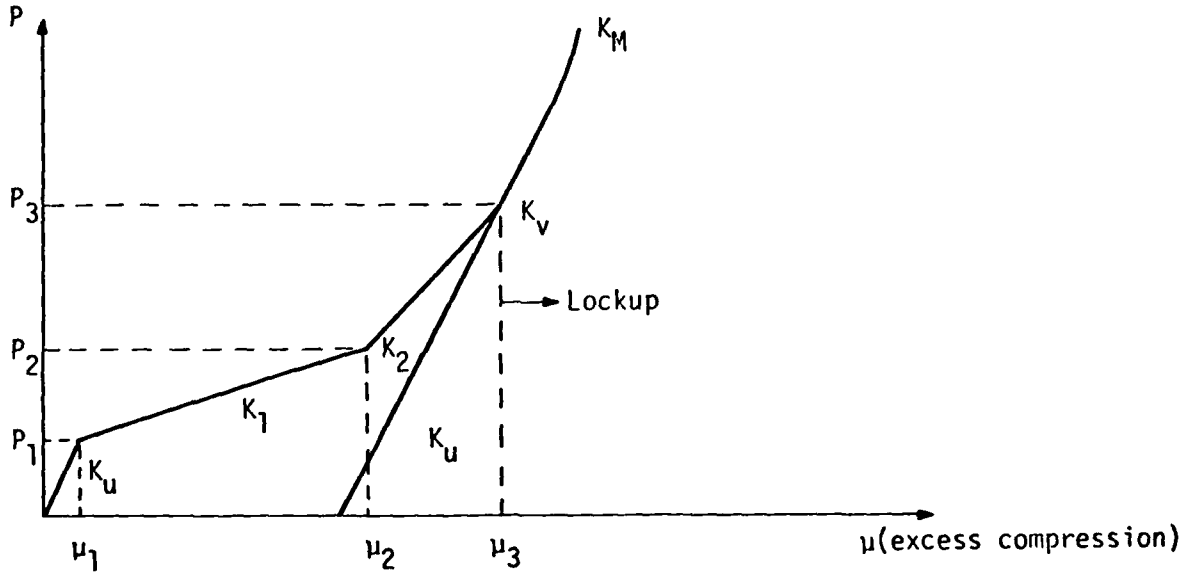

b) Hydrostat

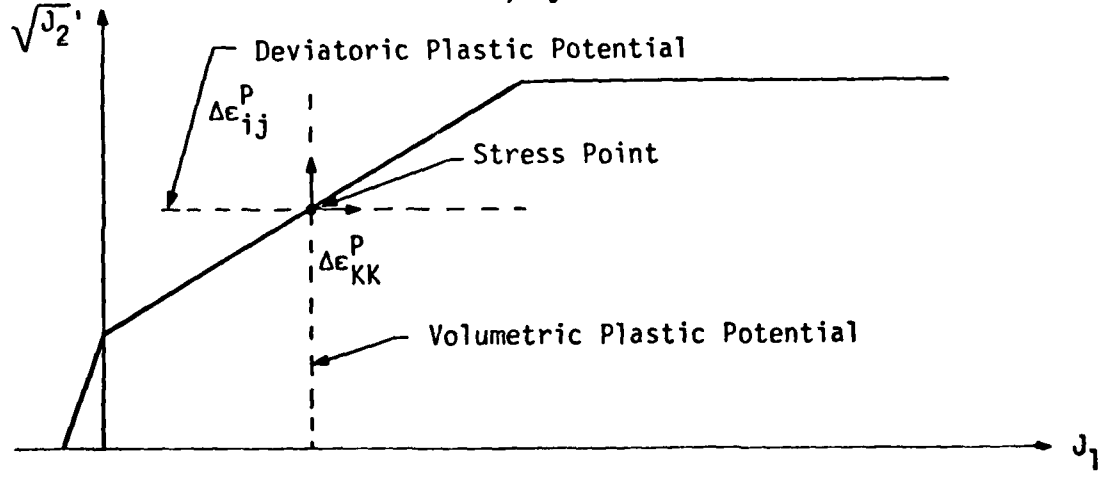

c) Plastic Potentials

Figure 3.4. AFWL engineering model.

allows irrecoverable volume strain as defined by the difference in the loading and unloading modulii. Note that the excess compression, μ, is used instead of ε_{kk}, the volume strain, to define the volume pressure relation. As a result, it is not quite correct to call the hydrostat slopes bulk modulii. Specifically:

$$K = \frac{P}{\varepsilon_{kk}} \tag{3.9}$$

wnere

$$\varepsilon_{kk} = \frac{\Delta V}{V_o} - 1 \tag{3.10}$$

But

$$\mu = \frac{\rho - \rho_o}{\rho_o} = \frac{V_o}{V} - 1 = \frac{\varepsilon_{kk}}{\varepsilon_{kk} + 1} \tag{3.11}$$

Thus

$$\frac{P}{\mu} = \frac{P}{\varepsilon_{kk}} (\varepsilon_{kk} + 1) \tag{3.12}$$

and, BKL = K + P

where BKL is the hydrostat slope and K is bulk modulus. The relationship between BKL and K is pressure dependent with the difference becoming significant only at higher pressures.

The failure surface (see figure 3.4a) consists of a Drucker - Prager frictional segment in combination with a von Mises cut-off. Below the failure surface, the material behaves elastically:

$$d\sigma_{ij}^{E} = 2\,G\,e_{ij}^{E} + 3\,K\;\varepsilon_{kk}^{E}\,(\delta_{ij}) \tag{3.13}$$

where

$$K = K(\mu)$$

$$G = 3/2\,(K)\left(\frac{1 - 2\nu}{1 + \nu}\right)$$

At the failure surface, there are two plastic potentials which effectively uncouple distortional and volumetric plastic strain (see figure 3.4c). The volumetric flow rule is associative:

$$d\,\varepsilon_{kk}^{p} = dP\,\left(\frac{K_u - K_l}{K_u\,K_l}\right) \tag{3.14}$$

and the deviatoric flow rule is non-associative, with stress being vertically corrected back to the failure surface:

$$de_{ij}^{p} = \lambda\,(S_{ij} + d\,S_{ij}) \tag{3.15}$$

$$\text{where,}\quad \lambda = \frac{d\sqrt{J_2'}}{2\,G\sqrt{J_2'}} \tag{3.16}$$

3.3.5. Effective Stress Cap Model

The SEM contains a version of the cap model which is intact from Baladi's original SANDR code. At present only one modification has been made to allow for a curved failure surface.

The cap model is an elastic-plastic constitutive model which has been developed in accordance with the rules of classical plasticity (see, for example, Hill (Ref. 3)). As a result, its mathematical description is a little more complicated than that of the AFWL model, which was developed with calculational results in mind. The cap model was an important development, because it effectively couples shear and volumetric behavior.

The behavior of the model in the elastic range is governed by the elastic bulk and shear modulii. The bulk modulus is a function of J_1 only:

$$K = \frac{K_i}{1 - K_1} \{ 1 - K_1 \exp [- K_2 (J_1 - 3 G_r)]\} \tag{3.17}$$

where K_i, K_1 and K_2 are material constants and G_r is the overburden stress due to gravity. G, the shear modulus, is taken to be a function of the second invariant of the stress deviator tensor, J_2':

$$G = \frac{G_i}{1 - G_1} [1 - G_1 \exp (- G_2 \sqrt{J_2'})] \tag{3.18}$$

where G_i, G_1 and G_2 are material constants. The parameters for the bulk and shear modulii are evaluated by fitting curves to match the unloading hydrostat behavior and the unloading stress difference - strain difference triaxial behavior, respectively.

The plastic behavior of the model is described in stress space by two functions (see figure 3.5a). A modified Drucker-Prager failure surface is defined by:

$$f(J_1) = (C_s + C) - C \exp (BJ_1) + \alpha J_1 \tag{3.19}$$

where C_s, C, B and α are material parameters which can be obtained from triaxial test data. C_s represents a cohesive strength, α a frictional strength, B defines a gradual increase in strength, and C a maximum shear strength. By properly defining the constants, a curved or linear failure surface may be specified.

An elliptical strain-hardening surface is defined by:

$$F (J_1, \kappa) = \frac{1}{R} \{[X(\kappa) - L(\kappa)]^2 - [J_1 - L(\kappa)]^2\}^{0.5} \tag{3.20}$$

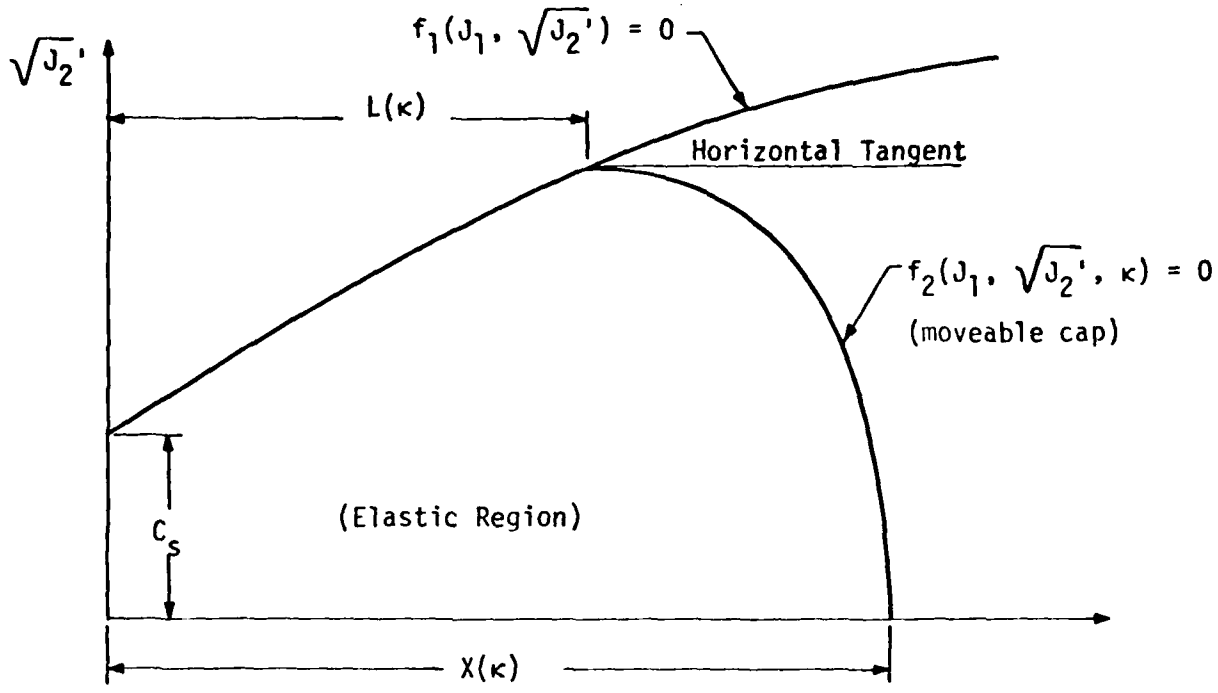

a) Yield Surfaces

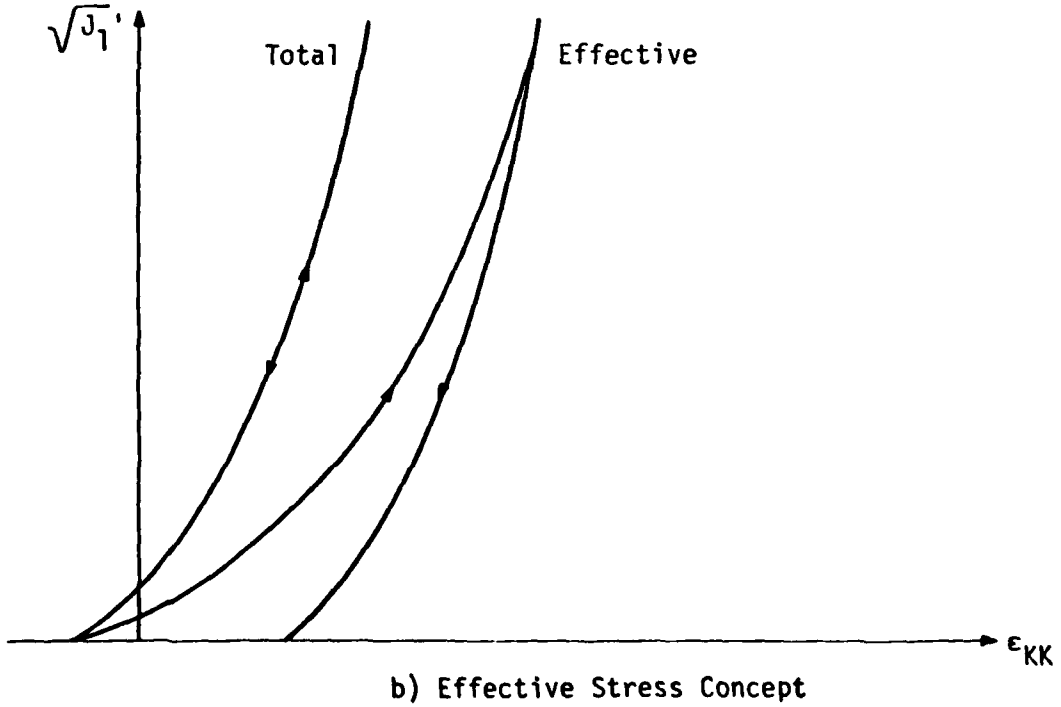

b) Effective Stress Concept

Figure 3.5. Effective stress cap model.

where $X(\kappa)$ and $L(\kappa)$ are as shown in figure 3.5a. R is the ratio of the major to minor axes of the elliptical yield surface. is the hardening parameter and controls cap movement:

$$X(\kappa) = -\frac{1}{D} \ln\left(1 - \frac{\varepsilon_{kk}^{p}}{W}\right) + 3\,G_r \qquad (3.21)$$

with D and W material constants. Thus, hardening of the cap is a function of plastic volumetric strain.

The cap model is an "effective" stress model in that it has both drained and undrained responses for the volumetric behavior (figure 3.5b). The undrained model, obtained from an undrained test, simulates total stress behavior. The drained model, obtained from a drained set of tests, simulates effective stress behavior. Since total stress equals effective stress plus pore pressure, the pore pressure response of the material is quite readily calculated.

The computation of stress given a strain increment in the cap model subroutine procedes by first assuming an elastic trial. Checks are then made to see if any control surfaces have been exceeded. If the failure surface is exceeded plastic strain is calculated according to an associative flow rule and the hardening parameter is updated to account for plastic volumetric strain. Iteration is needed to maintain consistency between location of the stress point, the cap, and the value of κ, the hardening parameter.

3.4 Test Paths

The SEM model is capable of exercising any of the installed constitutive relations over the following test paths:

i) isotropic compression/consolidation (undrained/ drained)
ii) uniaxial strain

iii) standard triaxial ($\sigma_2 = \sigma_3$)

iv) cubical triaxial (strain controlled, i.e. rigid platens)

v) simple shear (strain controlled)

vi) arbitrary strain paths

Several of these paths are shown in figure 3.6 for the triaxial plane. Note that one can also simulate the results of proportional loading tests, i.e. those with arbitrary directions in the triaxial plane.

3.5 Sample SEM Exercises

Appendix C illustrates the use of the Soil Element Model with six examples. The first five examples deal with one material, McCormick Ranch Sand (Ref. 4), for which several models have been preliminarily fit. The models were then subjected to various loading conditions, with the results shown by the figures in the appendix. The last example is of the effective stress cap model, which has been fit to model a deep-sea sediment (Ref. 1). Table 3.1 summarizes the paramters which are necessary to describe each of the models.

Further exercises of this type will be done to study material model responses. The models will be compared with data from both laboratory and insitu experiments.

3.6 Continuing Work

The SEM will play an important part in the dynamic soil properties effort which is continuing at ARA. The following enhancements and modifications constitute the direction of development for the computer code itself. Other additional areas of improvement may later become evident.

i) Model refinement. Enhance the response of the models already installed in the code. Examples are allowing for non-linear elasticity, isotropic hardening or softening of the elastic plastic model, and combining Pyke's shear model with the volumetric portion of various other models.

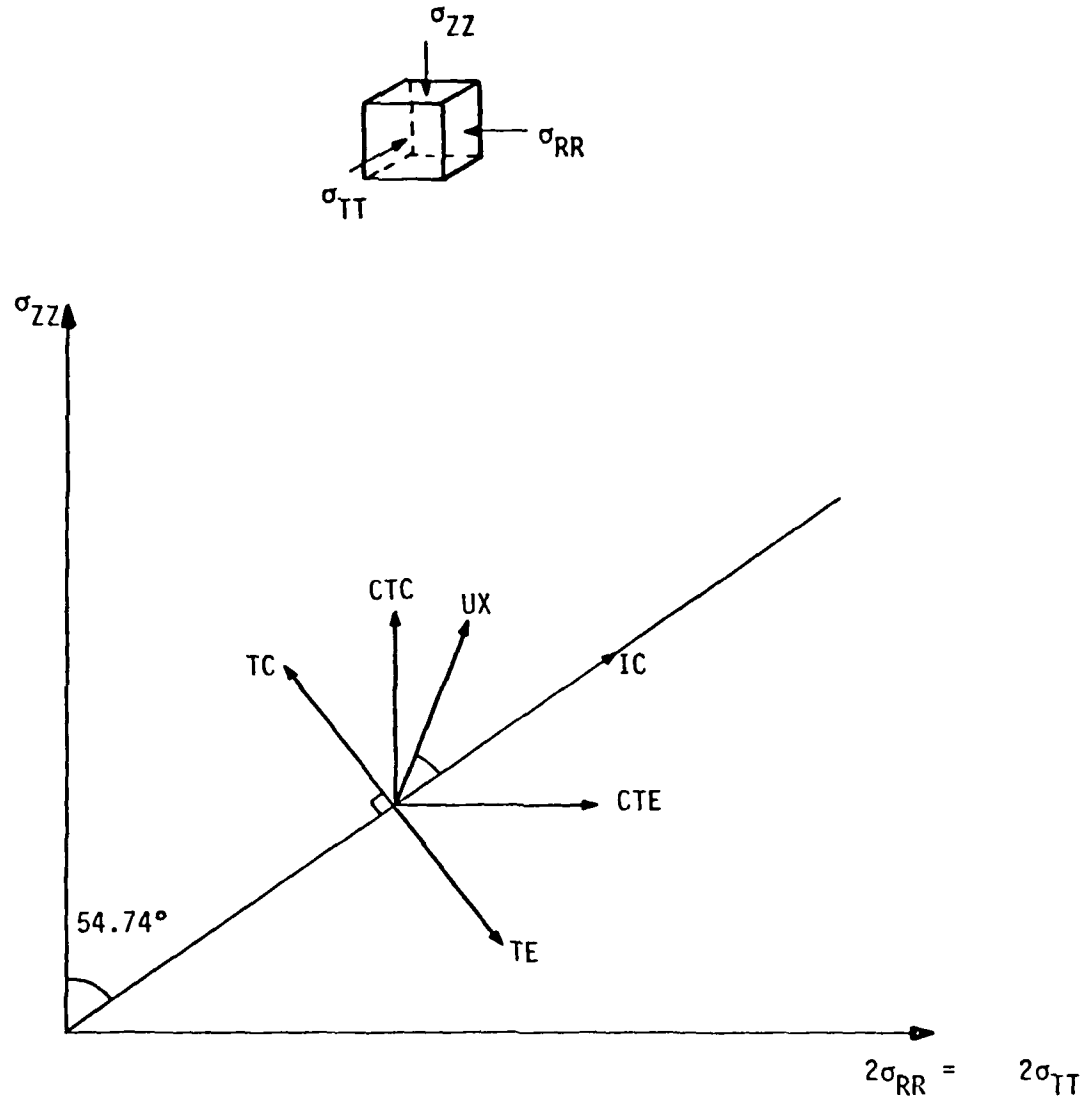

IC - isotropic consolidation $\sigma_{ZZ} = \sigma_{RR} = \sigma_{TT}$

CTC - conventional triaxial compression $\sigma_{RR} = \sigma_{TT}$ = constant

CTE - conventional triaxial extension σ_{ZZ} = constant
$\sigma_{RR} = \sigma_{TT}$

TC - triaxial compression (constant mean stress test, pure shear $\sigma_{RR} = \sigma_{TT}$, $\frac{\sigma_{RR} + \sigma_{TT} + \sigma_{ZZ}}{3}$ = constant

TE - triaxial extension $\sigma_{RR} = \sigma_{TT}$, $\frac{\sigma_{RR} + \sigma_{TT} + \sigma_{ZZ}}{3}$ = constant

UX - uniaxial strain (α varies with Poisson's ratio)

Figure 3.6. Strain paths for some laboratory test configurations.

TABLE 3.1. MATERIAL MODEL PARAMETERS

Model	Symbol	Identifier	Units	Response Defined	Description
Elastic	K	BKL3	Stress	Volumetric	Bulk Modulus
	G	SHEAR3	Stress	Deviatoric	Shear Modulus
Elastic-Plastic	K	BKL	Stress	Volumetric	Bulk Modulus
	G	SHEAR	Stress	Deviatoric	Shear Modulus
	C_a	CA	Stress	Failure Surface	Shear Strength
	C_b	CB	$(\text{Stress})^{-1}$	Failure Surface	Failure Surface Curvature
	C_c	CC	Stress	Failure Surface	CA - CC = Cohesion Intercept
	T	TCUT1	Stress	Failure Surface	Tensile Pressure Cut-off
Pyke's 1-D Curve fit	K	BKL4	Stress	Volumetric	Bulk Modulus
	y	TAUY	Stress	Initial Loading Hyperbola	Shear Strength
	G_{MAX}	GMAX	Stress	Initial Loading Hyperbola	Initial (maximum) shear modulus

TABLE 3.1. (Continued)

Model	Symbol	Identifier	Units	Response Defined	Description
	ρ_z	RHOZ	Density	Elastic Behavior	Initial and Reference Density
	ν_L	POISL	---	Elastic Behavior (loading) (loading)	Loading Poisson's Ratio
	ν_V	POISL	---	Elastic Behavior (unloading)	Unloading Poisson's Ratio
	K_1	BKL1	Stress	Volumetric and Elastic Shear	Loading Bulk Modulus
	K_2	BKL2	Stress	Volumetric and Elastic Shear	Loading Bulk Modulus
	K_u	BKU	Stress	Volumetric and Elastic shear	Initial and Unloading Bulk Modulus
AFWL	K_z	BKZ	Stress	High Pressure Region (initial)	Initial Modulus for High Pressure
	K_m	BKM	Stress	High Pressure Region	Maximum Bulk Modulus
	P_1	P1	Stress	Volumetric	Pressure Limit for Seismic Region
	P_2	P2	Stress	Volumetric	Hydrostat Break Point
	P_3	P3	Stress	Volumetric	Hydrostat Break Point
	T	ST1	Stress	Failure Surface	Tensile Pressure Cutoff
	Y	Y1	Stress	Failure Surface	Cohesion
	S	S1	---	Failure Surface	Slope of Failure Surface
	VM	VM1	Stress	Failure Surface	Von Mises Limit

TABLE 3.1. (Continued)

Model	Symbol	Identifier	Units	Response Defined	Description
Cap	K_{is}	AKI	Stress	Drained Elastic Volumetric	Initial Elastic Bulk Modulus
	K_{1s}	AK1	Stress	Drained Elastic Volumetric	Curve Fit Parameter (K_{max})
	K_{2s}	AK2	$(Stress)^{-1}$	Drained Elastic Volumetric	Curve Fit Parameter (curvature)
	K_{im}	AKIM	Stress	Undrained Elastic Volumetric	Initial Bulk Modulus (undrained isotropic compression test)
	K_{1m}	AK1M	Stress	Undrained Elastic Volumetric	Curve Fit Parameter (K_{max})
	K_{2m}	AK2M	$(Stress)^{-1}$	Undrained Elastic Volumetric	Curve Fit Parameter (curvature)
	G_i	AGI	Stress	Elastic Shear	Initial Elastic Shear Modulus
	G_1	AG1	Stress	Elastic Shear	Curve Fitting Constant (curvature)
	G_2	AG2	$(Stress)^{-1}$	Elastic Shear	Curve Fitting Constant (G_{max})
	α	AM	---	Failure Surface	Linear Slope, "Frictional" Strength
	C_s	AC	Stress	Failure Surface	"Cohesive" Strength
	B	BB	$(Stress)^{-1}$	Failure Surface	Defines Amount of failure surface curvature

TABLE 3.1. (*Concluded*)

Model	Symbol	Identifier	Units	Response Defined	Description
Cap (cont.)	C	CCC	Stress	Failure Surface	von Mises Level = C_S + C
	R	ARI	---	Strain Hardening (CAP)	Ratio of Major to Minor Ellipse Axes
	D	AD	$(Stress)^{-1}$	Hardening Parameter	Controls Cap Position
	W	AW	---	Hardening Parameter	Controls Cap Position

ii) Additional Models. Install other constitutive models such as Lade's model, Duncan and Chang's hyperbolic model, Prevost's model, endochronic model.

iii) Time Dependence. Introduce rate effects into the SEM by associating a time increment with each strain increment. Having accomplished this, such models as viscoelasticity, viscoplasticity, and rate-type fluid may be studied.

iv) Stress Controlled Driving. This is important for simulating laboratory tests (which are usually stress controlled) and for reproducing arbitrary stress paths. Rather than mathematically inverting the models, it is anticipated that stress control will be accomplished by iterating until the desired stress state is satisfied for each increment.

v) Anisotropy. Modify the installed models to allow for anisotropic material response. Also allow for initial anisotropic (K_o) consolidation prior to triaxial shearing.

vi) Plot Enhancement. Increase the available catalog of plots as needed. Additional plots already planned are principle stress space plots, invariant plots, time domain plots, and model comparison (overlay) plots.

4.0 INSITU MATERIAL BEHAVIOR

4.1 Introduction

Any attempt to model insitu soil behavior based on laboratory test results encounters several difficulties. First, there are the problems involved with obtaining representative samples and minimizing sample disturbance. Secondly, the loading conditions of conventional lab tests limit the type and number of stress/strain paths to a relatively simple few. As a result, studying the response of soil under insitu conditions (either controlled test conditions or actual field conditions) is a necessity. This section deals with one type of dynamic insitu testing.

4.2 The Cylindrical In-Situ Test

The particular test which will be emphasized here is known as the Cylindrical In-Situ Test (CIST) (Ref. 5) and was developed by The Air Force Weapons Laboratory in the early 70's. A CIST involves the detonation of a PETN explosive in a vertical cylindrical borehole and the subsequent measurement of ground motions in the soil or rock around the cavity (fig. 4.1). CIST provides information on material response in a large strain regime and under rapid loading conditions. A large data base for many geologies and materials has been developed since the first CIST in 1971 (table 4.1).

Ideally, a CIST event produces axisymmetric motion about the centerline of the explosive cavity. In addition, it is assumed that simultaneous loading occurs along the entire cavity. In reality, conditions may be somewhat different, depending on the particular site conditions and care with which the test is performed. In an actual geology there may occur lens-like deposits, non-horizontal layers, material non-homogeneties, etc, all undetected by any subsurface investigation. Any of these will tend to produce non-axisymmetric motions, and this is occasionally observed where there have been redundant radial measurements.

An attractive feature of CIST geometry is that several soil layers having different properties can be simultaneously tested in what is

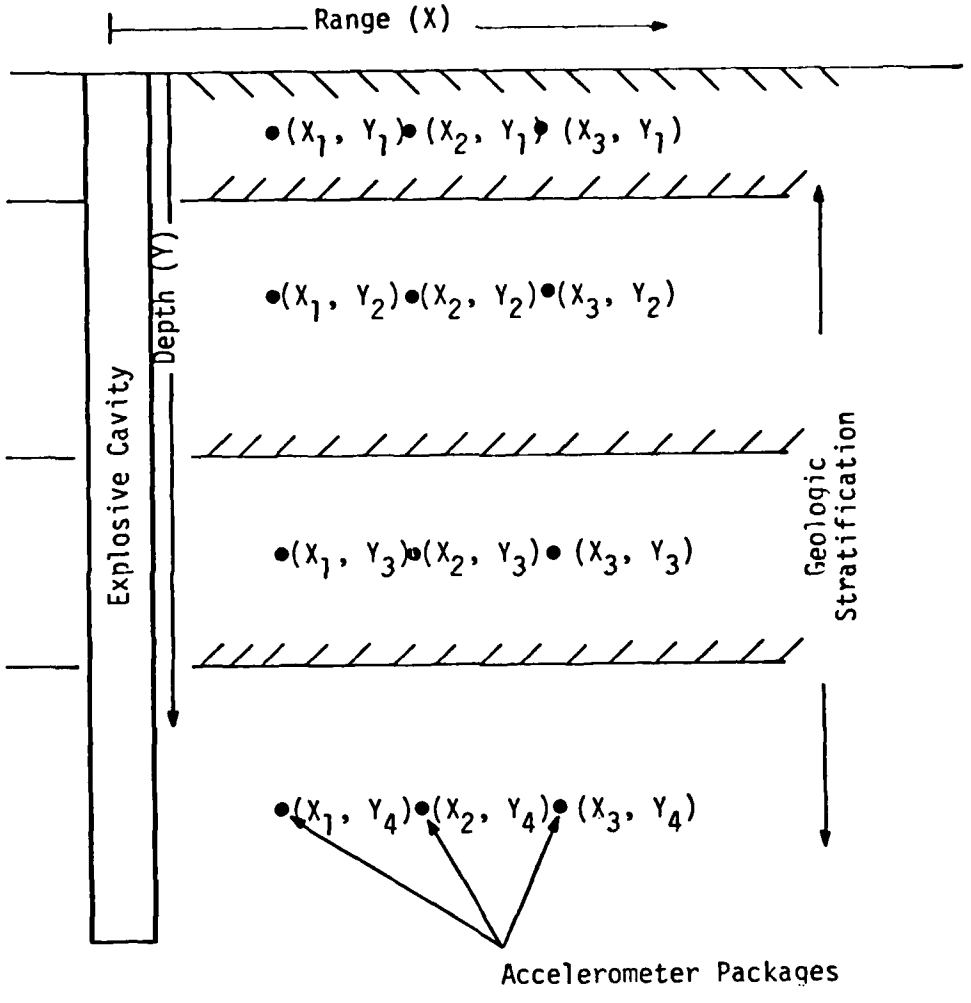

Figure 4.1. CIST cavity with geologic stratification. (From Ref. 6, p. 10)

TABLE 4.1. CIST EVENT SUMMARY

CIST No.	Location	Date	Geology	Associated Ground Motion Event(s)
1	MIDDLE GUST Wet Site, Colorado	16 Nov 71	Wet Clay-Shale	MG III
2	MIXED COMPANY Test Site, Colorado	28 Sep 72	Sandstone	MC I, II, III
3	MINUTEMAN Site D-1, Nebraska	02 Nov 72	Alluvium (dry)	HEST Test II
4	MIDDLE GUST Dry Site, Colorado	17 Jan 73	Dry Clay-Shale	MG IV
5	Nevada Test Site (Area 10)	22 May 73	Alluvium (dry)	JANGLE
6	Nevada Test Site (Area 6)	04 Jun 73	Playa	Pre-MINE THROW II
7	Nevada Test Site (Area 5)	23 Aug 73	Playa	SMALL BOY, PRISCILLA
8	MINUTEMAN Site P-1, Montana	30 Nov 73	Wet Clay-Shale	
9	MIDDLE GUST Wet Site, Colorado	07 Feb 74	Wet Clay-Shale	MG I, II, III
10	Aranit Island, Eniwetok Atoll	12 Jul 74	Coral Sand	PACE 1-KT
11	MINUTEMAN Site N-11, Missouri	22 Apr 74	Interbedded Limestone-Shale	
12	HARD PAN Test Site, Kansas	12 Jul 74	Interbedded Limestone-Shale	HARD PAN I
13	MINUTEMAN Site F-9, South Dakota	27 Sep 74	Wet Clay Shale	
14	MINUTEMAN Site M-28, North Dakota	18 Oct 74	Wet Clay	HEST TEST III

TABLE 4.1. (Concluded)

CIST No.	Location	Date	Geology	Associated Ground Motion Event(s)
15	Pre-DICE THROW Test Site, New Mexico	16 Jul 75	Wet Alluvium	Pre-DICE THROW I, II
16	Pre-DICE THROW Test Site, New Mexico	19 Feb 76	Wet Alluvium	Pre-DICE THROW I, II
17	Fort Wainwright, Alaska	07 Apr 76	Perma Frost (Loess)	
18	HAVE HOST Test Site, Arizona	22 Oct 76	Dry Alluvium	HAVE HOST
19	MISERS BLUFF Test Site, Arizona	03 May 77	Wet and Dry Sand	MB II
20	Ralston Valley, Nevada	26 Aug 77	Wet and Dry Rhyolite	
21	Hot Creek Canyon, Nevada	07 Sep 77	Silt and Tuff	
22	Ralston Valley, Nevada	13 Mar 79	Dry Sand	
23	Dry Lake Valley, Nevada	17 Sep 80	Dry Sand	

theoretically a "uniaxial"-like stress state at early times. If this assumption is true, models may be formulated by using one-dimensional wave propagation theory and iteratively matching calculational and experimental velocity waveforms. Usually, however, the motions are at least two-dimensional in nature especially at late times (and, unfortunately, sometimes three-dimensional). Two-dimensional motion results from waves eminating from the ends of the cavity and the ground surface (fig. 4.2), cratering effects, and from the effects of layering. For these reasons, a two-dimensional axisymmetric simulation tends to produce results more closely approximating the experimental results.

4.3 CIST Calculations - Description

There were several goals in performing these calculations:

a) To better define the ground motion experienced during a CIST explosion.

b) Study the effects of varying material model parameters on the calculated ground motion.

c) Arrive at insitu models by matching calculational and experimental results.

Two-dimensional CIST simulation is basically a dynamic axisymmetric boundary value problem. Constitutive relationships are chosen and material interfaces are specified. The calculation may be driven by several means. A pressure boundary may be specified along the cylindrical cavity which best represents measured experimental pressure time histories. Unfortunately, few reliable sets of cavity pressure measurements have been made for a CIST. (This is primarily because the harsh cavity environment has usually destroyed one or more components of the measurement system.) Measured horizontal velocity time histories at the 3 ft. range gages have been used to drive some one-dimensional calculations (e.g., Ref. 6). This method avoids the uncertainty surrounding cavity pressures. The method used in this study was to model the gases in the cavity using a simple γ-Law gas relation:

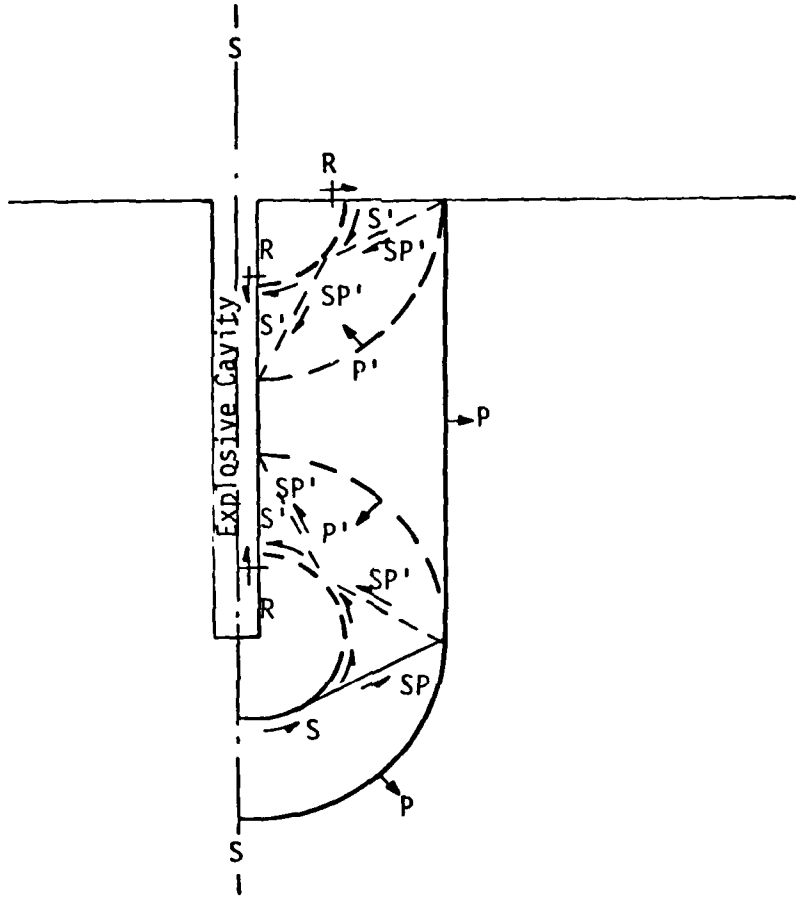

KEY:

Prime indicate relief waves.

——— Loading Wave
– – – Relief Wave
P Compression Waves
S Shear Waves
SP *von Schmidt-Like* Waves
R Rayliegh Waves

Figure 4.2. Major wavefronts from a cylindrical explosion in an elastic medium.

$$P = (\gamma - 1)\ \rho\ e$$

where P = Pressure

ρ = Density

e = Energy

γ = Coefficient

An initial energy, e_0 is introduced at the beginning of the calculation sufficient to provide the desired peak pressure. From experience (Ref. 7) the best representation of CIST waveforms has been:

$$P_{max} = 40.0 \text{ MPa}$$
$$\rho_{mixture} = 0.00225 \text{ g/cc}$$
$$\gamma = 1.25$$

The decaying pressure in the cavity produces calculated ground motion which seems to be qualitatively appropriate.

AFTON, a two-dimensional finite difference code (Ref. 8), was used to perform the calculations. Actually, a specialized version, known as CISTAFTON, which was developed at the Air Force Weapons Laboratory circa 1972, was used. AFTON, in addition to being axsymmetric as required by CIST geometry, has the feature of allowing arbitrary (generalized) grid motion (as opposed to strictly Lagrangian or Eulerian). During a CIST event, a crater develops directly adjacent to the cavity at the ground surface. If grid motion is restricted to purely Lagrangian, the grid stretches out in a narrow zone in the cratering region and causes the necessity for a very small calculational timestep. If done properly, arbitrary grid motion can circumvent this problem .

The AFWL Engineering Model was used in these calculations. The AFWL model was developed for this kind of study in an effort to make parameter variation and selection somewhat simplified. (This is why the hydrostat and failure surface have been linearized.) The model and its parameters, as they appear in CISTAFTON, are shown and defined, in fig. 4.3 and Table 4.2, respectively. (This version of the model varies somewhat from the version which appears in the SEM.) Note that the model contains an energy dependence which is not usually exercised during a CIST calculation.

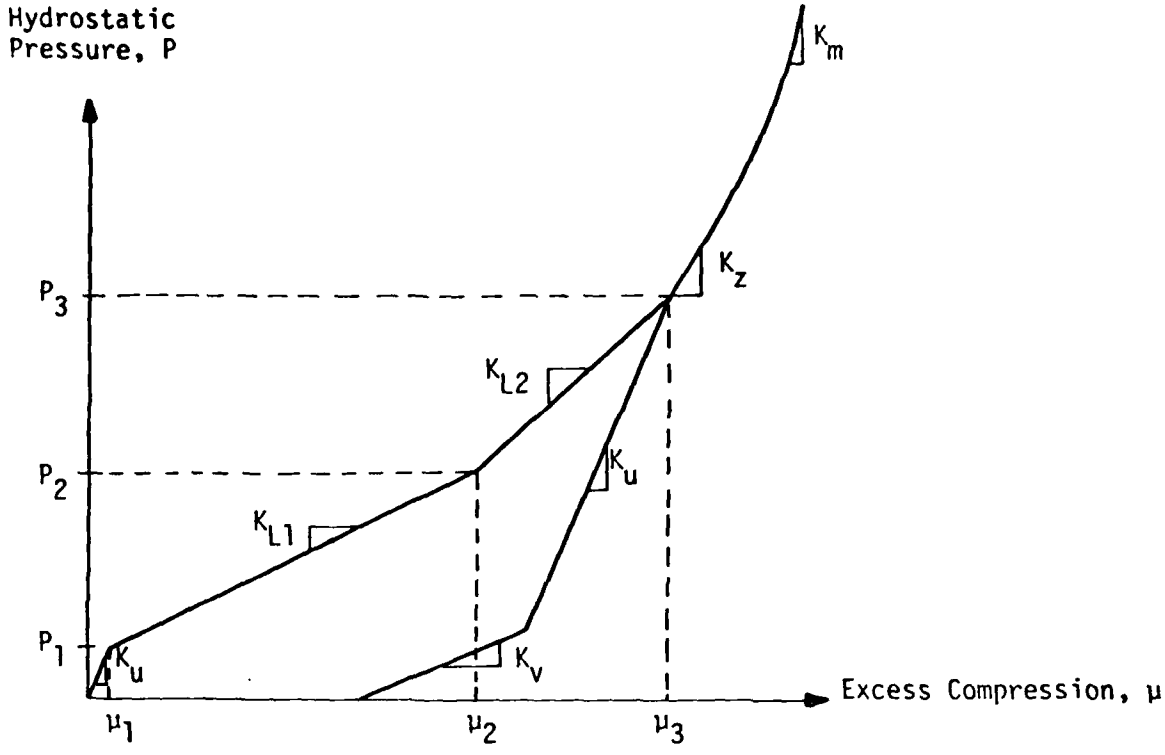

a) Hydrostat

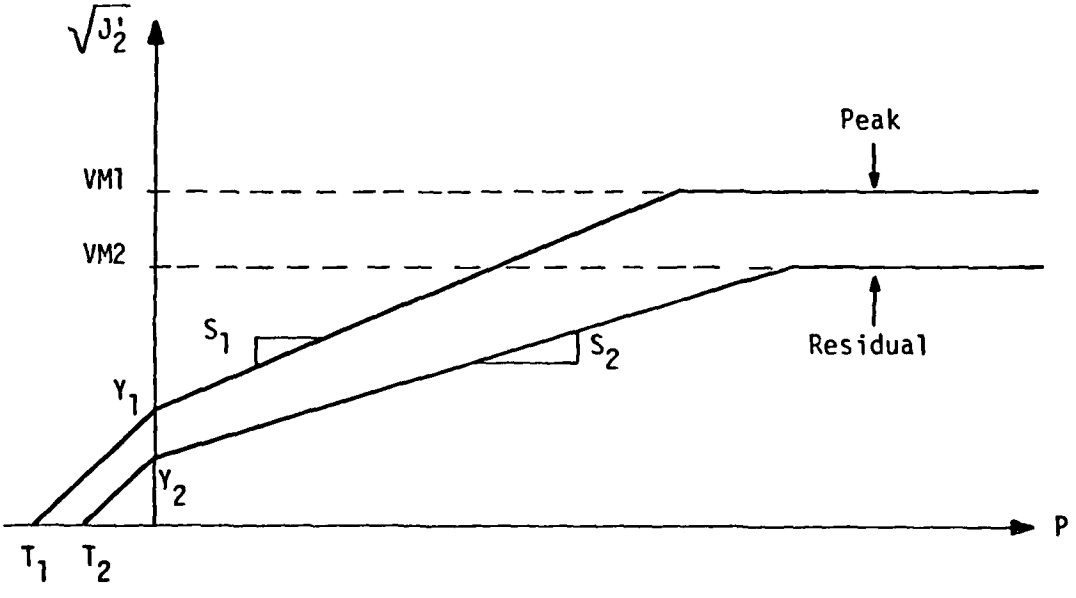

b) Failure Surface

Figure 4.3. CISTAFTON AFWL Engineering Material Model.

Variable	Symbol	Description	Units
RHOZ	= ρ_o	= initial material density	g/cc
POISL	= ν_L	= loading Poisson's ratio	----
POISU	= ν_U	= unloading Poisson's ratio	----
CL1	= C_{L1}	= constrained loading velocity	fps
CL2	= C_{L2}	= constrained loading velocity	fps
CU	= C_u	= seismic velocity, unloading	fps
CZ	= C_Z	= constrained loading velocity, corresponding to initial slope of high pressure/density portion of hydrostat	fps
CV	= C_V	= Constrained Velocity, corresponding to tail of unloading hydrostat	fps
P1	= P_1	= hydrostatic pressure at break between initial unloading and C_{L1} portion	psi
P2	= P_2	= hydrostatic pressure at break between C_{L1} and C_{L2}	psi
P3	= P_3	= hydrostatic pressure at initiation of high pressure/density portion	psi
AM3	= μ_3	= excess compression at P_3	----
ST1, 2	=T_1,T_2	= tensile strengths of peak and residual failure surfaces, respectively	psi
Y1, Y2	=Y_1,Y_2	= $\sqrt{J_2'}$ - axis intercepts of failure surfaces	psi
S1, S2	=S_1,S_2	= slopes of Drucker-Prager portion of failure surfaces	----
VM1, VM2		= peak and residual von Mises limits	psi
AMS	= μ_s	= material parameter, high energy/ density (HED)	----
BKM	= K_M	= material parameter (HED)	psi
TILA	= A	= material parameter (HED)	----
TILB	= B	= material parameter (HED)	----
TILE	= e_o	= initial internal specific energy	ergs/gm x 10^{12}
ES	= e_S	= material parameter, energy	ergs/gm x 10^{12}

TABLE 4.2. GUIDE TO CISTAFTON AFWL MATERIAL MODEL INPUT PARAMETERS

In an effort to evaluate the material sensitivities to the various model parameters, a few simplifications of the model were used for some of the calculations. These included purely elastic (with no shear failure) and hydrodynamic (elastic, with no shear strength). In addition, various combinations of elastic-plastic parameters were used.

Thirteen calculations have been performed to date. Emphasis was placed on CIST 9 and 10, which are wet clay and sand sites respectively, and CIST 23, a dry sand site. Two calculations were done for "CIST 00" a hypothetical CIST site. This generic site is used for studying model and geometry effects. Table 4.3 summarizes the calculations and should be used as a guide for the following discussions.

4.4 CIST Calculations - Results

4.4.1. Cavity Pressure

Figures 4.4 and 4.5 summarize the cavity pressure time histories which were generated for several of the AFTON calculations. It is seen that because the gases vent from the top of the cavity, the pressures decay much more rapidly in this region than in the middle or bottom regions of the cavity. Note that the pressure near the top decays to zero within about 6 ms.

At depth, decay of cavity pressure also depends significantly on the amount of cavity expansion. This is controlled by the amount of material deformation directly around the cavity. Both the hydrostat and failure surface influence deformations. By comparing the 8.5 m and 12.2 m depths of CIST calculations 00.1 and 00.2 (fig. 4.5) one can easily see that a stiff hydrostat causes the pressure to "hang up" much longer. The effect of shear failure can be seen by comparing cavity pressures for calculations 903 and 904. The hydrodynamic case (904) of no shear strength allows more deformation of the cavity (and therefore lower pressures) than the material with significant shear strength (903).

In general, a two term exponential of the form:

TABLE 4.3. SUMMARY OF CISTAFTON CALCULATIONS

CIST No. and Location	Material Models used for Calculation Set	Calc. No.	Description	Hydrostat Type	Failure Surface Type	Calculated out to ... (ms)
CIST 9 MIDDLE GUST Wet Site Colorado	1. (2) Partially Sat. Sandy Clay	901	Elastic	Elastic	No failure	9.6
	2. Wet Sandy Clay	902	Lab Models	Trilinear	D-P w/VM	7.9
	3. Stiff Clay	903	Elastic W/lab failure surf.	Elastic	D-P w/VM	8.0
	4. Frac. Clay Shale	904	Hydrodynamic	Elastic	Zero Strength	8.0
	5. Clay Shale					
CIST 10 Eniwetok Atoll, South Pacific	1. (2) Sat. Coral Sand Sand and Gravel	1001	Calc. and Lab	Bilinear	D-P w/VM	8.2
	2. Sat. Coral-Algal Grainstone	1002	Modification	Bilinear	D-P w/VM	8.1
		1003	Modification	Bilinear	D-P w/VM	13.9

(Continued next page)

TABLE 4.3. (Concluded)

CIST No. and Location	Material Models used for Calculation Set	Calc. No.	Description	Hydrostat Type	Failure Surface Type	Calculated out to ... (ms)
CIST 23 Dry Lake Valley, Nevada	1. (6) Dry Silty Sand with fine gravel	2302	Lab Models	Trilinear	D-P	15.1
		2303	Rerun for C.P.	Trilinear	D-P	3.1
		2304	1-D Models	Trilinear	D-P	15.1
CIST 00 Generic	1. Elastic = 305 m/s C_L	2305	Modification	Trilinear	D-P	14.7
		00.1	Elastic	Elastic	No failure	10.2
	2. Elastic 1067 m/s C_L	00.2	2-Layer Elastic	Elastic	No failure	14.0

Note: D-P = Drucker-Prager
D-P w/VM = Drucker-Prager with Von Mises Cut-off

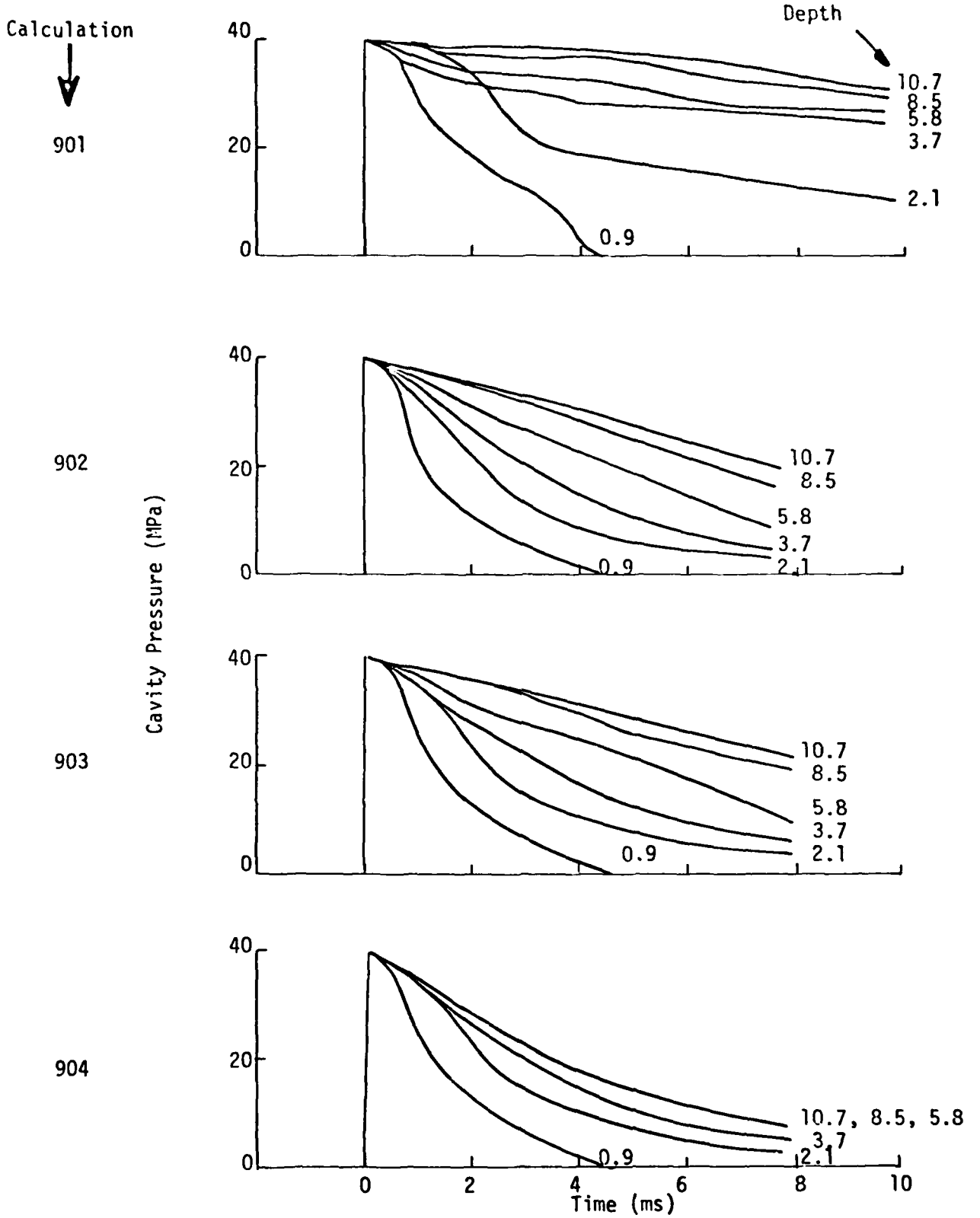

Figure 4.4. Cavity pressure time-histories for CIST 9.

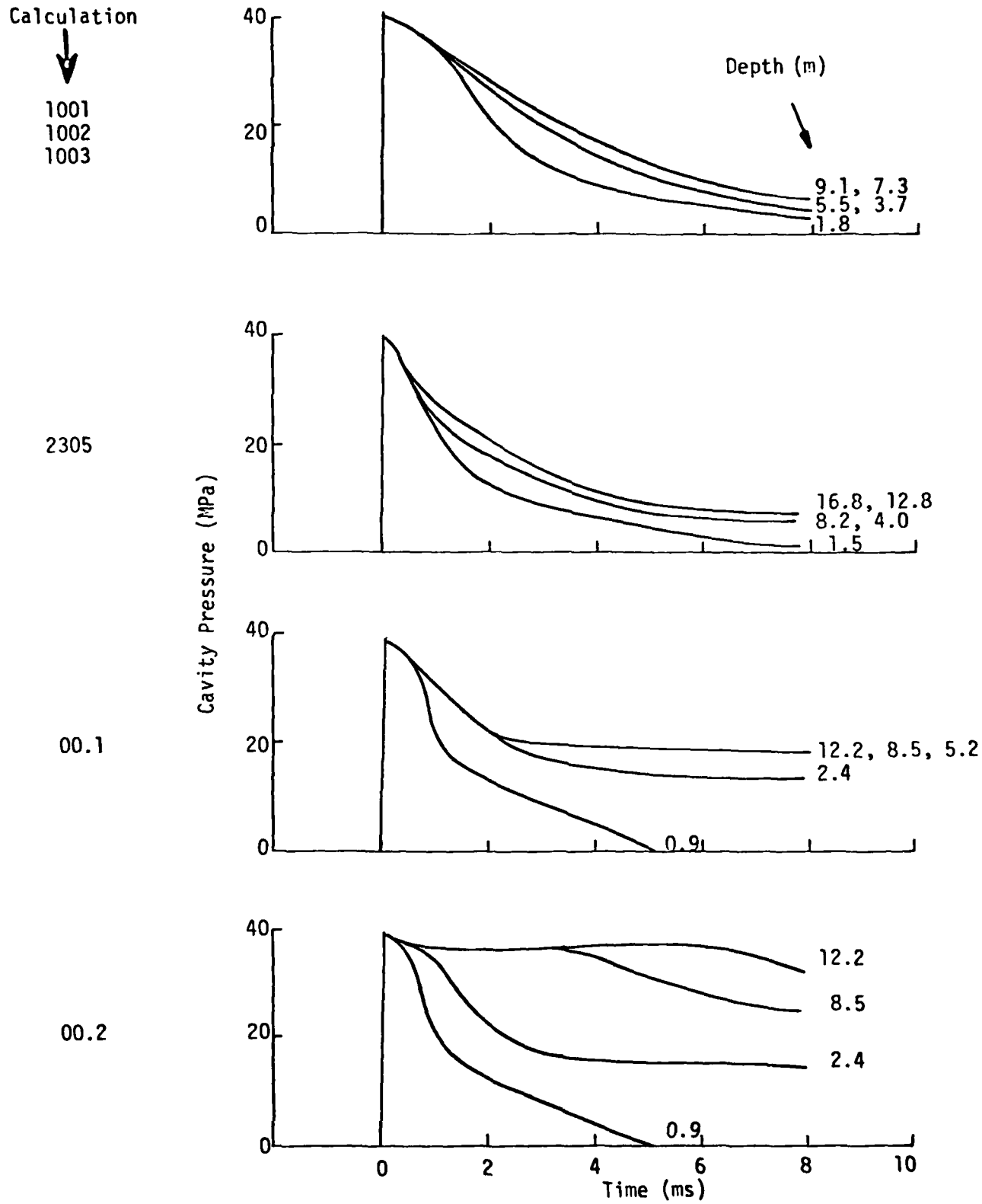

Figure 4.5. Cavity pressure time-histories for CIST 10, CIST 23, and CIST 00.

$$P(t) = C_1 e^{-C_2(t)} + C_3 e^{-C_4(t)} \quad (4.1)$$

where C_1, C_2, C_3 and C_4 are constants, determined to fit the calculated waveform, is adequate for mathematically describing these pressure-time histories. These fits could then be used as approximate driving pressure boundaries for one-dimensional calculations. The pressures generated here are also important if one wishes to compare experimental data with calculated cavity environments in order to check validity. Unfortunately, this is an area still open to question due to lack of high confidence cavity pressure measurements.

4.4.2. Generic CIST

The hypothetical site conditions for CIST 00 calculations 00.1 and 00.2 are shown in figure 4.6. The first calculation was for a uniformly elastic site and the second was for a two-layer elastic site, with soft material overlaying stiff material.

Figure 4.7 illustrates the basic response differences for the fast and slow materials. The stiff material transmits the stress pulse at a much higher frequency and at a somewhat higher level, but sustains much less material deformation.

Velocities for the two cases are compared in figures 4.8 thru 4.11. The frequency difference is again readily apparent. Decay of velocity and stress is compared in figures 4.12 and 4.13. According to Reinhart, (Ref. 9), the theoretical decrease in stress with range for a cavity of infinite extent would be:

$$\sigma_H = (a/r)^{1/2} P_{max} \quad (4.2)$$

where a = Cavity Radius
r = Radius
P_{max} = Peak Cavity Pressure

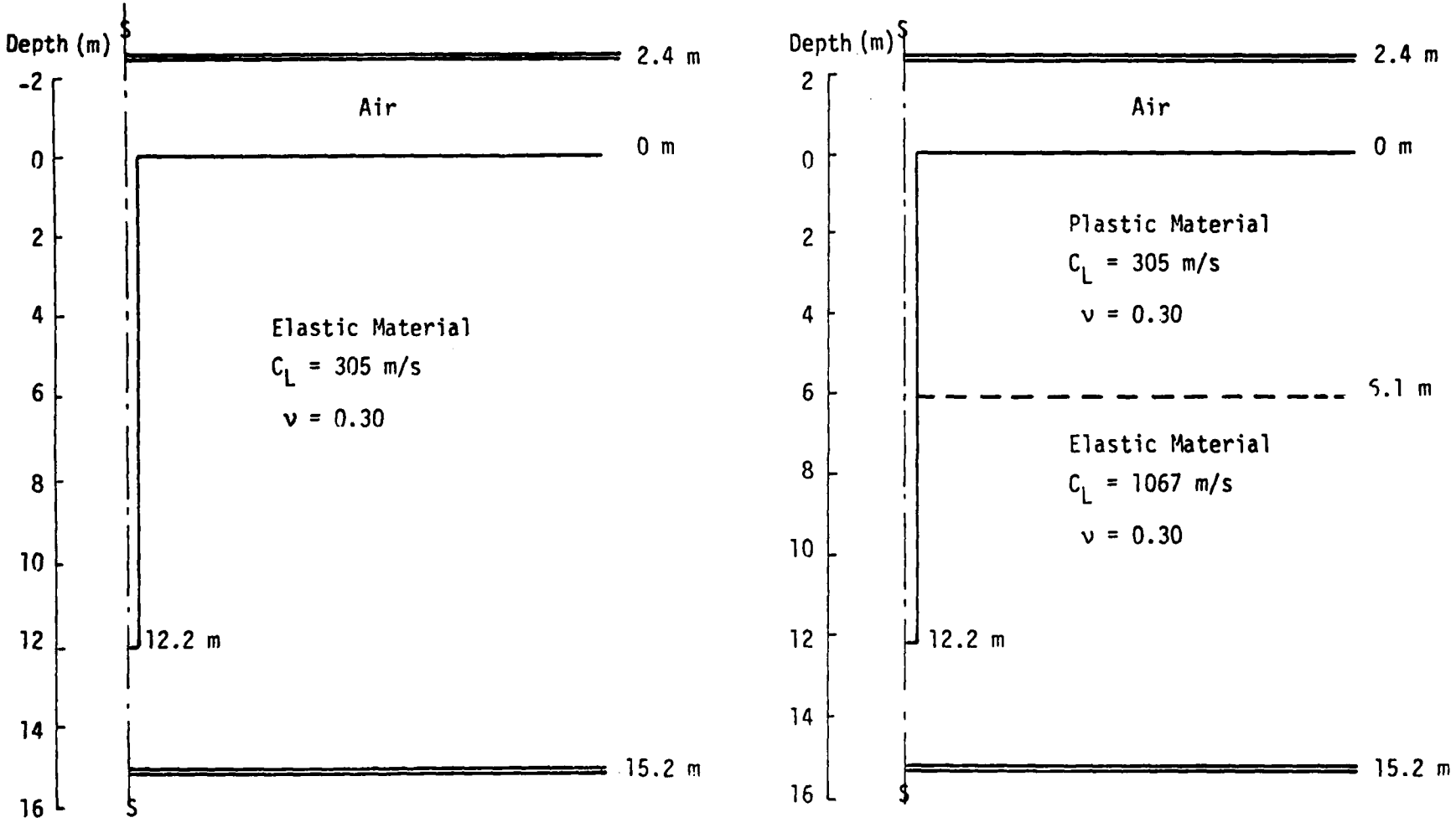

Figure 4.6. Generic CIST calculational profiles (CIST 00).

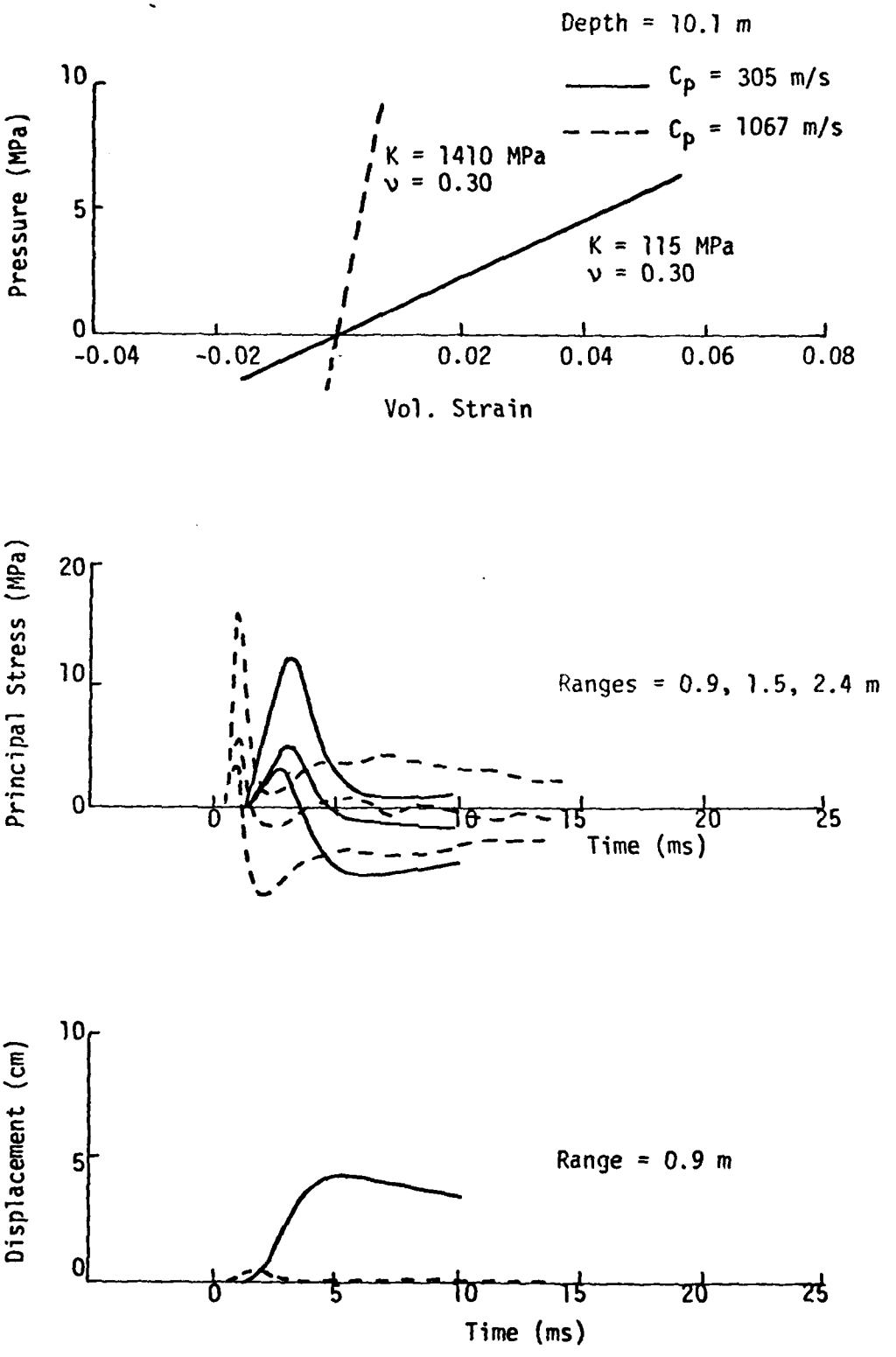

Figure 4.7. Response comparison of elastic materials having different P-wave velocities.

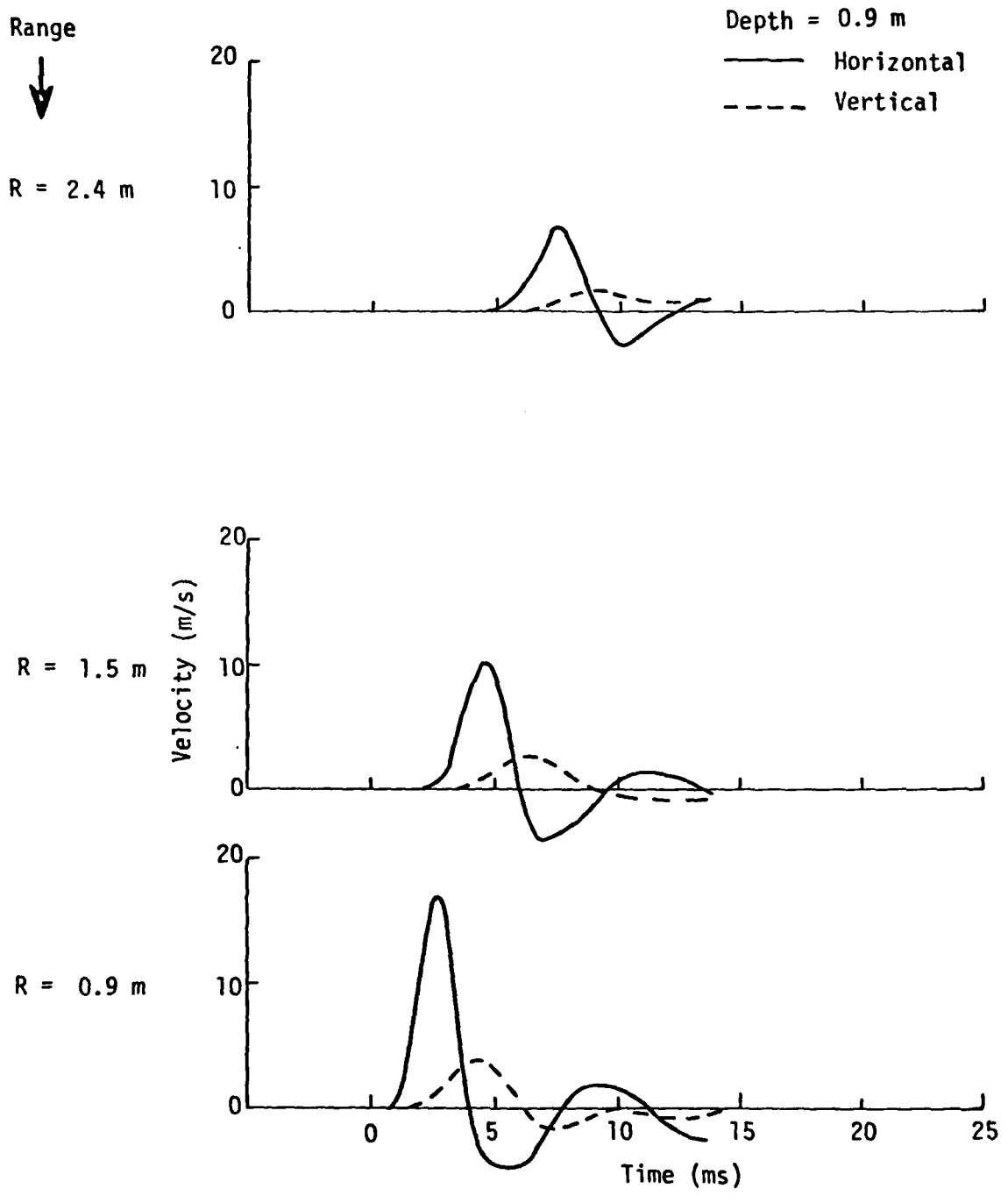

Figure 4.8. Velocity time histories for elastic (00.1) and 2-layer elastic (00.2) calculations at depth = 0.9 m.

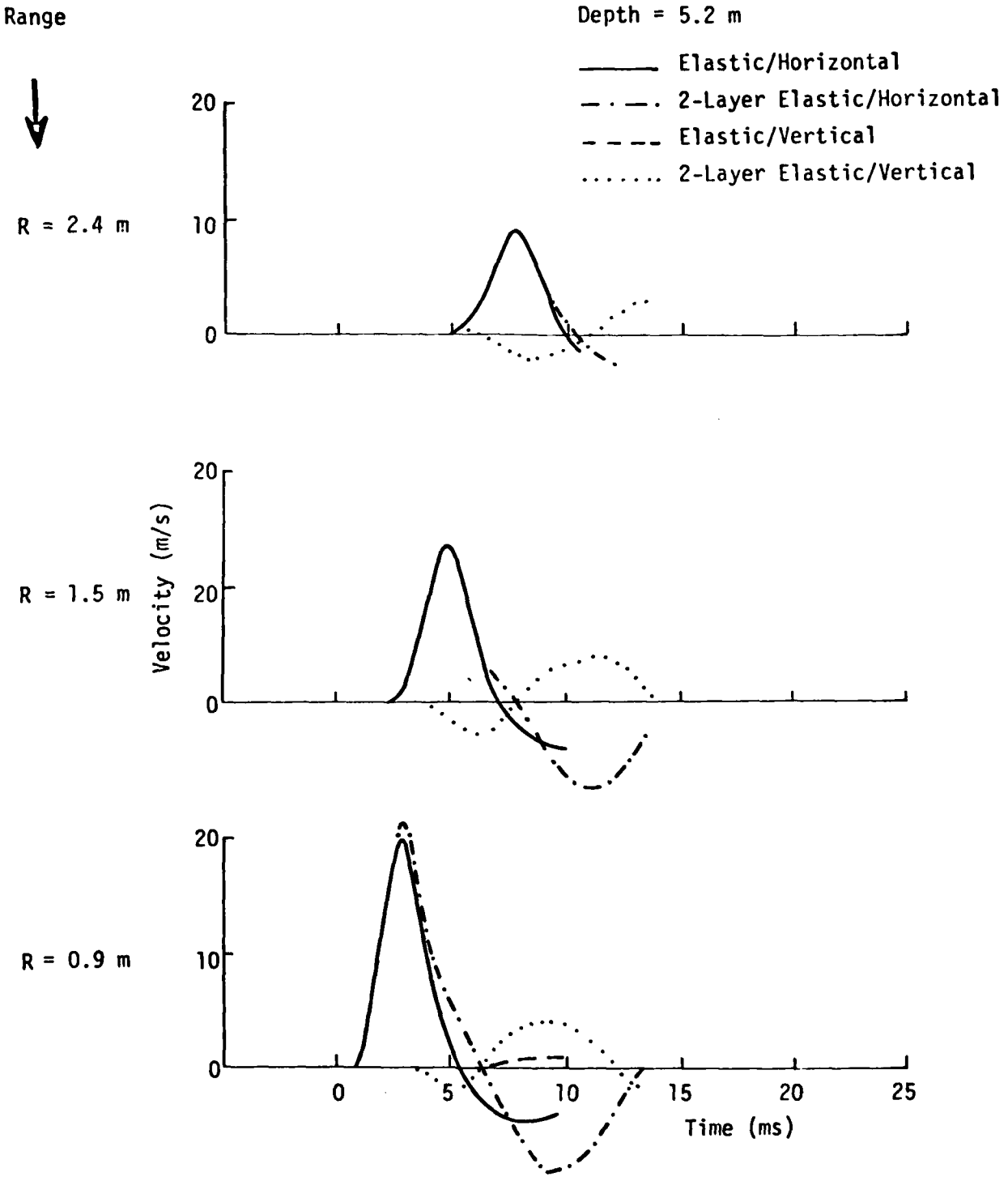

Figure 4.9. Velocity time histories for elastic (00.1) and 2-layer elastic (00.2) calculations at depth = 5.2 m.

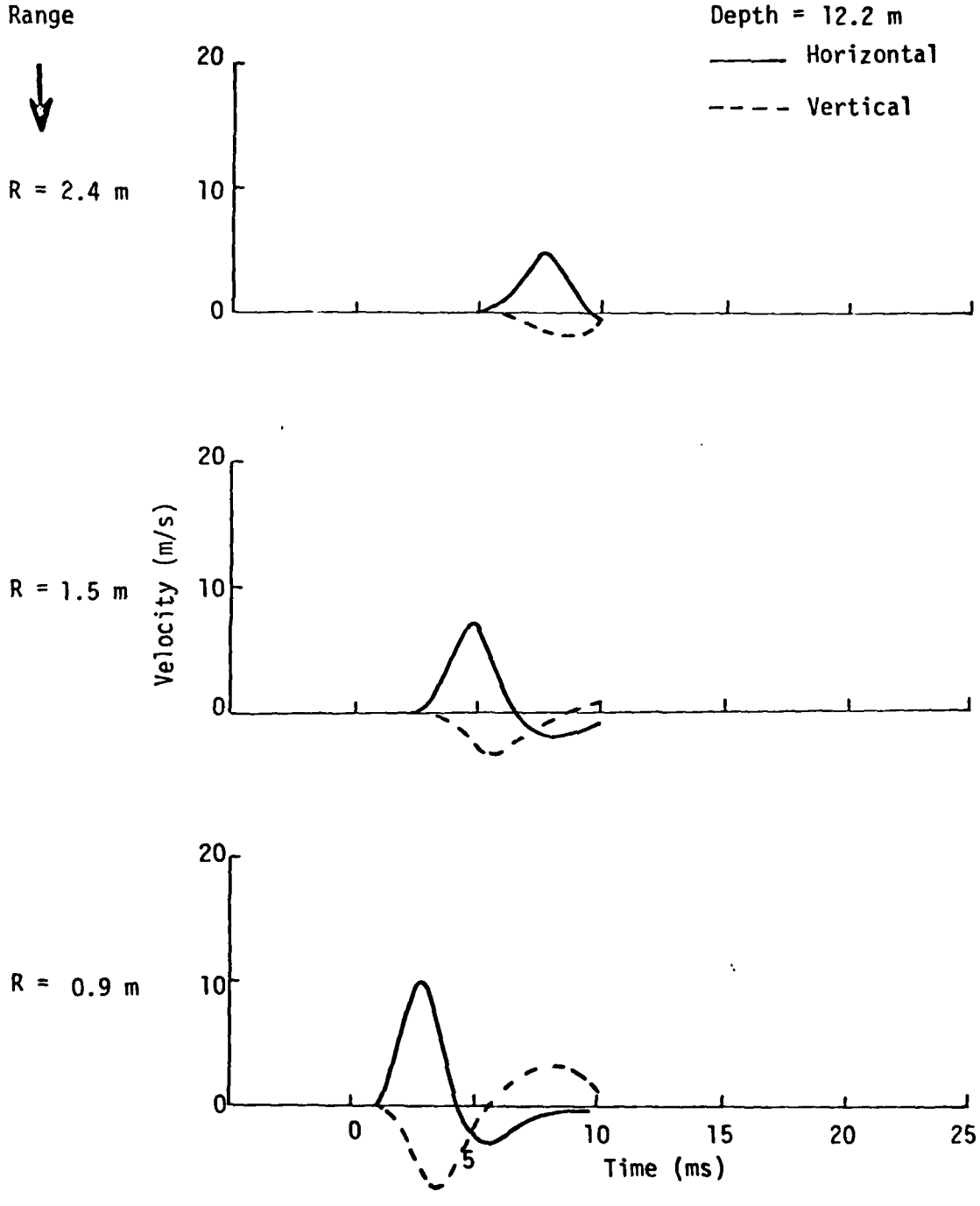

Figure 4.10. Velocity time histories for elastic (00.1) calculation at depth = 12.2 m.

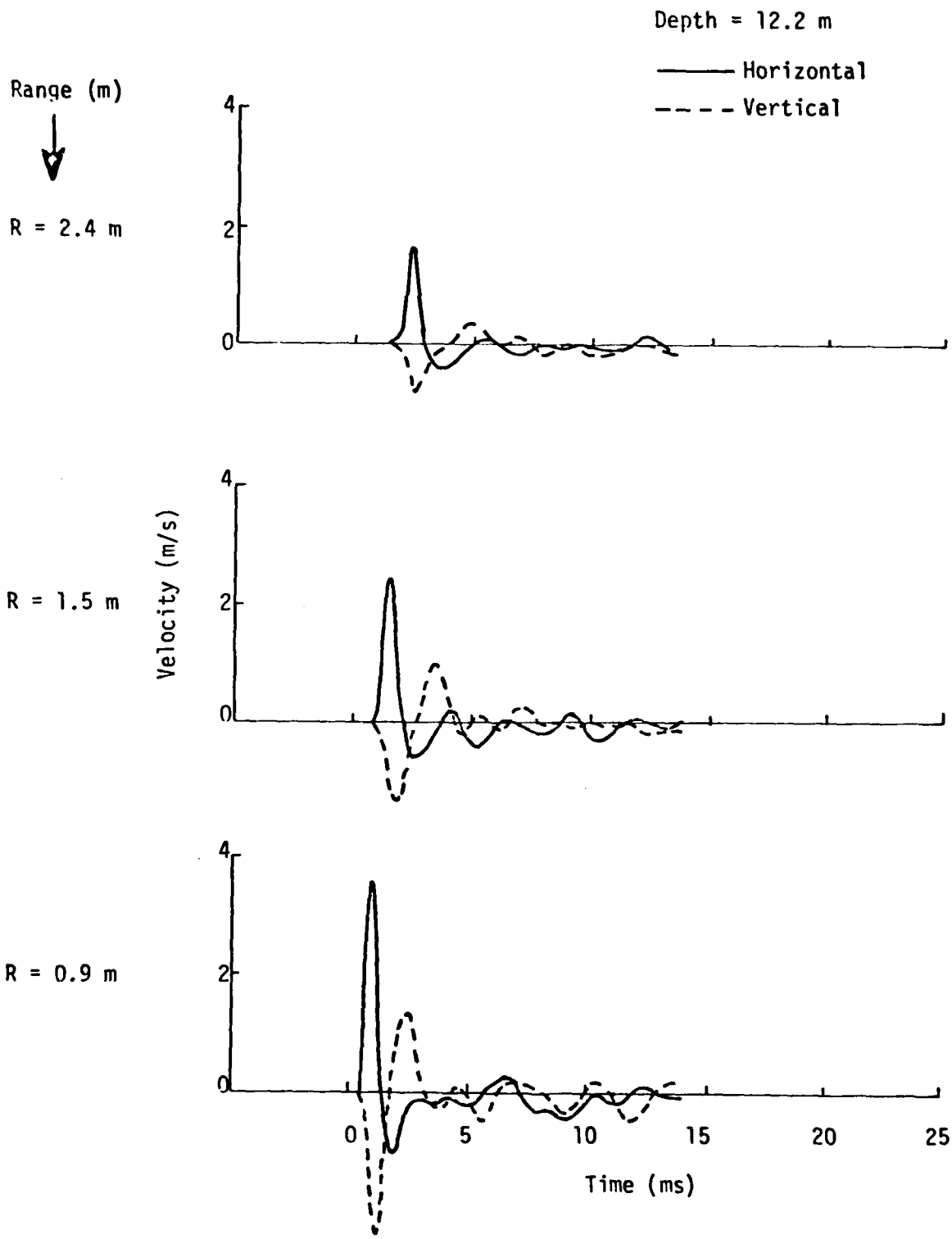

Figure 4.11. Velocity time histories for 2-layer elastic (00.2) calculation at depth = 12.2 m.

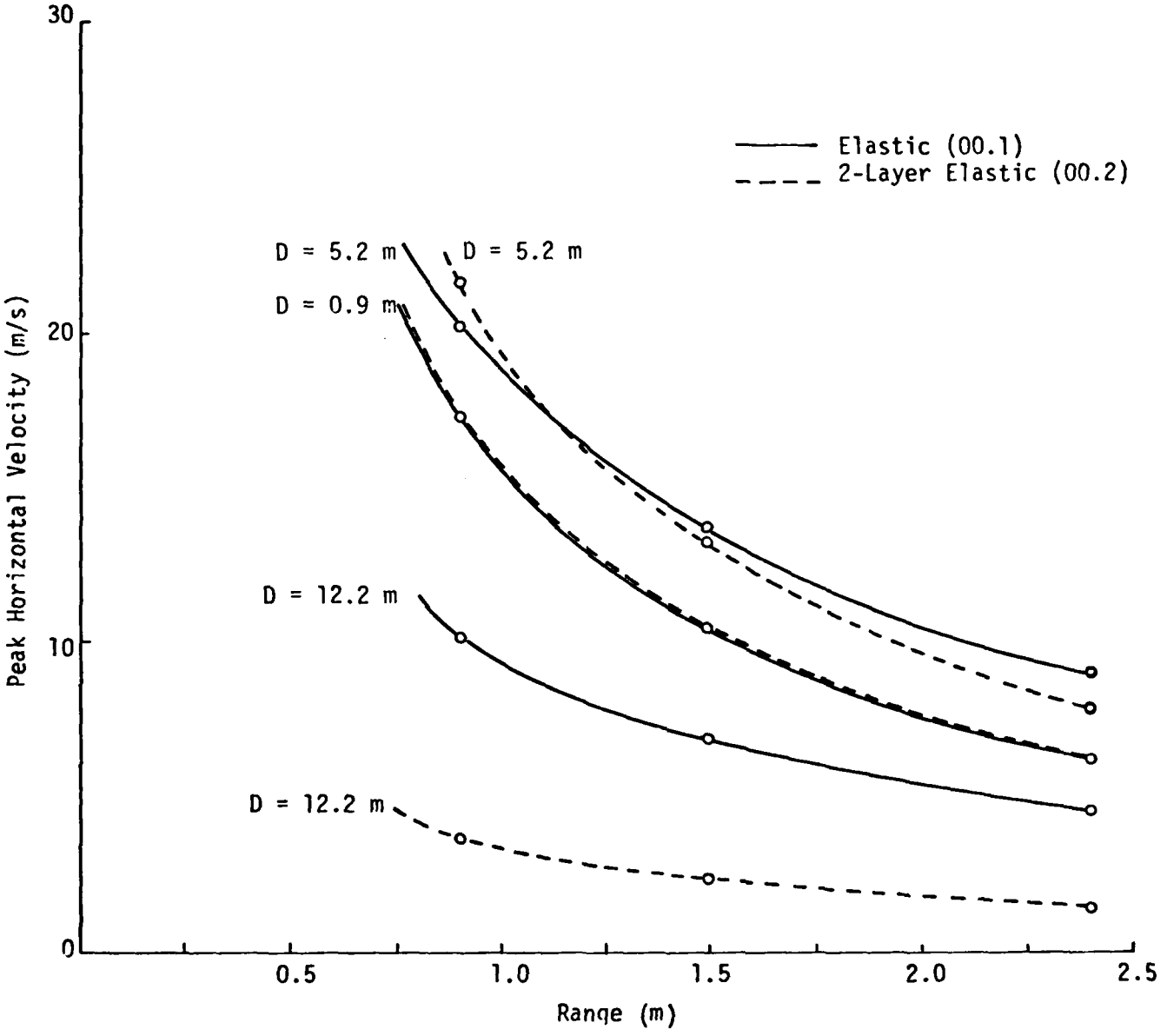

Figure 4.12. Variation of peak horizontal velocity with range for CIST 00 calculations.

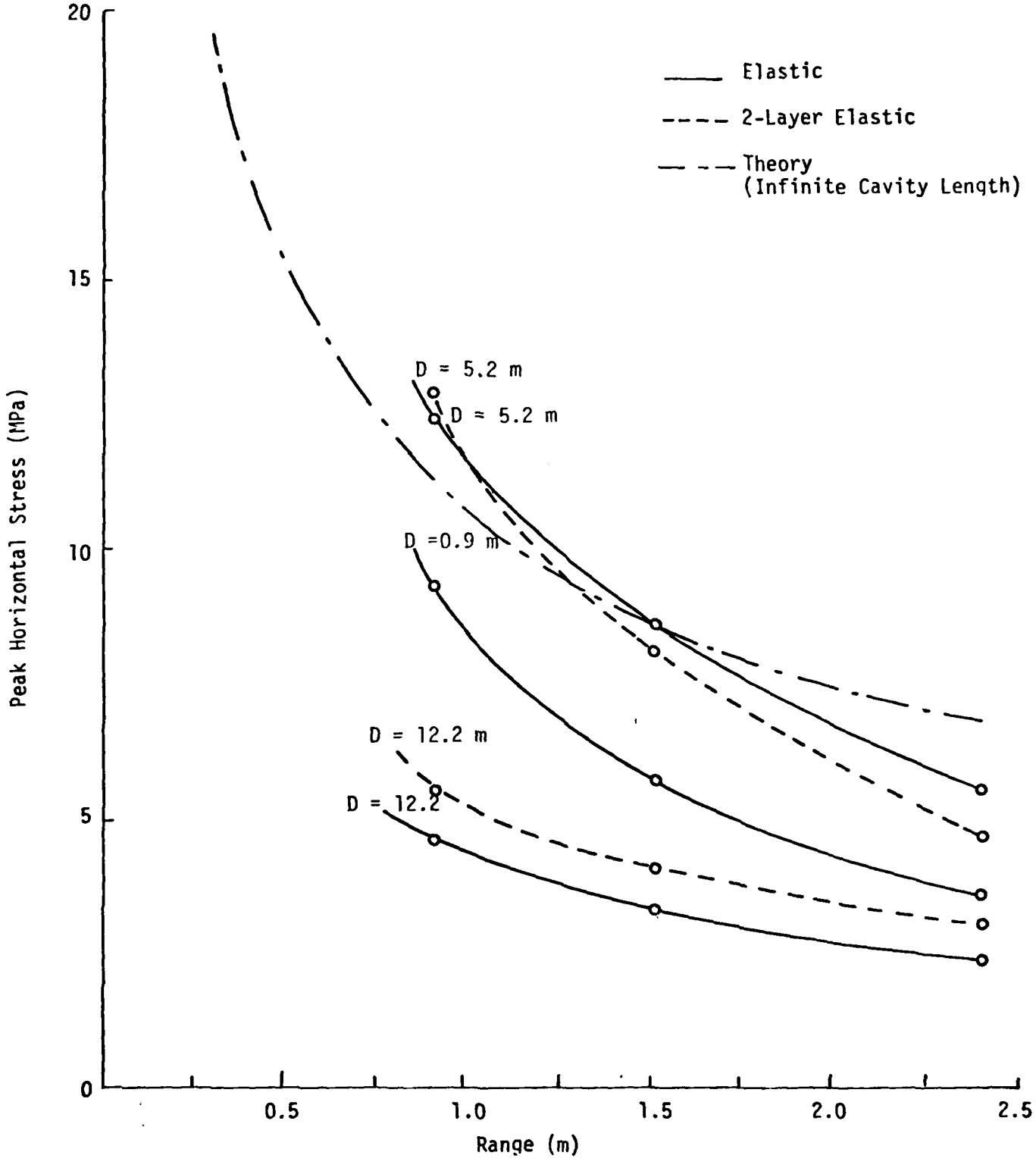

Figure 4.13. Variation of peak horizontal stress with range for CIST 00 calculations.

This is also plotted in figure 4.13. The differences observed between theory and calculation are accounted to the finite length of cavity (two dimensional effects) in a CIST experiment. This is illustrated by the fact that the theory agrees best with the calculation of the stresses at the mid height of the cavity.

The finite two-dimensional nature of the CIST geometry can be summarized by looking at the stress-strain behavior (fig. 4.14). Note the vertical strains near the top and bottom of the cavity due to relief effects. The cylindrical effects are shown in the tangential stress-strain response. In general, the stress state becomes very complex after passage of the initial wavefronts.

End effects and layering of materials with different wave propagation properties will also affect site response. The increased vertical motion near the interface of calculation 00.2 is an example of this (fig. 4.9). Velocity vector plots (figs. 4.15 and 4.16) can sometimes illustrate these effects. In figure 4.15, for example, one can easily see the shear wave propagating from the bottom of the cavity at later times. In figure 4.16, one can pick out waves propagating both due to end effects and layering effects. The shear wave coming off the bottom of the cavity (see 4.2 ms VV plot) can also be picked of the shear stress/strain plots or the principal stress/strain angle rotation plot. Anticipated arrival at a 5 ft. radius from the cavity bottom is calculated as follows:

$$C_S = C_p \frac{1 - 2\nu}{2(1 - \nu)}$$

$$C_S = (1070 \text{ m/s}) (0.53)$$

$$C_S = 567 \text{ (m/s)} \qquad (4.3)$$

Figure 4.17 points out the passage of this shear wave as seen in the time histories.

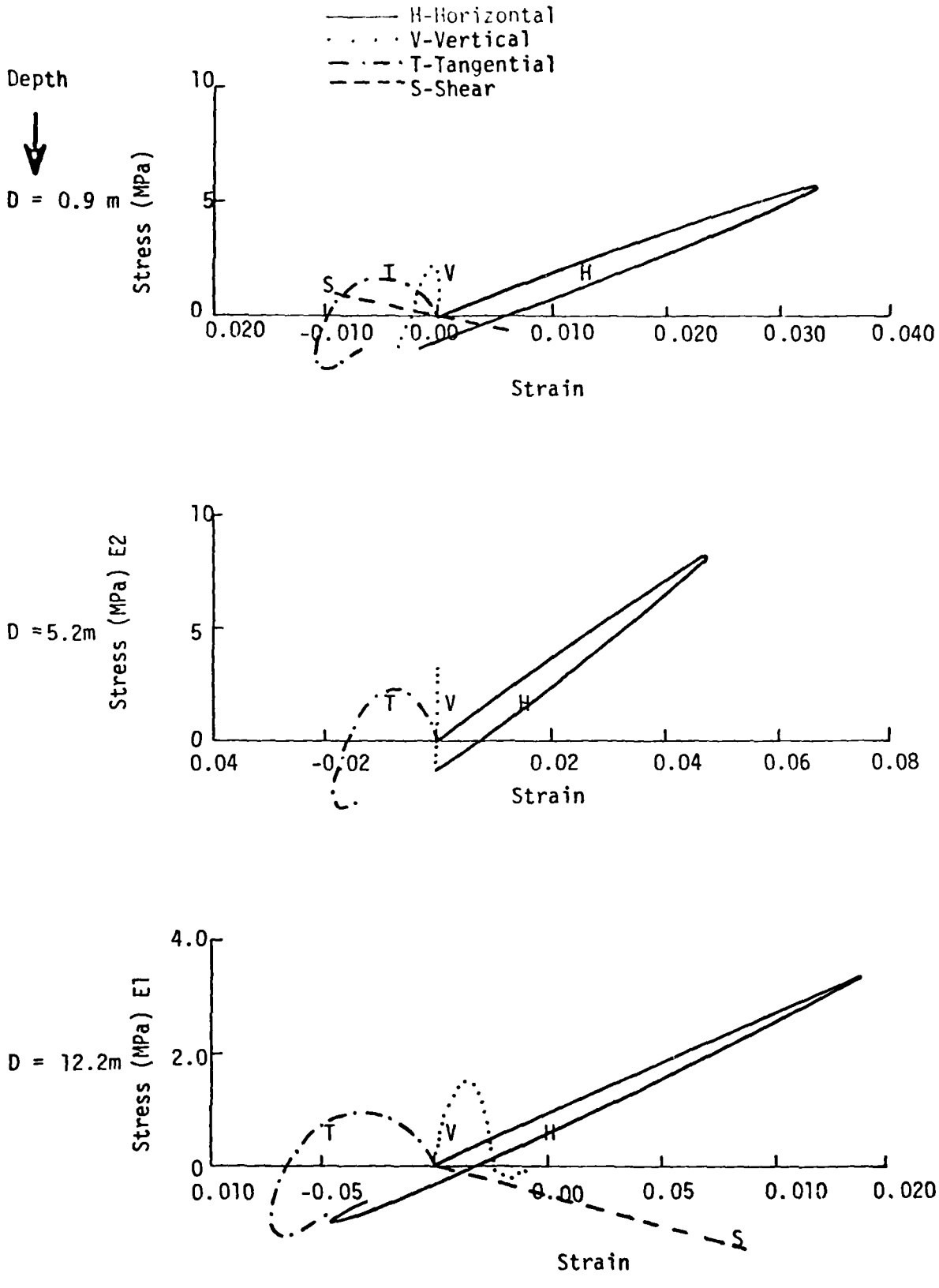

Figure 4.14. Stress-strain behavior for elastic case at range = 1.5 m.

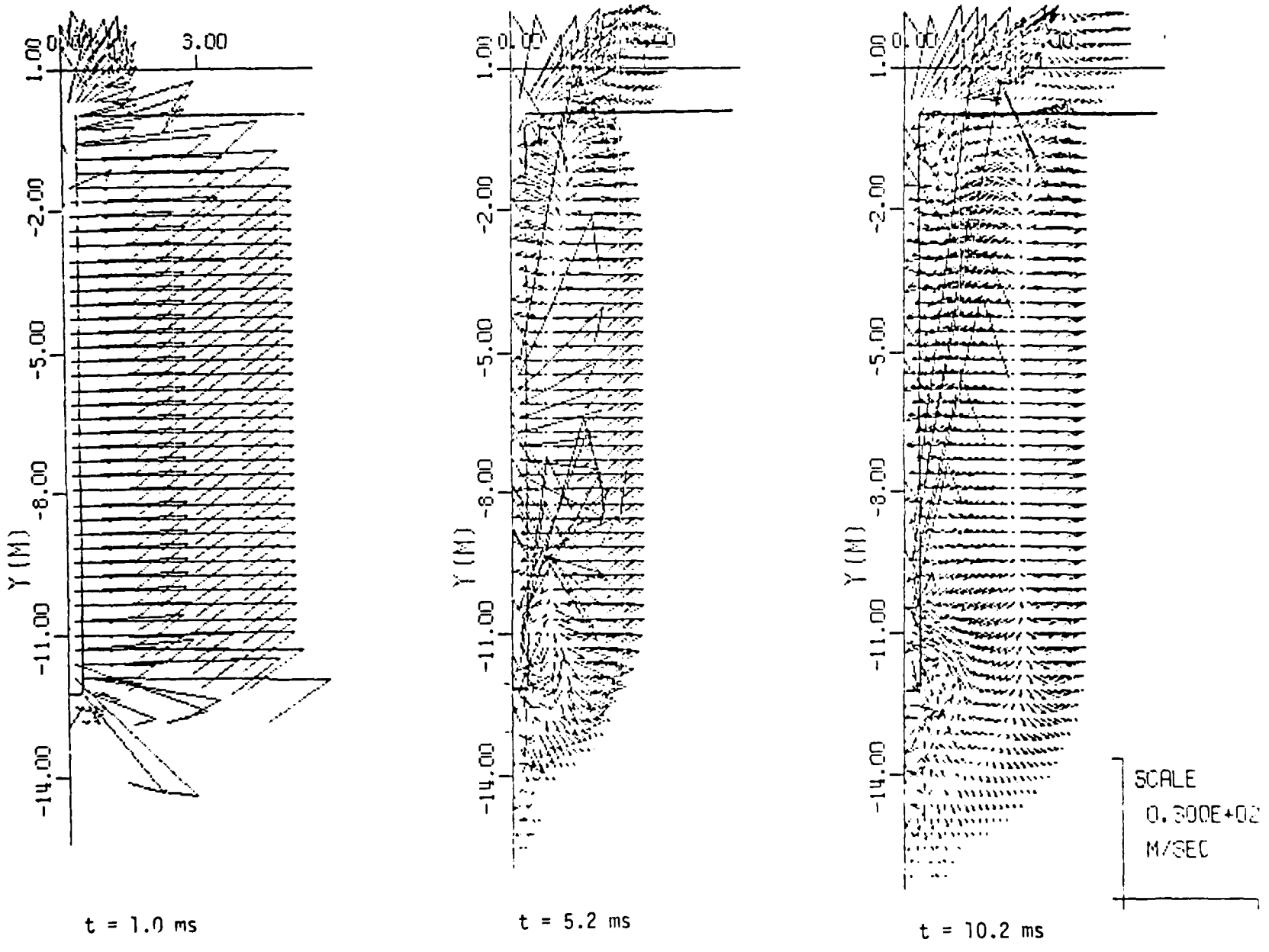

Figure 4.15. Velocity vector snapshots for an elastic CIST.

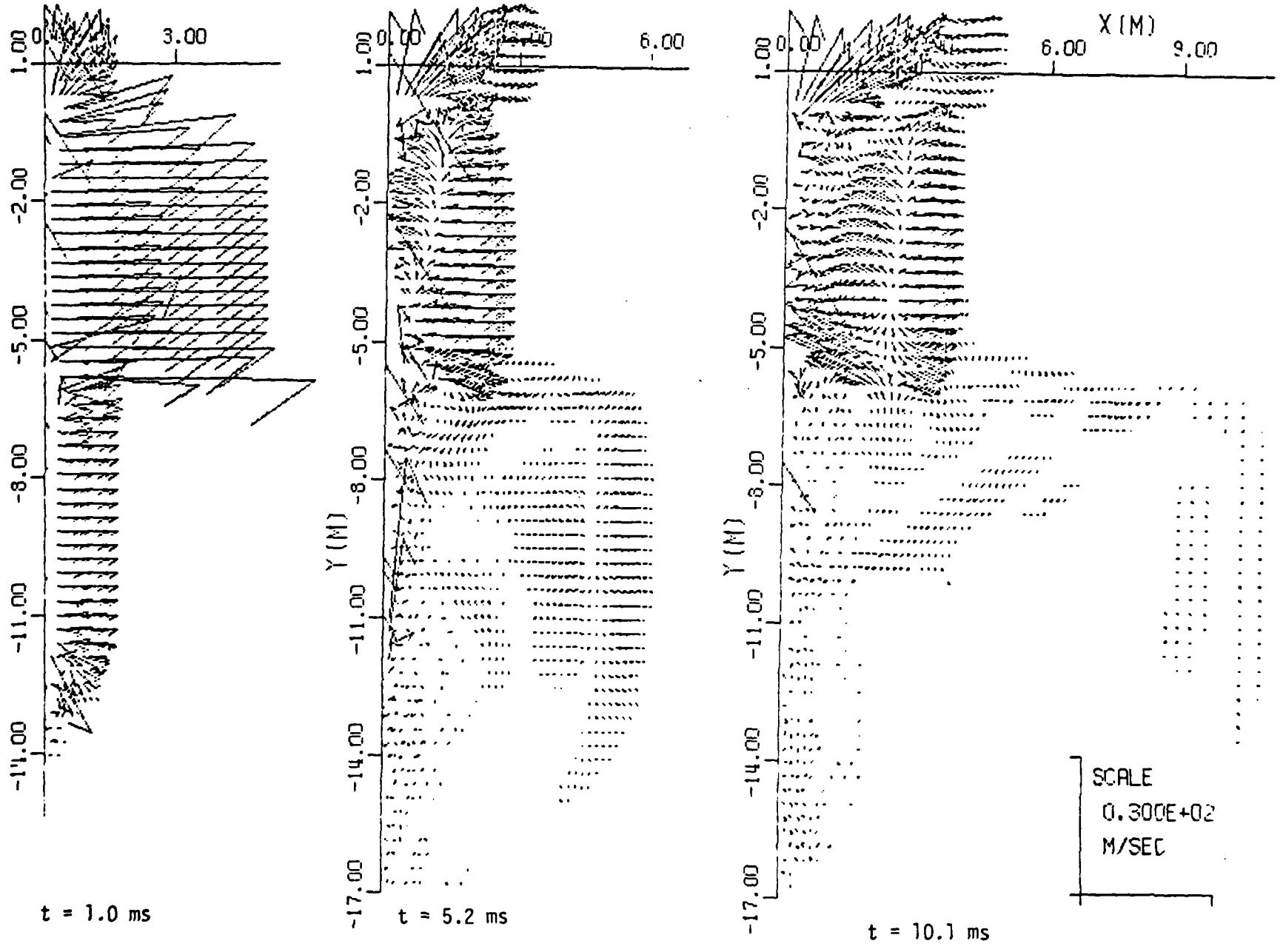

Figure 4.16. Velocity vector snapshots for 2-layer elastic CIST.

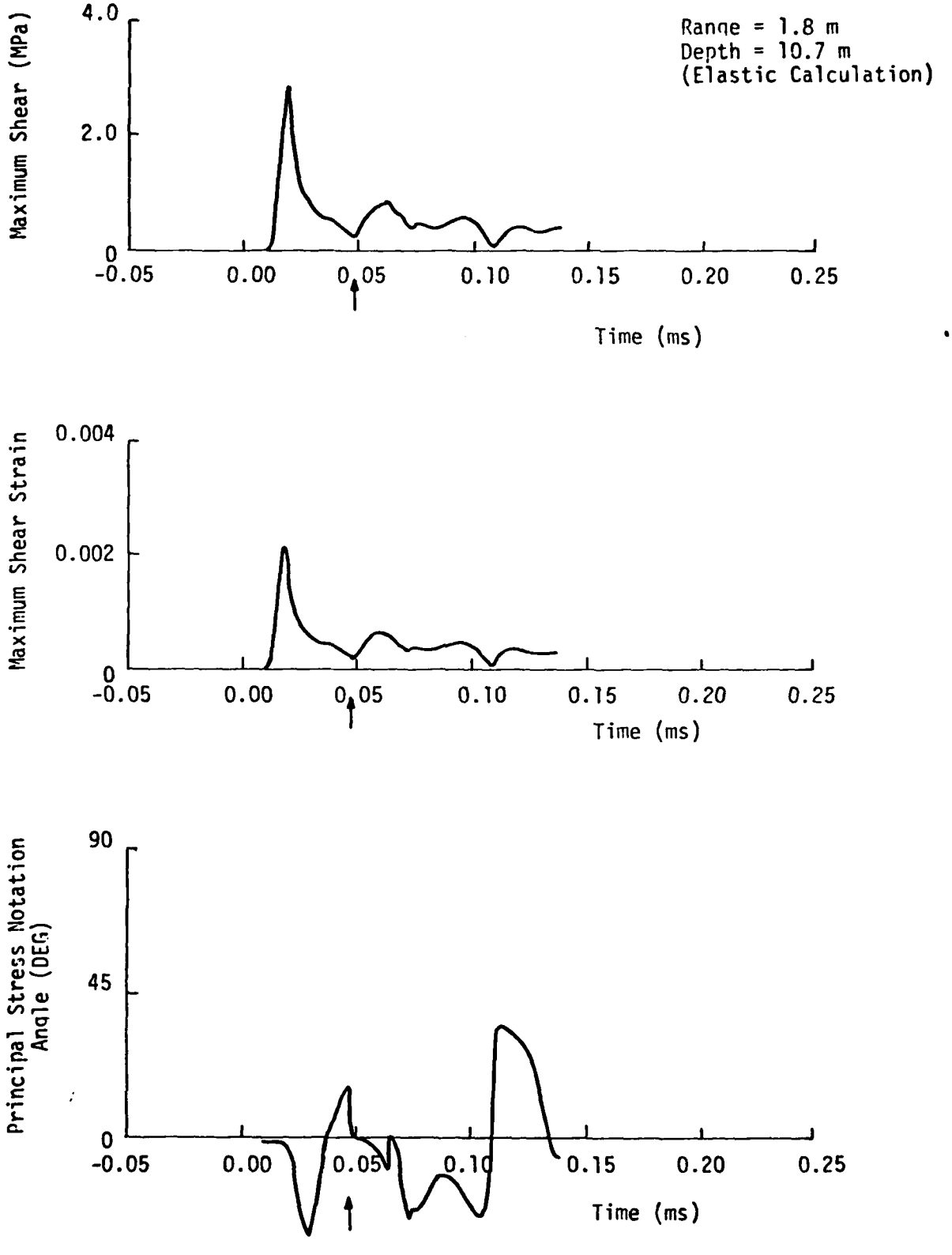

Figure 4.17. Shear wave propagation.

4.4.3 AFWL Model Variation

A series of calculations for CIST 9 was performed in which the material model type was varied to study the effect on resulting ground motion. Figure 4.18 gives site geology and layering for these calculations.

Four cases were run. Case 901 was an elastic calculation, with wavespeeds determined from CIST 9 arrival times as shown in figure 4.19. Case 902 used models based on laboratory data, as determined by WES (Ref. 10). Case 903 was elastic, as in 901, but used the lab failure surfaces as used in 902. Case 904 was elastic with no shear strength and is called the "hydrodynamic" case. The material models for the four calculations are shown in figures 4.20 and 4.21.

The results of the model study are summarized in figures 4.22 and 4.23. The elastic case (901) shows a peak velocity with rebound and a subsequent negative phase of velocity. At the other extreme, the hydrodynamic material (904) flows outward due to lack of shear strength. (Figures 4.24 and 4.25 show the resulting large deformations for this case. Note the significant upward velocity component in the upper soil layers.) For case 903, the upper layers do not have appreciable strength to behave significantly different from the hydrodynamic material. At the 5.8 m depth, however, shear strength is high enough to bring the velocity waveform down quite a bit, and limit continuing outward flow.

As is expected, based on the hydrostats the lab models yield considerably slower propagation velocities for the soil layers. Also because of the softer nature of the hydrostat, the particle velocities are much higher. The material does not have much shear strength and tends to maintain outward velocity after failure. Notice that at the shallow depth the lab models are in close agreement with the hydrodynamic model but at the deeper depth they are more like the elastic-plastic models. By comparing results of type with data for the events, general conlcusions can be made with regard to the controlling portion of the material model.

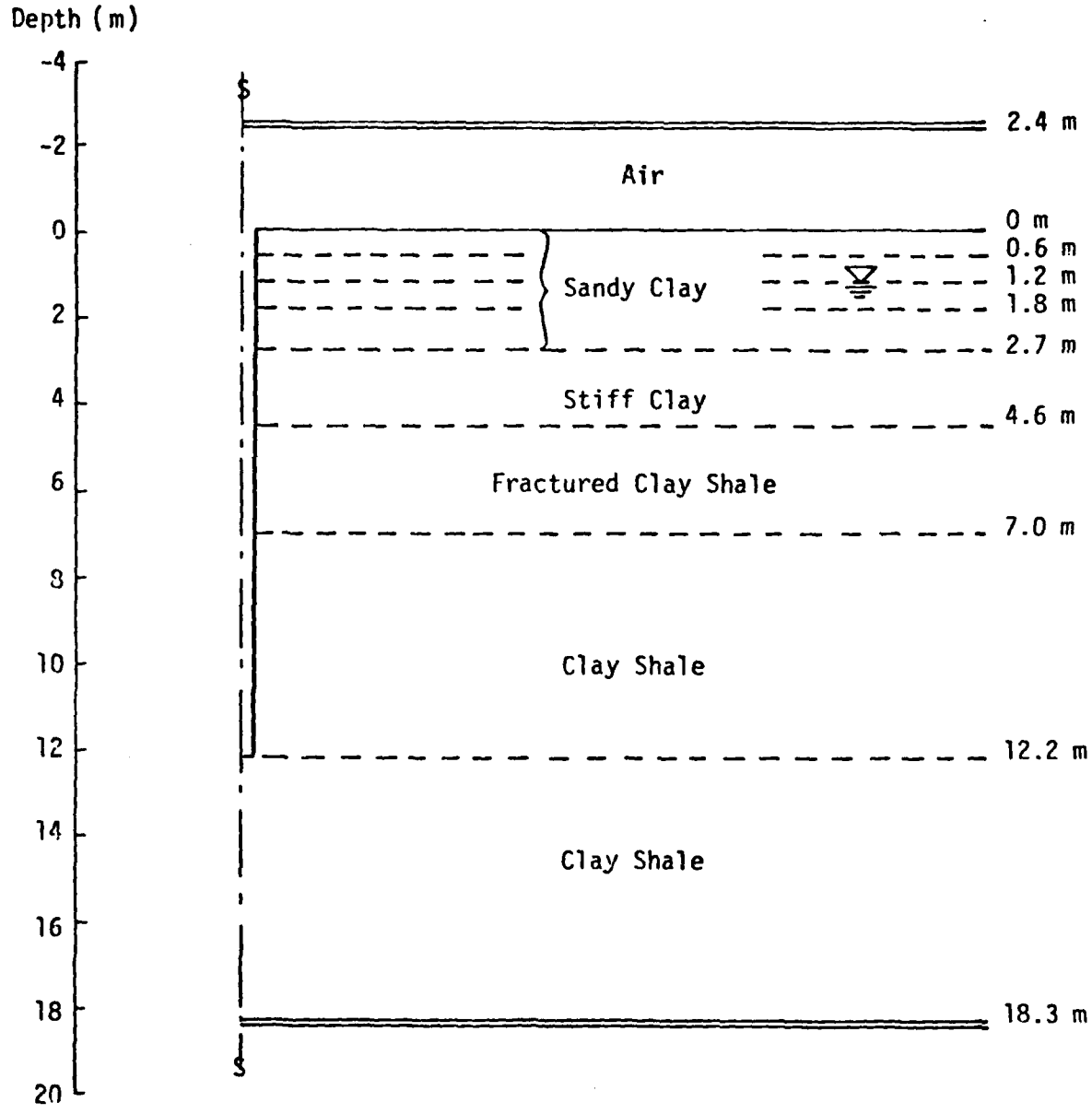

Figure 4.18. CIST 9 geology and calculational layering.

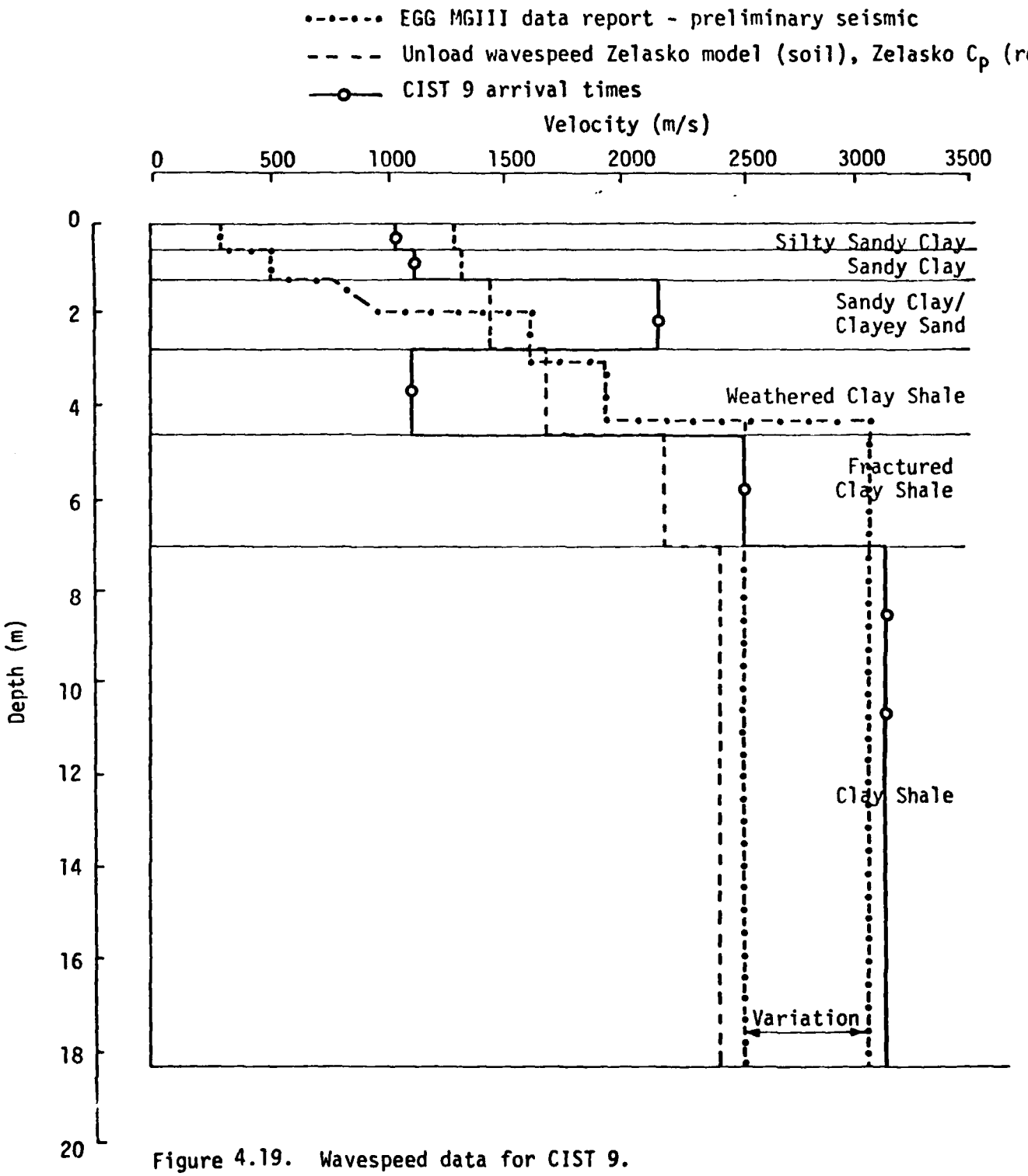

Figure 4.19. Wavespeed data for CIST 9.

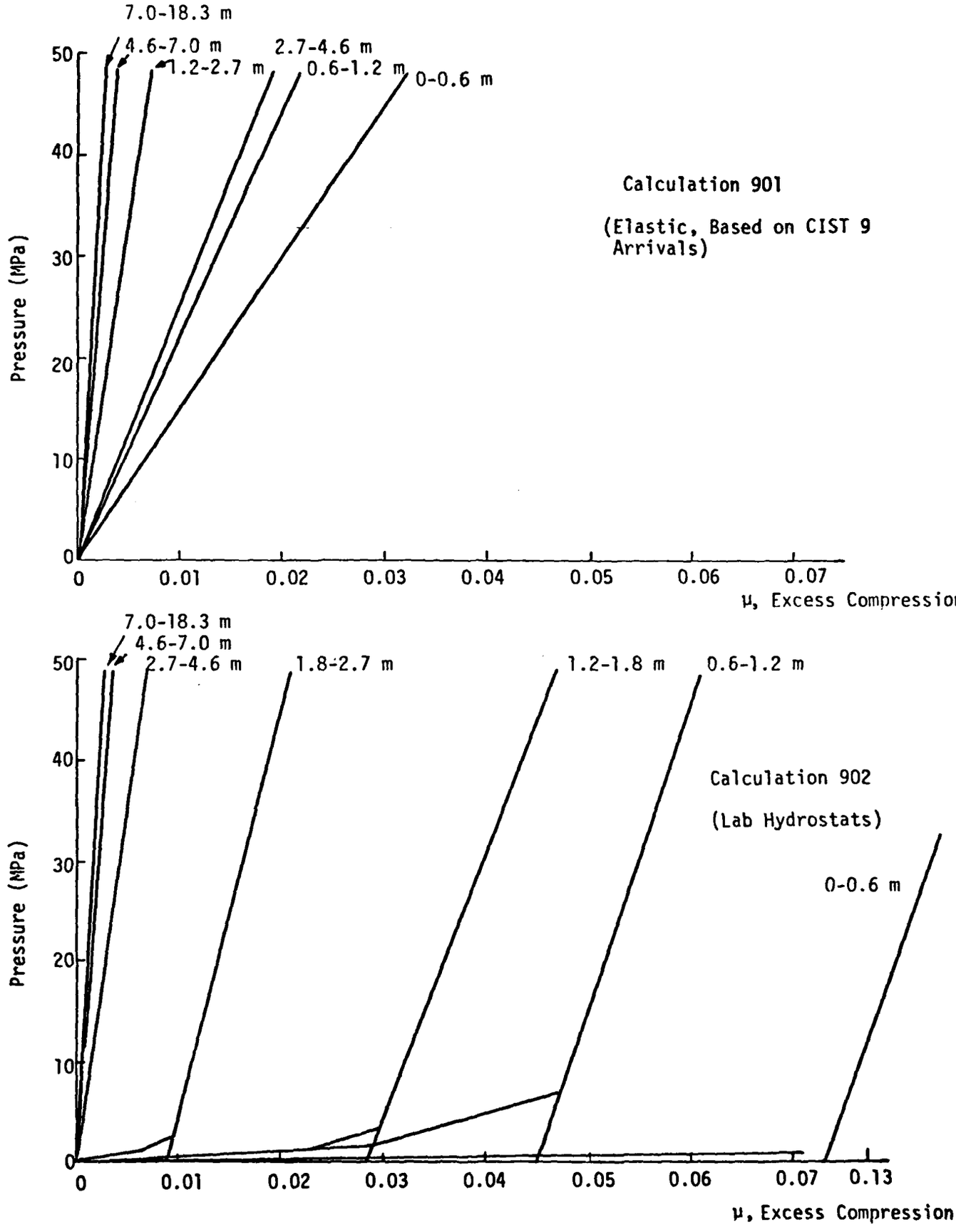

Figure 4.20. CIST 9 hydrostats.

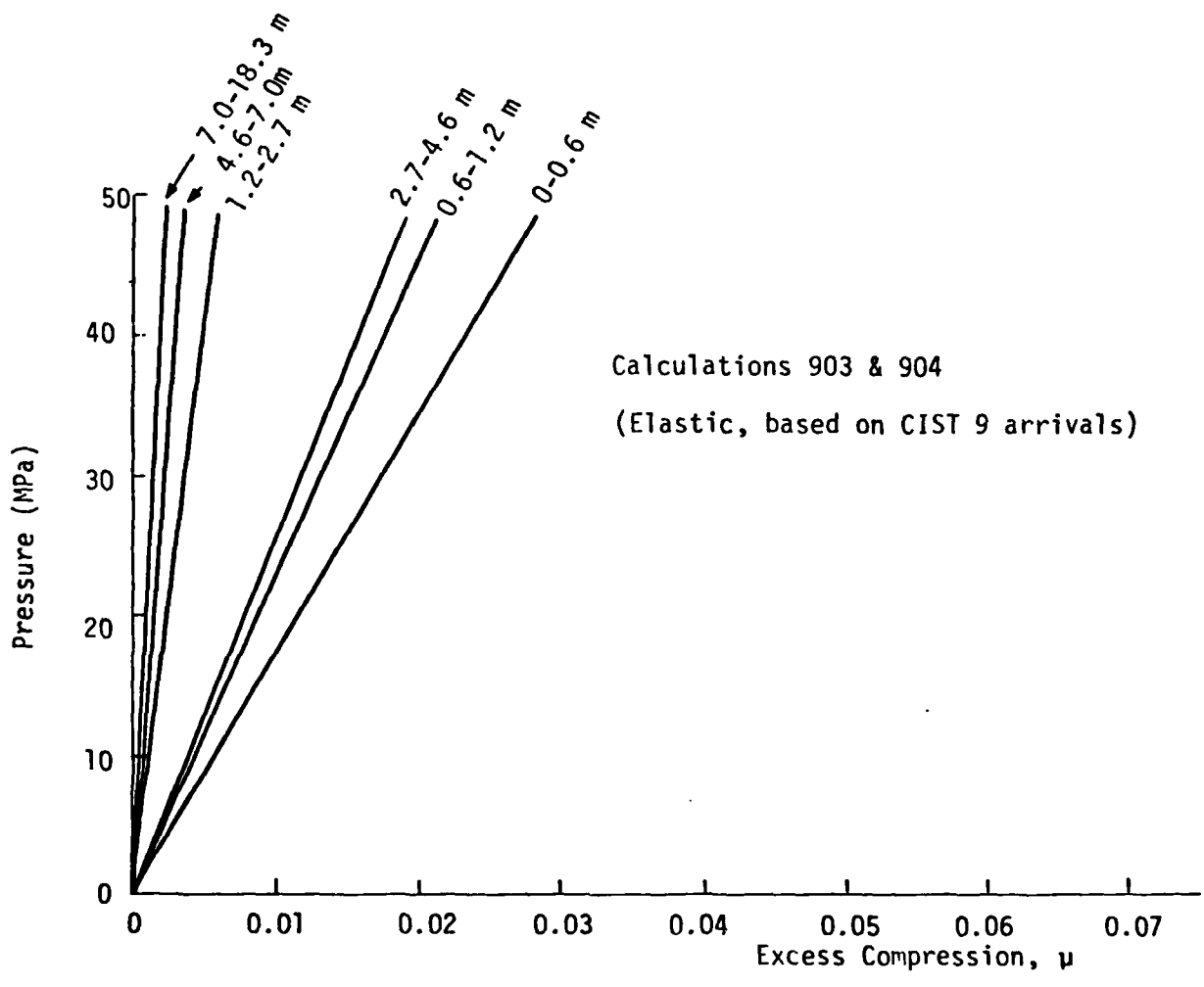

Figure 4.20 (concluded). CIST 9 hydrostats.

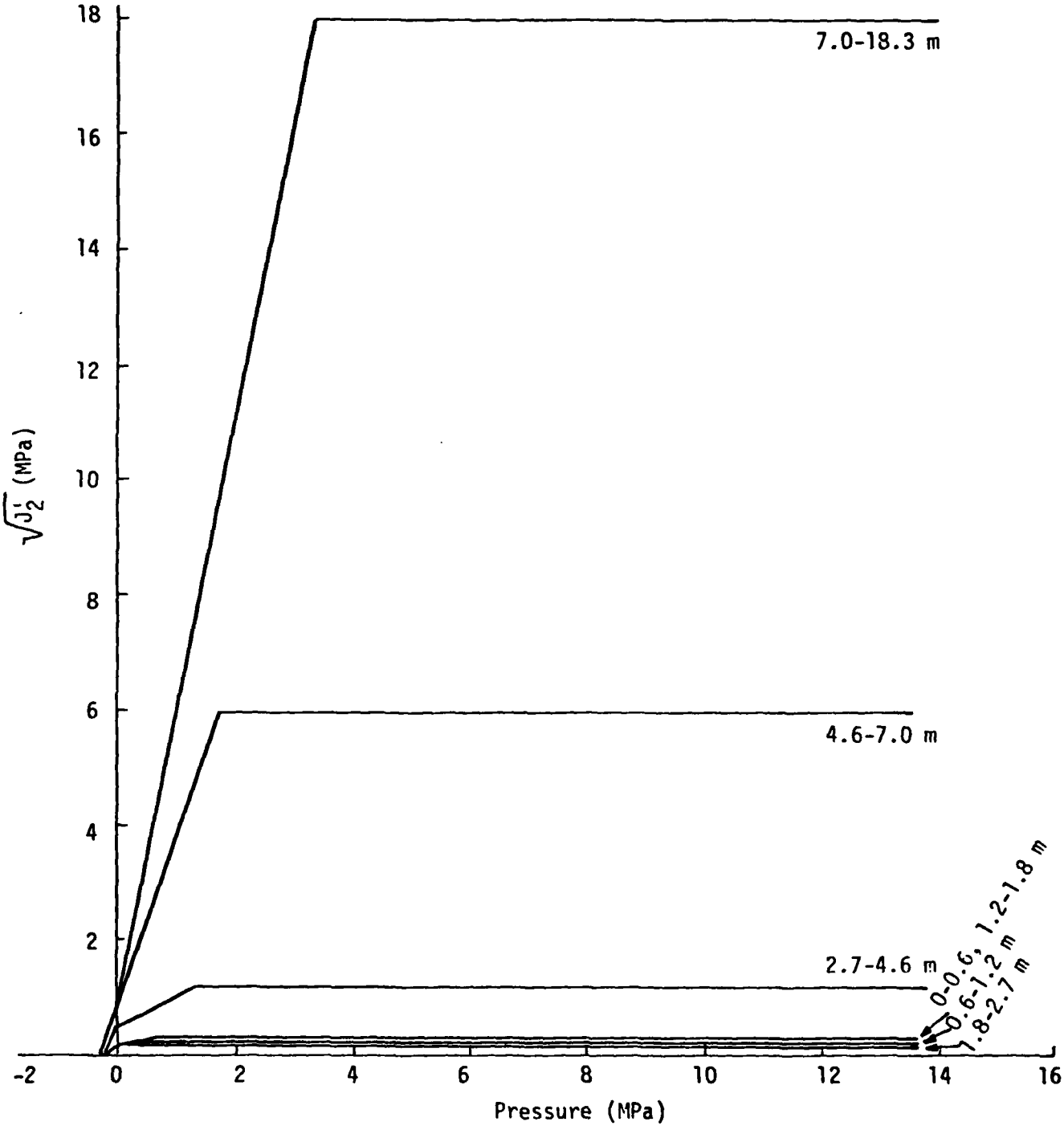

Figure 4.21. Failure surfaces for CIST 9, calculations 902 and 903.

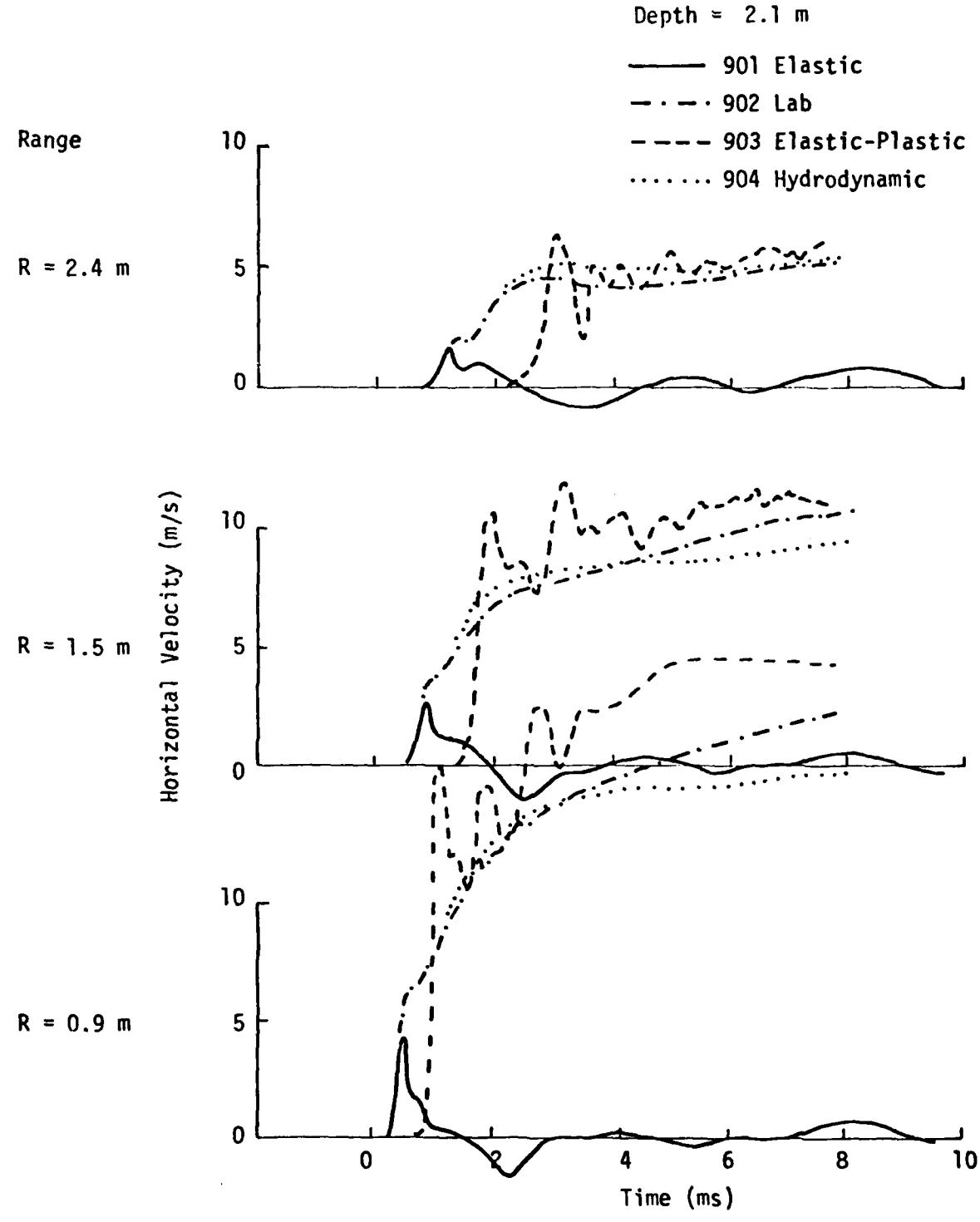

Figure 4.22. Velocity waveform comparisons at depth = 2.1 m, CIST 9 calculations.

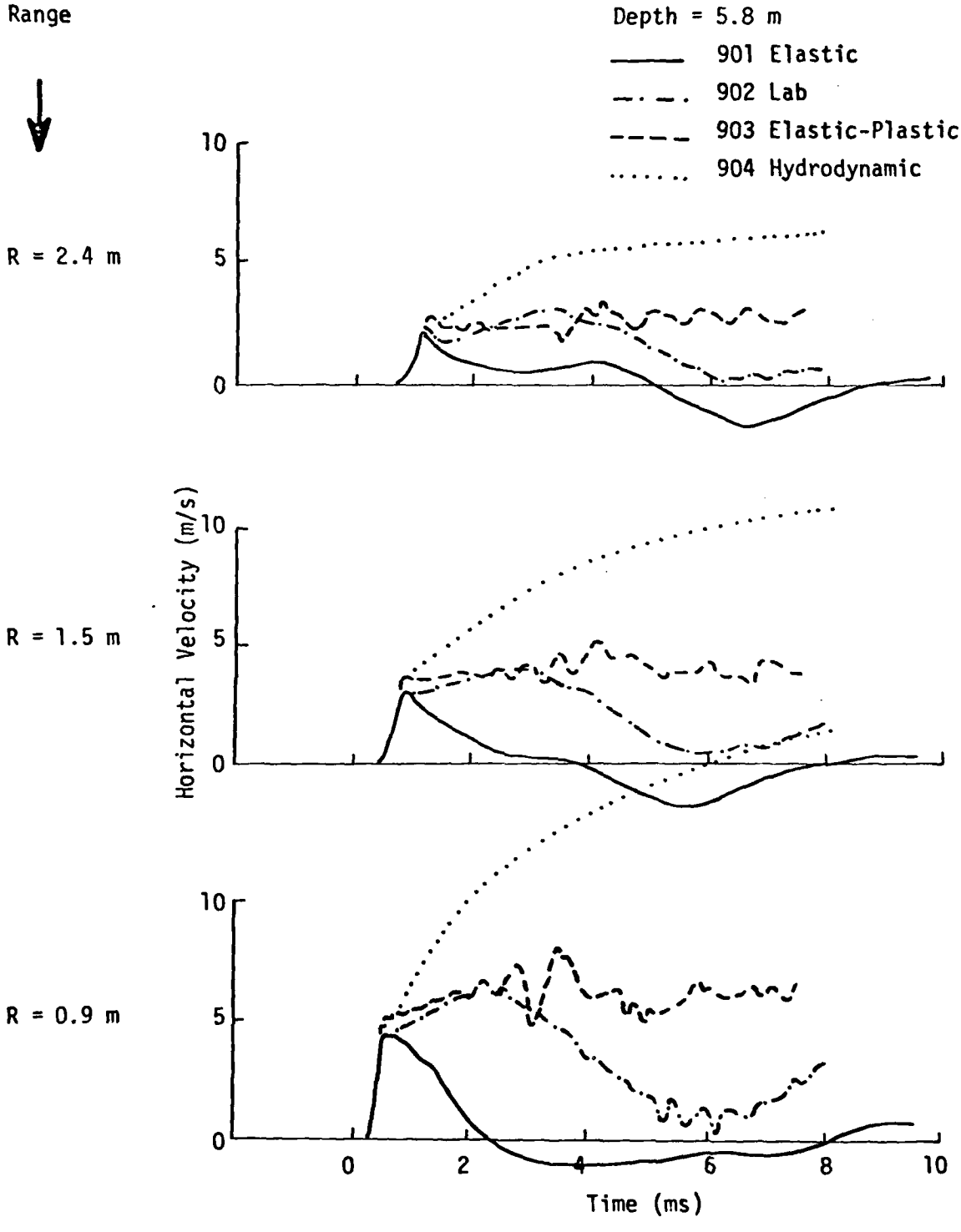

Figure 4.23. Velocity waveform comparisons at depth = 5.8 m, CIST 9 calculations.

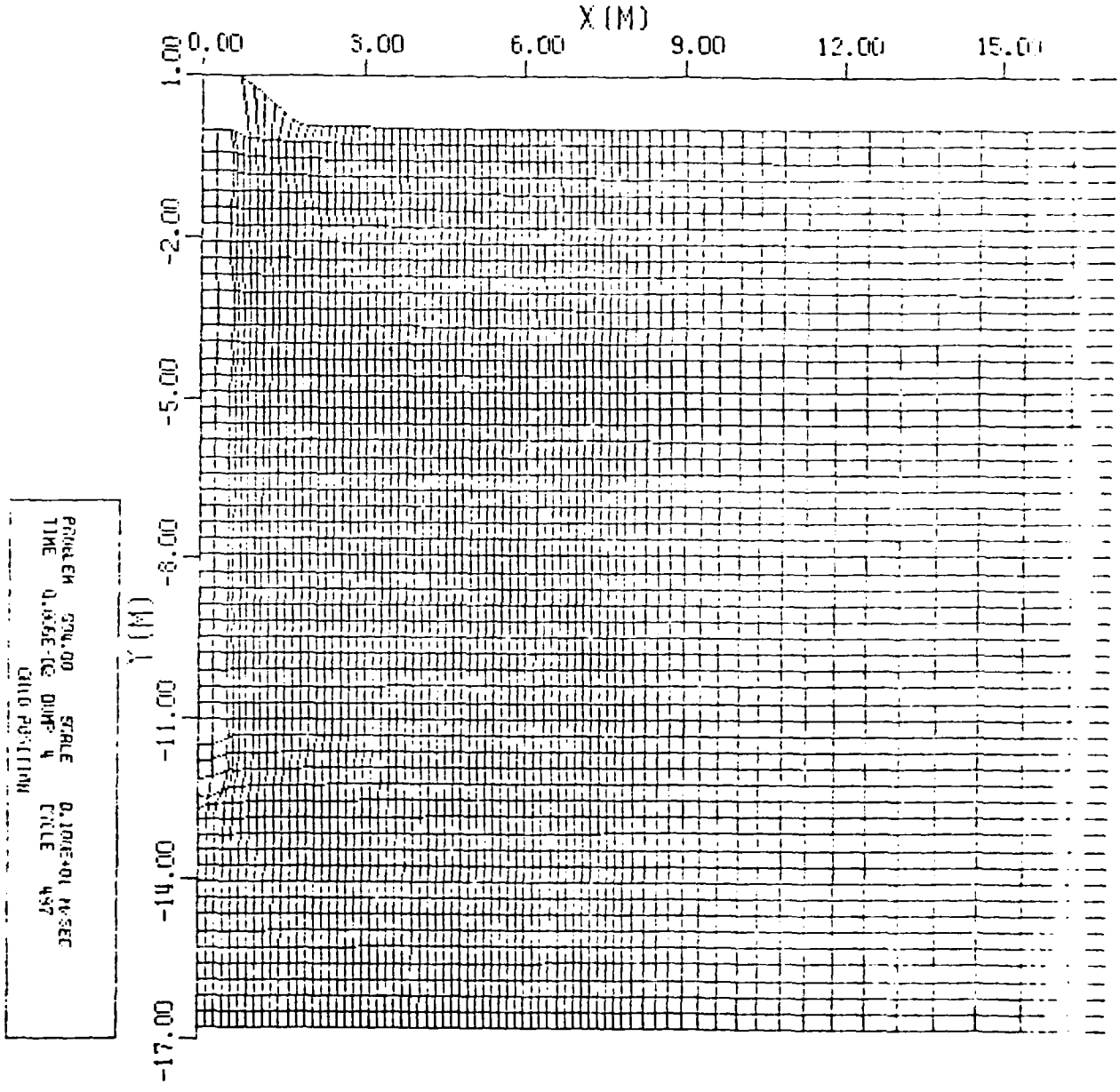

Figure 4.24. Grid plot for hydrodynamic CIST 9 at t = 8.1 ms.

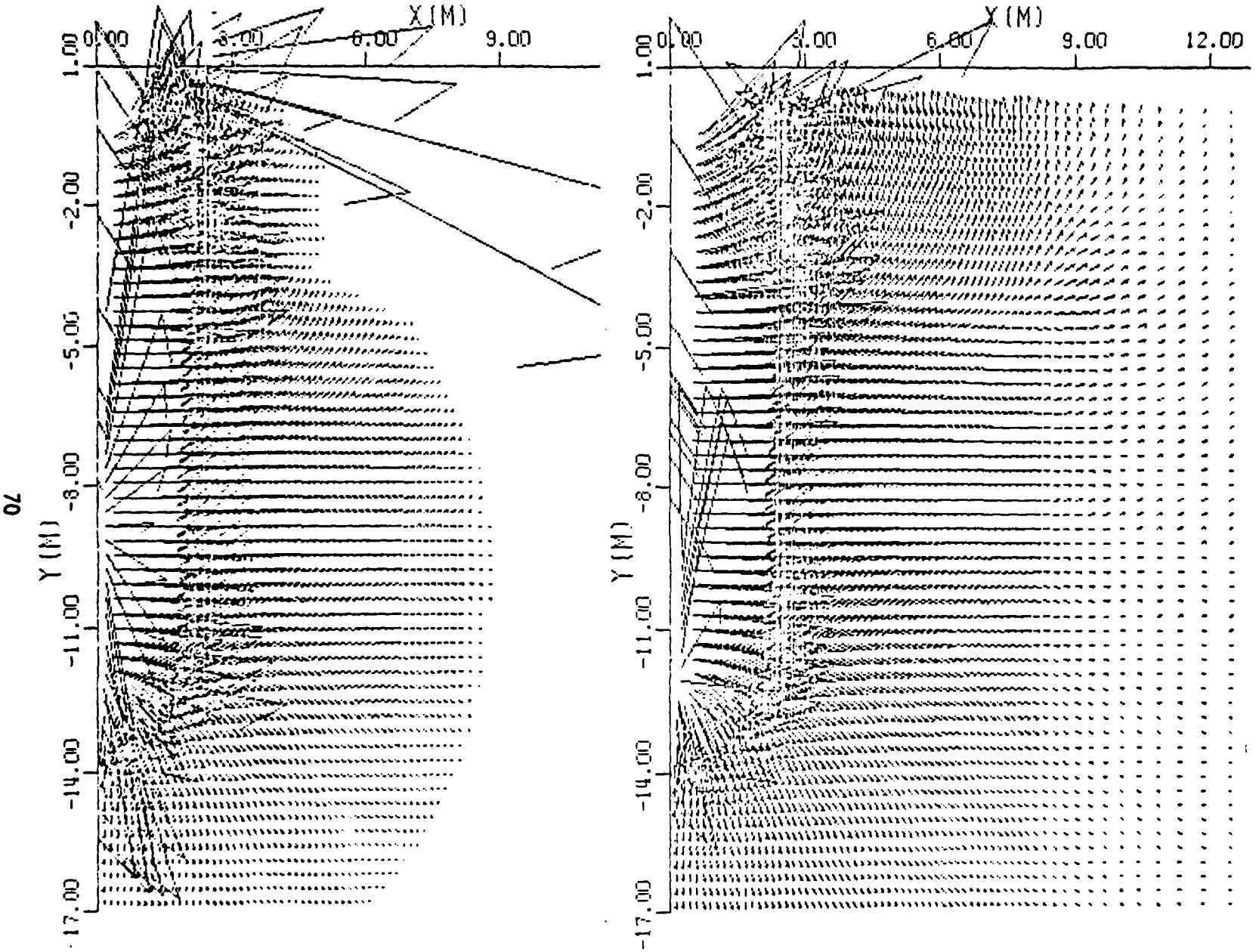

Figure 4.25. Velocity vector snapshots for hydrodynamic CIST 9.

4.4.4. CIST 10 and CIST 23

CIST 10 was conducted in the saturated coral sands at the Eniwetok Proving Ground. The variation of materials with depth was relatively minor and the water table at the time of the experiment was at the ground surface. The ground motion data also showed little variation with depth and quite simple wave forms at all locations. The particle velocity rose rapidly to a peak value and after a slight recovery began to indicate essentially constant horizontal velocity continuing for significant times. Close to the CIST cavity this velocity increased slightly with time and at the more distant ranges was constant at approximately the peak value reached during the initial rise. This indicates that the material reached the failure surface during the initial loading and then began to flow outward much like a heavy fluid. The material model parameters discussed in the previous section indicates that this behavior could be reproduced with a very simple model. In fact the hydrodynamic model yielded wave forms quite similar to those observed in CIST 10. The model used to fit these data involved a bilinear loading hydrostat with a small amount of air and a von-Mises type failure surface with a low value of shear strength. Because the material was essentially saturated, a Poisson's ratio of 0.49 was used. This allowed the material to load up below the failure surface but fail almost immediately upon unloading. Figure 4.26 shows representative data and the calculated waveforms for the 3.7 m depth. The comparison here is good, indicating that a quite simple model is quite adequate for representing the behavior of the saturated sand. Initially, the fit of the material parameters necessary to represent this data was obtained almost completely by examination and knowledge of the laboratory testing results. Only a couple of iterations were necessary to produce the agreement indicated on figure 4.26. The material model used for this calculation is shown in figure 4.27. Clearly, for this saturated sand, a very simple material model is quite adequate.

This behavior is contrasted to that of a dry sand (CIST 23) and a clay shale (CIST 9) in figure 4.28. The most obvious differences between the wet and dry sand are the initial arrival time and the rise time to peak velocity. The early time comparisons between the clay shale and the saturated sand indicate very similar performance, however, at late time the essentially strengthless wet sand continues to flow outward whereas the clay

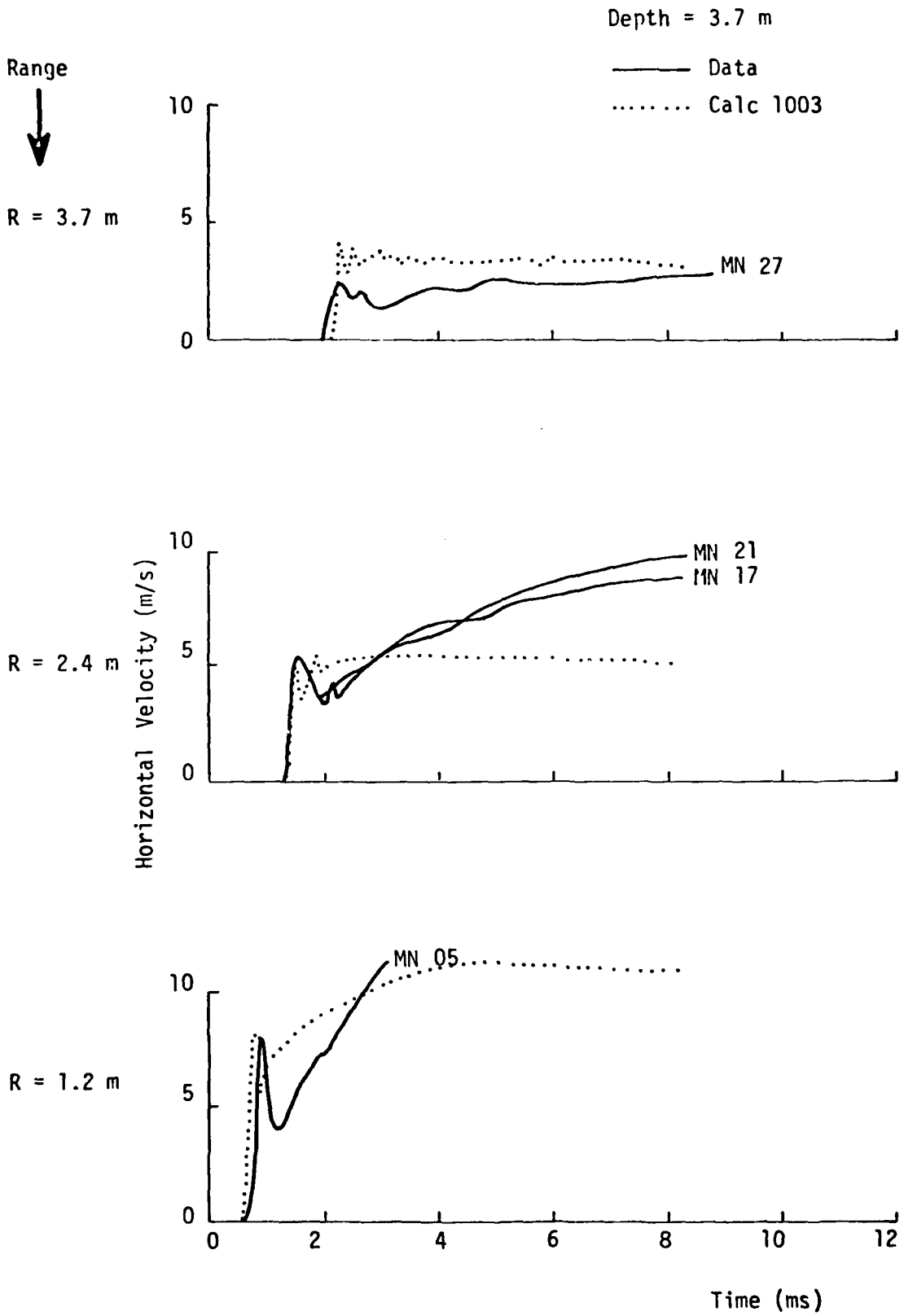

Figure 4.26 CIST 10 velocity waveform comparisons, depth = 3.7 m.

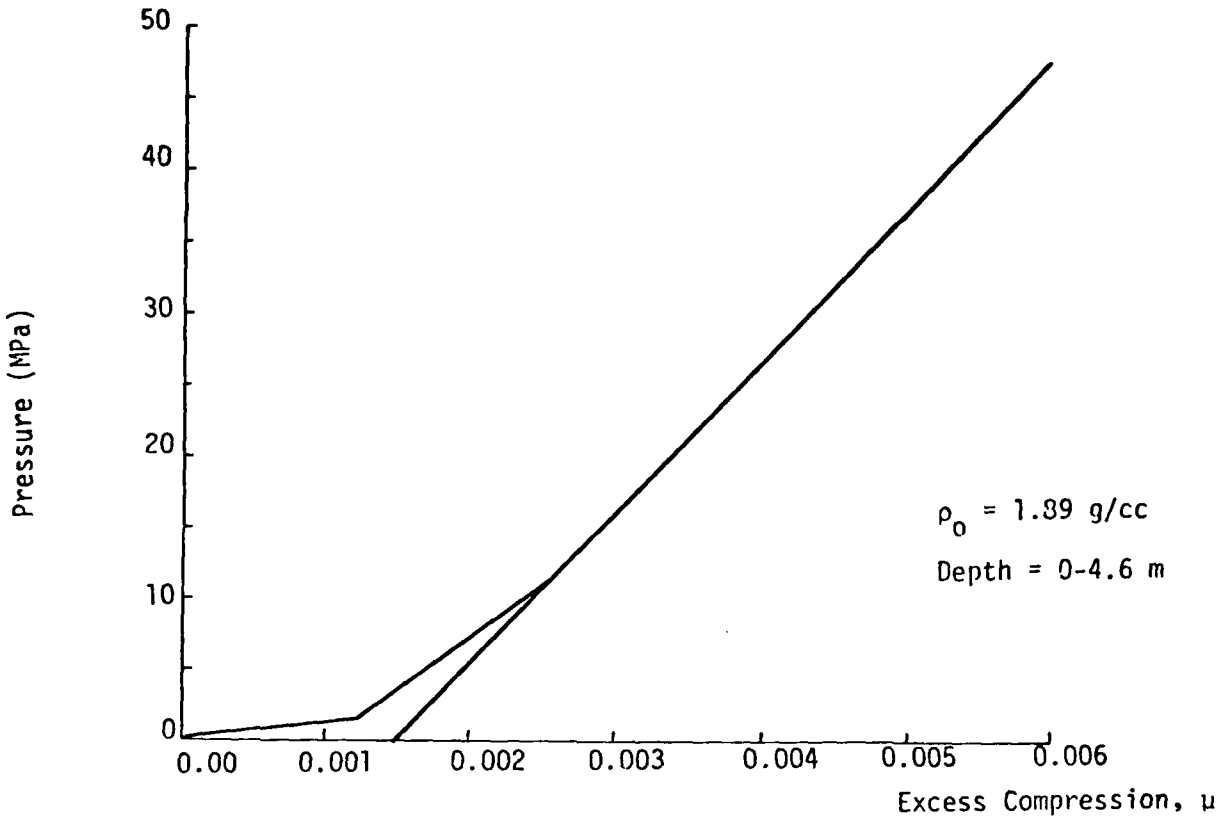

a) Hydrostat

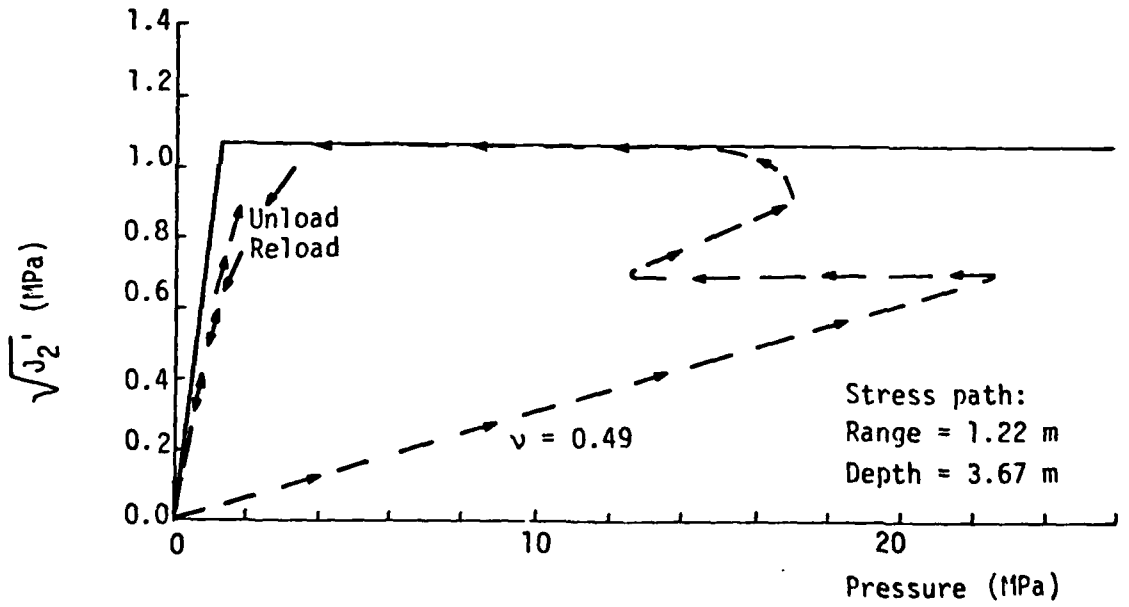

b) Failure surface (0-4.6 m) and representative stress path.

Figure 4.27 CIST 10 hydrostat and failure surface (calculation 1003).

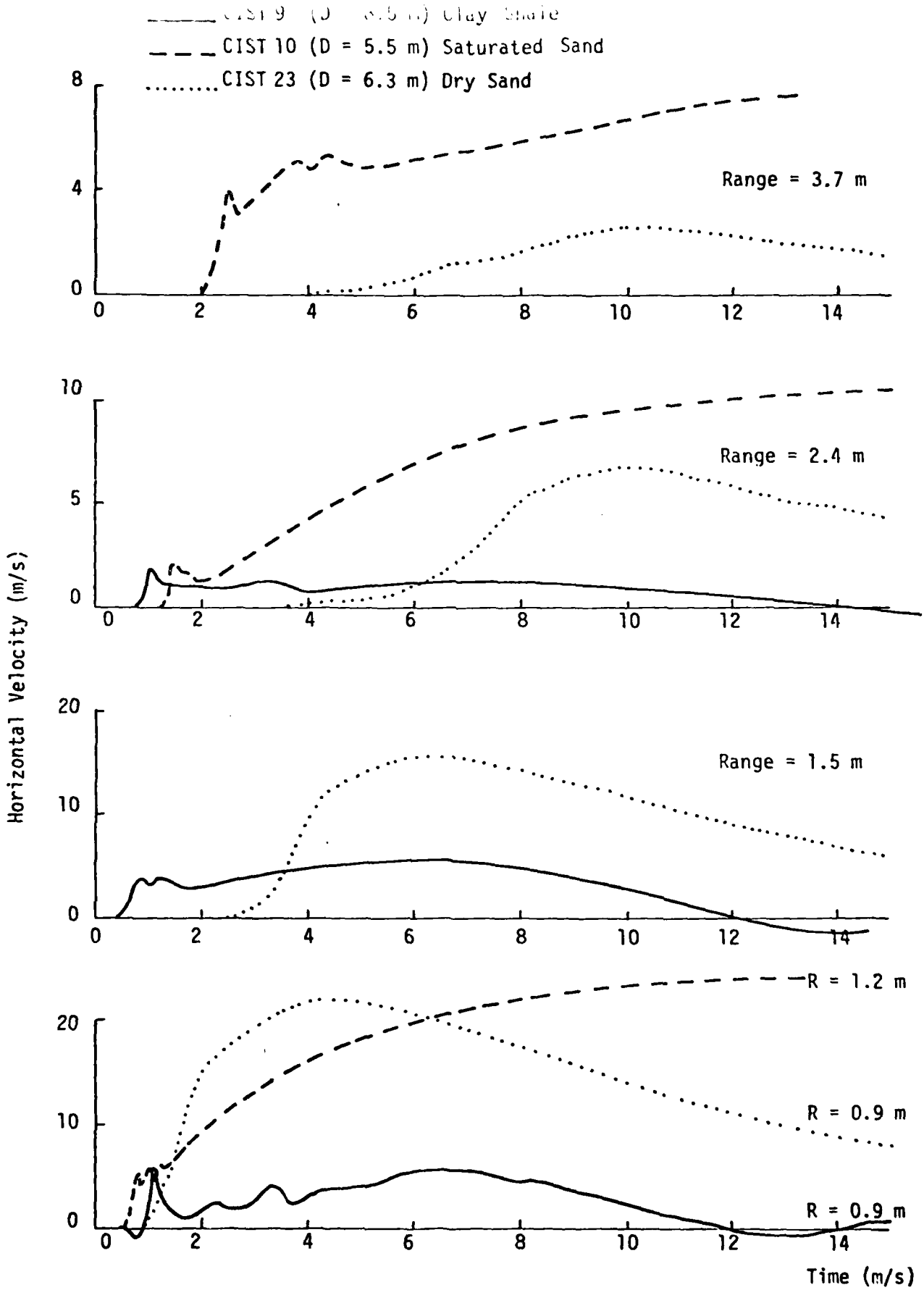

Figure 4.28 Data comparisons for various CIST tests and geological materials.

shale tends to recover and exhibits negative velocities during the times of comparison. This figure illustrates the large differences in response exhibited by the different materials for the same basic loading condition. This suggests that not only will the parameters in a model be quite different for the different materials but that different response mechanisms may be governing the behavior of the material. If this is true, then these experiments should provide a test for the generality of the basic model formulation.

The CIST 23 data shown on figure 4.28 is repeated in figure 4.29 and compared to the calculated behavior. The AFWL Engineering Model used here was developed based on laboratory data, and then improved by iterating the solution to obtain a better match to the experimental data. Notice that neither of the calculations match the exact qualitative features of the experimental data at all ranges. In general, however, the model developed by iteration is a reasonable fit. Comparisons of this kind indicate that for dry sand materials a somewhat more complex model may be required in order to reproduce both the qualitative and quantitative features of experimental data. A similar comparison for CIST 23 from the 12.8 m depth is shown in figure 4.30. In this case both the laboratory derived model and the model developed by iteration are in quite good agreement with the qualitative features of the experimental data and reproduced the magnitudes quite well. The model developed by iteration, however, seems to reproduce the detailed features of the waveform better than the model based on laboratory data.

4.5 Discussion of Results

The CIST calculations have helped to better isolate the behavior of soils under insitu conditions. By comparing various geologies under similar loading conditions, fundamental differences in material behavior may be studied. In addition, the basic wave types produced in a CIST test can be better quantified by calculations of this type.

The comparisons presented in the previous sections have illustrated that the cylindrical insitu test also provides a reasonable method to evaluate various material models and to check their generality against a reasonably simple insitu experiment of a complex dynamic nature. The ability of a material model to reproduce the qualitative nature of wave

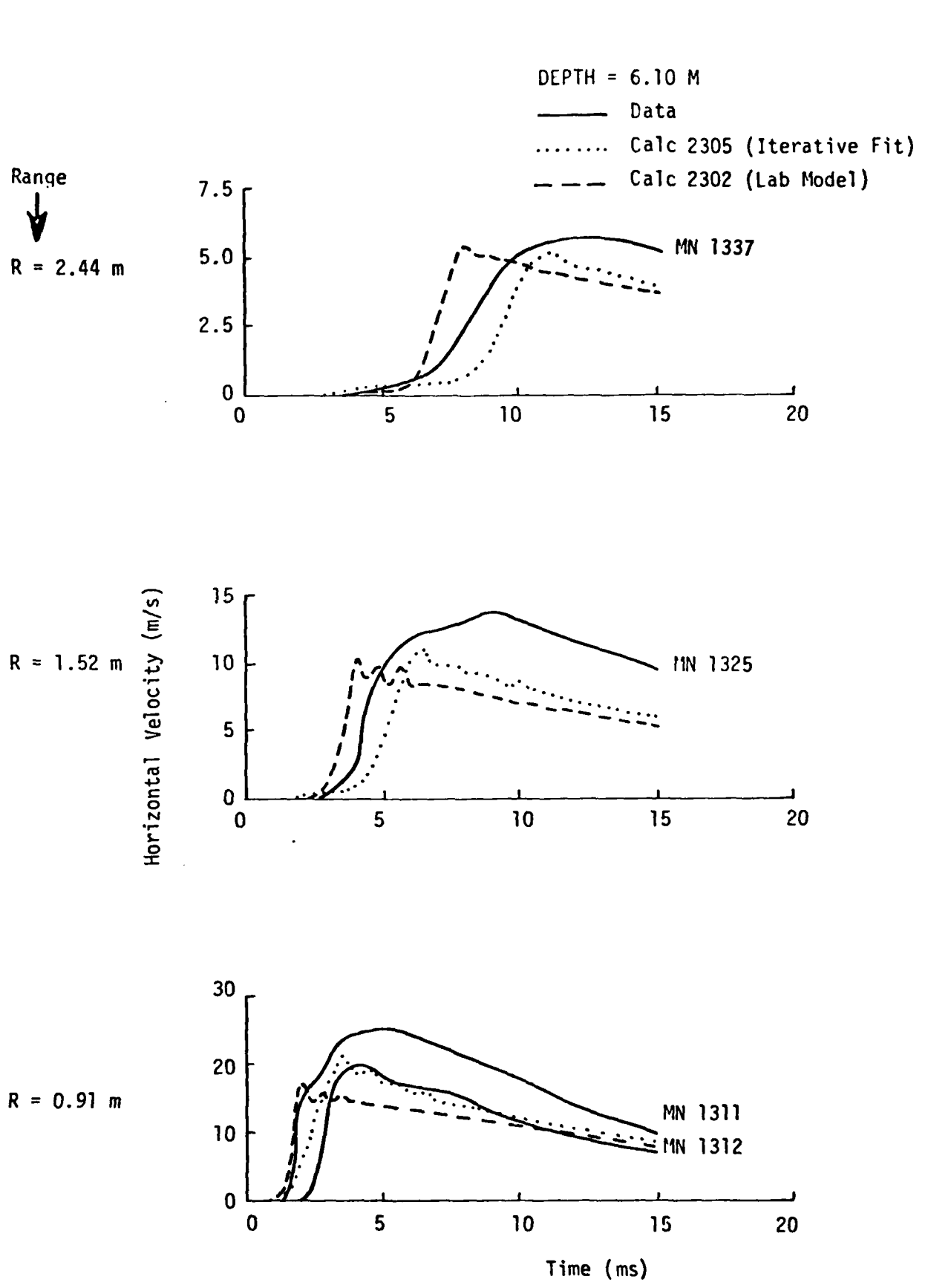

Figure 4.29 CIST 23 velecity waveform comparisons, depth = 6.1 m.

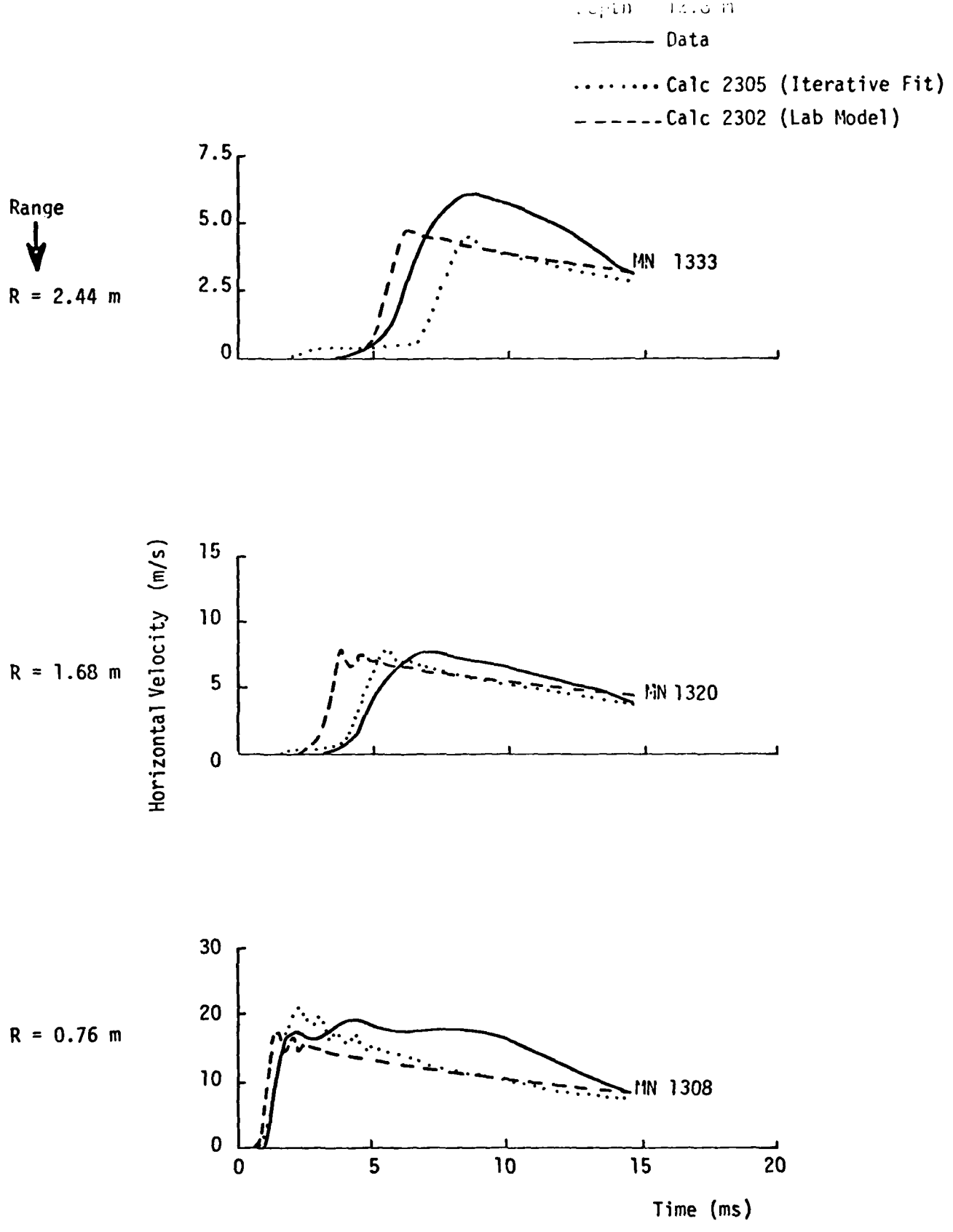

Figure 4.30 CIST 23 velocity waveform comparisons, depth = 12.8 m.

forms generated in the CIST experiments provide a first order screening process for models which have previously demonstrated a capability to reproduce laboratory data.

It is clear that two-dimensional CIST calculational studies contribute to a better understanding of the effect of material properties on observed material response and should be pursued. A number of problems with the AFTON code can be circumvented by using either the recent update of AFTON (CRALE, California Research Arbitrary Lagrangian - Eulerian) or STEALTH a newer code which we are currently using on other calculational programs.

Additional calculations will also study the effects of model variations and will further examine basic material response differences. In this way, CIST remains a valuable tool in studying insitu soil behavior.

5.0 SPECIAL PROBLEMS IN MODELING SOIL BEHAVIOR

5.1 Snear Behavior

The study of the calculations as presented in the previous sections has indicated tnat, while the CIST provides a good method for studying the behavior of materials and the effect of various material models on that behavior, the technique is not ideally suited for identifying propagating shear waves upon which to base estimates of the material shear modulus. The primary shear waves in a CIST experiment are generated at the top and bottom of tne cavity and propagate toward the center. This geometry (especially in layered sites) then does not lend itself particularly well to fundamental study of the shear behavior of the materials. Comparisons of a number of calculations of explosive events with experimental data indicate, on the other hand, that the shear behavior of the materials plays a significant role in the response of materials to explosive loadings. In addition, the importance of shear waves in earthquake problems has long been recognized and has precipitated many laboratory studies of the response of soils to shear loadings.

These laboratory investigations have demonstrated, conclusively, that the shear modulus of soils depends strongly on the shear strain to which the soil is subjected; the shear modulus decreases significantly as the maximum shear strain increases. Therefore, viable insitu testing techniques must be capable of attaining large shear strains. These laboratory studies certainly suggest the importance of the shear modulus in the material response. The actual determination of shear properties in the laboratory presents significant problems associated with sample disturbance and removal of insitu stresses in addition to those associated with the boundary conditions imposed by the laboratory test devices. In a state-of-the-art address to the ASCE conference on "InSitu Measurement in Soil Properties" Wroth (Ref. 11) stated,

> "The main reason for the need for insitu measurement of the parameters of deformation is that as our knowledge of the behavior of real soil expands, so does our appreciation grow for the inadequacy of conventional laboratory testing. The marked consequence of the inevitable disturbance that is caused in any soil specimen, however carefully it is sampled, are all to evident."

Insitu measurement of the fundamental properties necessary for ground response analysis, therefore, has become an area of major concern.

Two recent papers have presented an excellent review of the state-of-the-art in the in-situ material property determination. The first of these by Anderson and Espana of Fugro, Inc. (Ref. 12) was sponsored by the Electrical Power Research Institute and focuses on the entire spectrum of insitu testing techniques from the earthquake engineering perspective. Therefore, this review emphasized the measurement of shear modulus. The authors of this paper divide the test techniques into what they call wave propagation methods, dynamic system response methods, and direct/load strength metnods. For each of these methods the basic concept is discussed, the methods of data analysis are presented and the operational systems are described. A number of proposed test techniques are also presented even though they have not yet been reduced to practice. In summarizing their findings, Anderson and Espana stated,

> "A comparison of the three general classes of test methods, (wave propagation, dynamic-system response and direct/load strength) determined that no single existing test method or concept for a new test method satisfies all the requirements for a high-strain amplitude, dynamic in-situ property determination."

They went on to state, in conclusion, that although a number of techniques were presently available for making dynamic insitu soil property measurements that new insitu testing methods are required to extend the present capability and to varify the significance of various earthquake loading and related parameters presently thought to be of importance.

The second report, by Lodde (Ref. 13), was prepared for the AFWL and focused on only those techniques for evaluating insitu, high amplitude, shear behavior. This report was concerned with the properties required for nuclear weapons effects calculations. It concluded that since the shear stresses which could be propagated were limited by the shear strength of the material, the techniques used in earthquake studies were equally applicable to the weapon effect problem. Therefore, after a review of the existing laboratory shear tests, this report reviewed the same existing insitu test techniques covered by Anderson and Espana. Lodde also concluded that none

of the currently existing testing procedures are completely adequate for the problem at hand. As a result, the current state-of-the-art still involves a combination of insitu and laboratory testing. In all probability, such a condition will obtain for a considerable time in the future. However, the corrections currently used for the high strain portion of the laboratory data to account for insitu properties certainly requires evaluation.

Both of these studies suggest that the best currently available single test is the insitu Impulse Test developed by Shannon and Wilson, and Agbabian Associates for the Nuclear Regulatory Commission. This technique is described by Miller, et. al. in Reference 14. It is similar in nature to the cross-hole seismic test but involves a larger magnitude shear input. This input is generated in an anchor hole approximately 10 inches in diameter by impacting an anchor seated against the walls of the bore hole. This impact produces a vertically polarized shear wave which propagates radially and is detected at various ranges by sensors located in additional, smaller diameter bore holes. By comparing the waveforms as a function of radius from the center of the loading, the characteristic shear wave can be identified and its velocity of propagation determined. The corresponding shear strains are estimated using elastic theory. The primary disadvantage of this technique, at the current time, is that the largest amplitude strains are generated in the immediate vicinity of the 10 inch diameter anchor hole. This zone has been significantly disturbed and the geostatic stresses have been altered by the drilling of the anchor hole. Therefore, the large amplitude strains do not occur in an undisturbed material.

The major disadvantage of current techniques which attempt to generate high amplitude shear strains are that the largest strains are generated in a material distrubed by the drilling of a fairly large diameter bore hole for placement of the shear generation device. The CIST also would suffer from this limitation even if it were modified to generate a larger shear wave by propagating the detonations from the top to the bottom of the explosive hole.

A possible solution to this is to use an explosive charge configuration involving three charges near the ground surface. The detonation sequence and timing of the charges can be selected so that the explosive energy is directed into a skewed region, thereby creating an asymmetry in the

airblast. Asymmetries tend to generate large shear waves. A schematic plan and profile of this configuration is shown in Figure 5.1. The yields of the three explosive sources could be similar to those used in conventional refraction surveys but could be varied depending upon the depth of penetration desired and the nature of the materials involved. The relative location of the charges could be varied such that the pressure when the blast wave from the simultaneous detonation of charges 1 and 1a impinges upon charge 2, it would be approximately equal to the shear resistance (strength) of the soil. Charge 2 would be detonated just as the blast wave from charges 1 and 1a reaches it. The confinement of the charge 2 effects by the airblast from charges 1 and 1a would direct the energy into a limited region. This will create an asymmetry which will generate the large amplitude shear waves which will be measured by instruments located in bore holes at various ranges and depths. The depths and ranges of measurement would depend upon the layering of the site and the levels to which the shear wave measurements were desired.

Since no large diameter bore hole is required, and no large piece of equipment must be transported from site to site, this technique should be more economical than any of the existing large amplitude techniques. Utilizing this explosive technique, shear modulus data should be obtainable for strains up to those corresponding to the shear failure limits of the materials. The more distant measurements, on the other hand, would provide information at the lower strain levels so that a comparison with existing low strain amplitude in-situ techniques would be possible. In addition, a much larger volume of material would be tested than in the techniques utilizing a bore hole device for generation of the shear impulse. For this technique the cost would be directly proportional to the number of measurement locations. Therefore, would vary with the type of application.

The shear modulus plays an important role in the response of soils to dynamic, complex loadings. Since current insitu test techniques are not capable of generating the large shear strains required for constitutive modeling, the technique discussed provides a possible significant enhancement in insitu testing capability.

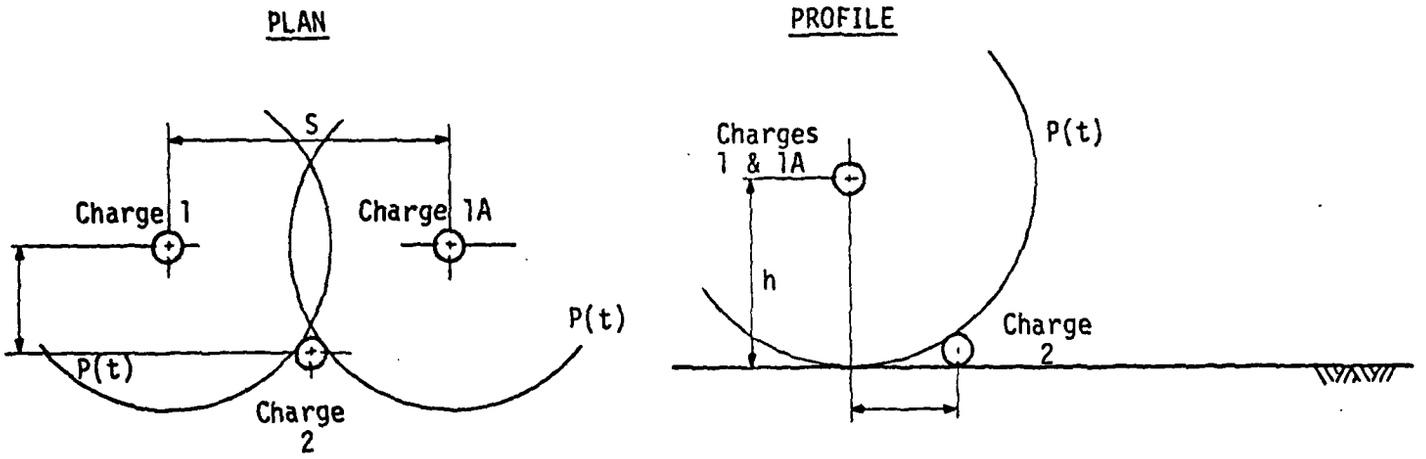

a). Schematic of Charge Configuration Showing the Location of the Blast Waves From Charges 1 & 1A of the Time of the Detonation of Charge 2.

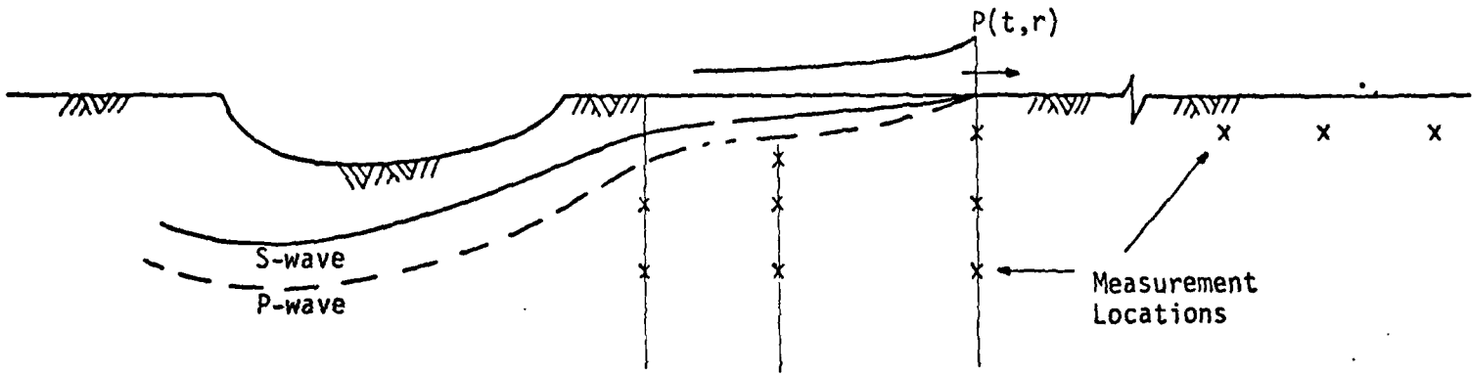

b). Initial Boundary Loading Conditions.

Figure 5.1. Explosive Shear Wave Generator.

5.2 Effective Stress Modeling

5.2.1 Introduction

Natural soils are three phase media consisting of solid grains, water and air. Most constitutive modeling has treated soil as an equivalent single continuum material. It is natural to ask if improved soil material modeling requires a more detailed and specific treatment of the individual components of the soil, and the interaction between these components. The main concern is over the effect of pore fluid, especially the water component, on the behavior of the soil. There are three main areas of concern:

- Effective stress and soil strength
- Pore pressure increase and potential liquefaction
- Lubrication effects on stiffness and strength of the soil.

The following paragraphs discuss some of the main points associated with effective stress and liquefaction, and present some preliminary conclusions with regard to future work that must be performed in order to include these effects in material models. Lubrication effects are not discussed because there is very little information available on this subject. It is believed, however, that some relatively simple experiments (dry soil versus wetted soil) would yield insight into the area. Comments are also presented on the computer requirements, in terms of memory and computing time, that might be introduced by a fuller treatment of the individual components of the soil media.

5.2.2 Strength and Effective Stress

Of the three components of natural soil, only the soil grain matrix has strength. For all practical purposes, the water and air phases can only carry hydrostatic loads. The soil grain matrix achieves its strength from friction and/or intramolecular forces developed between the particles. Dry and fully drained tests on natural soils show a dependence of strength on the normal stress applied to the sample. When a soil containing pore fluid is loaded, part of the load is carried in the grain matrix and part of the load is carried in the air-water phase, depending on the relative

compressibility of the individual components and on the ability of the pore fluid to flow. If fully saturated, the majority of the load is carried in the water phase. If less than fully saturated, then most of the load is carried in the grain matrix. Since only the grain matrix has strength and since that strength is dependent upon the normal load applied to the grain matrix, it is apparent that only the normal stress carried through the intergranular contacts influences the strength of the natural soil. This is known as the effective stress principal and was established by Terzagi (Ref. 15) over 40 years ago. The effective stress is expressed quite simply by the equation

$$\bar{\sigma} = \sigma - u$$

where σ is the total stress acting on a given plane, u is the pore pressure in the pore fluid, and $\bar{\sigma}$ is the effective stress which is carried in the grain matrix.

Most modeling for dynamic purposes (blast and earthquake) has not treated the details of effective stress. This is because it has normally been assumed that the dynamic phenomena of interest occurs so fast that the material can be considered to be undrained during the dynamic process. As a result, flow does not occur and, therefore, the effective stress in the soil does not change. In turn, the strength does not change during the dynamic process. Hence, total stress models have been the rule.

In recent years, however, there has been increasing concern that effective stress should be treated in more detail. A significant model developed within the blast and shock community is that of Baladi (Ref. 16 and Appendix A.1.2c). Baladi developed an effective stress model for ground shock computations by considering two models for the material. One was a total stress model derived from undrained tests on the soil material. The second was an effective stress model derived from fully drained tests on the same material. It was assumed that lubrication effects on the stiffness and strength of the material was not important. In Baladi's model, computations of total and effective stress variables are made using the total stress model and also using the effective stress model. Using assumptions of volumetric strain compatibility and effective and total deviatoric stress compatibility, the results of the computations from the two models are used

AD-A111 901 APPLIED RESEARCH ASSOCIATES INC ALBUQUERQUE NM F/G 8/13
FUNDAMENTAL PROPERTIES OF SOILS FOR COMPLEX DYNAMIC LOADINGS.(U)
SEP 81 W C DASS, J L BRATTON, C J HIGGINS F49620-80-C-0088
UNCLASSIFIED AFOSR-TR-82-0101 NL

2 OF 2
AD A
111901

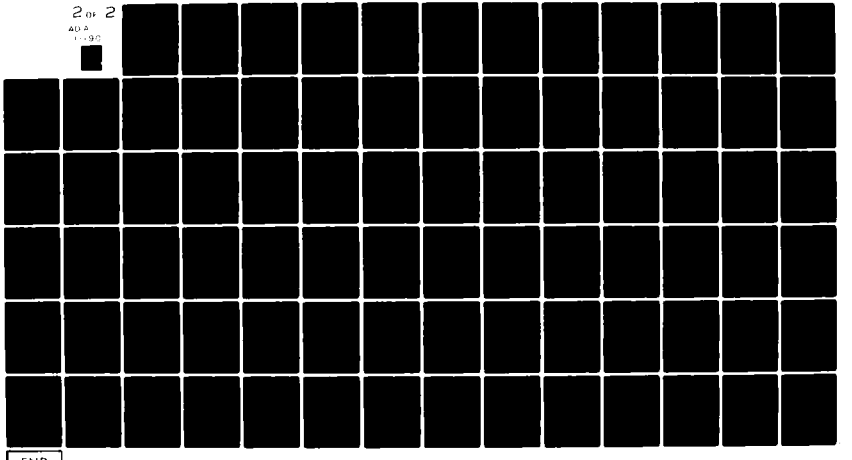

END
DATE FILMED
04-82
DTIC

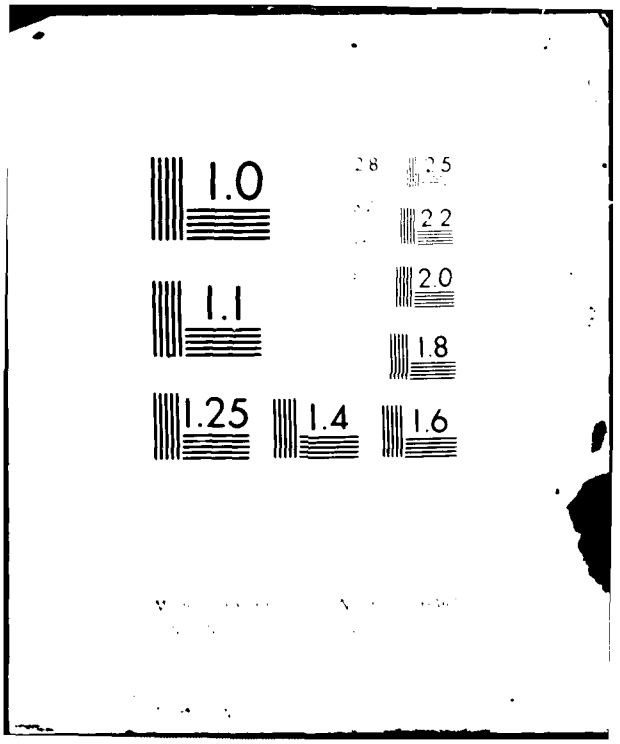
1.0
1.1
1.25
1.4
1.6
1.8
2.0
2.2
2.5
2.8

to determine the pore pressure. This pore pressure as a function of time is produced as part of the output of the ground motion calculation.

A detailed review of Baladi's model indicates that it really does not provide much more additional useful information beyond that available from a standard total stress model. This is because the ground motions computed by his method would be exactly the same as those computed with a total stress model alone (Baladi has not made such a comparison). Also, the loads or stresses produced on a structure embedded in the soil would be exactly the same since those loads are total stress loads rather than effective stress loads.

The usefulness of Baladi's model is limited primarily by the fact that it does not include fluid flow effects, which are potentially important even for general ground motion phenomena. Baladi's model does not include any flow because of the assumption that the phenomena of interest occurs so fast that flow is not important during the time of interest. As stated earlier, this has been a standard assumption throughout the blast and shock community over the past twenty or so years. However, there is another view that has never been studied in detail regarding the importance of flow. Ishihara (Ref. 17), in an analysis similar to that of Biot, derived equations of motion for the solid and fluid phases of a soil by representing the soil as an elastic porous matrix saturated with water. His main purpose was to derive results which could be interpreted in terms of standard soil mechanics concepts and tests. Two kinds of compression waves, the same as those found by Biot, were derived in a revised form. Evaluation of the deformation modulus in the frequency equation, with reference to specific soil test conditions, indicated that the first kind of wave travels through the solid-water phase system causing only compression of the solids and fluid but without any change in the pore volume due to flow. The second kind of wave can progress only when pore volume change takes place due to flow, and is associated with consolidation. The most interesting finding from Ishihara's work was that flow appears to be more important for what is normally considered to be high frequency, undrained loadings.

Ishihara states the usual assumptions and his findings very clearly: "In view of the usual hypothesis, it is expected that the wave that is encountered at higher frequency would be the one that does not permit the

drainage to take place, because the fluctuations in the pore pressure due to strain occurs so rapidly that there is little time for the water to flow from regions with higher pore pressure to those of lower pore pressure. On the contrary, the wave at lower frequency is expected to produce a condition where the pore water is allowed to move through the soil skeleton, because there may be sufficient time available for an equilibrium to be established for the fluctuation of the pore pressure. However, the above expectation is in complete contrast with what was found above. Nevertheless, the situation can also be considered from another point of view. It can be anticipated that at higher frequency the wavelength is short, so that, although there is little time for water to move, the distance that the pore water must travel is short. On the contrary, at lower frequency, although there is enough time for the water to flow, it has to traverse over a great distance because the wavelength is now large. According to this viewpoint, the stress condition that is encountered with a wave of lower frequency is an undrained condition, and the stress condition that is realized with a wave of higher frequency is a drained condition."

Ishihara's observations from his theoretical work are in marked contrast to the standard assumption based upon intuition which has been employed in dealing with dynamic problems assuming total stress models. Ishihara analyzed the one dimensional consolidation problem under a sinusoidally varying force to demonstrate his concept. The well known consolidation dimensionless time constant T_v (Ref. 15), which determines the time it takes to reach pore pressure equilibrium, is inversely proportional to the square of the distance and directly proportional to time. Hence, the distance seems to be more of a controlling factor for pore pressure equilibrium or water flow than time, supporting Ishihara's hypothesis. Although Ishihara's work was published in 1967 it has not been widely evaluated in the blast and shock community. Hence, it is a major conclusion of the authors here that his work be given a thorough evaluation in next years effort using available data and calculations.

5.2.3 Grain Matrix Degradation (Liquefaction)

The other major phenomena which is dependent upon pore fluid behavior and effective stress is that of liquefaction. Figure 5.2 shows some results from a computation given in reference 16. The calculation was for a

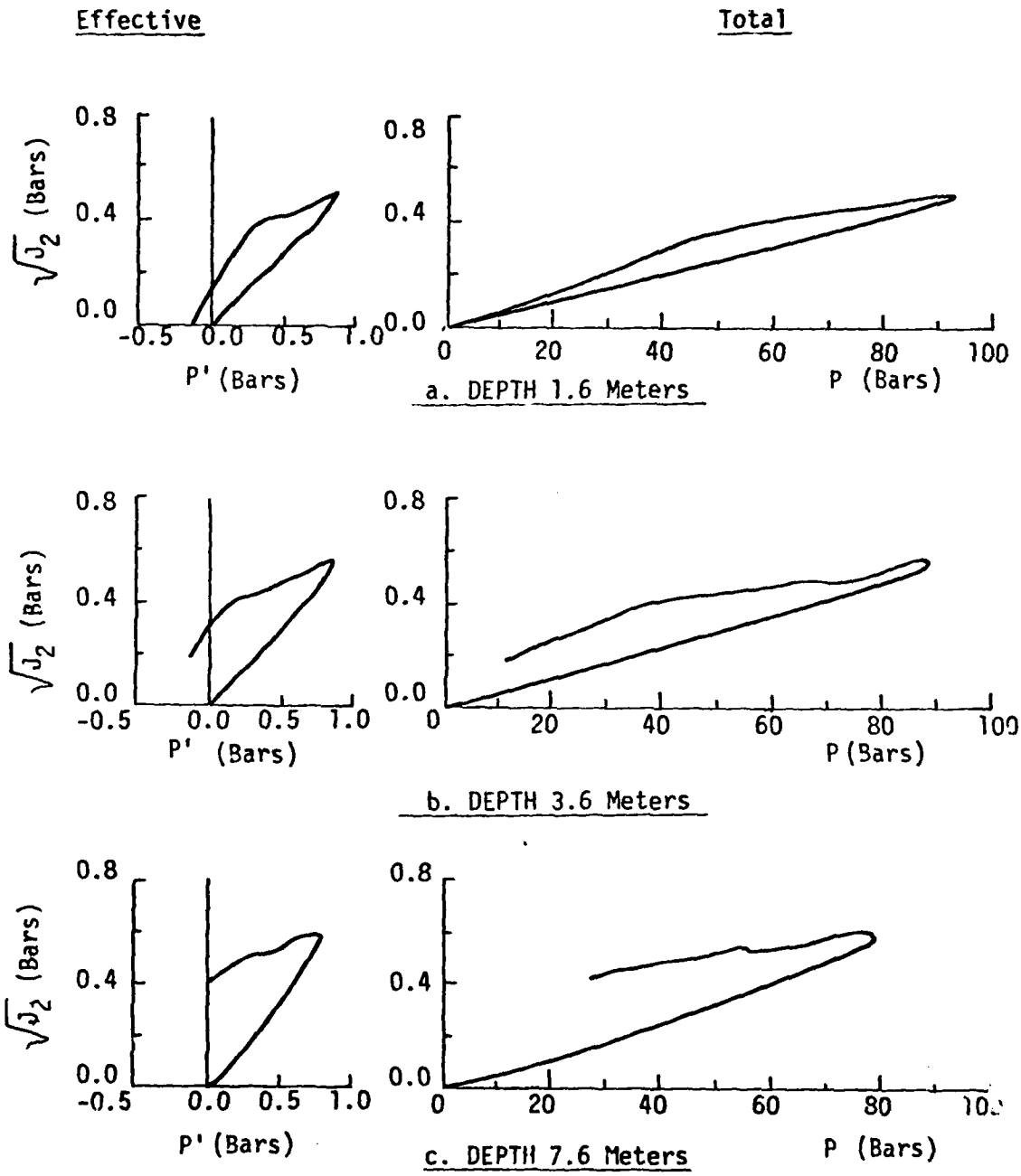

Figure 5.2 Comparison of total and effective stress paths range 15.6 meters. (After Ref. 16)

radially expanding airblast on a homogeneous halfspace of saturated sand. The figure shows the total and effective stress paths at three different depths at a range of 15.6 m from the origin. One of the most interesting points on these stress paths is that the effective stress at depths of 1.6 and 3.6 m become negative during unloading. This means, in a physical sense, that the grain matrix has been or is about to be broken down or degraded. Indeed, this is the onset of liquefaction under compressive loading and unloading. Baladi does not comment on this behavior at all in his report. However, it is here that one of the most interesting parts of the effective stress problem begins to occur, i.e., liquefaction.

In order to deal with liquefaction and post-liquefaction stability of soil, a model must be able to handle three complex problems:

- Air-water compressibility
- Pore pressure changes
- Fluid flow

Air-water compressibility is a major consideration because many soils, especially in regions near sea coasts, rivers, waterways or where water table fluctuations occur, are not in a state of 100 percent saturation. Minute amounts of air, which generally are impossible to measure by standard soil mechanics tests, can markedly affect the compressiblity of the air-water phase. As soon as the compressibility of the air-water phase becomes large compared with the compressibility of the soil grain matrix, even if the material is 98 percent saturated and above, the material behaves essentially as a soil grain matrix only. However, depending upon the magnitude of the load, the air contained in the air-water phase can be driven into solution and the material can become 100 percent saturated.

The phenomena by which these changes occur is extremely complex involving the behavior of free air bubbles, bubbles adhered to soil grains, surface tension, the solubility of air in water and a number of other factors including the dynamic behavior of these parameters. Air-water phase compressibility on a simplistic scale has been treated by Wood (Ref. 18) and, in Russia, by Lyakhov (Ref. 19). A recent investigation in the Netherlands by Barends (Ref. 20) provides a much more sophisticated treatment of all of the factors involved in air-water compressibility

including most of the factors mentioned above but not on a dynamic basis. Barends work indicates tnat the air-water phase compressibility does not vary continuously but, rather, that distinct pressures exist beyond which the free air becomes dissolved quite suddenly. Bubble collapse causes an unstable increase in compressibility. The main point here is not to confuse the issue but to make clear that air-water compressibility in and of itself is a major problem in the development of multi-phase models.

To illustrate the effect of small amounts of water upon the compressibility of the air-water phase, the pressure volume relationships for air-water mixtures at various degrees of saturation using the simpler model of the Russians (Ref. 19) have been calculated. The results are shown in Figure 5.3. The results indicate that degrees of saturation less than 99.99 percent yield a relatively large range of pressures over which the air-water phase shows very high compressibility. Indeed, for degrees of saturation below about 95 percent, the material can be considered essentially void of water except for any lubrication effects that might occur.

The second major concern in the analysis and prediction of liquefaction is the development of a model which will predict the pore pressure changes. These changes, of course, are due to changes in the pore volume. There are several models developed within the earthquake community which deal with pore pressure changes under multiple cycles of triaxial compression or simple shear. These models are generally restricted to these limited stress paths. Because of the simple assumptions in the models developed in the earthquake engineering community, they cannot be used for more general stress paths, particularly those related to blast and shock problems where compression is important. On the other hand, there are models which can deal with liquefaction under the influence of compressive loads. These models, however, cannot predict earthquake-type behavior because they generally lack coupling between deviatoric and volumetric strain.

The earliest work that has come to our attention which deals with compression (or blast)-induced liquefaction is that performed by the Russians (e.g. Refs. 19 and 21). This work was done in the 1950's and

1960's. More recent work has been done in Europe (e.g. Ref. 22), but the European models are very much like the Russian models.

To illustrate what might occur after the effective stresses go negative in Baladi's problem (fig. 5.2), consider the following simple illustration based upon the Russian models. Available information on explosion-induced liquefaction reveals that the pore pressure behavior is dependent upon the same parameters which are important for earthquake phenomena, i.e., air content, relative density, and all the other parameters which influence the grain skeleton compressibility (grain size, soil structure, grain roughness, cementation, etc.). The liquefaction mechanism currently accepted by the Europeans (e.g. Ref. 22) and proposed by the Russians in the 1960's (Ref. 21) is based upon irrecoverable strain in the soil skeleton upon unloading from some previous volumetric strain. If the fluid cannot flow during this period, residual pore pressures develop.

The basic mechanics for a simple model for composite fluid-skeleton behavior in uniaxial strain is given in Figure 5.4. On loading, both the fluid and the skeleton carry stress. The total stress is given by

$$\sigma = \bar{\sigma}\ (\varepsilon) + p(\frac{\varepsilon}{n})$$

where σ = total stress

$\bar{\sigma}$ = stress in the skeleton (intergranular stress)

p = pore pressure

The strain in the soil skeleton is the total strain , while the strain in the pore fluid phase is given by ε/n where n is the porosity. Because the fluid is usually much stiffer than the skeleton, most of the stress on loading is carried in the fluid. Upon unloading, the skeleton exhibits irreversible compaction so that the skeleton stress (effective stress) reaches zero while there is still pore pressure in the fluid. It is at this point that the soil matrix tends to break down or liquefy.

An example of the load-unload behavior for a soil which is 99 percent saturated and which has skeleton compressibility similar to that of

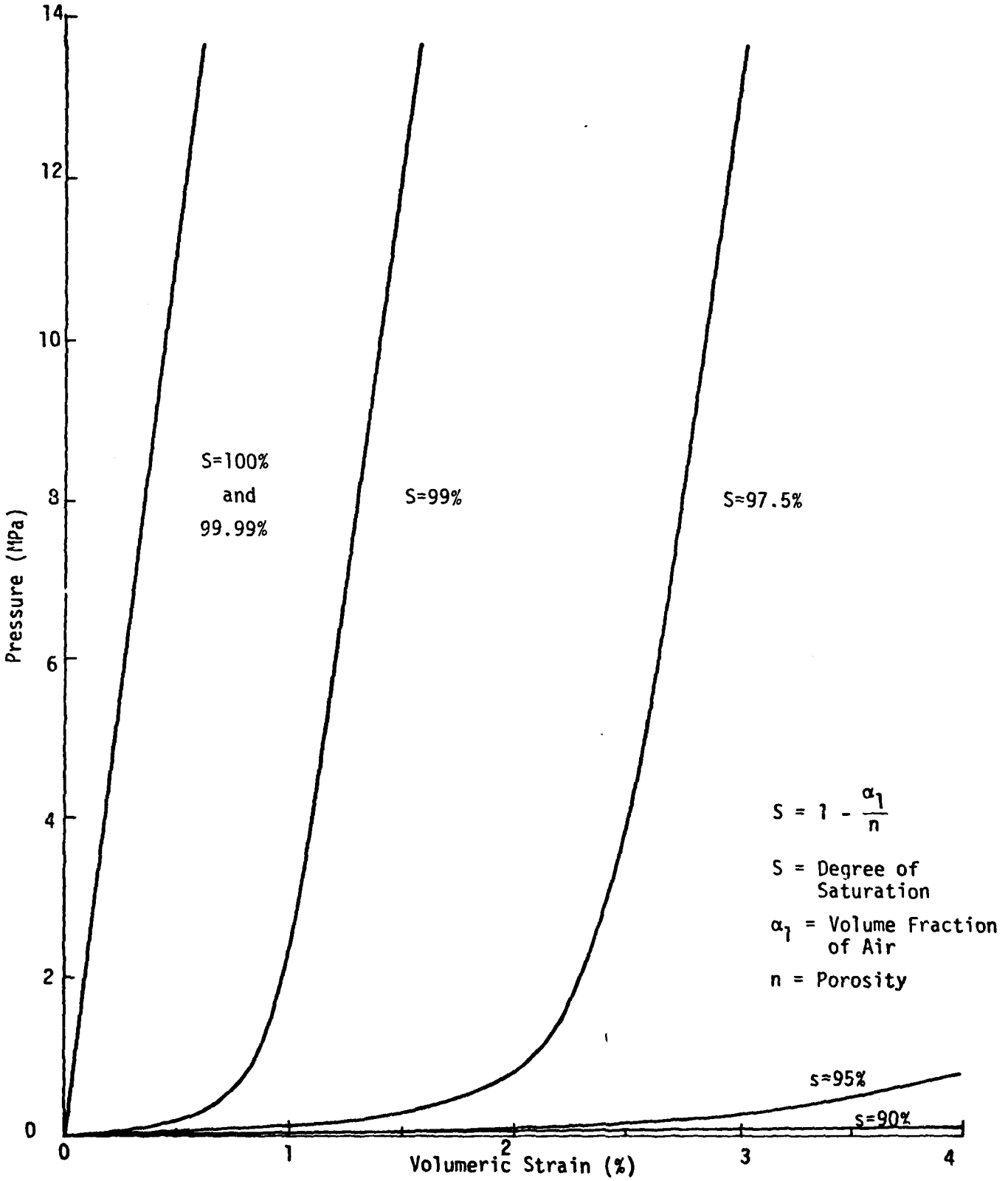

Figure 5.3. Pressure-volume relations in air-water phase for varying degrees of saturation.

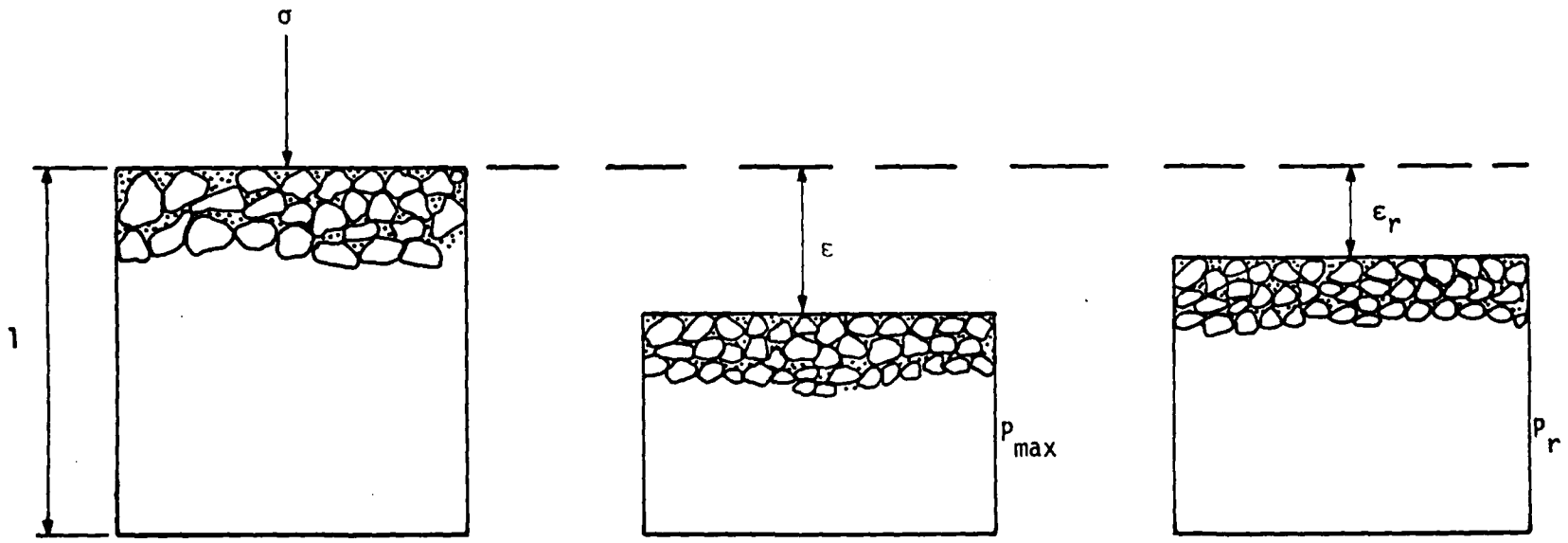

Assumptions:

Incompressible grains
Compressible fluid (nonlinearly ealstic)
Skeleton compressibility results from intergranular

ε = Maximum strain on loading = Maximum skeleton strain

ε_r = Residual skeleton strain at which the skeleton carries no stress

n = Porosity

P_{max} = Maximum fluid pressure = $f(\frac{\varepsilon}{n})$

P_r = Residual fluid pressure = $f(\frac{\varepsilon_r}{n})$

Figure 5.4. Concepts for a simple model for liquefaction in uniaxial strain.

McC rmick Ranch sand is given in Figure 5.5. The composite fluid-skeleton is loaded to a peak total stress above 28 MPa. Upon unloading, the skeleton, because of residual strain, reaches zero intergranular stress while the fluid phase still carries over 13 MPa. At this stage, the soil skeleton breaks down and further unloading occurs in a heavy fluid composed of grains and water. In a fully saturated soil, liquefaction would occur at lower stress levels. The example serves to illustrate both the mechanism of liquefaction and the importance of the air-water phase compressibility.

It is the relative compressibility between the soil skeleton and the air-water phase which controls whether liquefaction occurs and the stress levels needed to cause it. The relative compressibility can be affected by the skeleton stiffness on the one hand or the air-water phase compressibility on the other. Whenever the relative compressibility is such that the skeleton remains elastic (i.e., rebounds fully on unloading) or is stiffer than the air-water phase, liquefaction will not occur.

The simple model for liquefaction in a load/unload cycle of uniaxial strain will not predict liquefaction under shear conditions, just as simple shear models will not predict liquefaction in the uniaxial case just described. In order to provide a good prediction of pore pressure buildup and the potential for liquefaction under general stress paths, it is necessary to have a model for the grain matrix which includes a good model of deviatoric (shear) strain-volumetric strain interaction encompassing the entire range of potential stress paths which can be encountered in dynamic problems. None of the models in use in the blast and shock community today include deviatoric-volumetric strain interaction. The cap model, for example supresses volume change at the intersection of the cap and the standard yield surface. Models commonly need for earthquake related problems do not include this general capability either. Critical state models, although not generally in use for dynamic problems, to account for volume decrease or increase which is known to physically occur.

5.2.4 Conclusions and Recommendations

The key points that must be considered for effective stress modeling are, first, the importance of flow during the time of interest and its

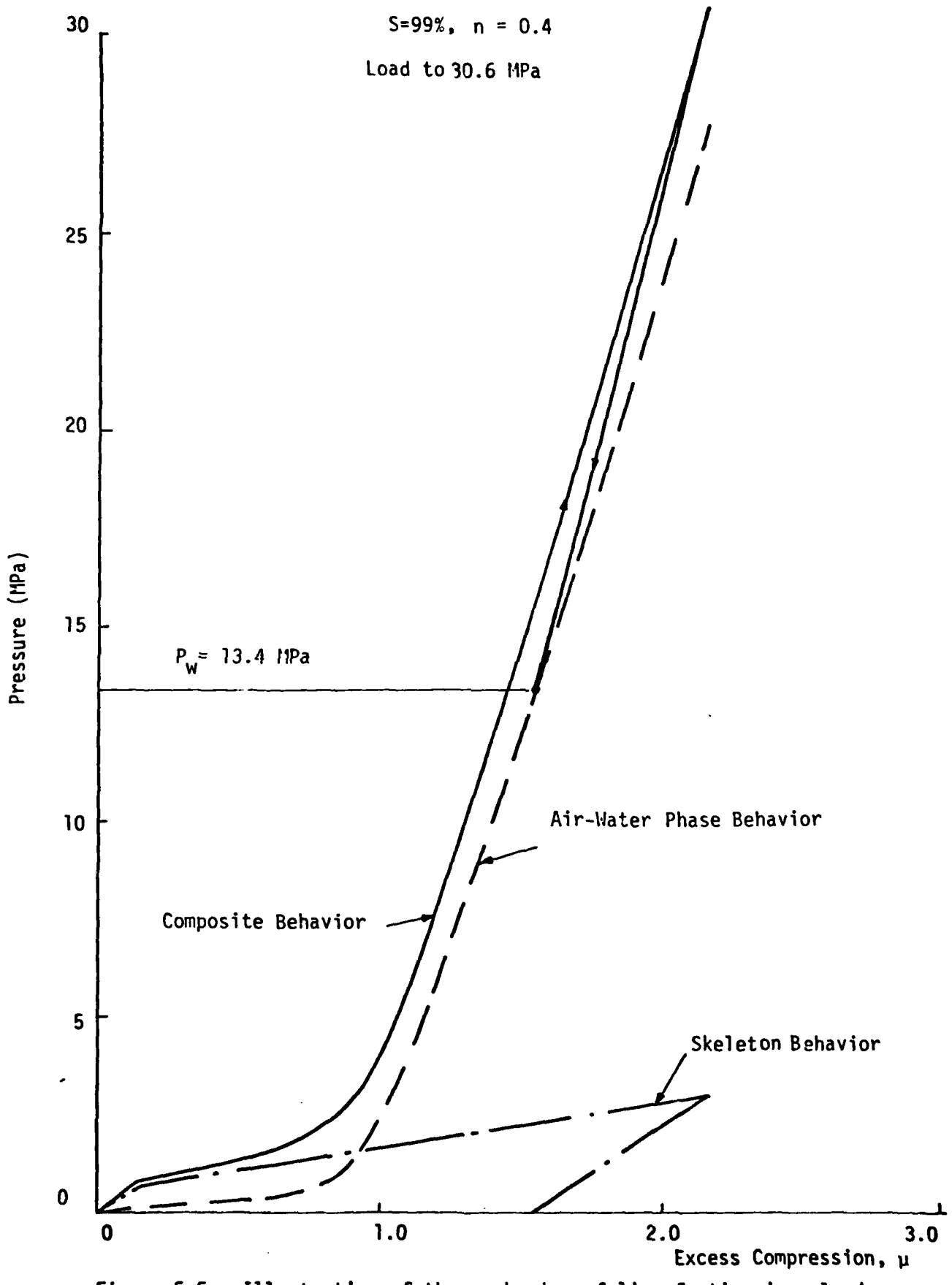

Figure 5.5. Illustration of the mechanism of liquefaction in a load - unload uniaxial . .rain cyc' ..

influence on effective stresses, and second, the ability of the grain matrix model to deal with deviatoric-volumetric strain coupling.

If flow occurs and causes a reduction in pore pressure during the time of interest, then those properties of the material which are dependent upon integranular or effective stress, especially strength, will change. In addition, the potential for liquefaction will also be affected. As discussed previously, Ishihara's work suggests that, even in dynamic problems associated with blast and shock, flow and resulting pore pressure changes may well be important. In fact, Ishihara also points out that for earthquake-related problems where frequencies are lower flow may not be important. It is essential that this position be evaluated.

The second major point bears on the ability of our models to deal with liquefaction phenomena. In order to do so, it is necessary to have a good model for the grain matrix which includes deviatoric-volumetric strain coupling over the entire credible set of stress and strain paths ranging from simple shear through hydrostatic compression in multiple loading cycles. In addition, it is necessary for a good air-water phase model to account for the effect of air-water phase compressibility on liquefaction. Finally, it is essential to have flow in the model to account for pore pressure changes which might affect intergranular stresses, as well as any pore pressure changes that would occur over a longer period of time after liquefaction has occured. This is necessary in order to predict ground motions as well as analyze instability of large bodies of soil due to liquefaction.

Regarding ground motion prediction, Figure 5.2 from Baladi indicated that the intergranular stress on unloading went to zero while there was still pore pressure in the fluid. At this point it is expected, physically, that the grain matrix will break down and the resulting mixture will be a heavy fluid consisting of grains and water. In a ground motion problem, whether it be blast and shock or earthquake-related, there may still be important waves propagating through the media. These waves will be propagating through a heavy fluid and not through a solid, as we normally assume. Hence, even for this part of the wave propagation problem, it is necessary to have a good model which considers flow and as appropriate, will

degenerate to a heavy fluid under proper physical conditions. One model that we are aware of which contains flow is due to Hart (Ref. 23).

Hart's model couples thermal, mechanical and fluid flow behavior. His treatment of flow appears to be reasonable. The model, however, does not include a modern representation for the grain matrix. He simply uses an elastic-perfectly plastic model. In order to make it applicable to most of the problems of interest in soils, the grain matrix model must be updated to include nonlinearity before failure, as well as an improved model of deviatoric-volumetric strain coupling. In addition, Hart's model must be updated to include a better air-water phase component model.

In summary, there is evidence to suggest that it is important to model effective stress in ground motion problems. This modeling must encompass more than just the modeling of effective stress. It is also necessary to model flow. The model must recognize the transition from a relatively solid tri-component medium to a heavy fluid when liquefaction occurs, subsequently track waves which propagate through this heavy fluid, and finally, track long term recovery to a stable state. There are bits and pieces available for such a model in various places. All of the bits and pieces however, have shortcomings. A program to overcome these shortcomings will be developed in the next phase of this project.

The limited experience that is available on the use of effective stress models in computations comes from Baladi's work and from some work performed at ARA using Hart's model. This work indicates that there are not major computer requirements associated with the incorporation of effective stress information or flow. Core requirements might increase by 10 to 15 percent in order to accommodate additional equation of state variables, as well as a few additional response variables. Computation time might increase on the order of 20 to 25 percent. It is believed that these additional requirements are relatively minor when compared with the improved predictions and analysis which would be available from the use of effective stress models.

6.0 SUMMARY

This report briefly describes the status of our research into the dynamic behavior of soils. With the initial year's effort at a close, we are continuing as outlined in the proposal for continued study.

The soil element model has been developed and will serve as a basic tool for studying the merits and applicability of various constitutive laws. This computer program will continue to improve as additional features are added.

Several two-dimensional calculations have been performed in order to better understand insitu soil behavior. The effect of varying material models was investigated as well as establishing some "best-fit" models, and this effort will be continued.

REFERENCES

1. Baladi, G.Y. and S. A. Akers, Constitutive Properties and Material Model Development for Marine Sediments in Support of The Subseabed Disposal Program, Sponsored by Sandia National Laboratories, Conducted by U.S. Army Engineer Waterways Experiment Station, Structures Laboratory, Vicksburg, Mississippi, March 1981.

2. Pyke, Robert, "Nonlinear Soil Models for Irregular Cyclic Loadings", Journal of the Geotechnical Engineering Division, ASCE, Vol. 105, No. GT6, June 1979.

3. Hill, R., The Mathematical Theory of Plasticity, Oxford University Press, New York, 1950, Reprinted 1964.

4. Kelly, M. and Baird, G. T., DSOT Geotechnical Data Report, Eric H. Wang Civil Engineering Research Facility, University of New Mexico, In-House Report prepared for Air Force Weapons Laboratory, Kirtland Air Force Base, June 1978.

5. Bratton, J. L. and Higgins C. J., "Measuring Dynamic In-Situ Geotechnical Properties", Proceedings of the ASCE Geotechnical Engineering Division, Specialty Conference on Earthquake Engineering and Soil Dynamics, held in Pasadena, California, Vol. I, June 1978.

6. Shinn, J. D., II and Brown, R, Cylindrical In-Situ Test at Dry Lake Valley, Nevada (CIST 23), AFWL-TR, Air Force Weapons Laboratory, Kirtland Air Force Base, July 1981.

7. Thomas, J. W., "On CIST Cavity Pressures", Memo, Technology and Applications Branch Civil Engineering Research Division, Air Force Weapons Laboratory, Kirtland Air Force Base, February 1980.

8. Applied Theory, Inc., The AFTON 2A Computer Code Revised User's Manual Part I. Theory and Explanations, AFWL-TR-75-111, Part I, Air Force Weapons Laboratory, Kirtland Air Force Base, June 1976.

9. Rinehart, J. S., Stress Transients In Solids, Hyperdynamics, Santa Fe, New Mexico, 1975.

10. Zelasko, J. S., "Son of MIDDLE-GUST", presentation in Late-Time Working Group Session, U.S. Army Waterways Experiment Station.

11. Wroth, C. P., "In-Situ Measurement of Initial Stresses and Deformation Characteristics", Proceedings of the Conference on In-Situ Measurements of Soil Properties, Vol. II, American Society of Civil Engineering, NY, NY, June 1975.

12. Anderson, D. G. and Espana, C., Evaluation of In-Situ Testing Methods for High Amplitude, Dynamic Property Determination, NP-920, Electrical Power Research Institute, Palo Alto, CA, November 1978.

13. Lodde, P.E., Review of Wave Propagation Techniques for Determining the In-Situ High-Amplitude Shear Behavior of Geologic Materials, AFWL-TR-79-152, Air Force Weapons laboratory, Kirtland AFB, NM, September 1980.

14. Miller, R. P. and Brown, F. R., "Shear Modulus Determination of Soils by In Situ Methods for Earthquake Engineering", Proceedings of the International Conference on Microzonation for Safer Construction, Research and Application, Vol. 2, pp. 545-558, Seattle, Washington, 1972.

15. Terzaghi, K., Theoretical Soil Mecnanics, Wiley, New York, 1943.

16. Baladi, G. Y., An Effective Stress Model for Ground Motion Calculations, Technical Report SL-79-7, U.S. Army Engineer Waterways Experiment Station, Vicksburg, MS, September 1979.

17. Ishihara, Kenji, "Propagation of Compressional Waves in a Saturated Soil", Proceedings, International Symposium on Wave Propagation and Dynamic Properties of Earth Materials, University of New Mexico Press, Albuquerque, NM, August 23-25, 1967.

18. Wood, A. B., A Textbook of Sound, G. Bell and Sons, London, 1930.

19. Lyakhov, G. M., "Shock Waves in the Ground and the Liquefaction of Water Saturated Sand", (Translation), Zhurnal Prikladnoy Medheniki I Tekhnicheskoy Fiziki, No. 1, pp. 38-46, 1961 (FTD-HS-108-71).

20. Barends, F. B. J., "The Compressibility of An Air-Water Mixture in a Porous Medium", IGM Mededalingen, Part XX, No. 2, Delft Soil Mechanics Laboratory, The Netherlands, August 1979.

21. Lyakhov, G. M. and Ployakova, N. I., Waves in Solid Media and Loads on Structures, Volny v Plotnykh Sredakh i Negruzki na Sooruzheniya, 1967 (FTD-MT-24-1137-71).

22. Rischbieter, F. "Soil Liquefaction - A Survey of Research", Proceedings, Fifth International Symposium on Military Applications of Blast Simulation, Stockholm, Sweden, May 1977.

23. Hart, R. D., A Fully Coupled Thermal-Mechanical-Fluid Flow Model for Nonlinear Geologic Systems, Ph.D. Thesis, University of Minnesota, March 1981.

APPENDIX A

Literature Survey

The following is a list of those references, by category, which were found to be useful or particularly important.

A.1 Constitutive Modeling

A.1.1 Review Papers

Armen, H., "Assumptions, Models, and Computational Methods for Plasticity", Computers and Structures, Vol. 10, pp. 161-174, 1979.

Desai, C. S. and Saxena, S. K., Implementation of Computer Procedures and Stress-Strain Laws in Geotechnical Engineering, Symposium Proceedings, Acorn Press, Durnam, N.C., Chicago, 1981.

Hardin, Bobby O., "Tne Nature of Stress-Strain Behavior for Soils" ASCE Sepc. Conf. Earthquake Engineering and Soil Dynamics, Vol. 1, pp. 3-90, Pasadena, CA, June 1978.

Marti, J. and Cundall, P. A., Constitutive Laws for Dynamic Modelling of Soils, EOARD-TR-80-7, Dames and Moore Job No. 11645-001-60, 1980.

Nelson, I., Baron, M. L. and Sandler, I., "Mathematical Models for Geological Materials for Wave-Propagation Studies" Chapter 13 of Shock Waves and the Mechanical Properties of Solids, Syracuse University Press, Syracuse N.Y., 1971.

Read, H. E., Evaluation of Material Models for MX siting Vol. 1: Soil Models, Final Report to AFBMO (Ballistic Missile Office) by Systems, Science, and Softward (S^3), La Jolla, California, 1979.

Schuster, S. H. and Isenberg, J., Equations of State for Geologic Materials, DNA 2925Z, Agbabian Associates, L.A. California, September 1972.

Yong, R. K. and Ko, H-Y (Editors), Limit Equilibrium, Plasticity and Generalized Stress-Strain in Geotechnical Engineering, Workshop Proceedings, McGill University, May 28-30, 1980, Sponsored by NSF and NSERC, ASCE, 1981.

A.1.2 Specific Models

a) Elasticity/Plasticity

Boresi, A., Sidebottom, O., Seely, F. B. and Smith, J., Advanced Mechanics of Materials, Third Edition, John Wiley, N.Y., 1932.

Bisplinghoff, R. L., Mar, J. W. and Pian, T. H., Statics of Deformable Solids, Massachusetts Institute of Technology, 1963.

Dougill, J. W., "Some Remarks on Path Independence in the Small in Plasticity", Quarterly of Applied Mechanics, October 1975, pp. 233-243, 1975.

Drucker, D. C., Gibson, R. E. and Henkel, D. J., "Soil Mechanics and Work Hardening Theories of Plasticity", Transactions ASCE, Vol. 122, pp. 338-346, 1957.

Drucker, D. C. and Prager, W., "Soil Mechanics and Plastic Analysis or Limit Design", Quarterly of Applied Mathematics, Vol. 10, pp. 157-165, No. 2.

Hill, R., The Mathematical Theory of Plasticity, Oxford University Press, London, 1950.

Isenberg, J., Nuclear Geoplosics, Part II: Mechanical Properties of Earth Materials, Prepared for DNA, Washington, by Agbabian Associates, El Segundo, CA, November 1972.

Koiter, W. T., "Stress-Strain Relations, Uniqueness and Variational Theorems for Elastic-Plastic Materials with a Singular Yield Surface", Quarterly of Applied Methametics, Vol. II, pp. 350-354, 1953.

b) "Curve-Fitting Models"

Duncan, J. M. and Chang, C. Y., "Nonlinear Analysis of Stress and Strain in Soils" Journal of the Soil Mechanics and Foundations Division, ASCE, Vol. 96, No. SM5, pp. 1629-1653, September 1970.

Pyke, Robert, "Nonlinear Soil Models for Irregular Cyclic Loadings" Journal of the Geotechnical Engineering Division, Vol. 105, No. GT 6, pp. 715-726, Proc. Paper No. 14642, June 1979.

c) Cap Model

Baladi, G. Y. and Akers, S. A., Constitutive Properties and Material Model Development for Marine Sediments in Support of the Subseabed Disposal Program, U.S. Army Engineer Waterways Experiment Station, Vicksburg, Miss., for Sandia National Laboratories, March 1981.

Baladi, G. Y., An Effective Stress Model for Ground Motion Calculations U.S. Army Engineer Waterways Experiment Station, Vicksburg, Miss. TR SL-79-7, September 1979.

Baladi, G. Y., An Elastic-Plastic Constitutive Relation for Transverse-Isotropic Three-Phase Earth Materials, U.W. Army Engineer Waterways Experiment Station, Vicksburg, Miss., August 1978.

DiMaggio, F. L. and Sandler, I. S., "Material Model for Granular Soils", Journal of the Engineering Mechanics Division, ASCE, Vol. 97, No. EM3, pp. 935-950, 1971.

Rubin, D. and Sandler, I., Development of a High Pressure Cap Model for Use in Computations of Ground Shock from Subsurface Explosions, Weidlinger Associates for DNA, 1977.

Sandler, I. S., Material Modeling Based on CIST Test and Laboratory Data, Report DNA 3970F Weidlinger Associates, N.Y., NY, March 1976.

Sandler, I.S., DiMaggio, F. L. and Baladi, G. Y., "Generalized Cap Model for Geological Materials" Journal of the Geotechnical Engineering Division, ASCE, Vol 102, No. GT7, pp. 683-699, 1976.

Sandler, I.S. and Rubin, D., Ground Shock on Alluvial Geologies; Study of the Effect of Cementation Breakdown and Pore Air Phenomena, Weidlinger Associates, N.Y., NY, 1980.

Schofield A. and Wroth, P., Critical State Soil Mechanics, McGraw-Hill Book Company, 1968.

d) Lade's Model

Lade, Poul V., "Elasto-Plastic Stress-Strain Theory for Cohesionless Soil with Curved Yield Surfaces", Int. J. Solids Structures, Vol. 13, pp. 1019-1035, 1977.

Lade, Poul V., "Prediction of Undrained Behavior of Sand" Journal of the Geotechnical Division, ASCE, Vol. 104, No. GT6, pp. 721-735, June 1978.

Lade, Poul V. and Duncan, J. M., "Elasto-Plastic Stress-Strain Theory for Cohesionless Soil", Journal of the Geotechnical Engineering Division, ASCE, Vol. 101, No. GT10, pp. 1037-1053, October 1975.

Lade, Poul, V. and Musante, H. M., "Three Dimensional Behavior of Remolded Clay", Journal of the Geotechnical Engineering Division, ASCE, Vol. 104, No. GT2, pp. 193-209, February 1978.

e) Prevost's Model

Prevost, J. H., "Plasticity Theory for Soil Stress-Strain Behavior", Journal of the Engineering Mechanics Division, ASCE, Vol. 104, No. EM5, October 1978.

Prevost, J. H., "Mathematical Modeling of Soil Stress-Strain-Strength Behavior" Proceedings, Third International Conference on Numerical Methods in Geomechanics, Aachen, pp. 347-361, 26 April, 1979.

Prevost, J. H. and Hoeg, K., "Soil Mechanics and Plasticity Analysis of Strain Softening", Geotechnique, Vol. 25, No. 2, pp. 279-297, 1975.

Prevost, J. H. and Hoeg, K., "Effective Stress-Strain-Strength Model for Soils", Journal of the Geotechnical Engineering Division, ASCE, Vol. 101, No. GT3, March 1975.

f) Endochronic Models

Bazant, Z. and Krizek, R., "Endochronic Constitutive Law for Liquefaction of Sand", Journal of the Engineering Mechanics Division, ASCE, Vol. 102, EM2, pp. 225-238, April 1976.

Cuellar, V., Bazant, Z., Krizek, R. and Silver, M., "Densification and Hysteresis of Sand Under Cyclic Shear" Journal of the Geotechnical Engineering Division, ASCE, Vol. 103, No. GT5, pp. 399-416, May 1977.

Dunger, R. and Nuh, S., "Endochronic-Critical State Models for Sand", Journal of the Engineering Mechanics Division, ASCE, Vol 106, No. EM6, October 1980.

Hsieh, B. J., "On the Uniqueness and Stability of Endochronic Theory", Transactions of the ASME, Vol. 47, December 1980.

Read, H. E. and Valanis, K. C., An Endochronic Constitutive Model for General Hysteretic Response of Soils, Systems, Science and Software, San Diego, CA, EPRI Report NP-957, Project 810, January 1979.

Read, H. E. and Valanis, K. C., New Endochronic Plasticity Models for Soils, Systems, Science and Software, La Jolla, CA, Final Report to EPRI, Report NP 1388, April 1980.

Valanis, K. C. and Read, H. E., "A Theory of Plasticity for Hysteretic Materials - I: Shear Response" Computers and Structures, Vol. 8, pp. 503-510, 1978.

g) Miscellaneous Modeling

Dafalias, Y. F. and Popov, E. P., "A Model of Non-Linearity Hardening Materials for Complex Loading", ACTA Mech., Vol. 21, pp. 173-192, 1975.

Davis, R. O. and Mullenger, G., Rate-Type Fluid Model for Granular Media with a Critical State, AFWL-TR-77-143, DNA, Washington, D.C., 1978.

Finn, W. D. L., Lee, K. W. and Martin, G. R., "An Effective Stress Model for Liquefaction", Journal of the Geotechnical Engineering Division, ASCE, Vol. 103, No. GT6, pp. 517-533, June 1977.

Mroz, Z, Norris, V. A. and Zienkiewicz, O. C., "Application of an Anisotropic Hardening Model in the Analysis of Elasto-Plastic Deformation of Soils" Geotechnique 29, No. 1, pp. 1-34, 1979.

Mroz, Z., "On the Description of Anisotropic Work Hardening", J. Mech. Phys. Solids, Vol 15, pp. 163-175, 1967.

Zienkiewicz, O. C., Humpheson, C. and Lewis R. W., "Associated and Non-Associated Visco-Plasticity and Plasticity in Soil Mechanics" Geotechnique, Vol 25, No. 4, pp. 671-689, 1975.

A.1.3 Calculational Studies/Modeling

Bathe, K. J., Ozdemir, H. and Wilson, E. L., Static and Dynamic Geometric and Material Nonlinear Analysis, Structural Engineering Laboratory, University of California, Berkeley, California, February 1974.

Blouin, S. E. and Wolfe, S. H., Analysis of Explosively Generated Ground Motions using Fourier Techniques, U.S. Army Cold Regions Research and Engineering Laboratory, Hanover, N.H. (CRREL Report 76-28) August 1976.

Bratton, J. L., Effects of Material Properties on Cylindrical Wave Propagation in Geologic Materials, AFWL-TR-77-184, CERF, University of New Mexico, Albuquerque, NM, October 1978.

Cooper, H. F., Jr., On the Application of Finite Difference Methods to Study Wave Propagation in Geologic Materials, AFWL-TR-70-171, April 1971.

Davis, R. O., Jr., One-Dimensional Wave Propagation in Bilinear Media, E. H. Wang CERF, AFWL-TR-70-117, December 1970.

Desai, C. S., Applications of the Finite Element Method in Geotechnical Engineering, Proc. WES Symp. Appl. Finite Element Method Geotech. Eng. U.S. Army Engineer Waterways Experiment Station, Vicksburg, Miss., 1972.

Desai, C. S. and Christian, J. T., Numerical Methods in Geotechnical Engineering, McGraw-Hill Book Company, 1977.

Fedock, J. J., Application of a Soil Cap Model to Ground Motion Analysis, AFWL-TR-77-134, University of New Mexico for DNA, 1978.

Isenberg, J., Vaughan, D. K. and Sandler, I., Non-Linear Soil-Structure Interaction, EPRI NP-945 (Project 810-2), Weidlinger Associates, Menlo Park, CA, December 1978.

Lodde, P. F., CIST 19 Analysis and Derivation of Dynamic Properties for Misers Bluff Site, AFWL-TR-78-252, CERF for AFWL/DNA, University of New Mexico, Albuquerque, NM, August 1979.

Prevost, J. H., Cuny, B., Hughes, T. J. R. and Scott, R. F., "Offshore Gravity Structures: Analysis", Journal of the Geotechnical Engineering Division, ASCE, Vol. 107, No. GT2, pp. 143-165, February 1981.

Sandler, I. and Rubin, D., A Modular Subroutine for the Cap Model, DNA001-75-C-0076, Weidlinger Associates, NY, NY, January 2, 1976.

Whitman, L. and Wright, J., Tensile Behavior of Geologic Material in Ground Shock Calculations DNA 001-75-C-0076, Weidlinger Associates, NY, NY, June 1975.

A.2 Insitu Behavior

A.2.1 Explosive Loading

Amend, J. H., III, Ullrich, G. W. and Thomas, J. N., Have-Host Cylindrical In-Situ Test (CIST) Data Analysis and Material Model Report, AFWL-TR-74-136, AFWL, KAFB, NM, October 1977.

Cooper, H. F., Jr. and Blouin, S. E., "Dynamic In-Situ Rock Properties from Buried High Explosive Arrays, Dynamic Rock Mechanics, Twelfth Symposium on Rock Mechanics, American Institute of Mining, Metallurgical, and Petroleum Engineers, Inc., N.Y., 1970.

Davis, S. T., Capt., General Test Plan for the Cylindrical In-Situ Test (CIST), AFWL-TR-74-136, AFWL, KAFB, NM, June 1974.

Hadala, P. F., Effect of Constitutive Properties of Earth Media on Outrunning Ground Shock from Large Explosions, U.S. Army Engineer Waterways Experiment Station, Vicksburg, Miss, TR S-73-6 August, 1973.

Higgins, C. J., Johnson, R. L. and Triandafilidis, G. E., The Simulation of Earthquake-Like Ground Motions with High Explosives, Report No. CE-45 (78) NSF-507-1 on NSF Grant ENG 75-21580, The University of New Mexico, Albuquerque, NM, July 1978.

Fedorovski, V. G., "Expansion of a Cylindrical Borehole in an Elastoplastic Medium", Translated from Osnovania, Fundameny i Mekhanika Gruntov, Plenum Publishing Corp., NY, NY, No. 2, pp. 28-30, March-April 1972.

Johnson, J. N., Dropek, R. K. and Schmitz, D. R., Simulation of the Load-Unload Paths Experienced by Rock in the Vicinity of Buried Explosions, DNA 4841F Terra Tek, Inc., Salt Lake City, Utah, December 1977.

Lyakhov, G. M. and Polyakova, N. I., Waves in Solid Media and Loads on Structures, (Translation) Volny v Plotnykh Sredakh i Nagruzki Na Soorruzheniya, pp. 1-232, 1967.

Trulio, J. G. and Vincent, C. T., "Trajectory Analysis, An Aid in Defining the MX System Ground Motion Part 2: Plan for a Key Proof Test: 10-TON HE Event in Dry Alluvium", ATR-80-52-1, for AFWL, March 1980.

Workman, J. W., Trulio, J. G. and Stokes, E. S., "Trajectory Analysis, an Aid in Defining the MX System Ground Motion, Part I: Uncertainty in Strain Paths form Observed Spherically Symmetric Motion and Methods for Determining Strain Paths in Axisymmetric Fields of Motion", ATR-80-52-1, for AFWL, March 1980.

Workman, J. W., Trulio, J. G. and Stokes, E. S., Modeling the Behavior of Geologic Materials in Explosive Field Events, Applied Theory, Inc., Las Angeles, California, AFWL-TR-80-66, January 1981.

A.2.2 Shear Testing

Arango, I. and Moriwaki, Y., "Comparison Between In-Situ and Laboratory-Determined Dynamic Shear Velocity and Modulus", Draft to ASCE, 1977.

Anderson, D. G. and Espana, C., Evaluation of the In Situ Testing Methods for High Amplitude, Dynamic Property Determination, Final Report to EPRI, Report No. NP-920 by Fugro, Inc., Long Beach, CA, November 1978.

Lodde, P. F., Review of Wave Propagation Techniques for Determining the In-Situ High Amplitude Shear Behavior of Geologic Materials, AFWL-TR-79-152, University of New Mexico, Albuquerque, NM, September, 1980.

Pyke, R., "Measurement of Dynamic Soil Properties-Discussion", ASCE Geotechnical Engineering Division Specialty Conference on Earthquake Engineering and Soil Dynamics, Pasadena, CA, June 1978.

Wilson, S. D., Brown, F. R., Jr. and Schwartz, S. D., "In-Situ Determination of Dynamic Soil Properties" Dynamic Geotechnical Testing, ASTM STP 654, American Society for Testing and Materials, pp. 295-317, 1978.

A.3 Laboratory Testing

Arthur, J. R. F., Chua, K. S. and Dunstan, T., "Dense Sand Weakened by Continuous Principal Stress Direction Rotation", Geotechnique, Vol. 29, No. 1, pp. 91-96, 1979.

Arthur, J. R. F., Chua, K. S. and Dunstan, T., "Induced Anisotropy in a Sand", Geotechnique, Vol. 27, No. 1, pp. 13-30, 1977.

Arthur, J. R. F. and Menzies, B. K., "Inherent Anisotropy in a Sand", Geotechnique, Vol. 22, No. 1, pp. 115-128, 1972.

Bishop, A. W. and Henkel, D. J., The Measurement of Soil Properties in the Triaxial Test, Edward Arnold Publishers, Ltd., London, 1957.

Bjerrum, L. and Landva, A., "Direct Simple-Shear Tests on a Norwegian Quick Clay", Geotecnnique, Vol. 16, pp. 1-20, January 1966.

Green, G. E. and Bishop, A. W., "A Note on the Drained Strength of Sand Under Generalized Strain Conditions", Geotechnique, Vol. 19, No. 7, pp. 144-149.

Hardin, B. O. and Drnevich, V. P., "Shear Modulus and Damping in Soils: Measurement and Parametric Effects", Journal of the Soil Mechanics and Foundations Division, ASCE, Vol 98, No. SM6, pp. 603-624, June 1972.

Hardin, B. O. and Richart, F. E., "Elastic Wave Velocities in Granular Soils", Journal of the Soil Mechanics and Foundations Division, ASCE, Vol. 89, No. SM1, pp. 33-65, February 1963.

Hirschfeld, R. C. and Poulos, S. J., "High-Pressure Triaxial Tests on a Compacted Sand and an Undisturbed Silt", Laboratory Shear Testing of Soils, ASTM Special Technical Publication, No. 361, September 1963.

Jackson, J. G., Jr., Ehrgott, J. Q. and Rohani, B., "Loading Rate Effects on Compressibility of Sand", Journal of the Geotechnical Engineering Division, ASCE, Vol. 106, No. GT8, pp. 839-852, August 1980.

Jackson, J. G., Jr., "Material Response Characterization", Miscellaneous Paper S-77-11, U.S. Army Engineer Waterways Experiment Station, Vicksburg, Miss., August 1977

Lee, K. L., and Seed, H. B., "Drained Strength Characteristics of Sand", Journal of the Soil Mechanics and Foundations Division, ASCE, Vol. 93, No. SM6, pp. 177-141, November 1967.

Prevost, J. H., "Undrained Shear Tests on Clays", Journal of the Geotechnical Engineering Division, ASCE, Vol. 105, No. GT1, pp. 49-64, January 1979.

Pyke, R., "Some Effects on Test Configuration on Measured Soil Properties Under Cyclic Loading", ASTM Geotechnical Testing Journal, Vol. 1, No. 3.

Silver, M. L. and Seed, H. B., "Deformation Characteristics of Sands Under Cyclic Loading" Journal of Soil Mechanics and Foundations Division, ASCE, Vol. 97, No. SM8, pp. 1081-1098, August 1971.

Youd, L. T., "Compaction of Sands by Repeated Shear Straining", Journal of the Soils Mechanics and Foundations Division, ASCE, Vol. 98, No. SM7, pp. 709-725, July 1972.

Zelasko, J. S., Comparisons of MAP-Relevant Material Models in Laboratory Coordinates, U.S. Army Engineer Waterways Experiment Station, Soils and Pavements Laboratory, Vicksburg, Miss, DNA, 1977.

APPENDIX B

Definitions and Notation

B.1 Coordinate System

For the soil element model code, a consistant set of coordinate axes has been maintained as much as possible. Z-axial, R-radial, and T-tangential, have been used as subscripts.

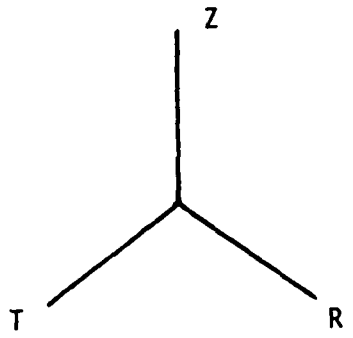

The stress and strain tensors for this system are then:

$$[\sigma] = \begin{bmatrix} \sigma_{RR} & \sigma_{RZ} & \sigma_{RT} \\ \sigma_{RZ} & \sigma_{ZZ} & \sigma_{ZT} \\ \sigma_{RT} & \sigma_{ZT} & \sigma_{TT} \end{bmatrix} \qquad [\varepsilon] = \begin{bmatrix} \varepsilon_{RR} & \varepsilon_{RZ} & \varepsilon_{RT} \\ \varepsilon_{RZ} & \varepsilon_{ZZ} & \varepsilon_{ZT} \\ \varepsilon_{RT} & \varepsilon_{ZT} & \varepsilon_{TT} \end{bmatrix}$$

Summation notation is occasionally used here to minimize cumbersome equations.

B.2 Invariants

Stress and strain invariants are useful in that they describe the stress/strain state in quantities which are independent of coordinate axes configuration. Stress invariants J_1, J_2, and J_3 are defined here, strain invariants I_1, I_2, and I_3 follow similarly.

The three invariants are the coefficients of the cubic equation:

$$\sigma^3 + J_1\sigma^2 + J_2\sigma + J_3 = 0$$

where σ_1, σ_2, and σ_3 are the roots of the cubic, also known as principal stresses, and:

$$J_1 = \sigma_{RR} + \sigma_{ZZ} + \sigma_{TT}$$

$$J_2 = \begin{vmatrix} \sigma_{RR} & \sigma_{RZ} \\ \sigma_{RZ} & \sigma_{ZZ} \end{vmatrix} + \begin{vmatrix} \sigma_{RR} & \sigma_{RT} \\ \sigma_{RT} & \sigma_{TT} \end{vmatrix} + \begin{vmatrix} \sigma_{ZZ} & \sigma_{ZT} \\ \sigma_{ZT} & \sigma_{TT} \end{vmatrix}$$

$$J_3 = \begin{vmatrix} \sigma_{RR} & \sigma_{RZ} & \sigma_{RT} \\ \sigma_{RZ} & \sigma_{ZZ} & \sigma_{ZT} \\ \sigma_{RT} & \sigma_{ZT} & \sigma_{TT} \end{vmatrix}$$

B.3 Deviatoric Stress/Strain

The stress deviator tensor is defined as:

$$[S_i] = \begin{bmatrix} (\sigma_{RR} - P) & \sigma_{RZ} & \sigma_{RT} \\ \sigma_{RZ} & (\sigma_{ZZ} - P) & \sigma_{ZT} \\ \sigma_{RT} & \sigma_{ZT} & (\sigma_{TT} - P) \end{bmatrix}$$

where P = pressure = $\dfrac{\sigma_{RR} + \sigma_{ZZ} + \sigma_{TT}}{3}$

The deviator tensor is also refered to as $[S_{ij}]$.

J_1', J_2' and J_3; are the invariants of the stress deviator tensor. A convenient derivable expression in terms of the full stress tensor is:

$$J_2' = \sigma_{RR}^2 + \sigma_{RR}\sigma_{TT} + \sigma_{TT}^2 + \sigma_{RZ}^2 + \sigma_{ZT}^2 + \sigma_{RT}^2$$

Invariants of the strain deviator tensor, I_1', I_2' and I_3', follow similarly.

B.4 Volume Behavior

As stated above P denotes mean confining stress, or pressure.

Volumetric strain, ε_{KK}, is defined as:

$$\varepsilon_{KK} = \varepsilon_{RR} + \varepsilon_{ZZ} + \varepsilon_{TT} = \frac{V - V_o}{V_o}$$

ε_{KK} is also known as the cubical dilitation, or the first strain invariant.

The excess compression, μ, which is used in the AFWL model, is defined as:

$$\mu = \frac{\varepsilon_{KK}}{\varepsilon_{KK} + 1} = \frac{\rho - \rho_o}{\rho}$$

where ρ = density, and

ρ_o = initial density

B.5 Modulii

In general, only three elastic modulii are used for defining elastic behavior in this study:

K = Bulk Modulus = P / ε_{KK}

G = Shear Modulus = $(\sigma_{ZZ} - \sigma_{RR}) / (\varepsilon_{ZZ} - \varepsilon_{RR})$

$$\nu = \text{Poisson's Ratio} = \frac{3K - 2G}{2(3K + G)}$$

B.6 Sign Convention

The SEM uses a sign convention which is typical of finite difference/finite element codes which are in use for geotechnical engineering. Tension is considered positive for the stress/strain tensor quantities and compression is positive when describing volume behavior quantities, such as mean confining stress. This is somewhat confusing to follow, but necessary if the models which are developed with this program are to be later implemented in larger codes.

APPENDIX C

Sample SEM Exercises

Six examples are given to illustrate use of the Soil Element Model. Note that units vary (SI, English, etc.) for each example. Any consistant set of units may be used in the Soil Element Model.

Example I

Material: McCormick Ranch Sand

Model: Elastic
K = 8375 psi
G = 3865 psi

Loading: a) Initial geostatic pressure = 0.0 psi
Drained isotropic compression
- Load to 20 psi
- Unload to 0 psi
- Load to 50 psi

b) Drained Std. Triaxial
- Load to 1 percent axial strain difference
- Unload to 0 psi stress difference
- Load to 3 percent axial strain difference
- Unload to 0 psi stress difference
- Load to 7 percent axial strain difference

Example II

Material: McCormick Ranch Sand

Model: Elastic - Plastic
K = 8375 psi
G = 3865 psi

C_a = 260 psi
C_b = 260 psi
C_c = 0.016 $(psi)^{-1}$
TCUT1 = 0.0 psi
FCUT1 = 0.0 psi

Loading: Same as Example I

Example III

Material: McCormick Ranch Sand

Model: Pyke's 1-D Curve Fit
K = 8375 psi
τ_y = 210 psi
G_{max} = 50,000 psi

Loading: Initial geostatic pressure - 0.0 psi
a) Drained Isotropic Pressure
- Load to 50 psi

b) Strain Controlled Pure Shear (using complete strain reversal)
- 5 cycles at γ_{RZ} = 1.0 percent
- 5 cycles at γ_{RZ} = 0.4 percent
- 5 cycles at γ_{RZ} = 2.0 percent

Example IV

Material: McCormick Ranch Sand

Model: AFWL Engineering
ρ_Z = 1.75 g/cc
ν_L = 0.30
ν_u = 0.30
K_u = 74,000 psi

K_1 = 5,400 psi
K_2 = 12,300 psi
K_Z = 74,000 psi
K_M = 74,000 psi
P_1 = 0 psi
P_2 = 150 psi
P_3 = 520 psi
T = 0 psi
Y = 0 psi
S = 0.54
VM = 260 psi

Loading: Initial geostatic pressure = 0.0 psi

a) Drained Isotropic Compression

- Load to 20 psi
- Unload to 0 psi
- Load to 50 psi
- Unload to 0 psi

b) Uniaxial Loading (Drained)

- Load to Axial Stress = 100 psi
- Unload to Axial Stress = 0 psi
- Load to Axial Stress = 200 psi
- Unload to Axial Stress = 0 psi
- Load to Axial Stress = 250 psi

Example V

Material: McCormick Ranch Sand

Model: Cap Model

K_{iS} = 7.50 ksi
K_{1S} = 0.94
K_{2S} = 1.0 $(ksi)^{-1}$
G_i = 40 ksi
G_1 = 0.75

G_2 = 3.0 $(ksi)^{-1}$
α = 0.0
C_S = 0.08 ksi
B = 0.214 $(ksi)^{-1}$
C = 0.39 ksi
R = 2.5
D = 0.7 $(ksi)^{-1}$
W = 0.066

Loading: Initial geostatic pressure = 0.0 ksi

a) Drained Isotropic Compression
- Load to 0.010 ksi
- Unload to 0.0 ksi
- Load to 0.050 ksi

b) Drained Std. Triaxial
- Load to 1 percent axial strain difference
- Unload to 0 ksi stress difference
- Load to 3 percent axial strain difference

Example VI

Material: Ocean Mud (Seabed Deposits)

Model: Effective Stress Cap

K_{iS} = 20.0 MPa
K_{1S} = 0.999
K_{2S} = 0.0002 $(MPa)^{-1}$
K_{iM} = 1875 MPa
K_{1M} = 0.35
K_{2M} = 0.05 $(MPa)^{-1}$
G_i = 0.60 MPa
G_1 = -1.0
G_2 = 200.0 $(MPa)^{-1}$
α = 0.133336
C_S = 0.00866 MPa

B = 0.0 $(MPa)^{-1}$

C = 0.0 MPa

K = 4.0

D = 1.20 $(MPa)^{-1}$

W = 0.42

Loading: Initial geostatic pressure = 0.037 MPa

a) Drained Isotropic Compression

- Load to 0.050 MPa
- Unload to 0.037 MPa
- Load to 0.086 MPa

b) Undrained Std. Triaxial Test

- Load to 2.0 percent axial strain difference
- Unload to 0.0 MPa stress difference
- Load to 4.0 percent axial strain difference
- Unload to 0.0 MPa stress difference
- Load to 8.0 percent axial strain difference

The following figures illustrate material response for the six examples as outlined above.

EXAMPLE I - ELASTIC MODEL

MCCORMICK RANCH SAND

EFF PRESS VS. VOLUMETRIC STRAIN

(ISOTROPIC CONFRESSION)

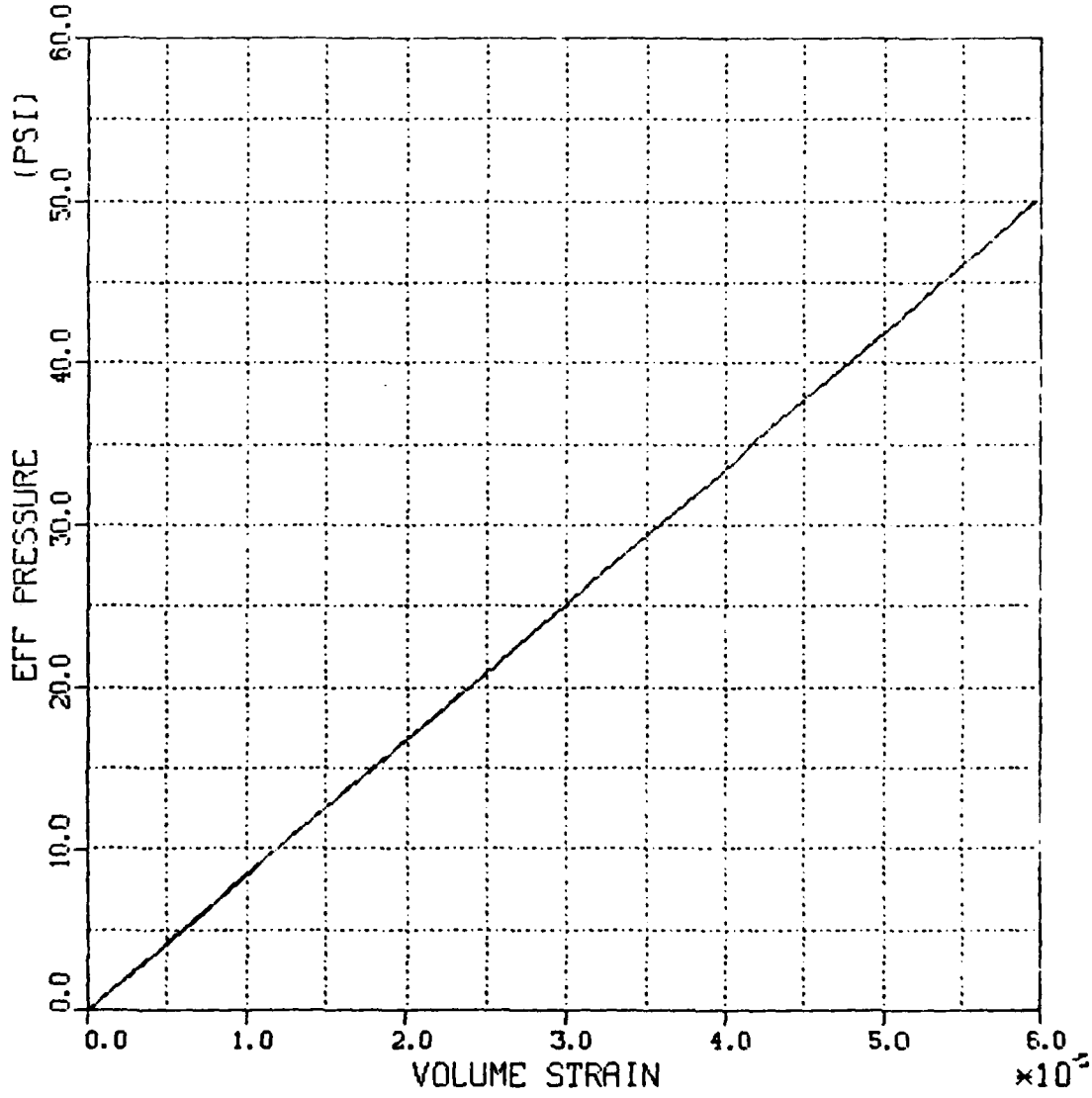

PLOT 1 18.12.51 MON 2 NOV, 1981 JOB-HARBINN , NPAL CRAY DISSPLA VER 9.0

EXAMPLE 1 - ELASTIC MODEL

MCCORMICK RANCH SAND

STRESS DIFFERENCE VS. EFF PRESS

(STANDARD TRIAXIAL TEST)

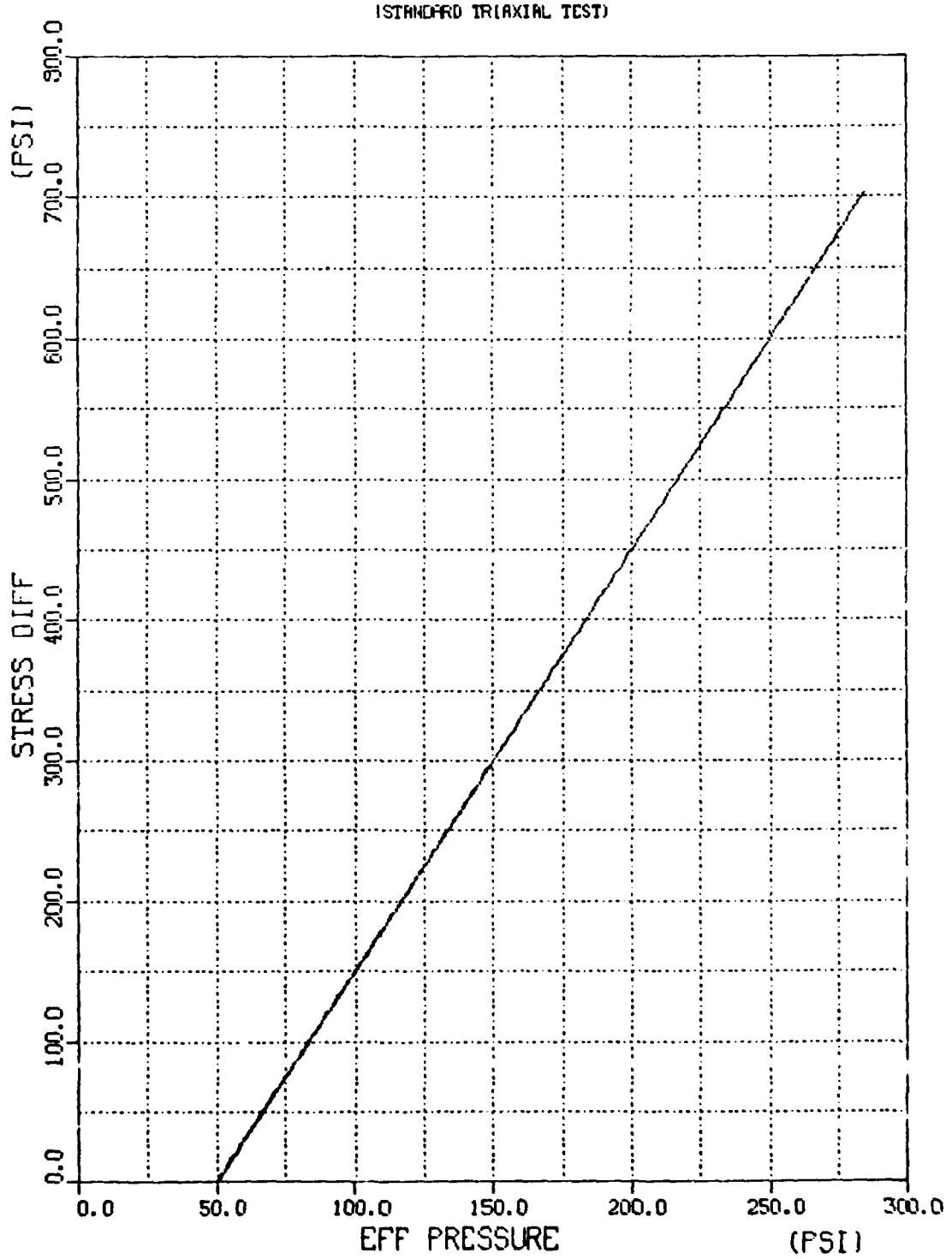

PLOT 1 18.12.53 MON 2 NOV, 1981 JOB-HARBINGER , ANAL CAM DISSPLA VER 9.0

EXAMPLE I - ELASTIC MODEL

MCCORMICK RANCH SAND

STRESS DIFF VS. AXIAL STRAIN

(STANDARD TRIAXIAL TEST)

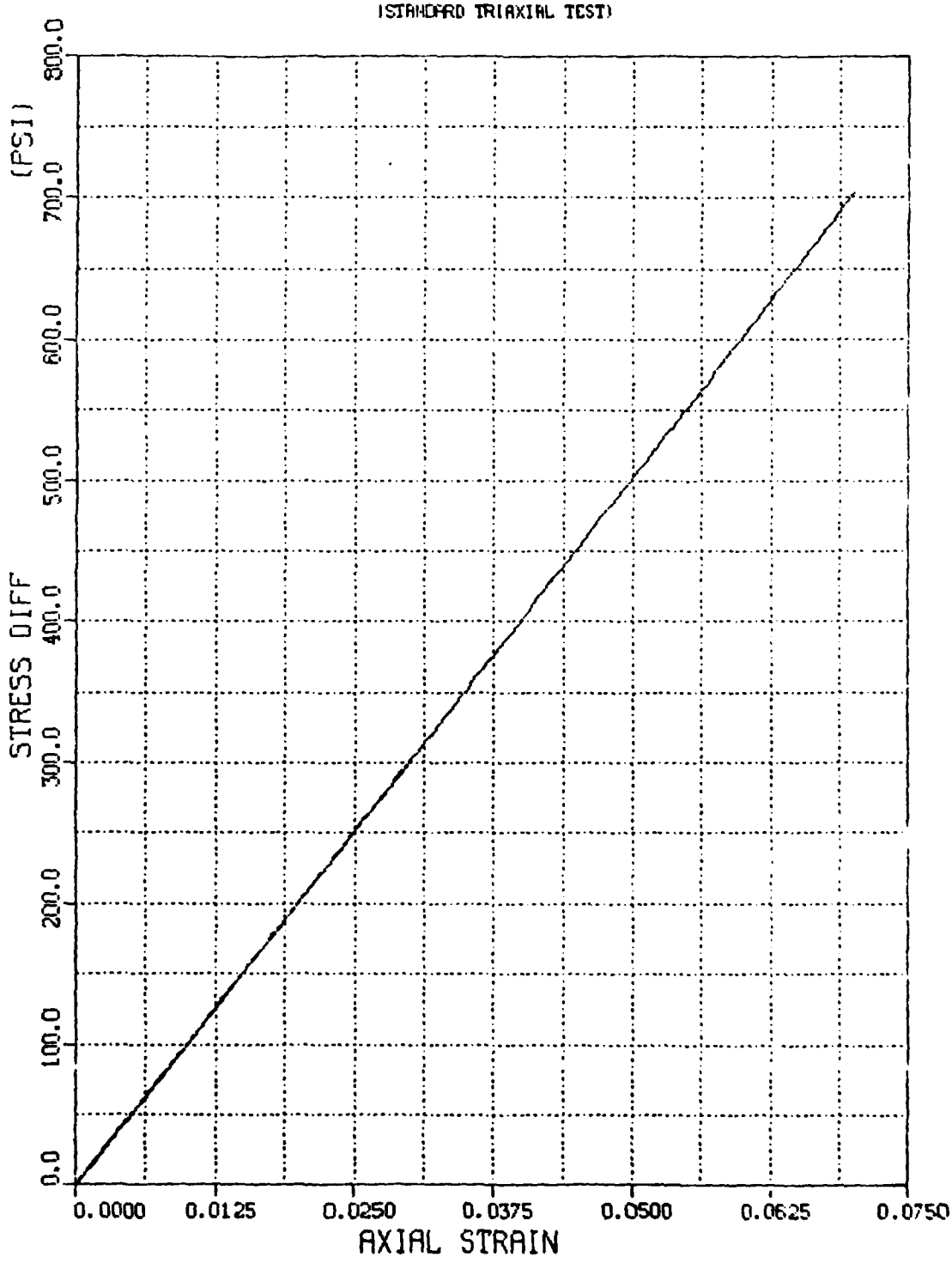

PLOT 1 18.12.53 MON 2 NOV, 1981 JOB-HARDIN , AFML CRA DISPLA VER 9.0

EXAMPLE I - ELASTIC MODEL

MCCORMICK RANCH SAND

STRESS DIFF VS. STRAIN DIFF

(STANDARD TRIAXIAL TEST)

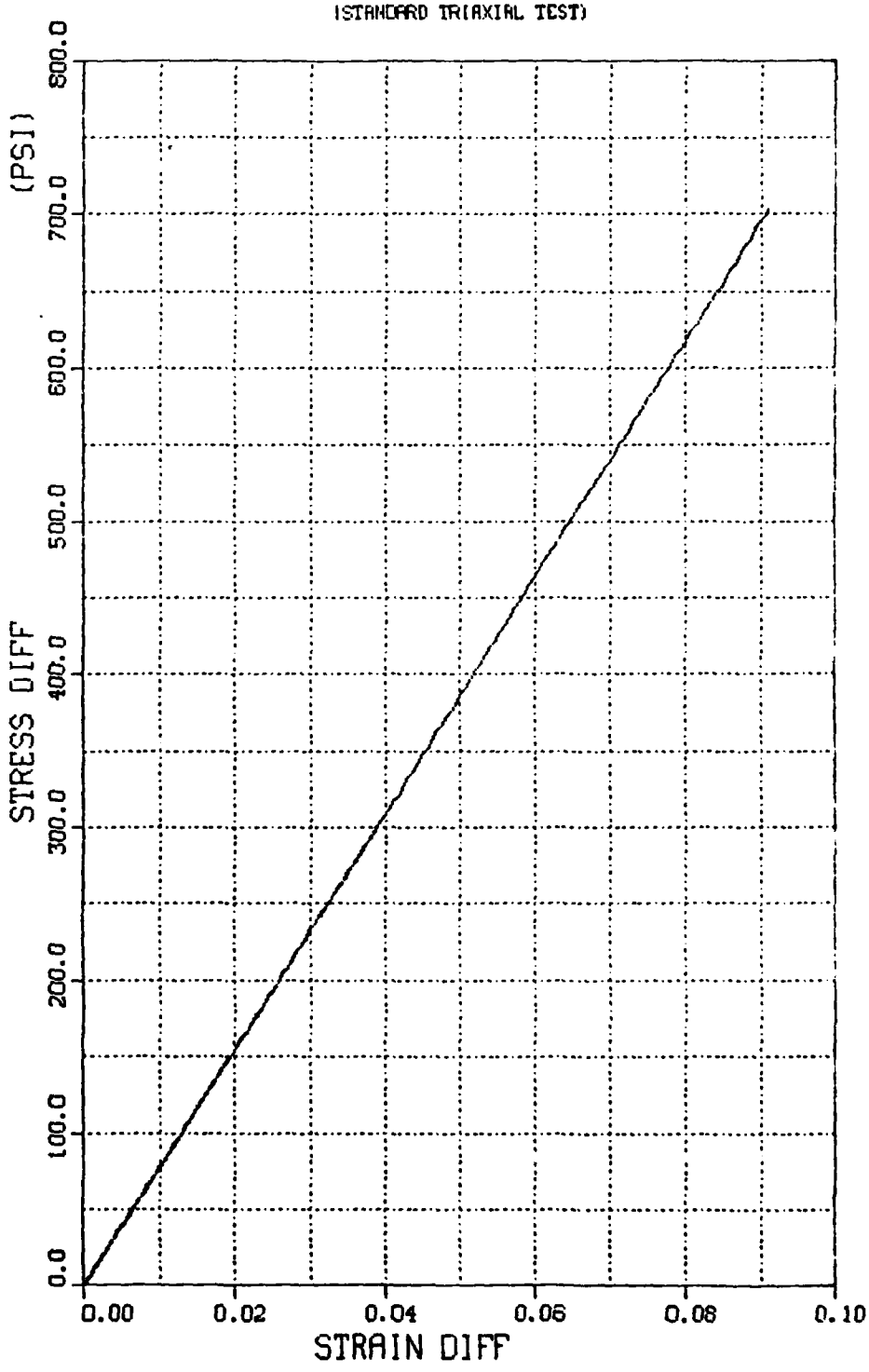

PLOT 1 18.12.54 MON 2 NOV, 1981 JOB-HARDIN , AFWL CRA DISSPLA VER 9.0

EXAMPLE I - ELASTIC MODEL

MCCORMICK RANCH SAND

EFF PRESS VS. VOLUMETRIC STRAIN

(STANDARD TRIAXIAL TEST)

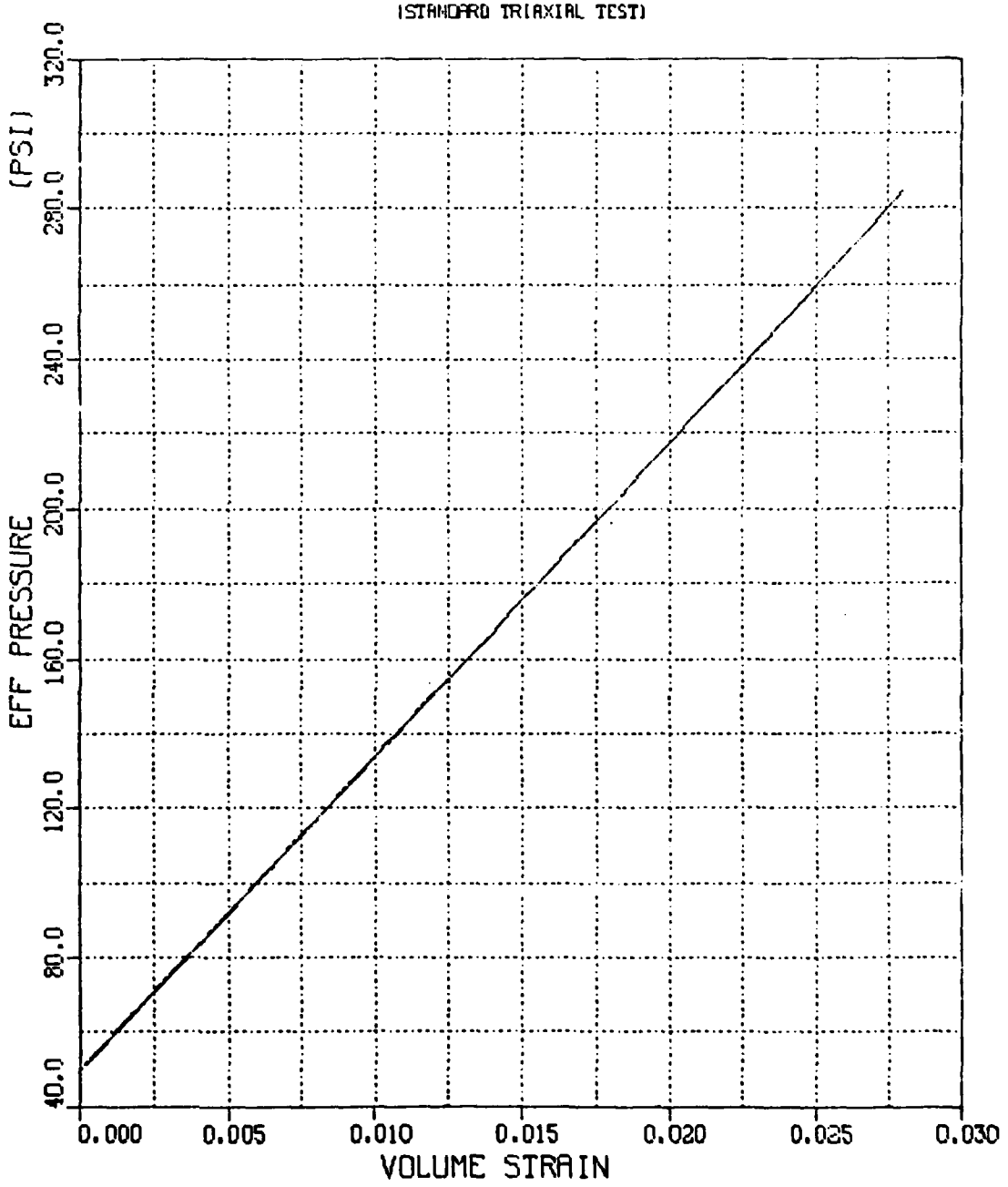

PLOT 1 18.12.54 MON 2 NOV, 1981 JOB-HARBHAN , NAVL CMR DISPLA VER 9.0

EXAMPLE I - ELASTIC MODEL

MCCORMICK RANCH SAND

STRESS RATIO VS. AXIAL STRAIN

(STANDARD TRIAXIAL TEST)

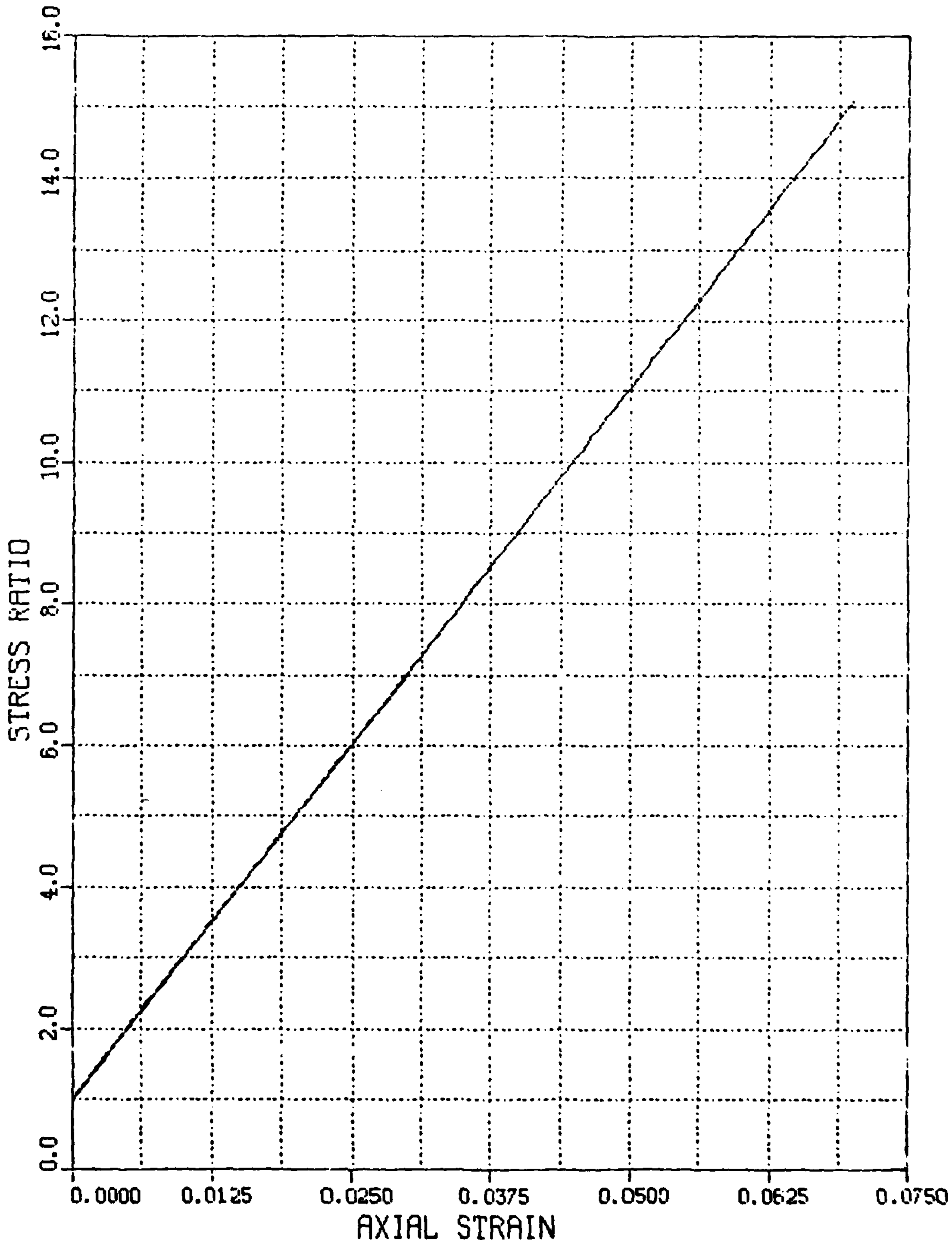

EXAMPLE 1 - ELASTIC MODEL

MCCORMICK RANCH SAND

AXIAL STRAIN VS VOLUME STRAIN

(STANDARD TRIAXIAL TEST)

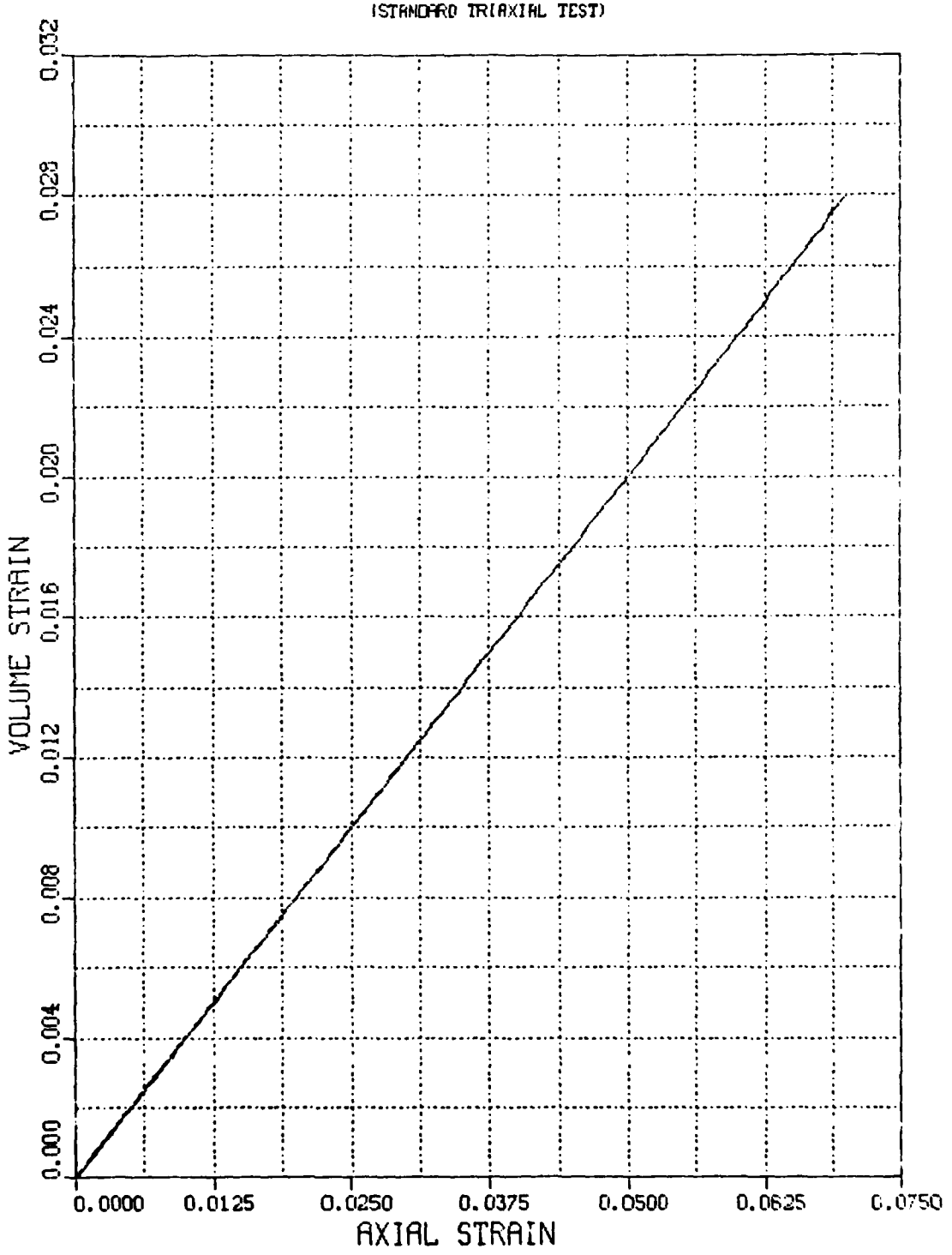

PLOT 1 18.12.58 MON 2 NOV, 1981 JOB=HARRISON , MAHL CAM DISSPLA VER 9.0

EXAMPLE I - ELASTIC MODEL

MCCORMICK RANCH SAND

STRESS RATIO VS. AXIAL STRAIN

(STANDARD TR(AXIAL TEST)

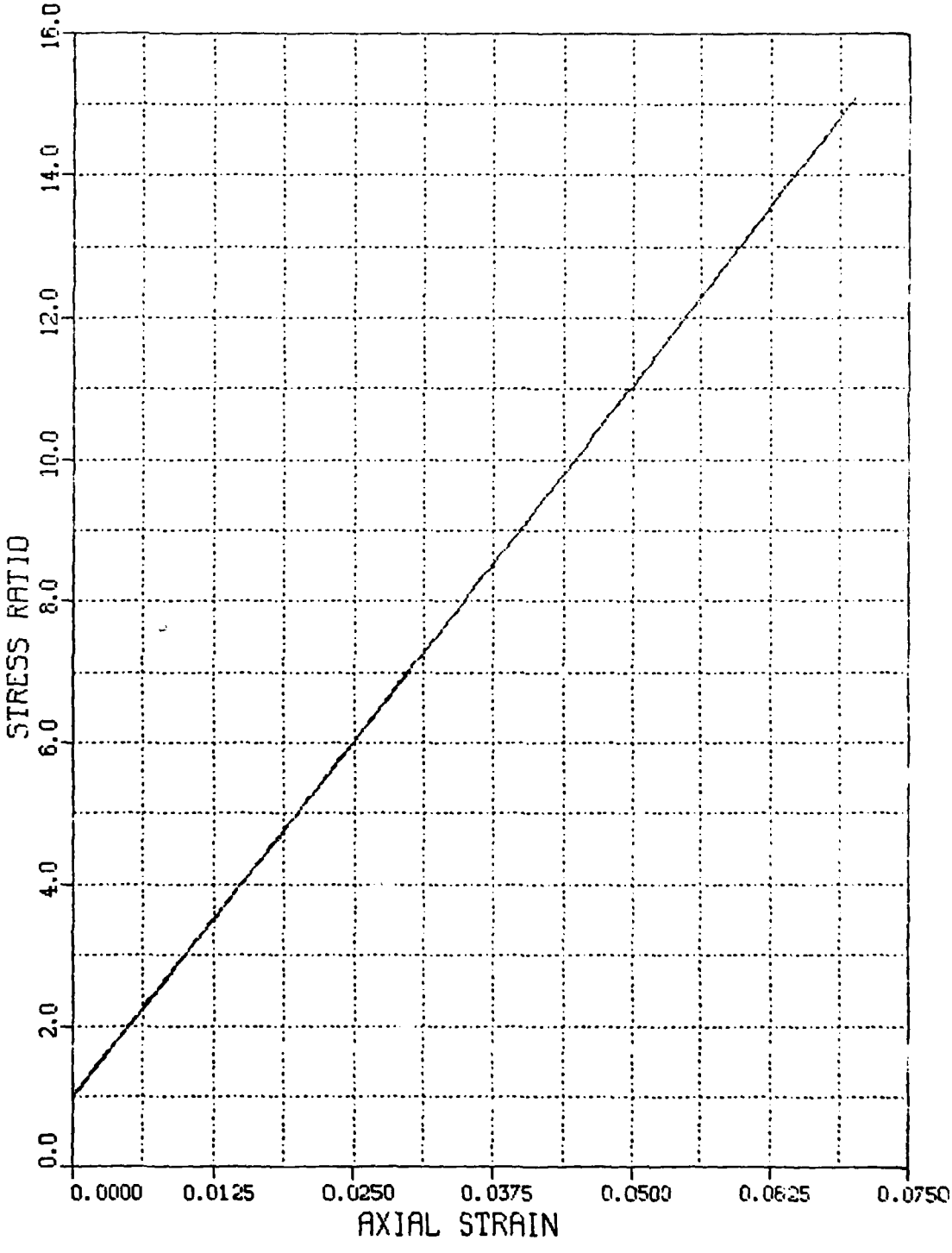

PLOT 1 10:12:56 MON 2 NOV, 1981 JOB=HARBHN , RMAL CRA DISPLA VER 9.0

EXAMPLE I - ELASTIC MODEL

MCCORMICK RANCH SAND

EFF AXL STRESS VS. AXIALSTRAIN

(STANDARD TRIAXIAL TEST)

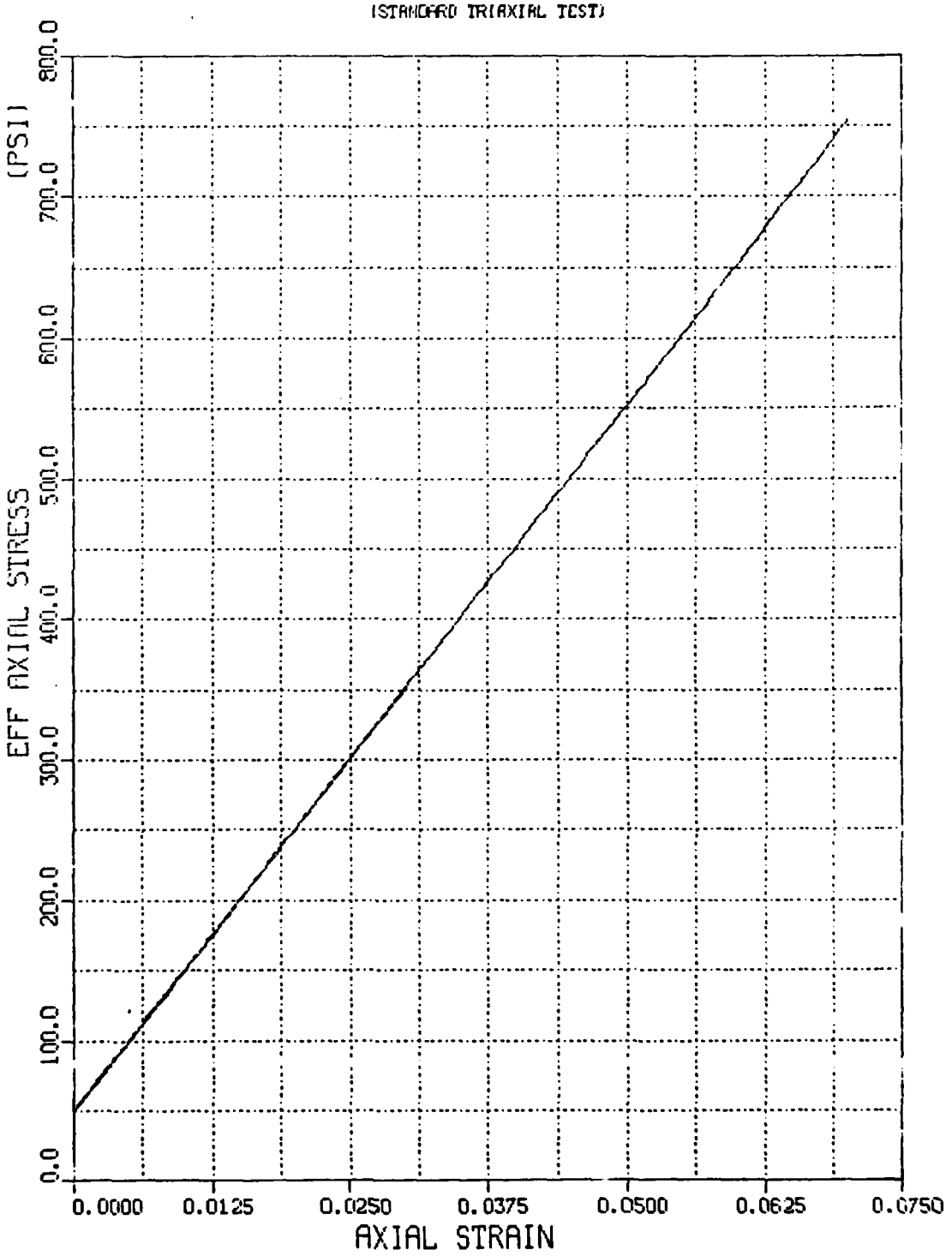

PLOT 1 10:12:57 MON 2 NOV, 1981 JOB-HARENIK , AFWL CRA DISSPLA VER 9.0

EXAMPLE II - ELASTIC-PLASTIC MODEL

MCCORMICK RANCH SAND

EFF PRESS VS. VOLUMETRIC STRAIN

(ISOTROPIC CONFRESSION)

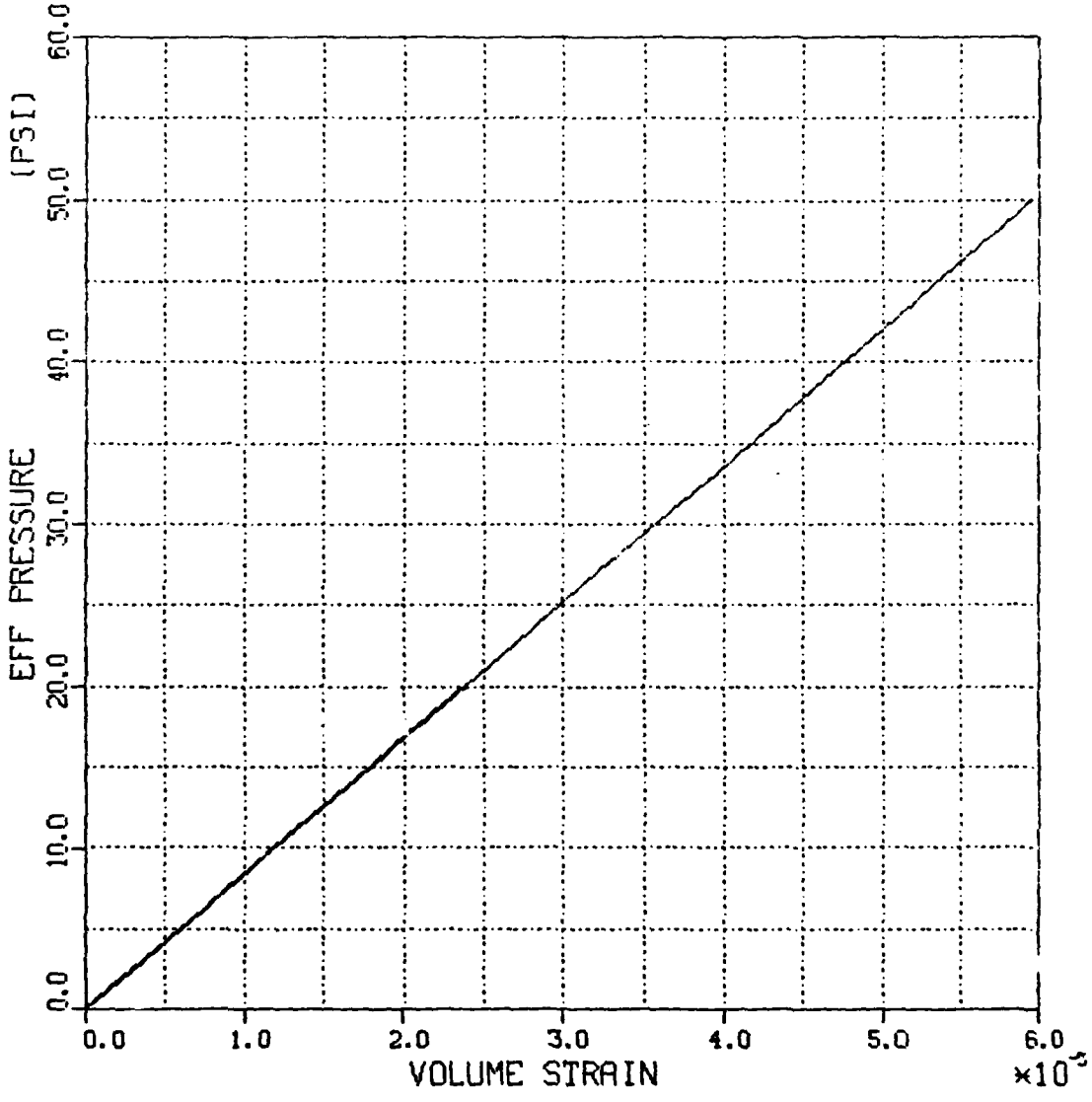

PLOT 1 18.12.59 MON 2 NOV, 1981 JOB=HARBIN , NTAL CAN DISSPLA VER 9.0

EXAMPLE II - ELASTIC-PLASTIC MODEL
MCCORMICK RANCH SAND
STRESS DIFFERENCE VS. EFF PRESS
(STANDARD TRIAXIAL TEST)

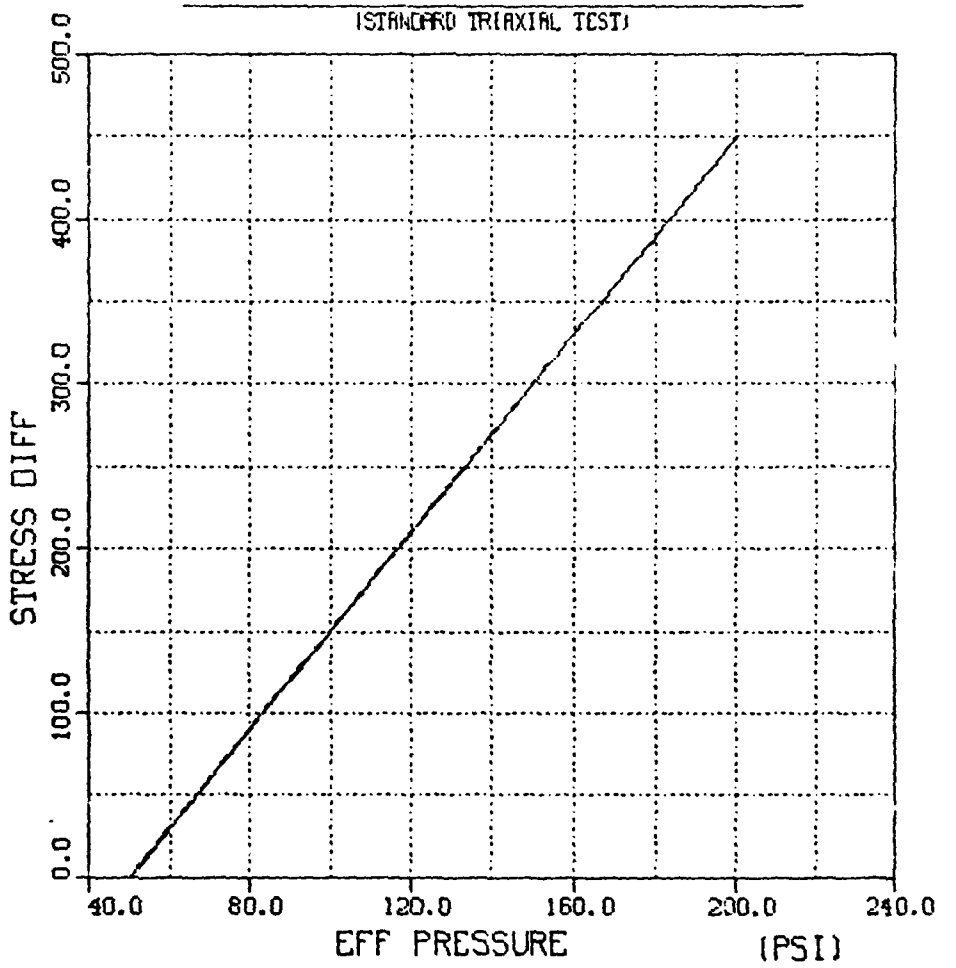

PLOT 1 18.15.00 MON 2 NOV, 1981 JOB-HARBINN , NMSL CRAY DISSPLA VER 9.0

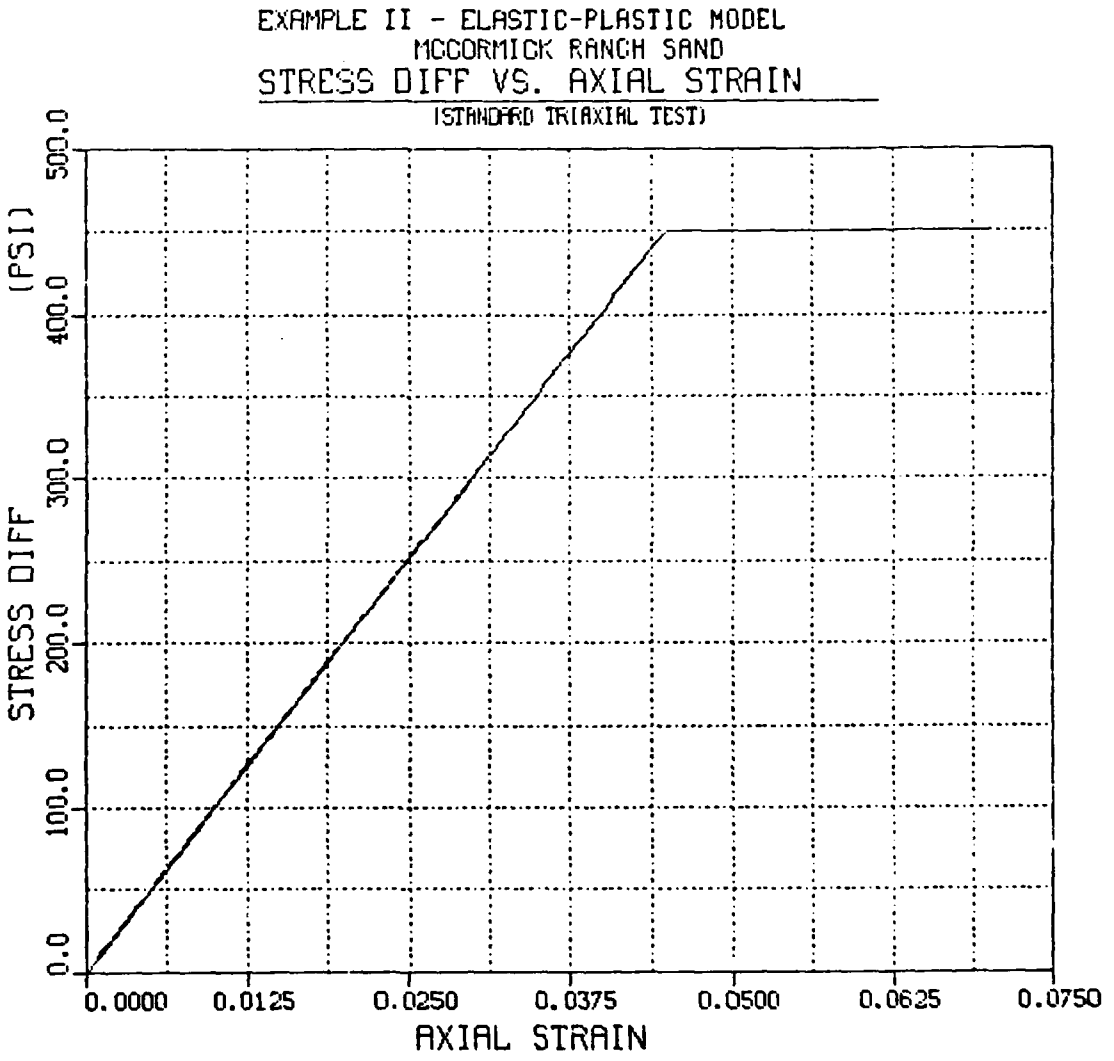

PLOT 1 10:13:00 MON 2 NOV, 1981 JOB=HARBHON , ATAL CAM DISSPLA VER 9.0

EXAMPLE II - ELASTIC-PLASTIC MODEL
MCCORMICK RANCH SAND
STRESS DIFF VS. STRAIN DIFF
(STANDARD TRIAXIAL TEST)

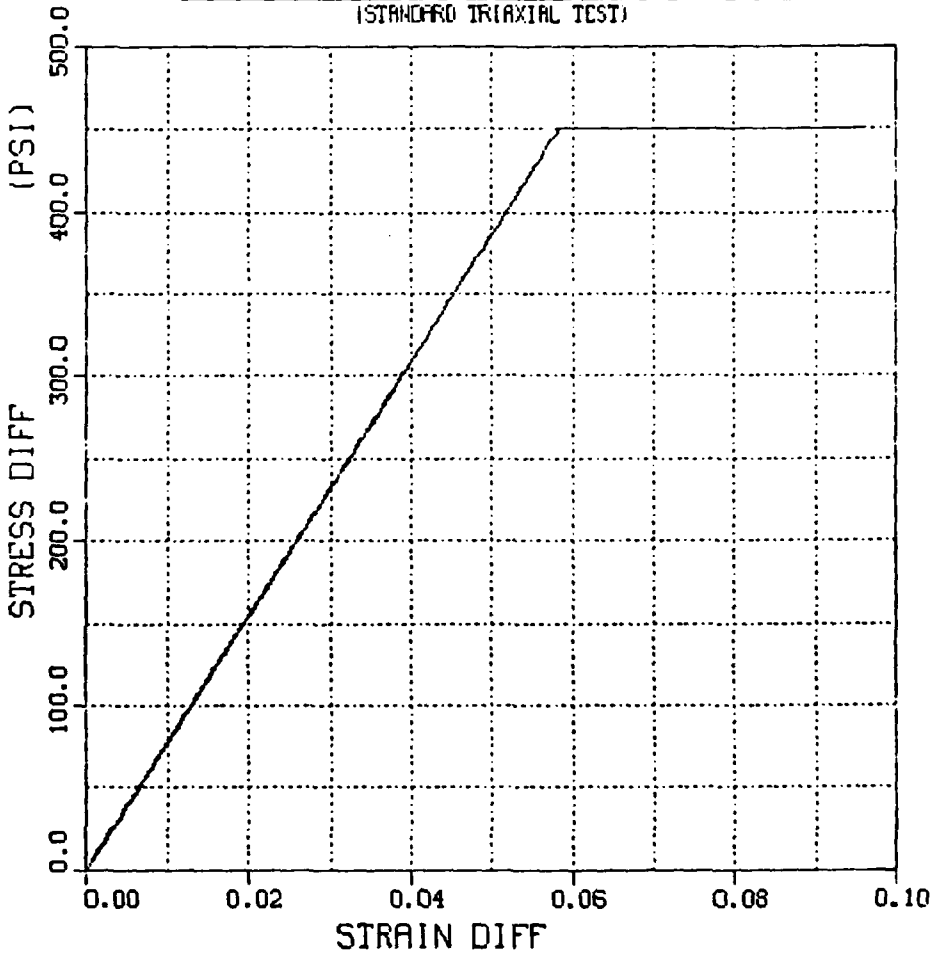

PLOT 1 18.13.01 MON 2 NOV, 1981 JOB-HARBINN , AFWL CRA DISSPLA VER 9.0

EXAMPLE II - ELASTIC-PLASTIC MODEL

MCCORMICK RANCH SAND

EFF PRESS VS. VOLUMETRIC STRAIN

(STANDARD TRIAXIAL TEST)

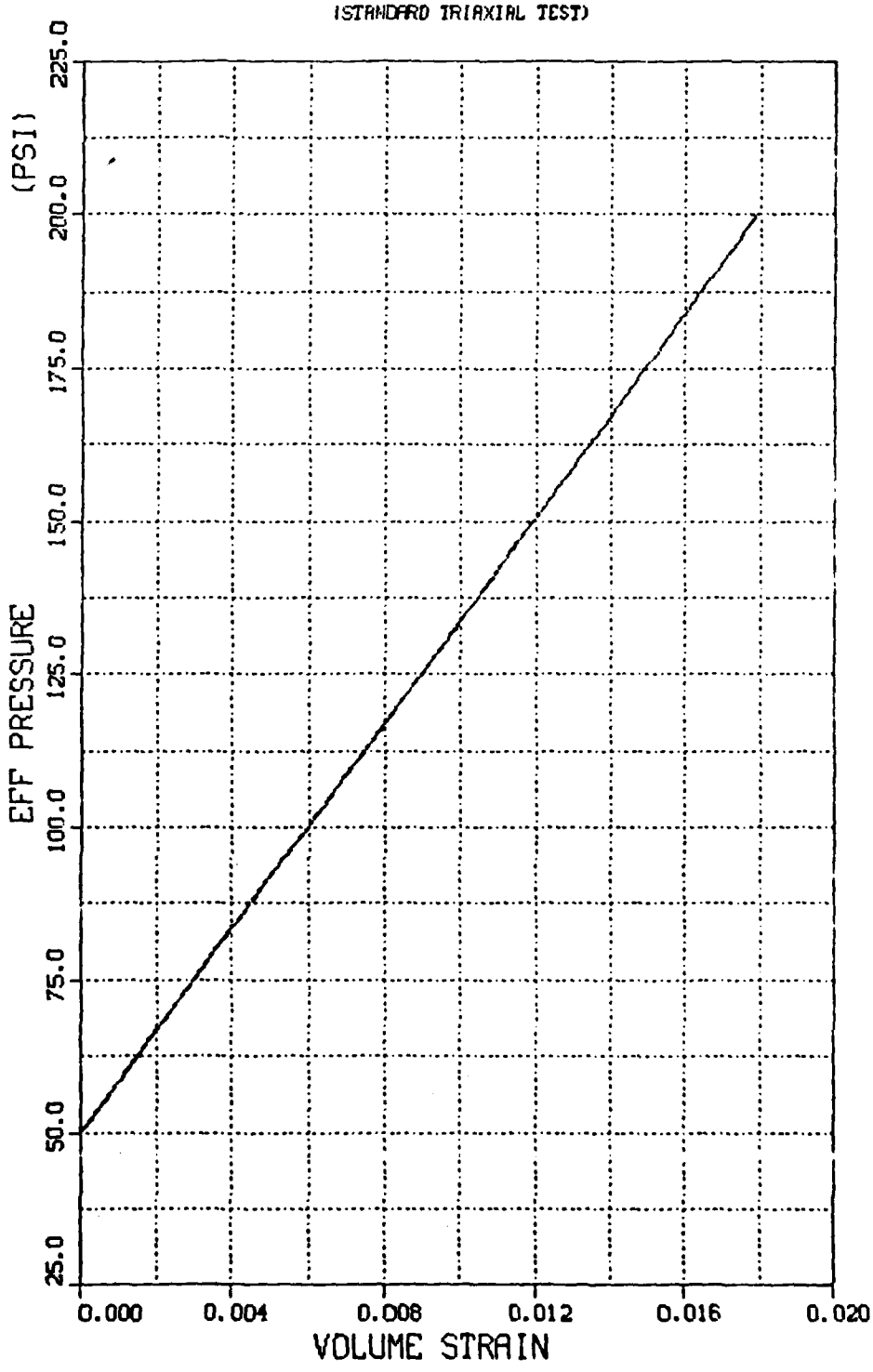

PLOT 1 16:13:02 MON 2 NOV, 1981 JOB=HARBHAN , AFWL CRA DISSPLA VER 9.0

EXAMPLE II - ELASTIC-PLASTIC MODEL

MCCORMICK RANCH SAND

AXIAL STRAIN VS VOLUME STRAIN

(STANDARD TRIAXIAL TEST)

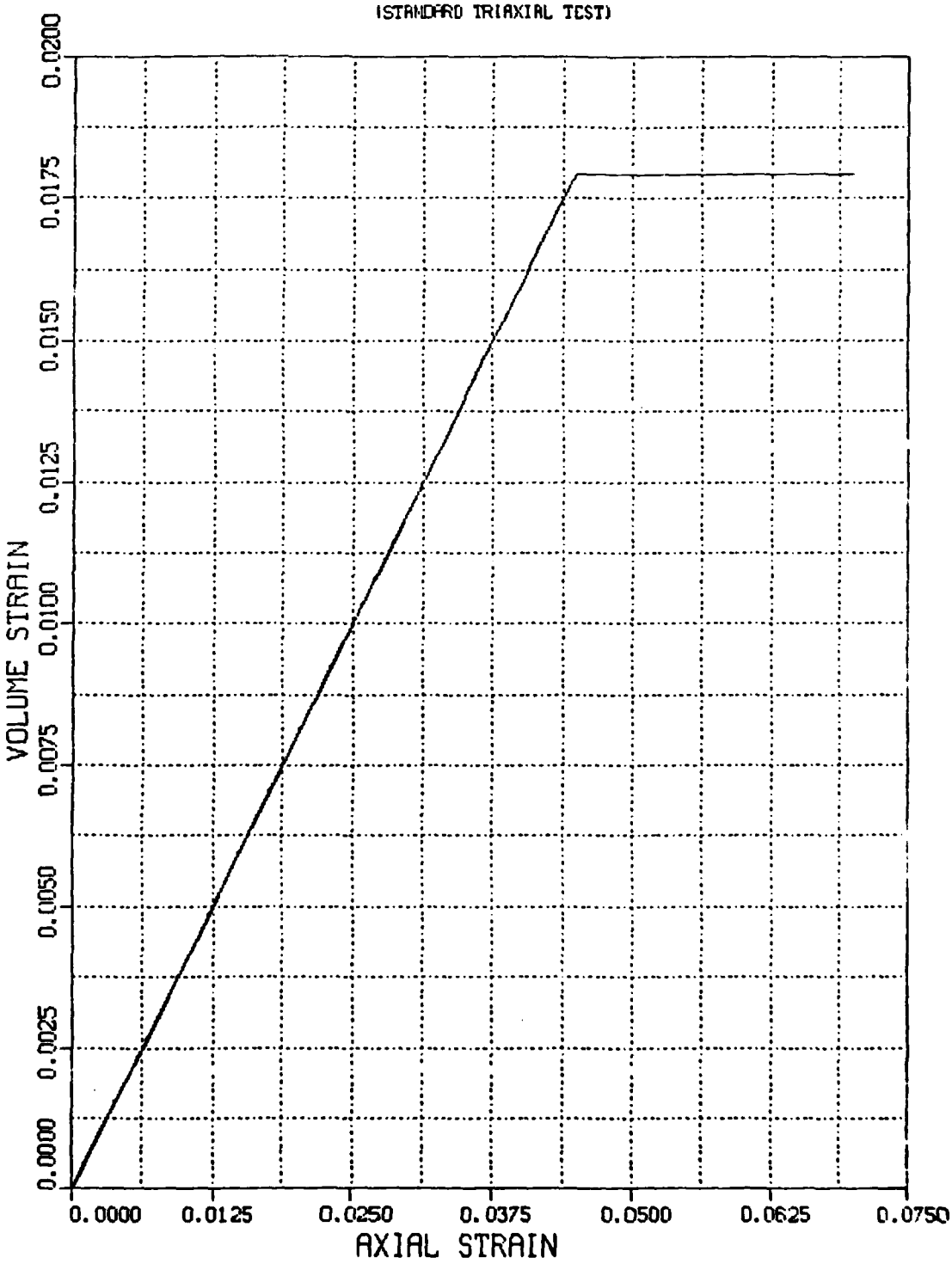

PLOT 1 18:13:03 MON 2 NOV, 1981 JOB=HARBINA , ATNL CRA DISSPLA VER 9.0

EXAMPLE II - ELASTIC-PLASTIC MODEL

MCCORMICK RANCH SAND

STRESS RATIO VS. AXIAL STRAIN

(STANDARD TRIAXIAL TEST)

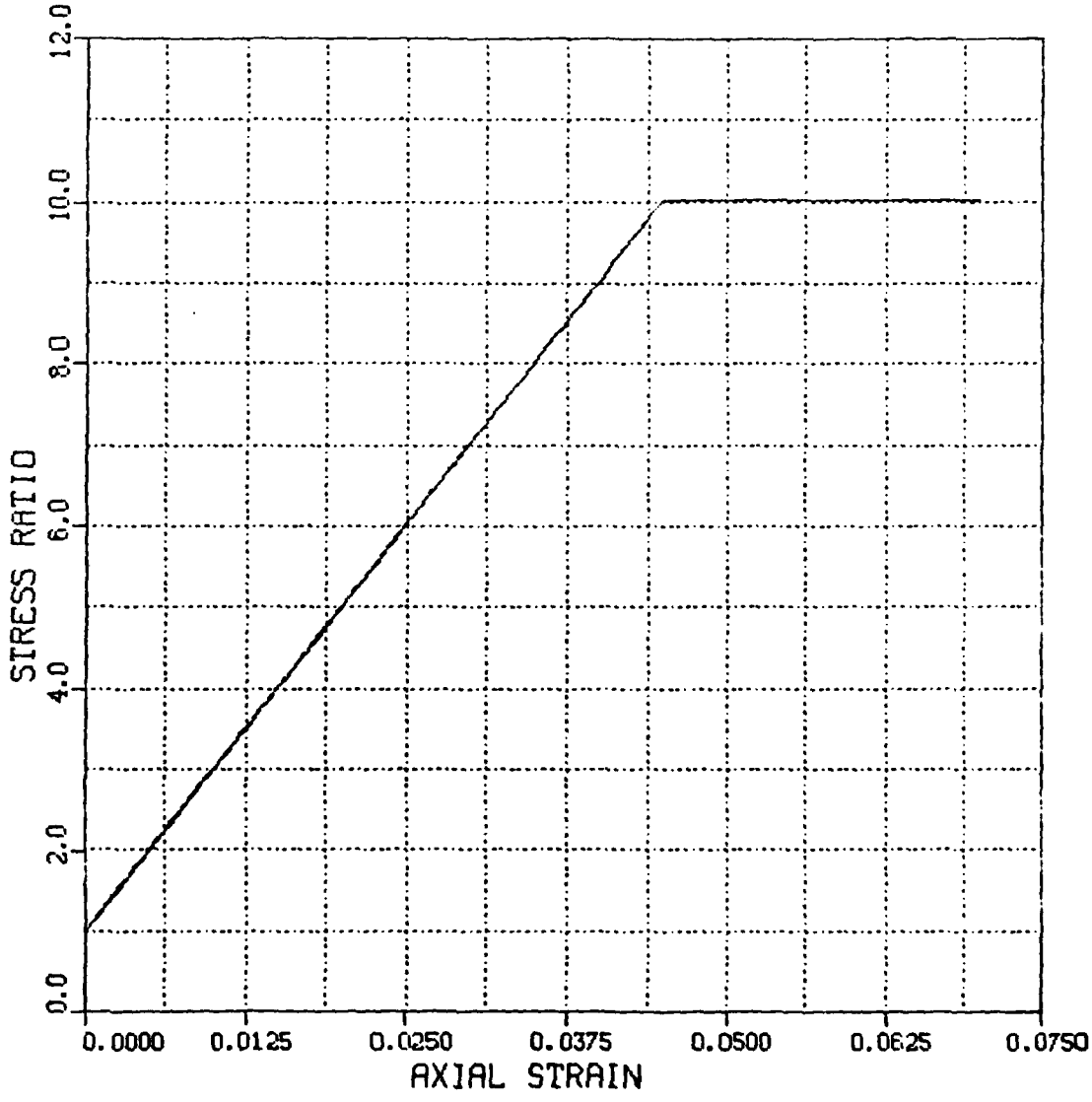

PLOT 1 18:13:03 MON 2 NOV, 1981 JOB-HARBISON , MTHL GRA DISPLA VER 9.0

EXAMPLE II - ELASTIC-PLASTIC MODEL

MCCORMICK RANCH SAND

EFF AXL STRESS VS. AXIALSTRAIN

(STANDARD TRIAXIAL TEST)

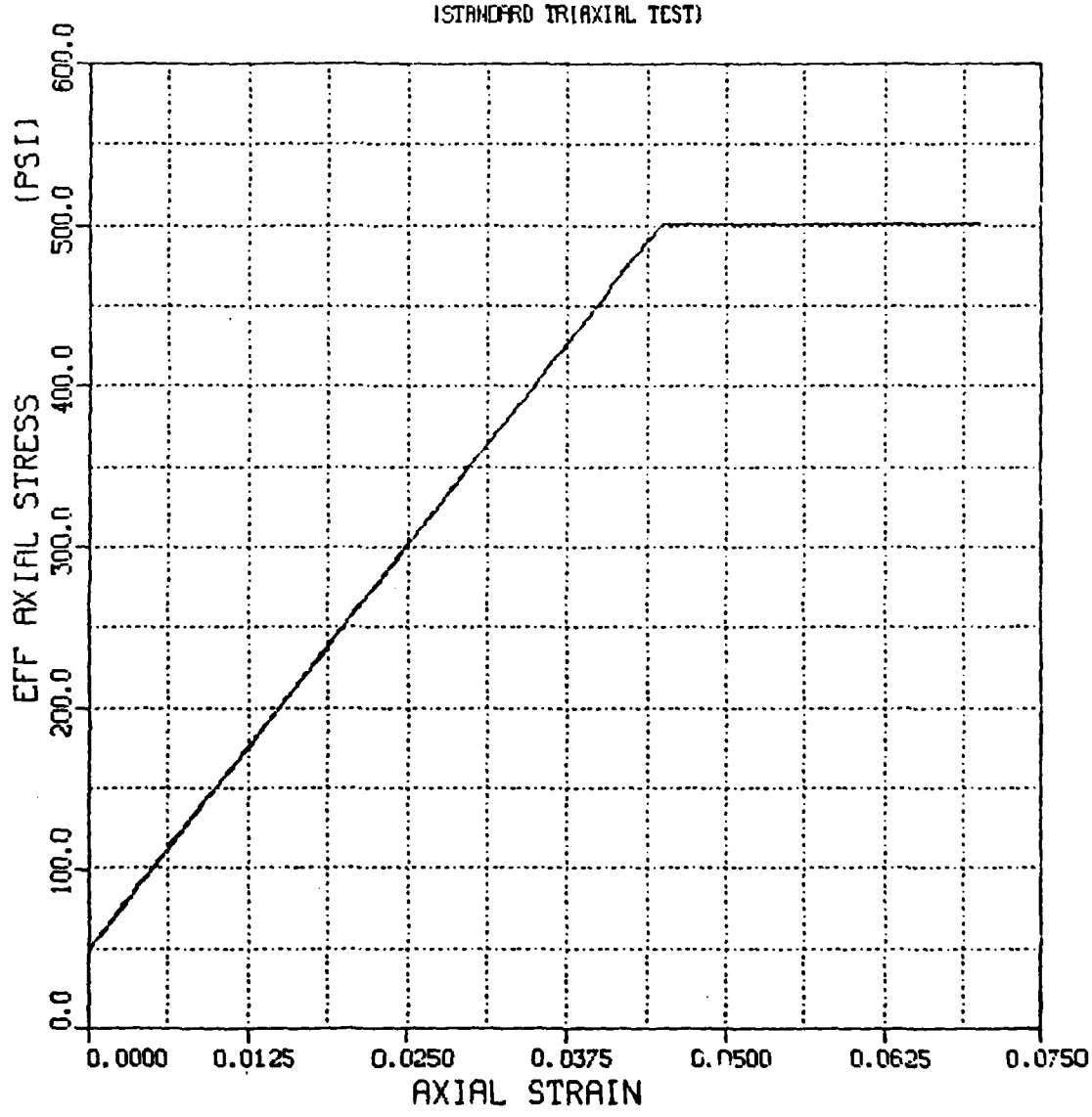

PLOT 1 10:13:04 MON 2 NOV, 1981 JOB=HARBINA , MTHL CRA DISPLA VER 9.0

EXAMPLE III - 1-D CURVE FIT (PYKE)

MCCORMICK RANCH SAND

EFF PRESS VS. VOLUMETRIC STRAIN

(ISOTROPIC COMPRESSION)

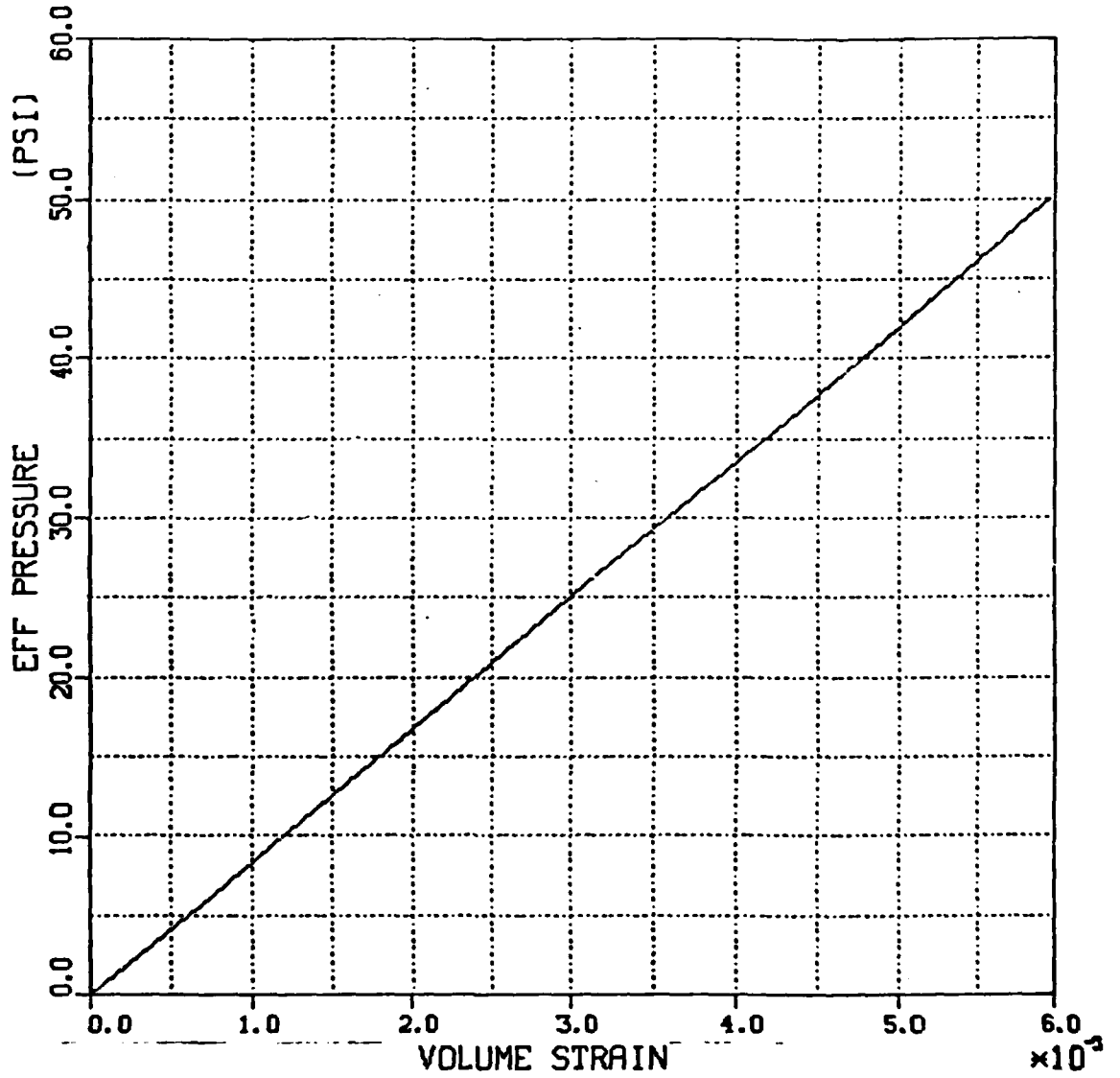

EXAMPLE III - 1-D CURVE FIT (PYKE)

MCCORMICK RANCH SAND

SHEAR STRESS VS. SHEAR STRAIN

(PURE SHEAR TEST)

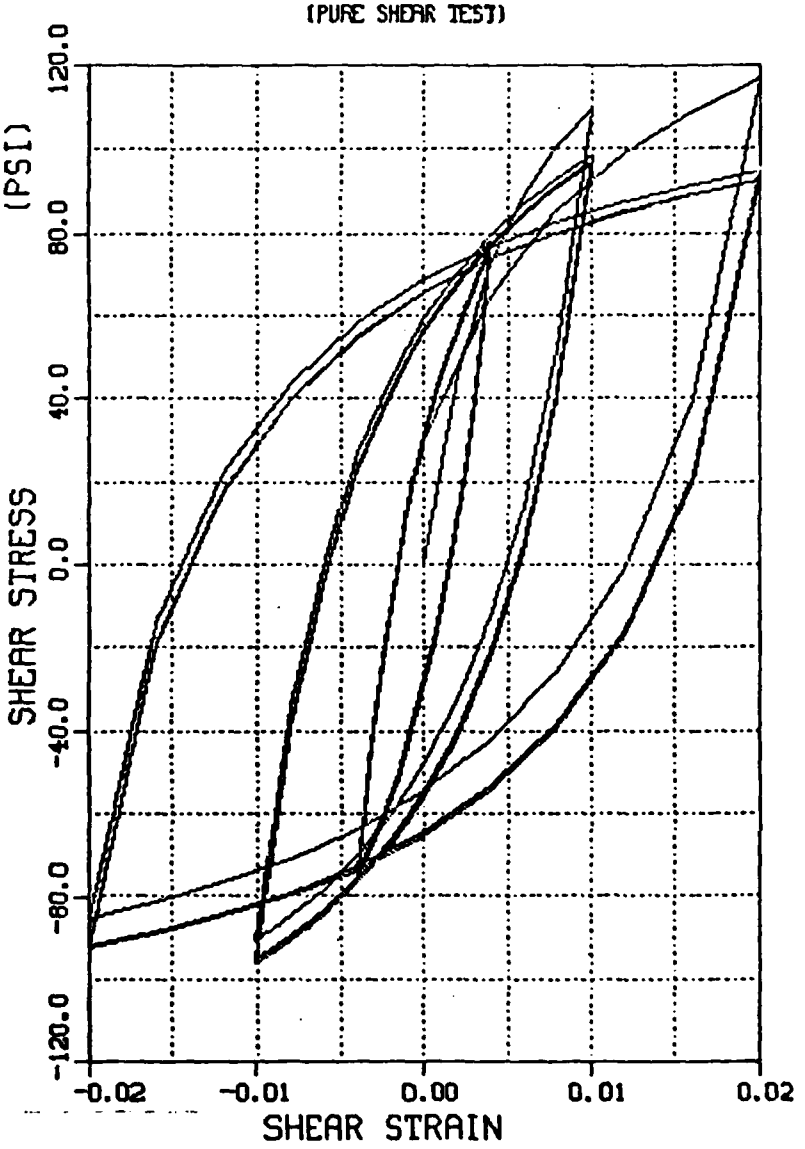

PLOT 1 04.05.30 MON 30 SEP, 1991 JOB=MARENTO , MVL CMA DISPLA VER 9.0

EXAMPLE IV - AFWL MODEL

MCCORMICK RANCH SAND

EFF PRESS VS. VOLUMETRIC STRAIN

(ISOTROPIC COMPRESSION)

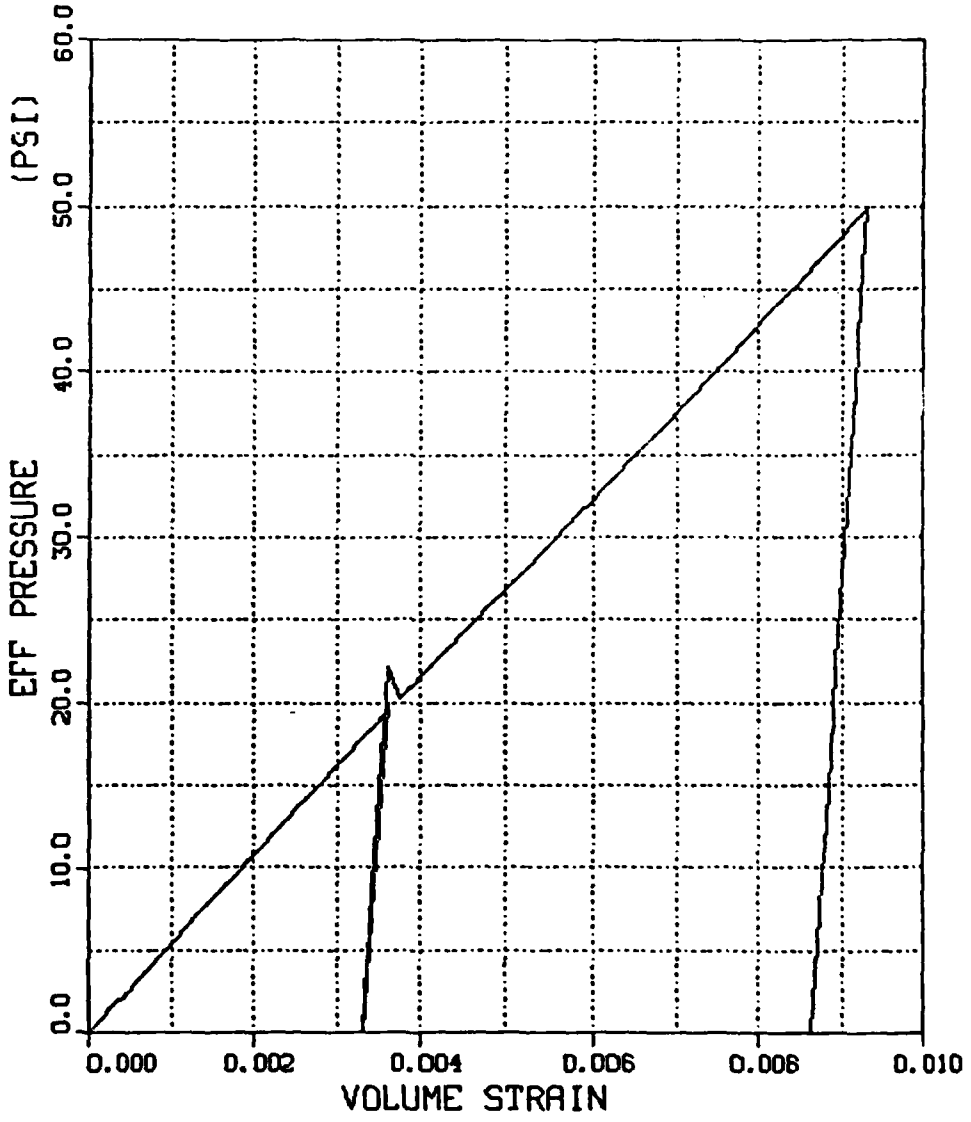

PLOT 1 04.05.38 WED 30 SEP, 1981 JOB-HARDYID, AFWL CRAY DISSPLA VER 9.0

EXAMPLE IV - AFWL MODEL

MCCORMICK RANCH SAND

EFF PRESS VS. VOLUMETRIC STRAIN

(UNIAXIAL TEST)

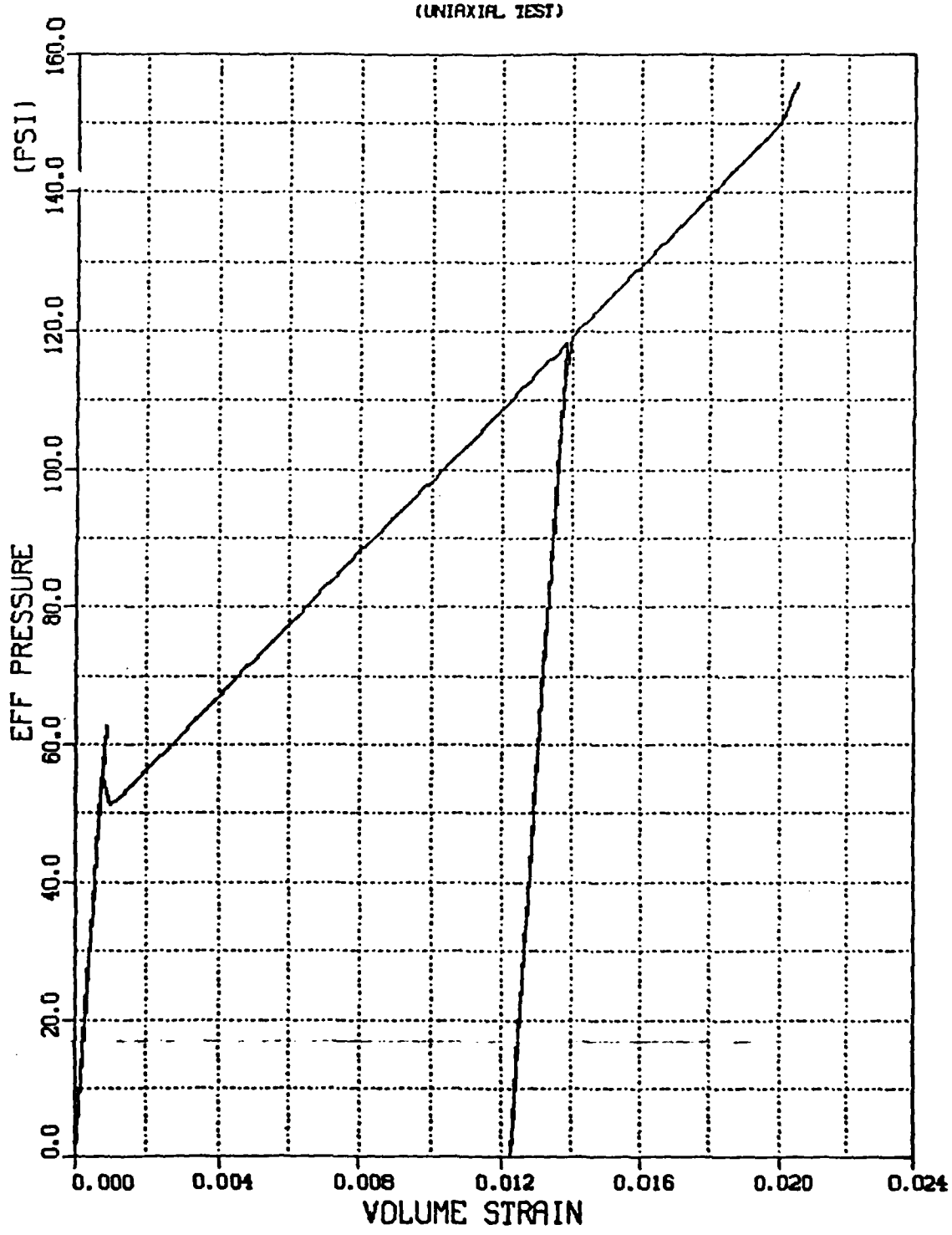

EXAMPLE IV - AFWL MODEL

MCCORMICK RANCH SAND

STRESS DIFF VS. AXIAL STRAIN

(UNIAXIAL TEST)

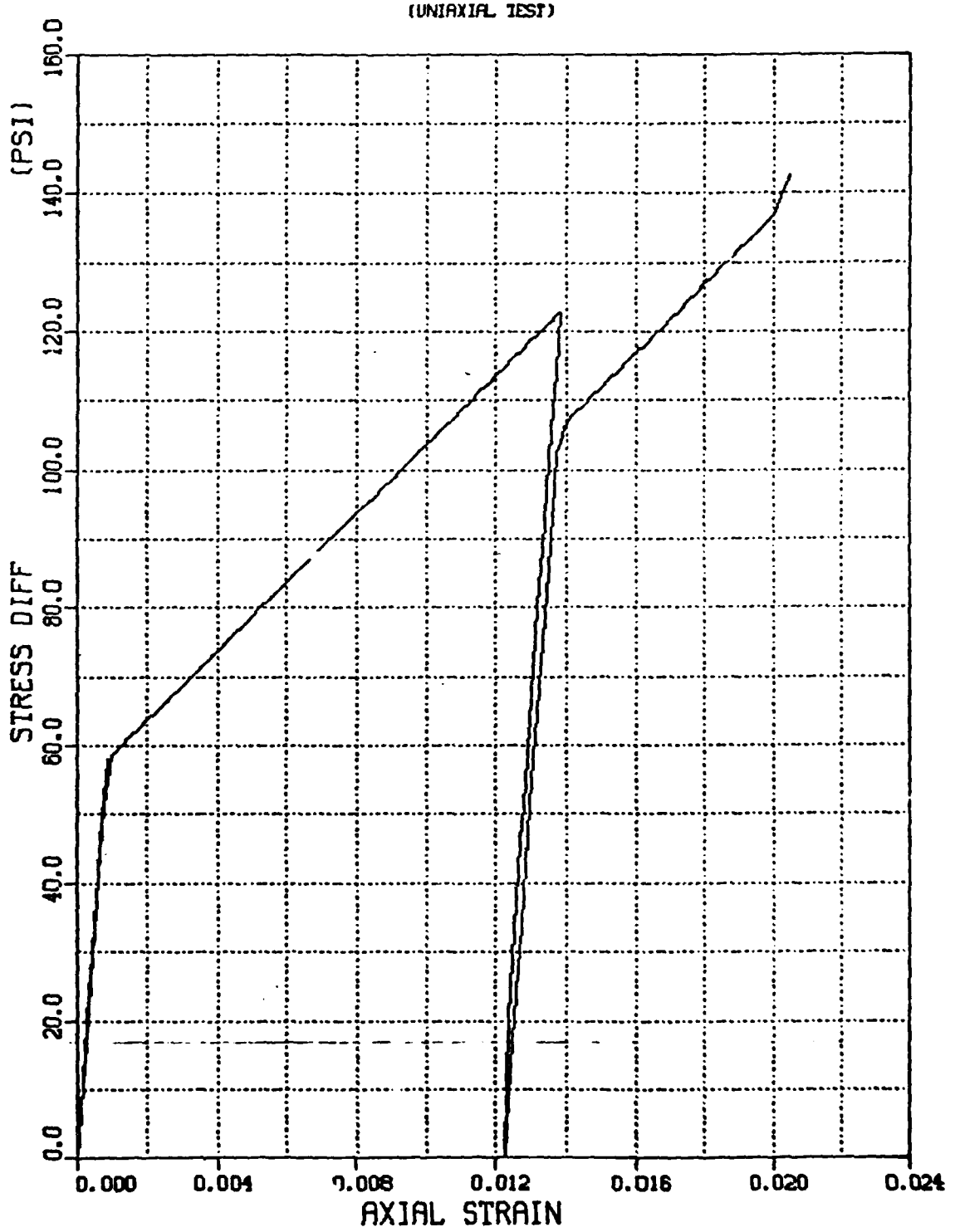

PLOT 1 08.05.58 WED 30 SEP, 1981 JOB=HARBIID , AFWL CRM DISPLAY VER 9.0

EXAMPLE IV - AFWL MODEL

MCCORMICK RANCH SAND

STRESS DIFF VS. STRAIN DIFF

(UNIAXIAL TEST)

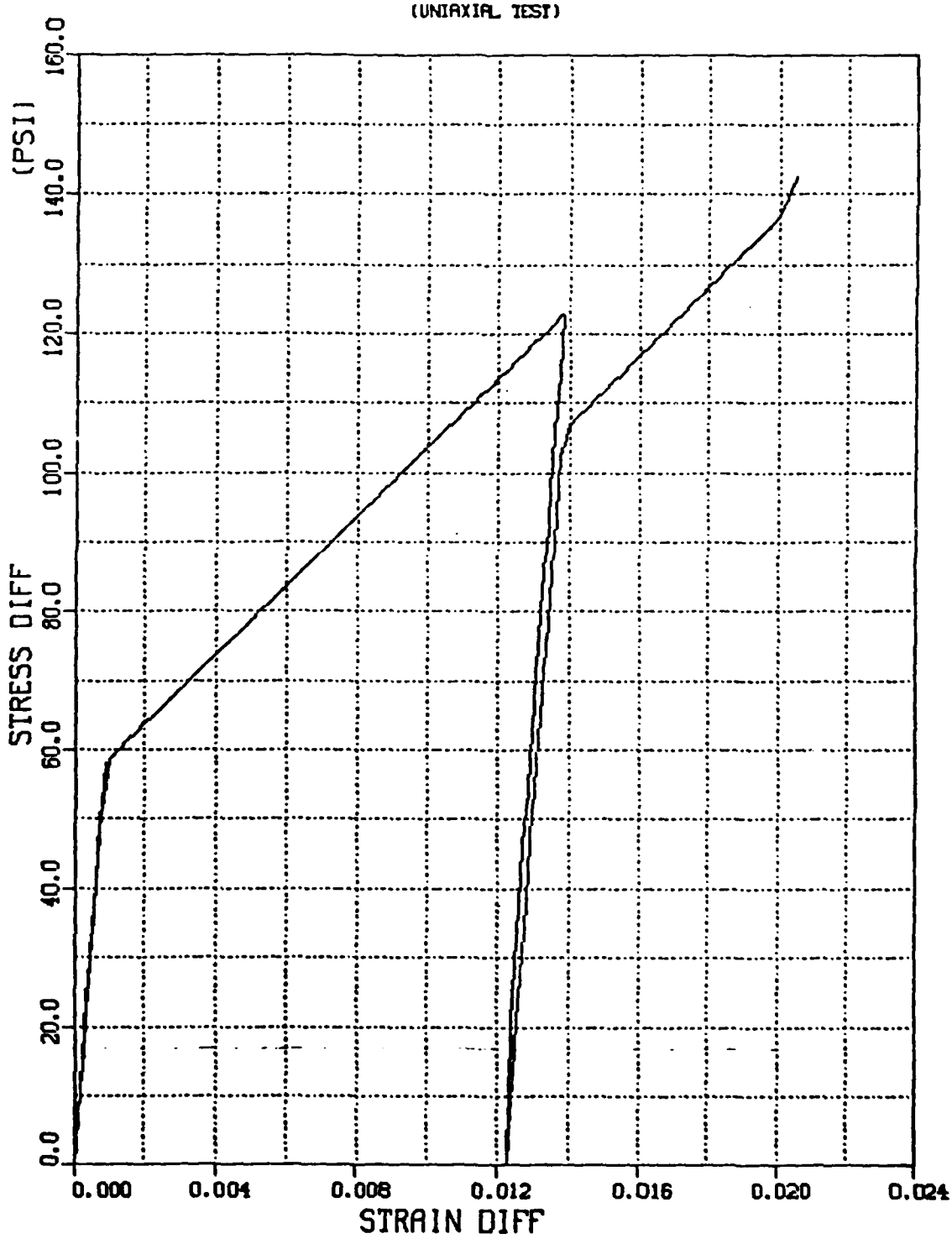

PLOT 1 08:05:58 MON 30 SEP, 1981 JOB=HARDNIO , AFWL GRAF DISPLAY VER 9.0

EXAMPLE IV - AFWL MODEL

MCCORMICK RANCH SAND

VOLUMETRIC STRAIN VS STRAIN DIFF

(UNIAXIAL TEST)

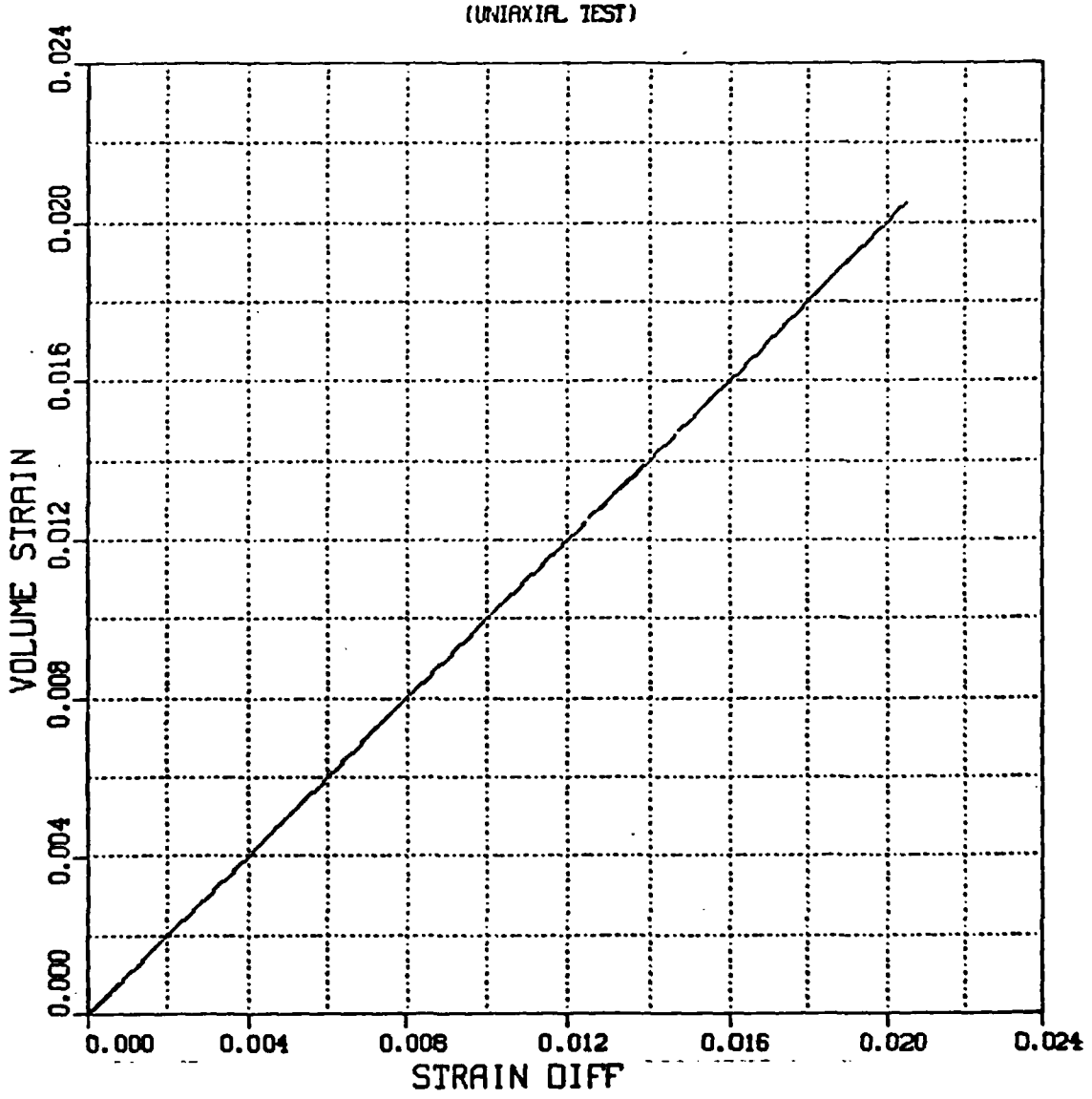

PLOT 1 08.05.57 MED 30 SEP, 1981 JOB-HARDIO , AFWL CRAY DISPLA VER 9.0

EXAMPLE IV - AFWL MODEL

MCCORMICK RANCH SAND

AXIAL STRAIN VS VOLUME STRAIN

(UNIAXIAL TEST)

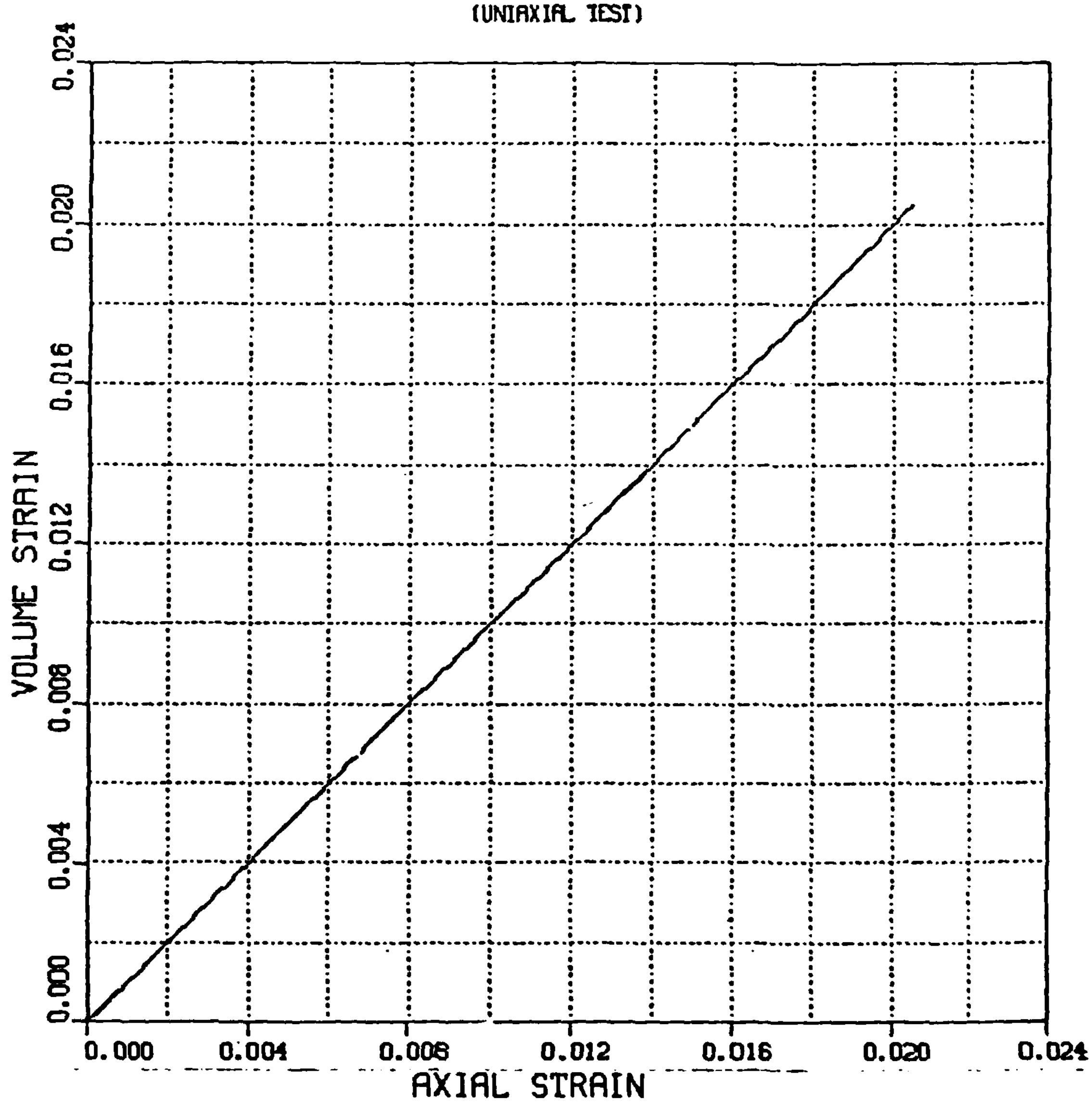

EXAMPLE IV - AFWL MODEL

MCCORMICK RANCH SAND

STRESS RATIO VS. AXIAL STRAIN

(UNIAXIAL TEST)

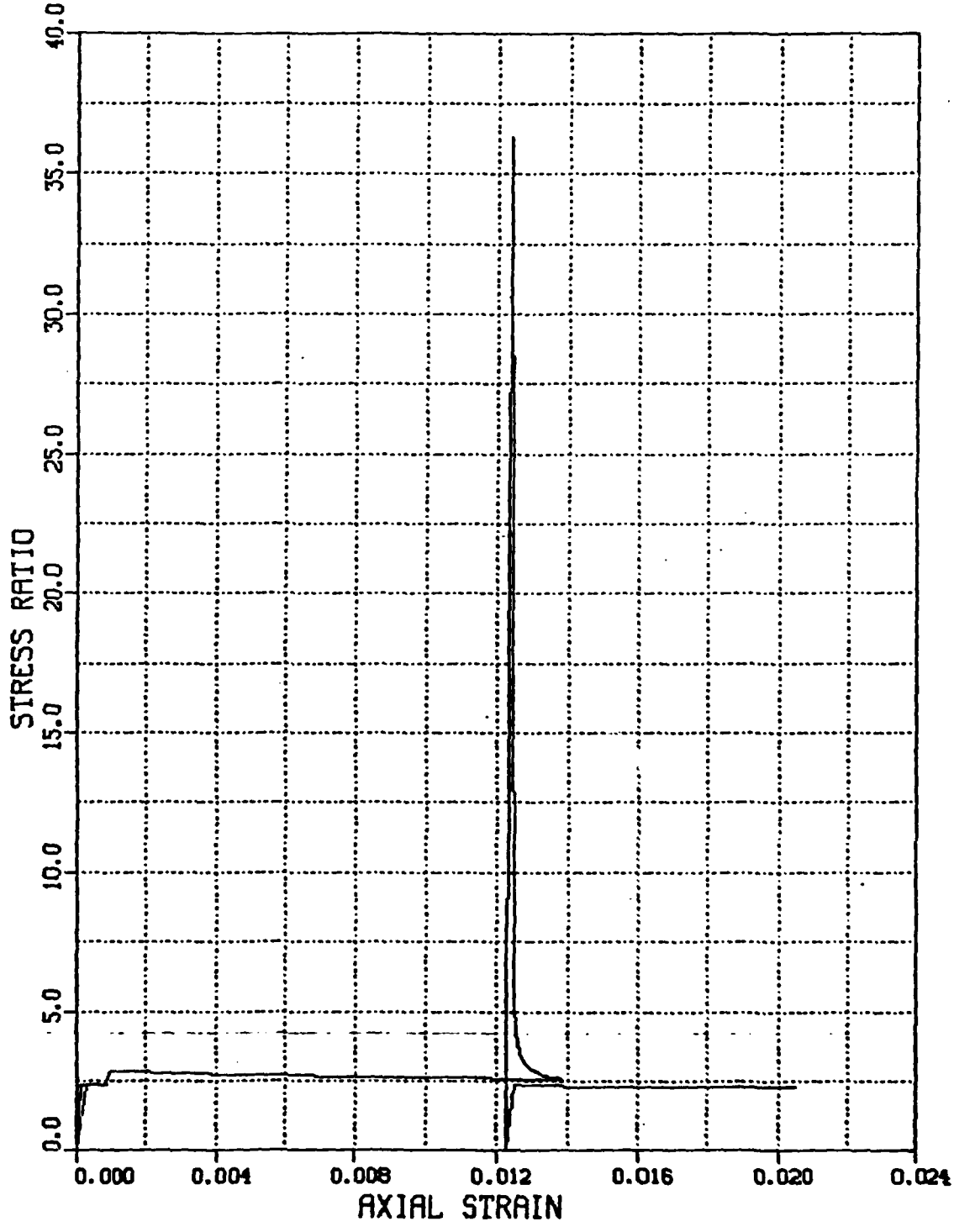

PLOT 1 08.05.58 WED 30 SEP, 1981 JOB-MRB110 , AFWL CRM DISPLA VER 9.0

EXAMPLE V - AFWL MODEL

MCCORMICK RANCH SAND

EFF AXL STRESS VS. AXIALSTRAIN

(UNIAXIAL TEST)

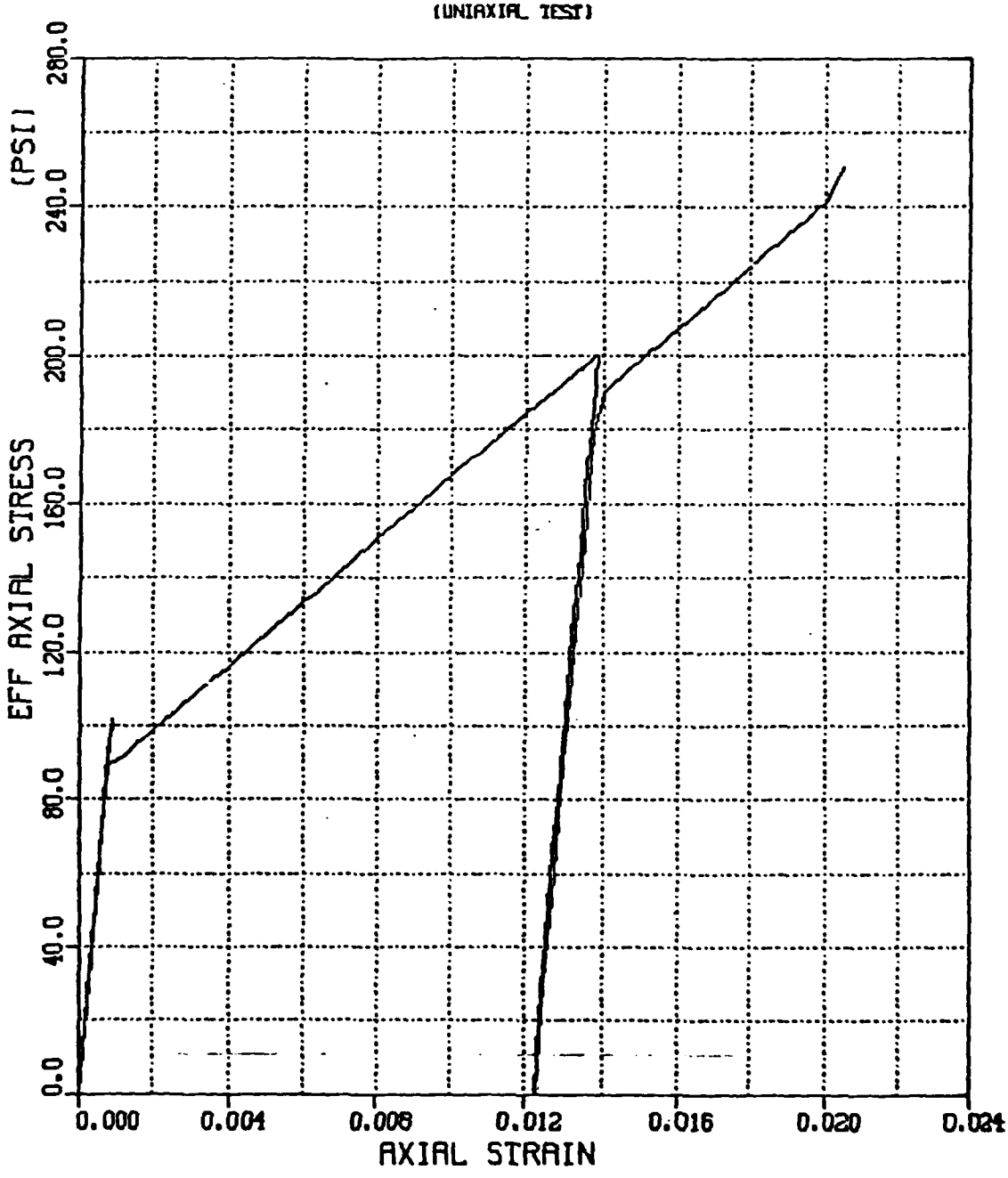

PLOT 1 08.05.59 MON 30 SEP, 1981 JOB-HARBITO , AFWL CAM DISPLA VER 9.0

EXAMPLE V - CAP MODEL

MCCORMICK RANCH SAND

EFF PRESS VS. VOLUMETRIC STRAIN

(ISOTROPIC COMPRESSION)

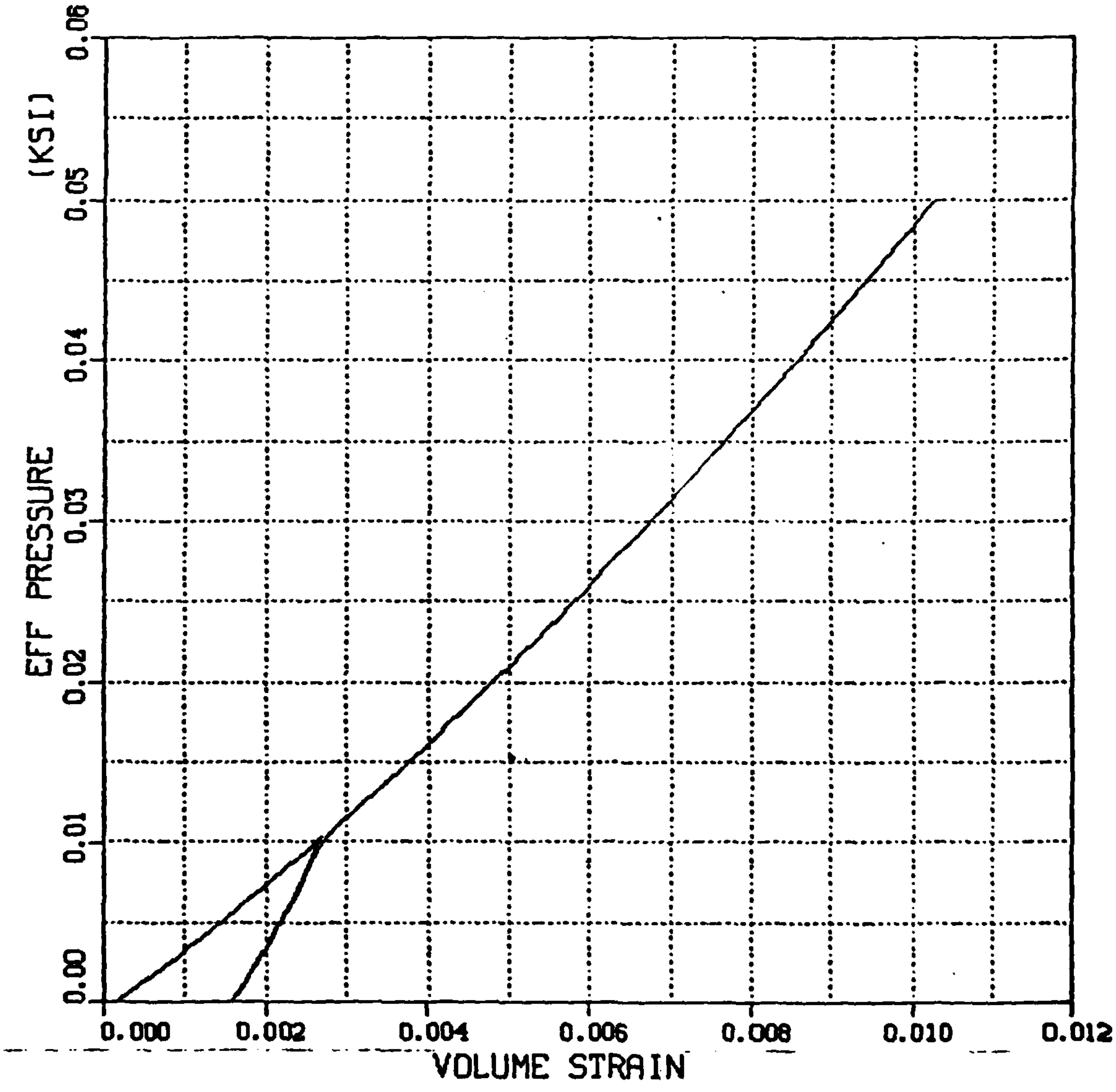

EXAMPLE V - CAP MODEL
MCCORMICK RANCH SAND
STRESS DIFFERENCE VS. EFF PRESS
(STANDARD TRIAXIAL TEST)

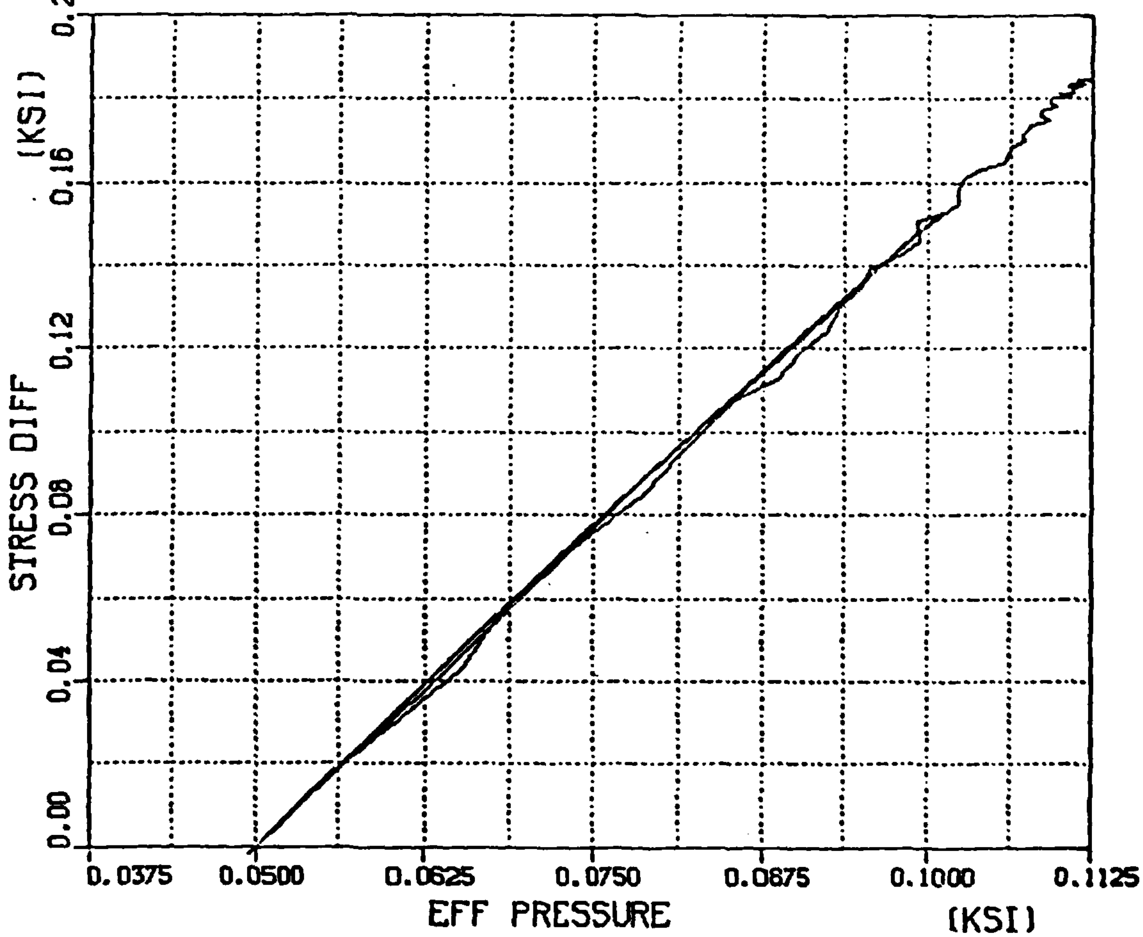

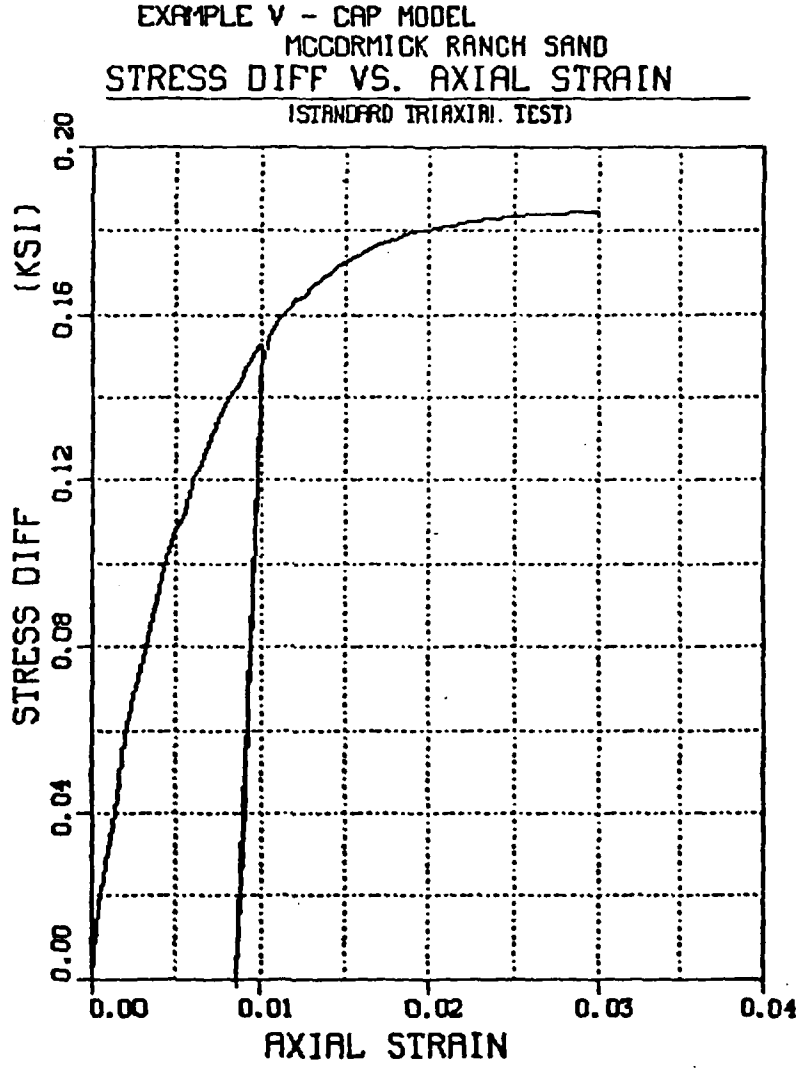

PLOT 1 08.08.07 WED 30 SEP, 1981 JOB-HARBIID, ANAL.DAN DISPLA VER 9.0

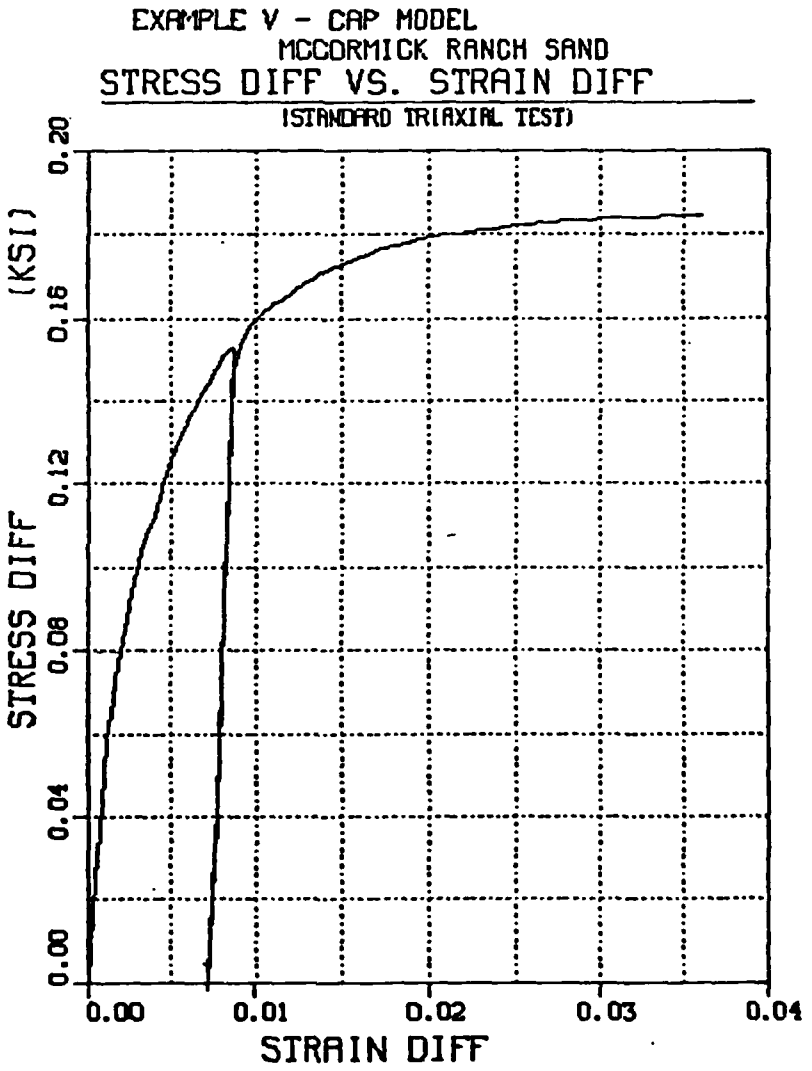
EXAMPLE V - CAP MODEL
MCCORMICK RANCH SAND
STRESS DIFF VS. STRAIN DIFF
(STANDARD TRIAXIAL TEST)
STRESS DIFF (KSI)
0.00
0.04
0.08
0.12
0.16
0.20
0.00
0.01
0.02
0.03
0.04
STRAIN DIFF

EXAMPLE V - CAP MODEL

MCCORMICK RANCH SAND

EFF PRESS VS. VOLUMETRIC STRAIN

(STANDARD TRIAXIAL TEST)

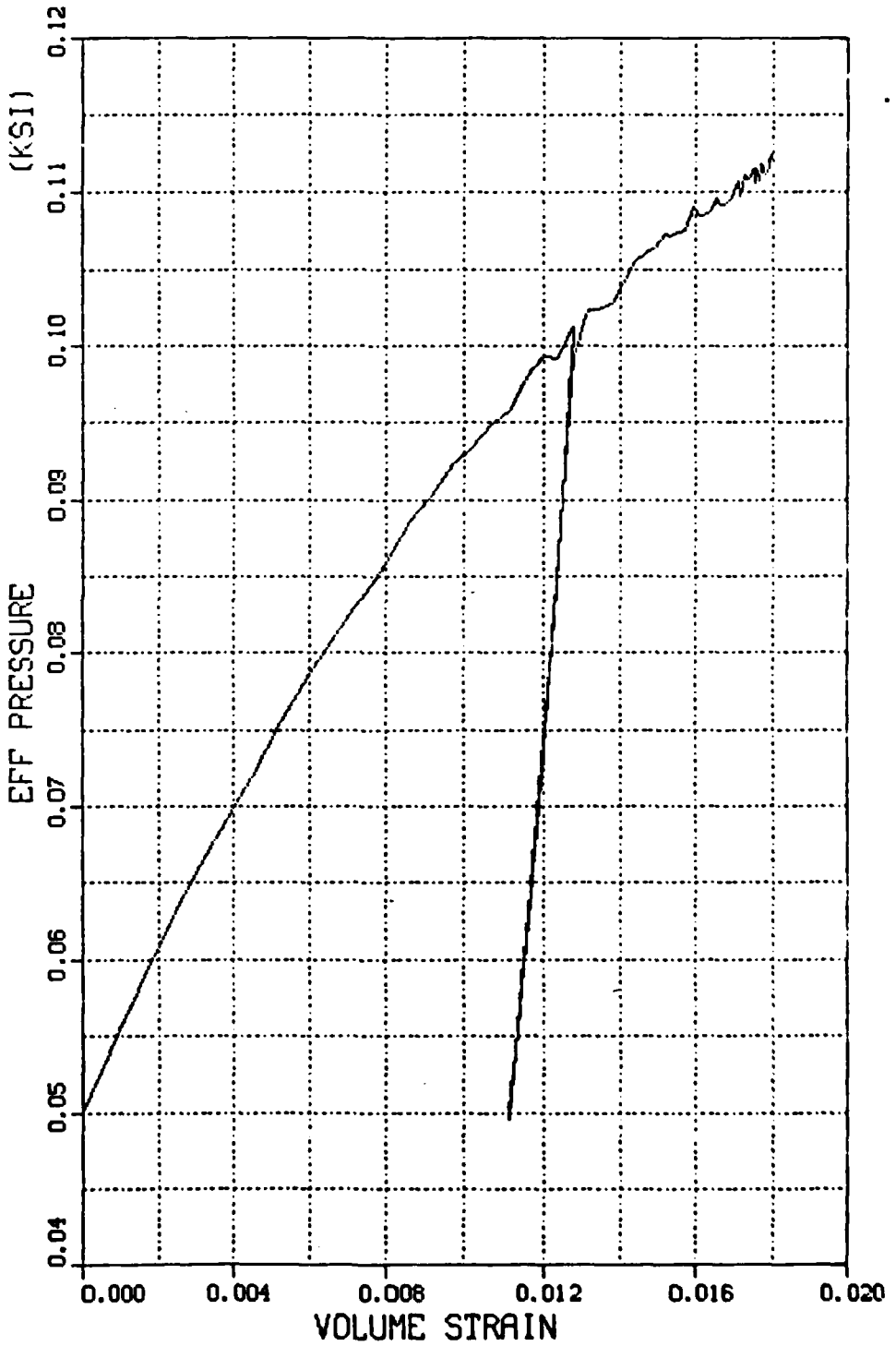

PLOT 1 08.06.88 WED 30 SEP, 1981 JOB=MARINO , MTHL CAP DISPLAY VER 9.0

EXAMPLE V - CAP MODEL

MCCORMICK RANCH SAND

VOLUMETRIC STRAIN VS STRAIN DIFF

(STANDARD TRIAXIAL TEST)

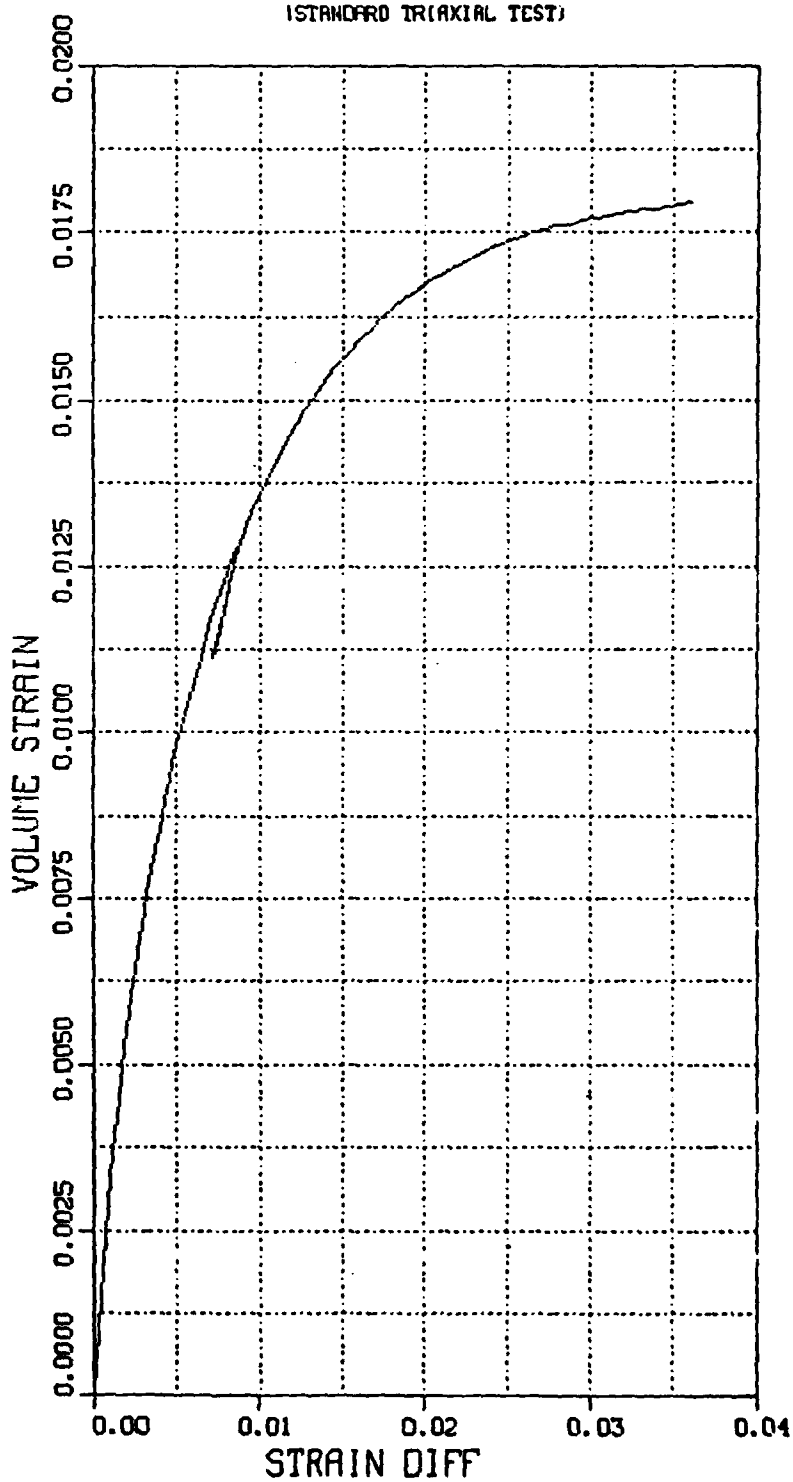

PLOT 1 08.08.09 WED 30 SEP, 1981 JOB-HARENTO , ATHL ORA DISSPLA VER 9.0

EXAMPLE V - CAP MODEL

MCCORMICK RANCH SAND

AXIAL STRAIN VS VOLUME STRAIN

(STANDARD TRIAXIAL TEST)

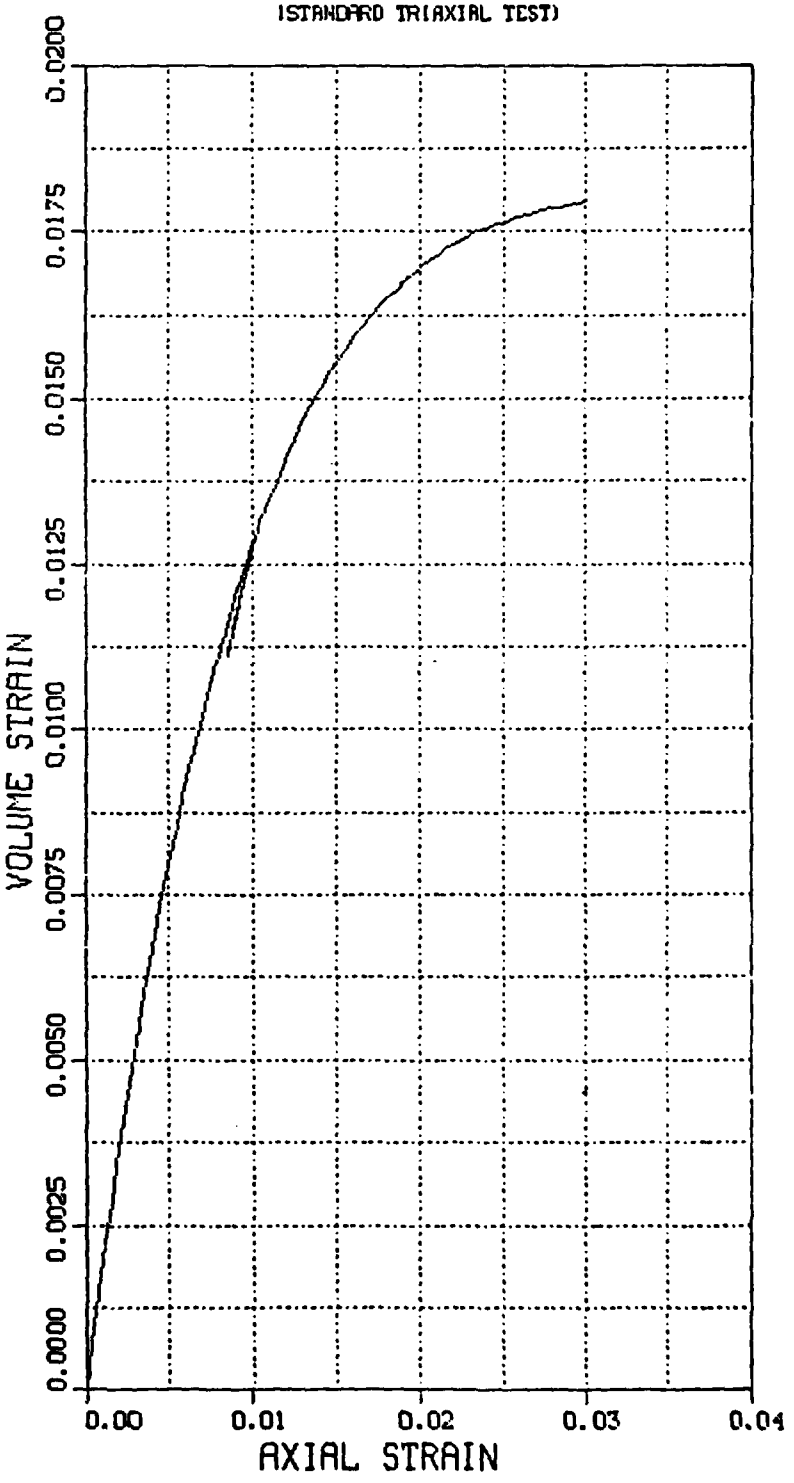

PLOT 1 08.08.89 WED 10 SEP, 1991 JOB-HARDTD , NAVAL CRA DISPLA VER 3.0

EXAMPLE V - CAP MODEL
MCCORMICK RANCH SAND
STRESS RATIO VS. AXIAL STRAIN
(STANDARD TRIAXIAL TEST)

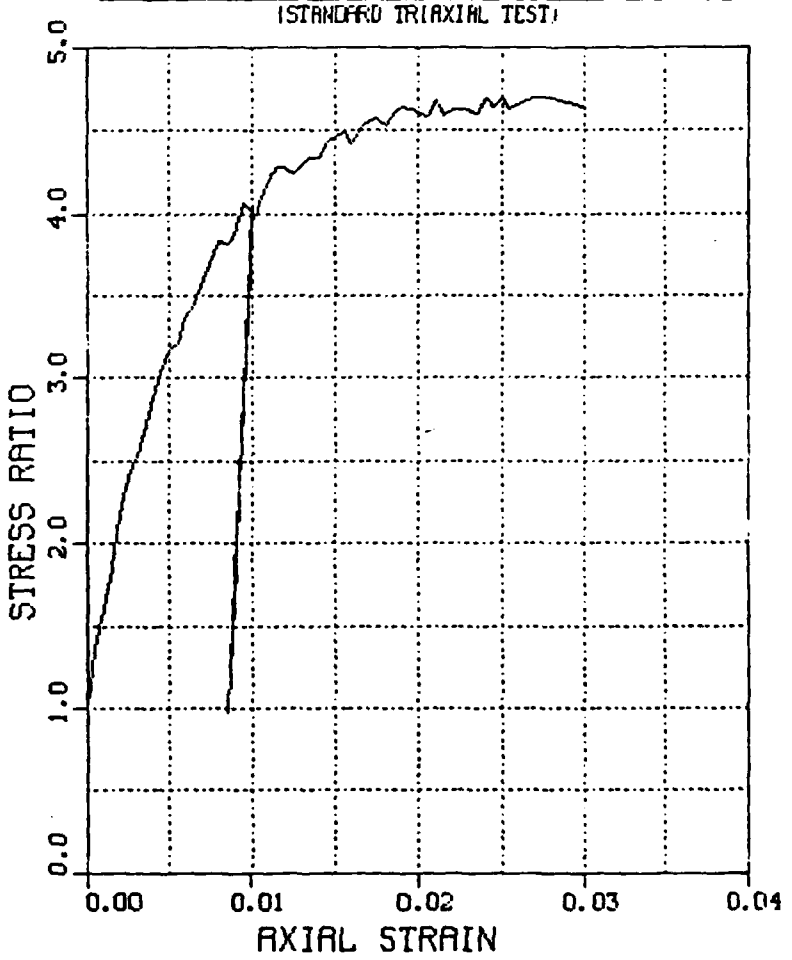

PLOT 1 08.08.17 WED 30 SEP, 1981 JOB-HARVID , ATAL CAM DISSPLA VER 9.0

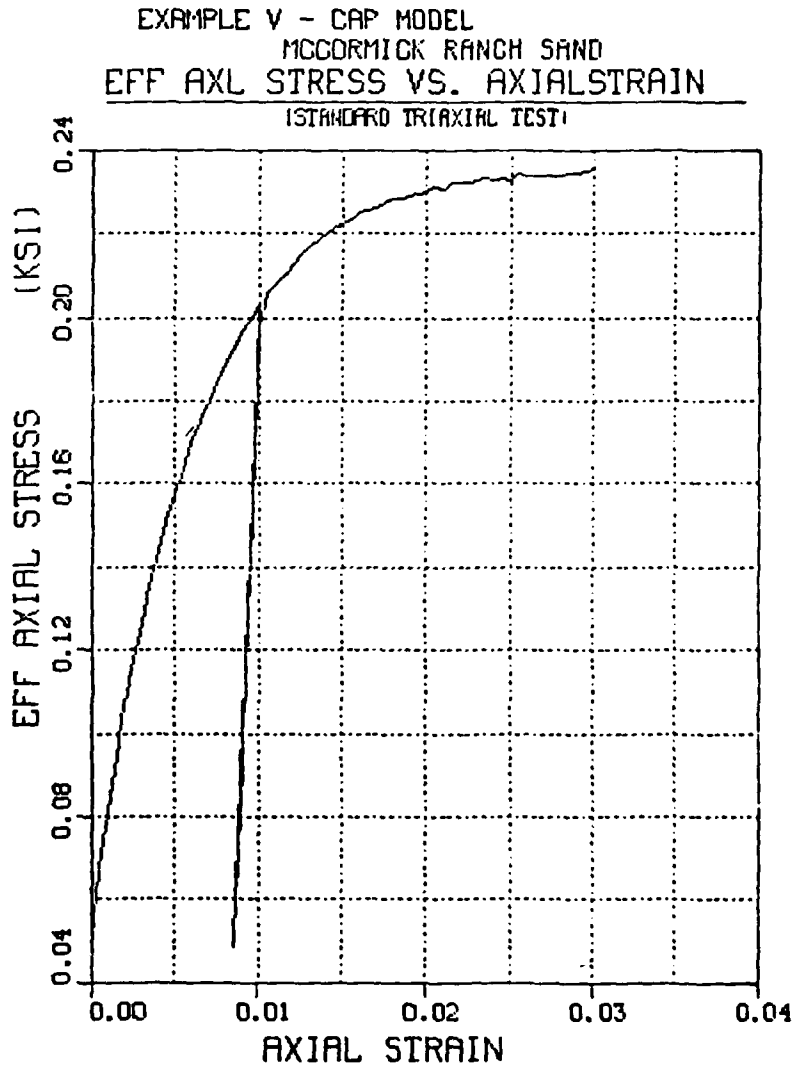

PLOT 1 08.08.28 WED 30 SEP, 1981 JOB-HARDITO , RIVAL CAP DISPLA VER 9.0

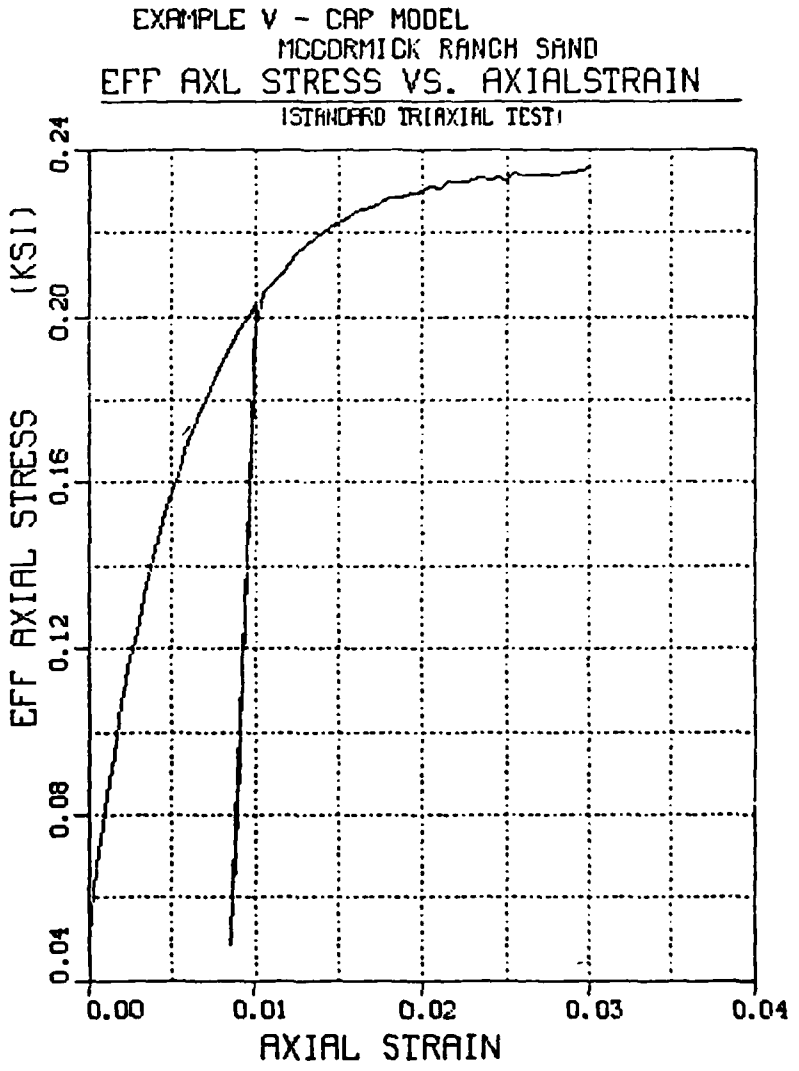

PLOT 1 08.08.28 WED 30 SEP, 1981 JOB=HARDIO , RIVL CRAY DISSPLA VER 9.0

EXAMPLE VI - EFFECTIVE STRESS CAP

OCEAN MUD

PRESSURE VS. VOLUMETRIC STRAIN

ISOTROPIC COMPRESSION

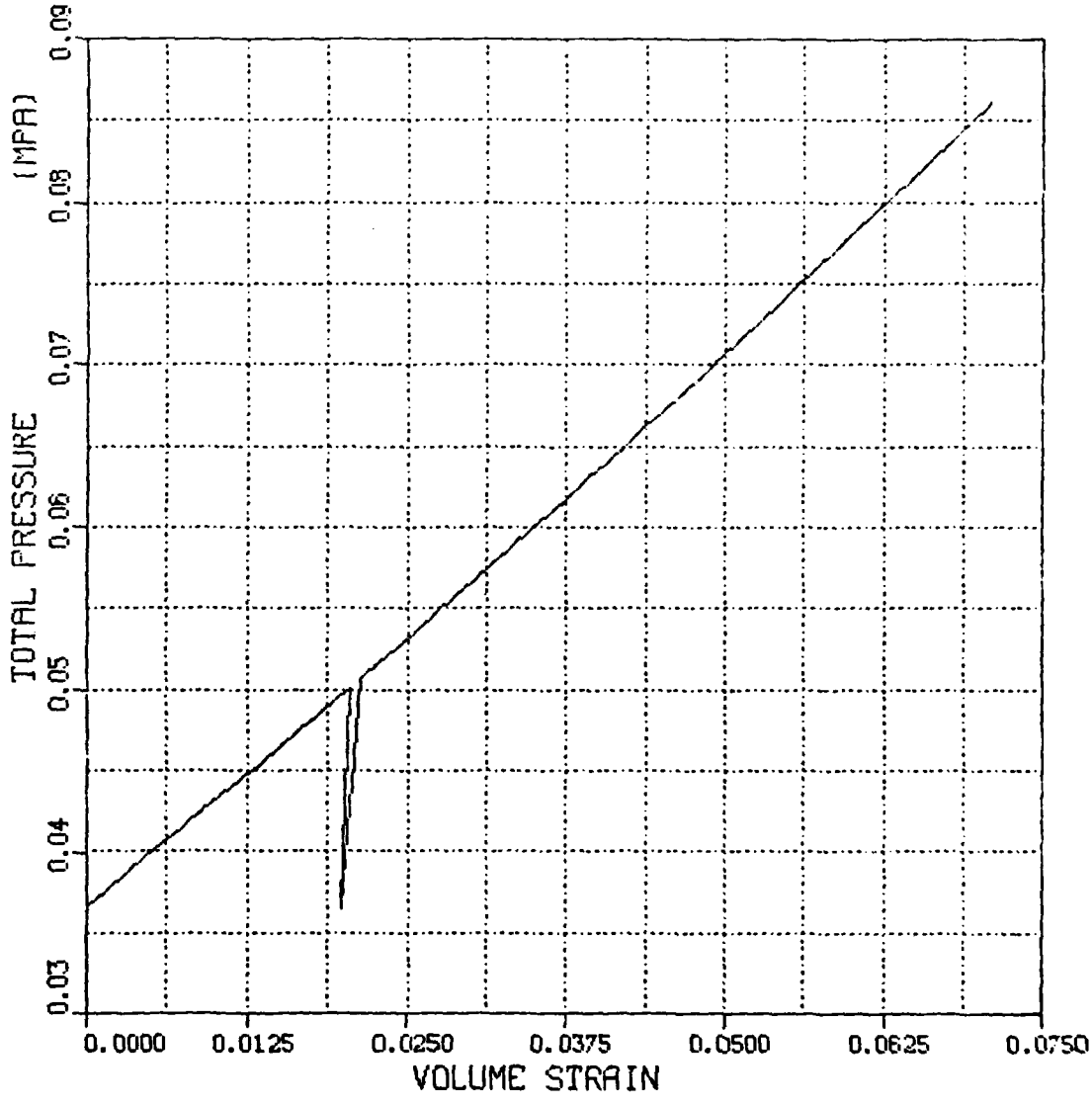

PLOT 1 10:13:21 MON 2 NOV, 1981 JOB=HARDMAN , ATML GRAF DISSPLA VER 9.0

EXAMPLE VI - EFFECTIVE STRESS CAP

OCEAN MUD

EFF PRESS VS. VOLUMETRIC STRAIN

(ISOTROPIC COMPRESSION)

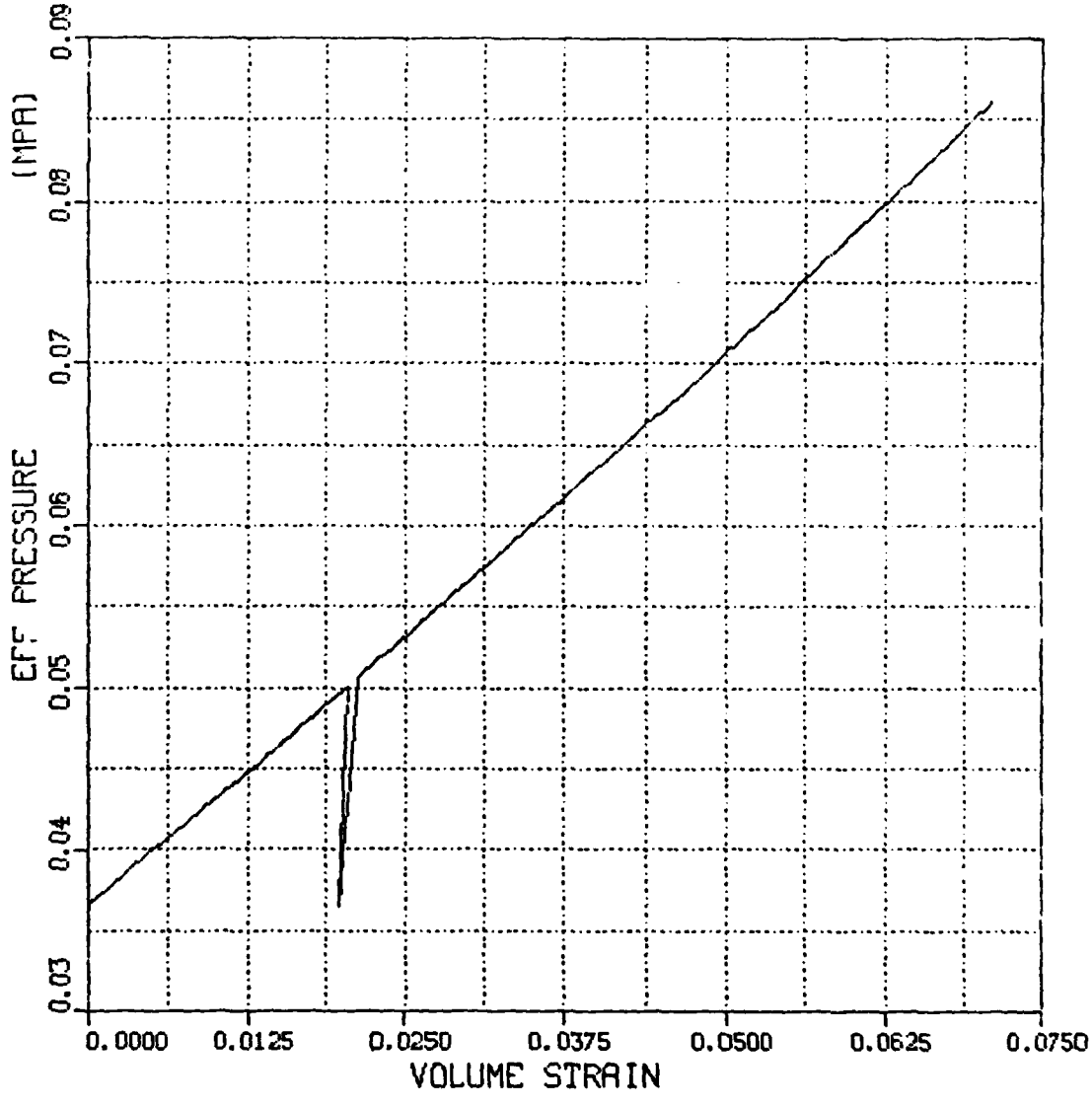

PLOT 1 10.13.21 MON 2 NOV, 1981 JOB-HARDIN , MTHL CAP DISPLA VER 9.0

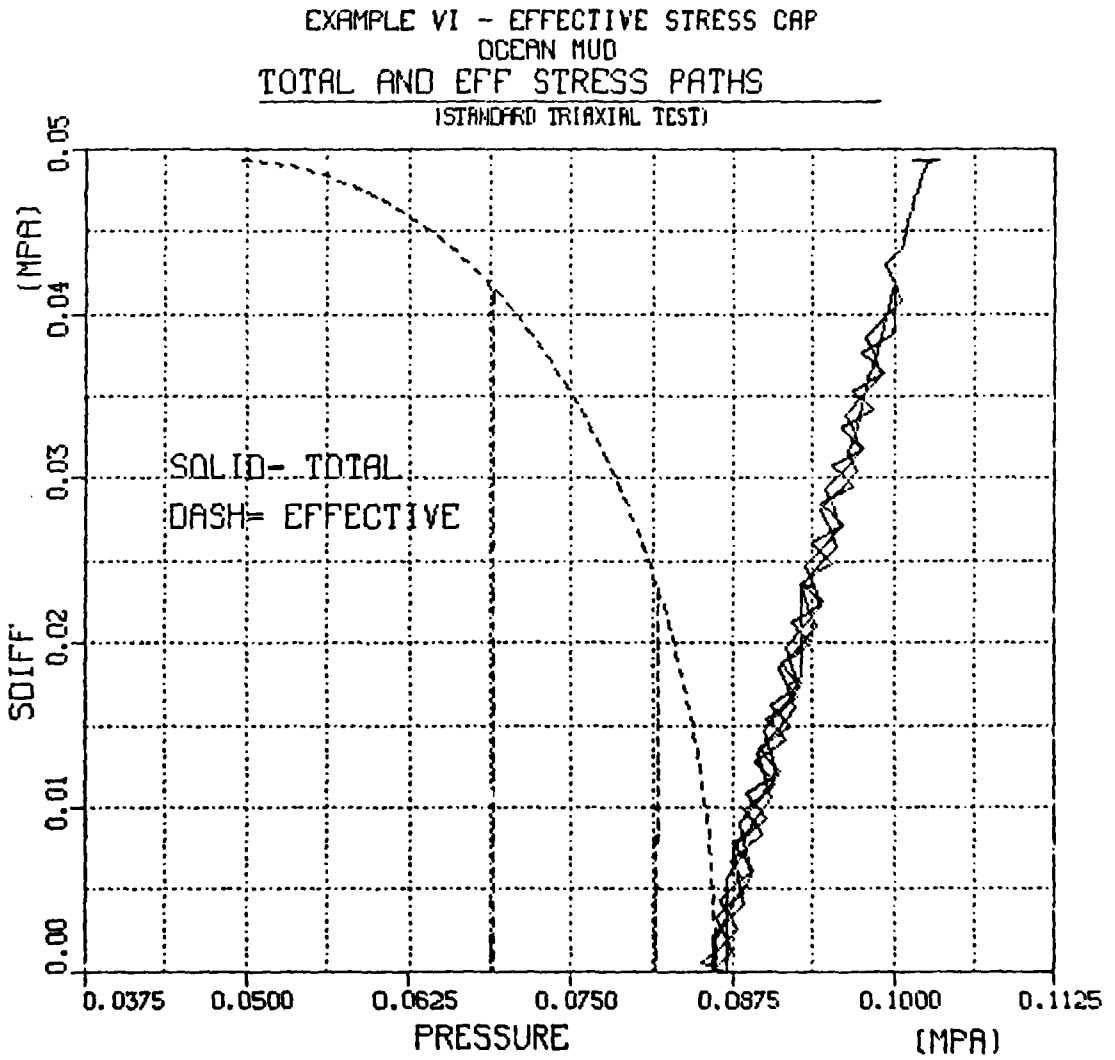

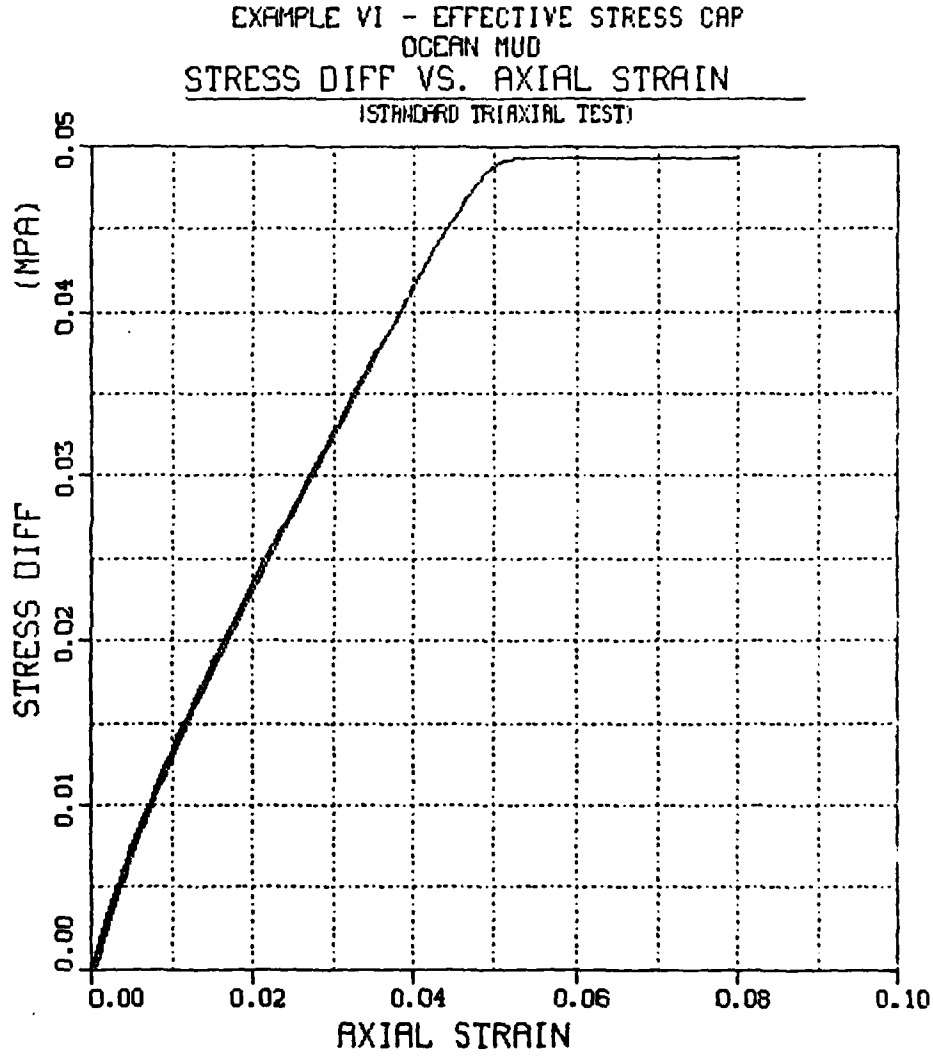

PLOT 1 18.13.23 MON 2 NOV, 1981 JOB=IRARENAN , NTAL CAP DISSPLA VER 9.0

EXAMPLE VI - EFFECTIVE STRESS CAP
OCEAN MUD
STRESS DIFF VS. STRAIN DIFF
(STANDARD TRIAXIAL TEST)

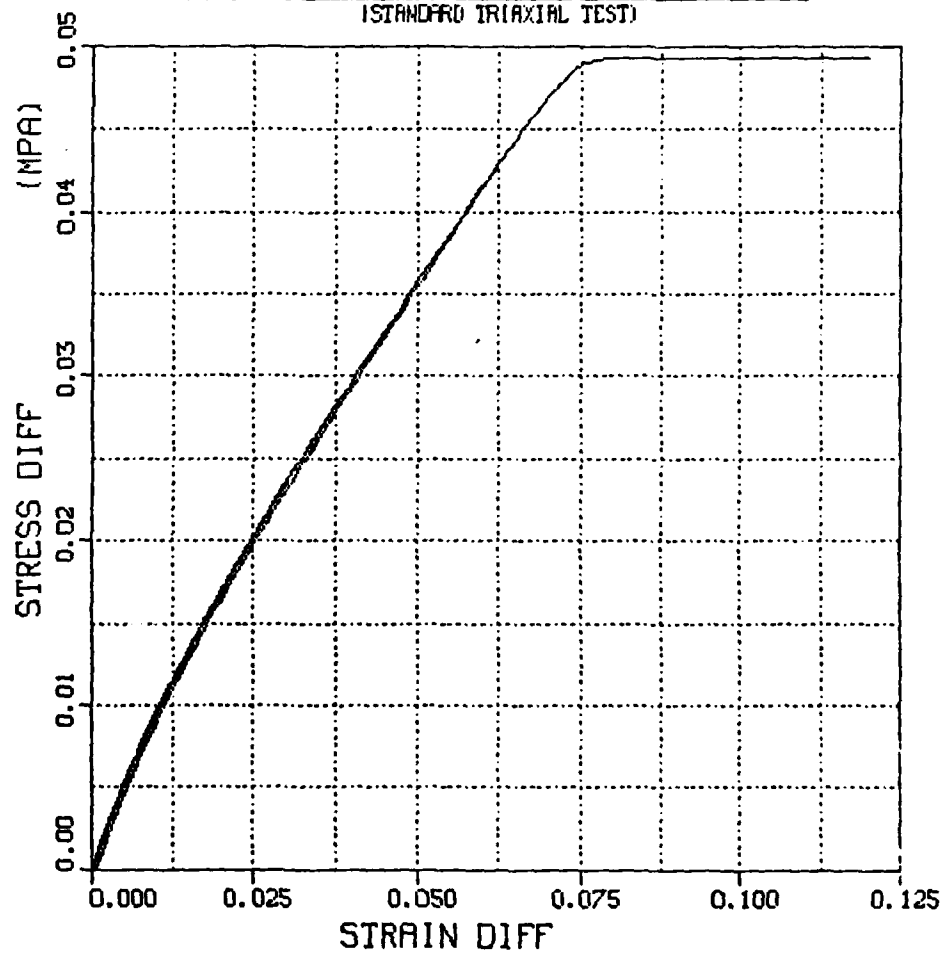

PLOT 1 10:13:23 MON 2 NOV, 1981 JOB=HARDIN, ATML CRA DISSPLA VER 9.0

EXAMPLE VI - EFFECTIVE STRESS CAP

OCEAN MUD

AXIAL STRAIN VS VOLUME STRAIN

(STANDARD TRIAXIAL TEST)

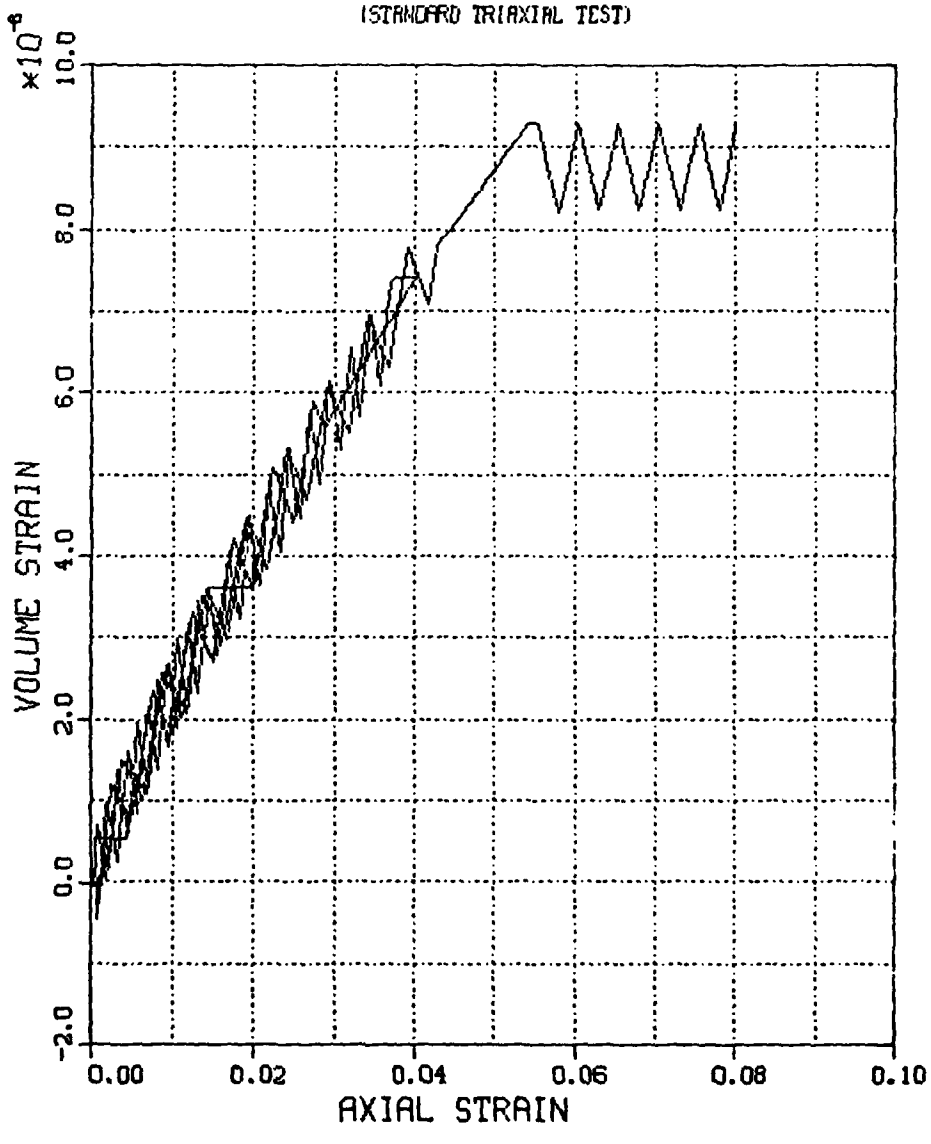

PLOT 1 10.13.25 MON 2 NOV, 1981 JOB-HARBINN , MTHL CRR DISSPLA VER 9.0

EXAMPLE VI - EFFECTIVE STRESS CAP

OCEAN MUD

PORE PRESSURE VS. AXIAL STRAIN

(STANDARD TRIAXIAL TEST)

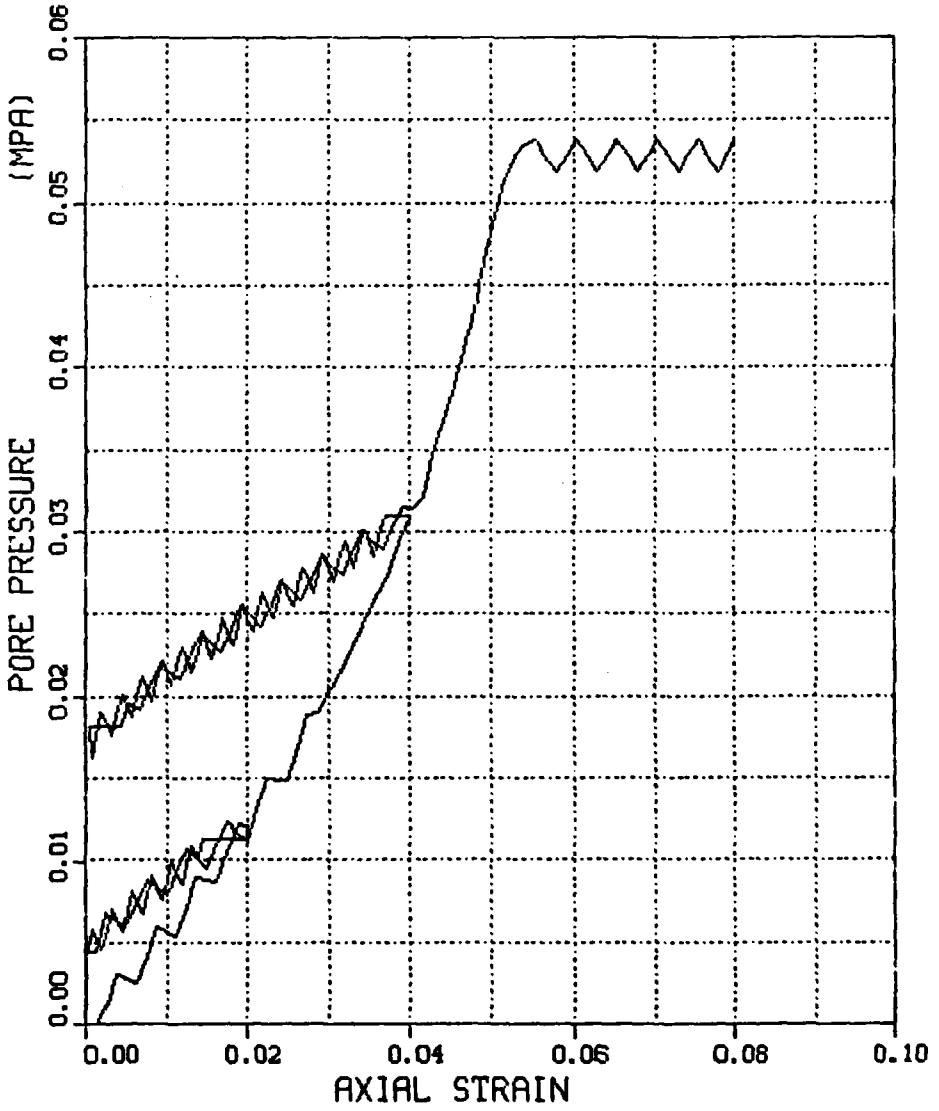

PLOT 1 10:15:25 MON 2 NOV, 1981 JOB-HARBIN , NAVAL CRM DISSPLA VER 9.0

EXAMPLE VI - EFFECTIVE STRESS CAP

OCEAN MUD

STRESS RATIO VS. AXIAL STRAIN

ISTANDARD TR(AXIAL TEST)

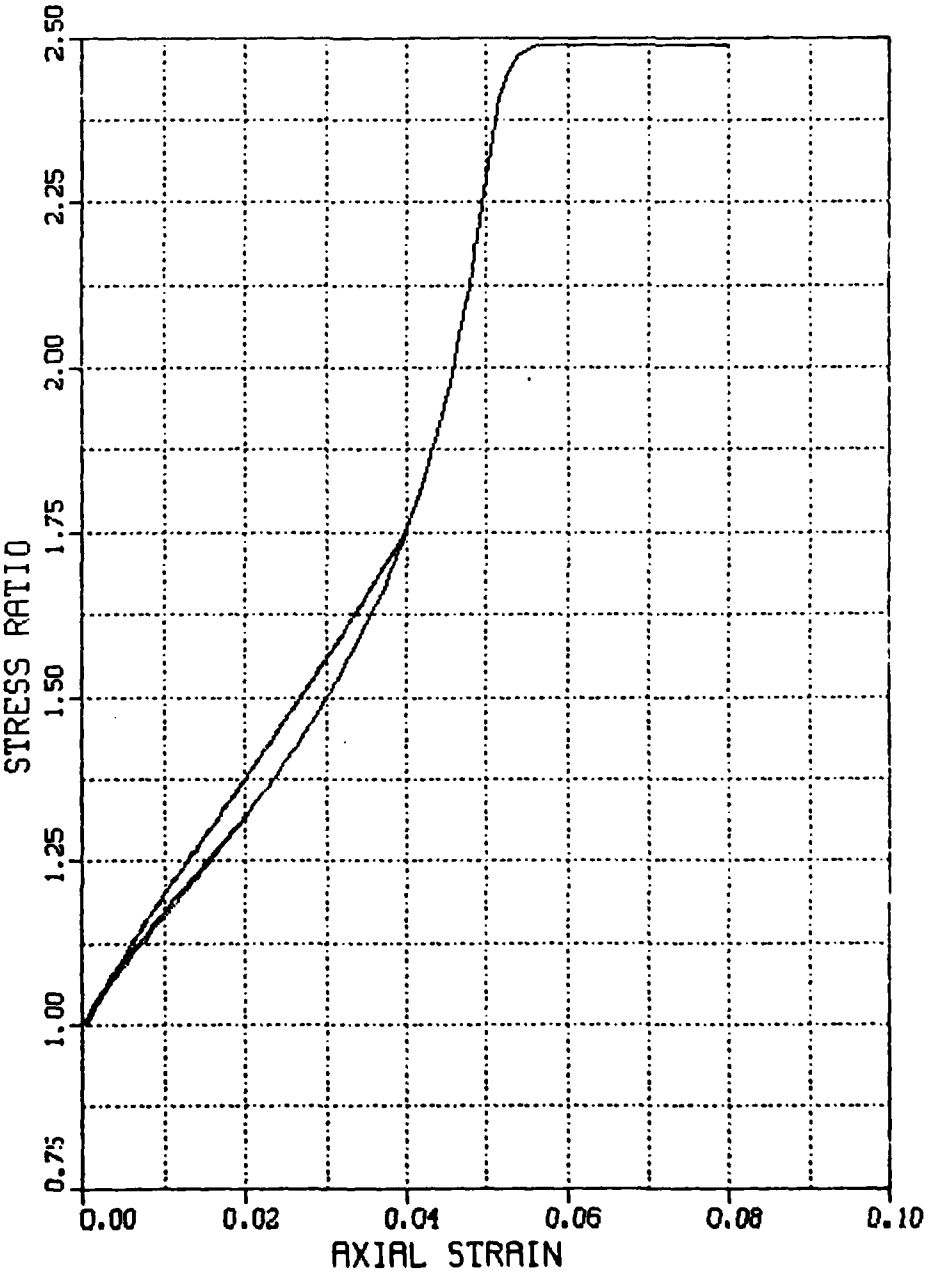

PLOT 1 11.13.28 MON 2 NOV, 1981 JOB-HARDMAN, NAVAL CMR DISSPLA VER 9.0

EXAMPLE VI - EFFECTIVE STRESS CAP

OCEAN MUD

EFF AXL S SS VS. AXIALSTRAIN

(STANDARD TRIAXIAL TEST)

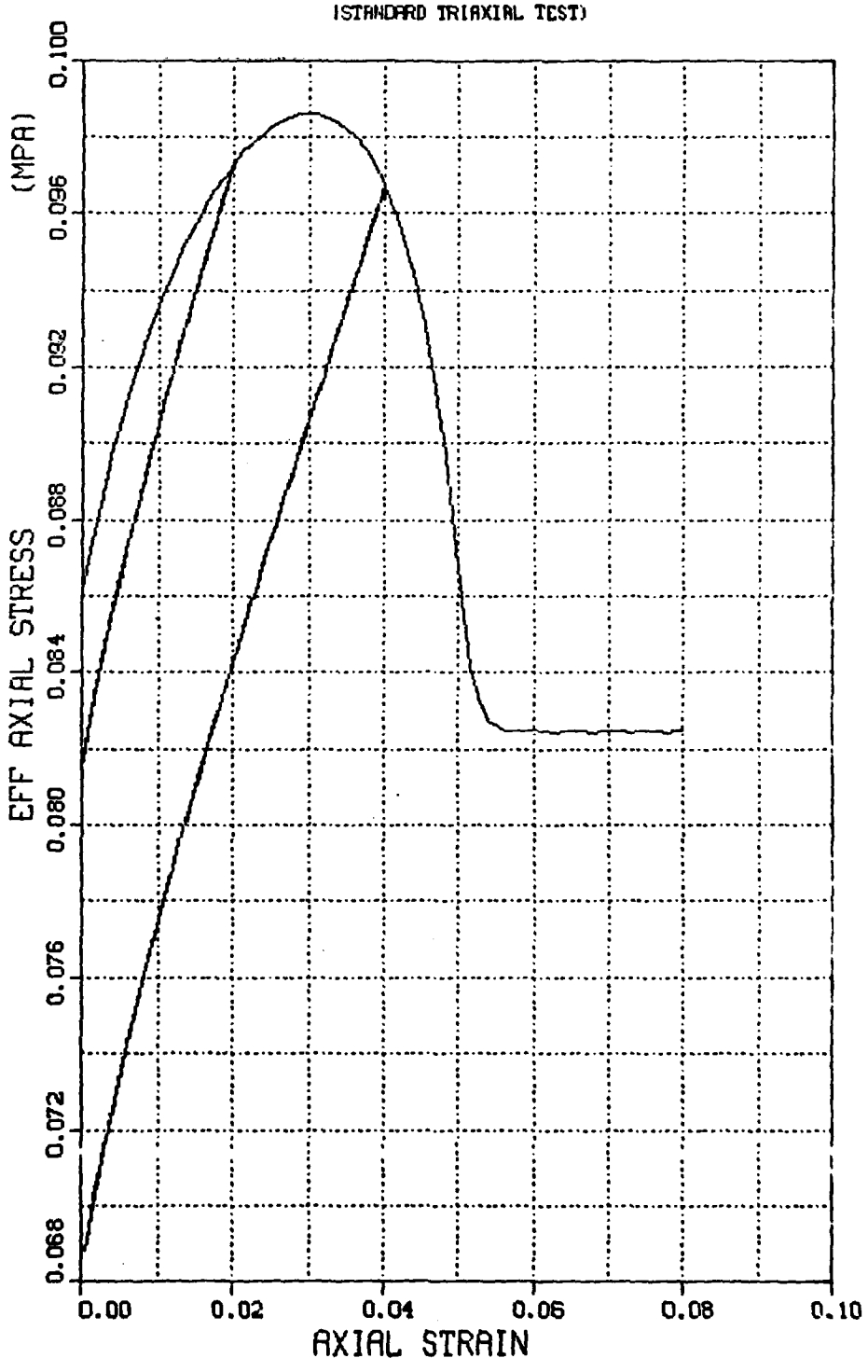

PLOT 1 18.15.28 MON 2 NOV, 1981 JOB=HARDIN , HTML CAP DISSPLA VER 9.0

EXAMPLE VI - EFFECTIVE STRESS CAP

OCEAN MUD

TOT AXL STRESS VS. AXIALSTRAIN

(STANDARD TR(AXIAL TEST)

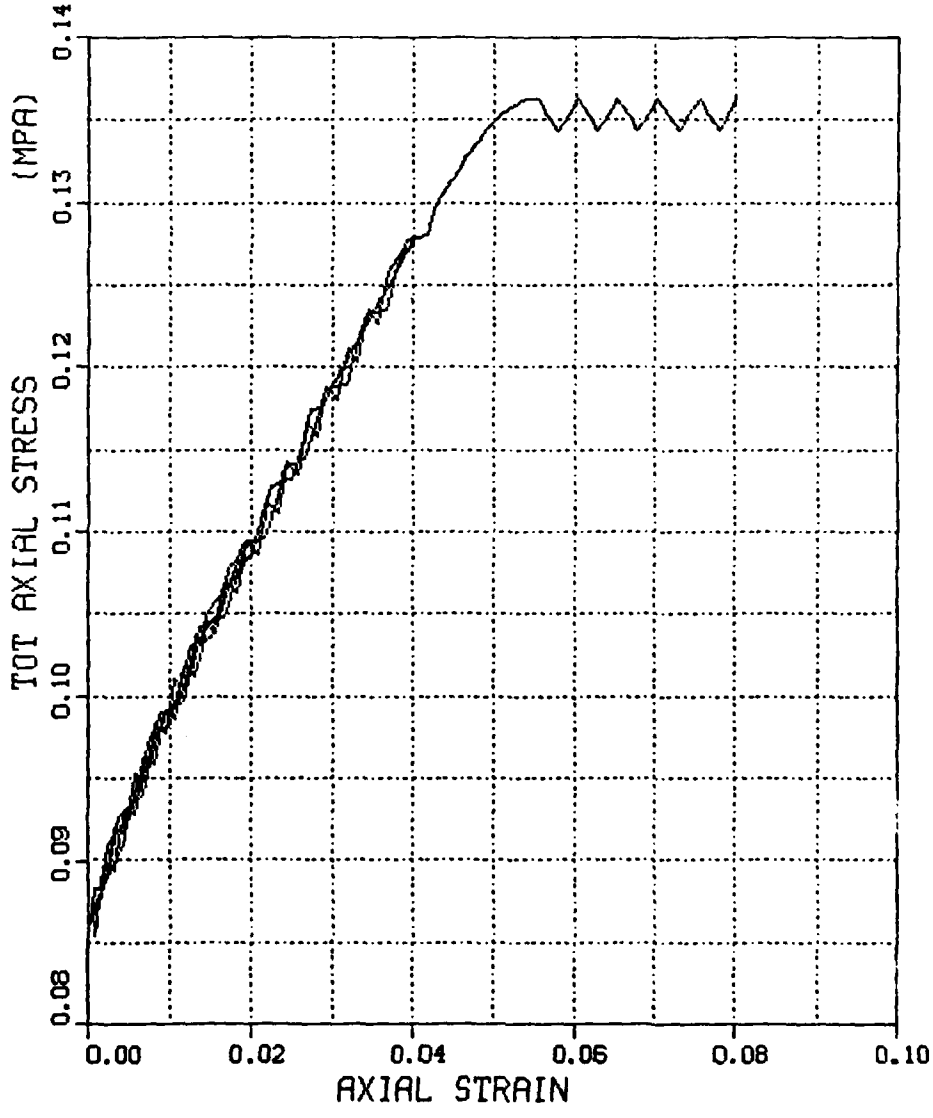

PLOT 1 10.13.27 MON 2 NOV, 1981 JOB-HARDING , MTWL CRA DISSPLA VER 9.0

APPENDIX D

Professional Personnel and Interactions

D.1 Professional Personnel

The following people were associated with this research effort:

1. Jimmie L. Bratton
   Principal, Applied Research Associates, Inc.

2. William C. Dass
   Research Engineer, Applied Research Associates, Inc.

3. Dr. Cornelius J. Higgins
   Principal, Applied Research Associates, Inc.

4. Peter Dzwilewski
   Senior Engineer, Science Applications, Inc.
   (presently, Senior Engineer, Applied Research Associates, Inc.)

5. David K. Rudeen
   Scientist, Science Applications, Inc.

6. Dr. Yoshi Moriwaki
   Senior Engineer, Science Applications, Inc.
   (presently with Woodward-Clyde Associates)

D.2 Interactions

A symposium entitled "Implementations of Computer Proceedures and Stress-Strain Laws in Geotechnical Engineering" was held in Chicago, Illinois on August 3-6, 1981, cosponsored by the Illinois Institute of Technology and the Virginia Polytechnical Institute. The conference was attended by Mssrs. Dass and Dzwilewski of ARA, and provided additional insight into the present status of research on constitutive laws.

In addition, ARA has submitted two abstracts for (see below) acceptance to the "International Conference on Constitutive Laws for Engineering Materials: Theory and Application", to be held in January 1983 at the University of Arizona. ARA will continue to prepare papers for the appropriate conferences and/or publications.

COMPARISON OF CONSTITUTIVE MODELS SUBJECTED TO VARIED STRESS-STRAIN PATHS

William C. Dass[1]

ABSTRACT

Many levels of constitutive models are available today to the practitioner, from very complex to simple linear-elastic. As a result, there is often confusion when the time comes to choose a model which will give the right combination of simplicity (and therefore cost-effectiveness) and accuracy.

This paper describes a small computer program which has been developed as a tool for studying material constitutive models. The program allows comparisons of model behavior, and with it one can perform parametric studies to determine the influence of model components. It is intended that the "Soil Element Model", as it is called, be an aid in model development and also in choosing a model which best suits a particular boundary value problem.

A study is presented which illustrates the use of this code to compare the ability of several material models to replicate laboratory test data. The test data (both static and dynamic) was taken from previous efforts and some data was generated specifically for this purpose. The study concentrates on parametric effects and on isolating areas for model improvement and development. In addition, complex loading paths, typical of those which are induced by blast loadings, are imposed on the models and some comparisons are drawn.

[1]Research Engineer, Applied Research Associates, Inc., Albuquerque, New Mexico

THE ROLE OF IN-SITU TESTING IN DEVELOPMENT OF CONSTITUTIVE LAWS FOR ENGINEERING MATERIALS

Jimmie L. Bratton[1]

ABSTRACT

Theoretical development of Constitutive Laws for engineering materials begins with a set of characteristics assumed to be representative of the behavior of the material under boundary conditions approximating those of the engineering problem of interest. Generally these characteristics are developed from laboratory tests of the material. Laboratory tests of geologic materials, however, are subject to many limitations. The sampling and specimen preparation procedures can lead to both quantitative and qualitative changes in the material behavior. In addition, the boundary conditions which can be applied and measurements which can be made are limited and not always the most indicative of the material behavior for the conditions of interest or sufficient to allow the generalization of the measured response necessary for development of a constitutive model.

In-situ testing has been shown to provide a necessary and important adjunct to laboratory testing for soils and rock. This is particularly true when the loadings of interest are complex and dynamic. In-situ testing techniques are briefly reviewed and their application to the establishment of the material response characteristics for constitutive modeling is discussed. The use of these tests for evaluating models is also reviewed and specific examples are presented. Characteristics of the material response which were not identified in laboratory testing are presented for specific cases and the role of in-situ testing in the development of constitutive laws for engineering materials is illustrated.

[1]Principal, Applied Research Associates, Inc., Albuquerque, New Mexico


DATE
ILME